IDENTIFICATION AND QUANTIFICATION OF TRANSIENT STRUCTURE-BORNE SOUND SOURCES WITHIN ELECTRICAL STEERING SYSTEMS

Michael STURM

Ph.D. Thesis 2013

IDENTIFICATION AND QUANTIFICATION OF TRANSIENT STRUCTURE-BORNE SOUND SOURCES WITHIN ELECTRICAL STEERING SYSTEMS

Michael STURM

Acoustics Research Centre

School of Computing, Science and Engineering

University of Salford, Salford, UK

Submitted in Partial Fulfilment of the Requirements of the

Degree of Doctor of Philosophy, September 2013

Contents

LIST OF FIGURES ..... **V**

ACKNOWLEDGEMENTS ..... **XXII**

NOMENCLATURE ..... **XXIII**

ABSTRACT ..... **XXX**

1. INTRODUCTION **1**

1.1. BACKGROUND 2

1.2. THE GENERAL APPROACH OF VIRTUAL ACOUSTIC PROTOTYPING 4

1.3. ON THE GENERATION AND ASSESSMENT OF STEERING INDUCED SOUND 7

1.4. THE PHYSICAL PROBLEM 8

1.5. TIME DOMAIN REPRESENTATION OF ELECTRICAL STEERING SYSTEMS 11

1.6. THESIS OBJECTIVES 13

2. LITERATURE REVIEW AND THEORY **16**

2.1. INTRODUCTION 17

2.2. ASSUMPTION OF LINEAR AND TIME-INVARIANT SYSTEM BEHAVIOUR 19

2.3. CHARACTERISATION OF STRUCTURE-BORNE SOUND SOURCES 21

2.3.1. Mechanical mobility and related frequency response functions 28

2.3.2. Direct measurement of free velocity and blocked force 31

2.3.3. Measurement of operational contact force 33

2.3.4. The in-situ blocked force approach 35

2.4. INVERSE FORCE IDENTIFICATION 38

2.4.1. Frequency domain inverse methods and related approaches 46

2.4.2. Direct deconvolution methods in time domain 48

2.4.3. Time domain modal filtering 49

2.4.4. Inverse filtering using state-space methods 53

2.4.5. Kalman filtering 60

2.4.6. Sensitivity methods 66

2.4.7. Adaptive method based on the LMS algorithm 67

2.5. SUMMARY AND CONCLUDING REMARKS 68

3. IDENTIFICATION OF INTERNAL SOURCE LOCATIONS 72

3.1. INTRODUCTION 73
3.2. ELECTRIC POWER STEERING SYSTEMS 73
3.2.1. The functional principle 75
3.3. SOUND PHENOMENA INDUCED BY ELECTRICAL STEERING SYSTEMS 78
3.3.1. Functional steering sound 78
3.3.2. Interfering steering sound 80
3.3.3. Contact noise 81
Stick-slip phenomenon 81
Impact phenomenon 84
3.3.4. Relevance ranking of steering induced (transient) sounds 88
3.4. THE CONCEPTUAL SOURCE-PATH-RECEIVER MODEL 91
3.4.1. The concept 91
3.4.2. Sub-structuring into active and passive parts 92
3.4.3. The source-path-receiver model 95
3.4.4. Discussion 96
3.5. SUMMARY 98

4. FORCE RECONSTRUCTION IN TIME DOMAIN USING AN ADAPTIVE ALGORITHM 100

4.1. INTRODUCTION 101
4.2. FUNDAMENTALS OF THE TIME DOMAIN INVERSE ROUTINE 102
4.2.1. The conventional Least Mean Square algorithm 102
4.2.2. Adaptive algorithm for the reconstruction of forces in time domain 105
4.2.3. The iterative adaptive process 109
4.2.4. Demonstration of the inversion routine for an ideal numerical model 113
4.3. THE MODELLING APPROACH 118
4.3.1. System and noise model 119
4.3.2. Performance evaluation 121
4.4. FORCE RECONSTRUCTION FOR SINGLE INPUT SINGLE OUTPUT SYSTEMS 125
4.4.1. Application to noise free system 126
4.4.2. Sensitivity to noise in the structural response 128

4.4.3. Sensitivity to errors in the system model 130
4.4.4. Conclusions 132
4.5. FORCE RECONSTRUCTION FOR SINGLE INPUT MULTIPLE OUTPUT SYSTEMS 134
4.5.1. The concept of over-determination and the averaged error gradient 134
4.5.2. Application to noise free system 138
4.5.3. Sensitivity to noise in the structural responses 142
4.5.4. Sensitivity to errors in the system model 146
4.5.5. Conclusions 149
4.6. FORCE RECONSTRUCTION FOR MULTIPLE INPUT MULTIPLE OUTPUT SYSTEMS 153
4.6.1. The generalisation of the method 153
4.6.2. Application to noise free system 157
4.6.3. Sensitivity to noise in the structural responses 162
4.6.4. Sensitivity to errors in the system model 165
4.6.5. Conclusions 172
4.7. SUMMARY AND CONCLUDING REMARKS 176

5. CHARACTERISATION OF STRUCTURE-BORNE SOUND SOURCES IN ELECTRICAL STEERING SYSTEMS 180

5.1. INTRODUCTION 181
5.2. THE TEST BENCH MEASUREMENT APPROACH 182
5.2.1. The test bench 183
5.2.2. State-of-the-art analysis 185
5.2.3. Operation and testing conditions 187
5.2.4. Conclusions 188
5.3. OBTAINING SUITABLE SYSTEM MODELS 189
5.3.1. Measurement of (in-situ) frequency response functions 189
5.3.2. Data evaluation criteria based on reciprocity principle 193
5.3.3. Data evaluation criteria based on conductance of the mobility matrix 195
5.3.4. Impulse response functions from transformation 204
5.3.5. Conclusions 207
5.4. CHARACTERISATION USING ARTIFICIAL EXCITATIONS 208
5.4.1. Experimental set-up 209
5.4.2. Steering system with single internal source: Numerical examples 210
5.4.3. Steering system with single internal source: Experimental example 216

5.4.4. Steering system with multiple internal sources: Numerical example 217
5.4.5. Steering system with multiple internal sources: Experimental example 220
5.4.6. Characterisation of the internal sources using test bench excitation 223
5.4.7. Conclusions 230
5.5. CORRECTION STRATEGIES FOR TEST BENCH MEASUREMENTS 231
5.5.1. Limitations of test bench approach 232
5.5.2. Strategy I: Correction of the measured operational responses 235
5.5.3. Strategy II: Reconstruction of an expanded set of input forces 237
5.5.4. Conclusions 241
5.6. SUMMARY AND CONCLUDING REMARKS 242

6. CONCLUDING REMARKS AND FUTURE WORK 245

REFERENCES 256

A APPENDICES 273

A.1 OVERVIEW OF TIME DOMAIN INVERSE FORCE IDENTIFICATION METHODS 273
A.2 ADDITIONAL RESULTS: INVERSE FORCE IDENTIFICATION IN TIME DOMAIN 277
A.3 FRAC AND PAC ANALYSIS 299

List of Figures

Figure 1.1: The physical problem behind steering induced noise in vehicles 9

Figure 2.1: Two-stage measurement approach for determination of contact forces in-situ. Assembled structure *C* comprising the source *A* which is active due to some internal source mechanisms s_k and the passive receiver *B*; *a*,*b* and *c* represent all degree of freedom on the corresponding interfaces of structures *A*, *B* and *C*, respectively; *o* indicates that operational measurements are conducted. 34

Figure 2.2: Two-stage measurement approach for determination of blocked forces in-situ. Assembled structure *C* comprising the source *A* which is active due to some internal source mechanisms s_k and the passive receiver *B*; *a*,*b* and *c* represent all degree of freedom on the corresponding interfaces of structures *A*, *B* and *C*, respectively; *o* indicates that operational measurements are conducted 35

Figure 2.3. Schemes of two inverse problems in structural dynamics: (a) inverse system identification, (b) inverse force identification. Problem solutions are underlined. 40

Figure 3.1. Application areas of different EPS systems according to standard values of steering rack force and mechanical performance for all vehicle classes [180]. 74

Figure 3.2. The electrical steering system EPSapa PL2: Schematic diagram [2] (a) and illustration of the physical assembly of the steering gear including the acting loads (b). 75

Figure 3.3. Functional block diagram of electric power assisted steering [180] 76

Figure 3.4. Configuration of servo gear system in EPS with paraxial servo unit. 77

Figure 3.5. Spectogram (frequency vs. time) of sound pressure level measured inside the passenger compartment and order contributions from associated functional steering sound sources [2]. 79

Figure 3.6. (a) Stick-slip phenomenon: Schematic illustration of the physical relationship between interfacing solids ; (b) simple mass-spring-model of interfacial relationship and (c) schematic of oscillating friction forces responsible for the generation of stick-slip noise..... 82

Figure 3.7. Groaning in EPS systems: Impulsive structural response (measured on the steering housing) resulting from stick-slip between bearing ring and housing while alternating left-right-steering is performed. 84

Figure 3.8. Impact phenomenon: (a) Exemplary model of driving mechanism forcing two neighbouring 'inactive' objects to vibrate; (b) Contact model descriptive for the duration of the impact between 'active' components. 86

Figure 3.9. Classification of sound phenomena in electric powered steering systems (EPS) .. 88

Figure 3.10. Domains and components of the EPSapa PL2 steering system. 93

Figure 3.11. Layers within gearbox and pinion/yoke domain of EPSapa PL2 steering system 93

Figure 3.12. Source-path-receiver model of the EPSapa PL2 steering system. 96

Figure 4.1. Block diagram of adaptive system modelling (a) and detailed structure of the adaptive filter (b) 103

Figure 4.2. Schematic of the steepest descent rule applied to the performance surface of a single-tap transversal filter with optimum value $\mathbf{h}_0$ 104

Figure 4.3. Block diagram for adaptive input reconstruction (Apostrophes indicate constrained conditions) 106

Figure 4.4. SISO system - force excited beam: Schematic of physical input identification problem (a), principle of cyclic iterative process achieved by consideration of additional constraints (b) and corresponding block diagram of adaptive input reconstruction algorithm (c). (Apostrophes indicate constrained conditions.) 109

Figure 4.5. Elementary numerical model to illustrate the iterative recursive process involved in the time domain inverse routine. Steps (a)-(d) are to be processed at each time step n_k while step (e) is to be performed after each full iteration cycle k. Diagram (e) illustrates the final solution after the last iteration cycle $k = 10$ was completed. 112

Figure 4.6. Simulation results for noise free underdamped second-order system: Original and reconstructed force time history in full length (a) and close up (d), desired and reconstructed acceleration time history (b), progression of relative mean prediction error (c). ── original signal, ---- reconstructed signal using $\eta = 0.1$ % as interruption criterion, ── reconstructed signal using $\eta = 0.001$ % 114

Figure 4.7. Simulation results for 3 different input force signatures (periodic - Simulation 1, constructed impulse sequence – Simulation 2, single transient –Simulation 3): Original and reconstructed force time history in full length (a) and close up (d), desired and reconstructed acceleration time history (b), progression of relative mean prediction error (c). ── original signal, ---- reconstructed signal using η = 0.1 % as interruption criterion, ── reconstructed signal using η = 0.001 % 116

Figure 4.8. Modelling approach to account for measurement noise in different data sets 121

Figure 4.9. Strategy invoked for identification of dynamic input forces using the time domain inverse method (TDM) and the standard frequency domain inverse method (FDM). Both methods rely on the same data sets. 123

Figure 4.10. Numerical result for noise free SISO system. Representation of signals in time domain (a, d, g, j), representation of signals in frequency domain (b, e, h,) and different estimation errors (c, f, i): ▬▬ true signal; ── reconstructed response using TDM; ─ ─ reconstructed force using TDM; ── identified force using FDM. 127

Figure 4.11. Numerical result for SISO system with 10% noise added to the acceleration response. Representation of signals in time domain (a, d, g, j), representation of signals in frequency domain (b, e, h,) and different estimation errors (c, f, i): ▬▬ true signal; ── reconstructed response using TDM; ─ ─ reconstructed force using TDM; ── identified force using FDM. 128

Figure 4.12. Numerical result for SISO system with 10% noise added to the impulse response function. Representation of signals in time domain (a, d, g, j), representation of signals in frequency domain (b, e, h,) and different estimation errors (c, f, i): ▬▬ true signal; ── reconstructed response using TDM; ─ ─ reconstructed force using TDM; ── identified force using FDM. 131

Table 4.2. Summary of all simulation results achieved with the novel time domain inversion routine and the standard frequency domain inverse method for force identification in single input single output (SISO) systems. 133

Figure 4.13. Principle of over-determination for structures with single degree of freedom excitation: Schematic of force excited beam (a) and corresponding block diagram for adaptive input reconstruction in single input multiple output (SIMO) systems. (Apostrophes indicate

constrained conditions; angle brackets denote the averaged error gradient used to update the estimated force at each time step.) 135

Table 4.3. Time domain inversion routine for identification of forces in single input multiple output systems. 137

Figure 4.14. Numerical result for noise free SIMO system. Representation of signals in time domain (a, d, g, j), representation of signals in frequency domain (b, e, h,) and different estimation errors (c, f, i): Quantities indicated by $\nabla\xi_m$ are obtained by the SISO recursion from Table 4.1 whereas $\langle\nabla\xi\rangle$ indicates that the SIMO recursion from Table 4.3 is used. 140

Table 4.4. Summary of simulation results achieved with the expanded time domain inversion routine and the standard frequency domain inverse method for the noise free SIMO system. 141

Figure 4.15. Comparison of the time domain inverse method (TDM) with the standard frequency domain inverse method (FDM) for the noise free SIMO system. Reconstructed force time history (left) and spectral estimation error in the identified force (right): ▬▬ true signal; ── reconstructed force using the SIMO TDM; ─ ─ identified force using the FDM. 142

Figure 4.16. Numerical result for SIMO system with 10% noise added to the acceleration responses. Representation of signals in time domain (a, d, g, j), representation of signals in frequency domain (b, e, h,) and different estimation errors (c, f, i): Quantities indicated by $\nabla\xi_m$ are obtained by the SISO recursion from Table 4.1 whereas $\langle\nabla\xi\rangle$ indicates that the SIMO recursion from Table 4.3 is used. 143

Figure 4.17. Evolution of the expanded relative mean prediction error (E-RMPE) as a function of noise added to all responses of the investigated SIMO system. The residual E-RMPE value after convergence is dependent on the noise level. 144

Figure 4.18. Comparison of the time domain inverse method (TDM) with the standard frequency domain inverse method (FDM) for SIMO system with 10% noise added to the responses. Reconstructed force time history (left) and spectral estimation error in the identified force (right): ▬▬ true signal; ── reconstructed force using the SIMO TDM; ─ ─ identified force using the FDM. 146

Figure 4.19. Numerical result for SIMO system with 10% noise added to impulse response functions. Representation of signals in time domain (a, d, g, j), representation of signals in

frequency domain (b, e, h,) and different estimation errors (c, f, i): Quantities indicated by $\nabla\xi_m$ are obtained by the SISO recursion from Table 4.1 whereas $\langle\nabla\xi\rangle$ indicates that the SIMO recursion from Table 4.3 is used. 147

Figure 4.20. Comparison of the time domain inverse method (TDM) with the standard frequency domain inverse method (FDM) for SIMO system with 10% noise added to system model. Reconstructed force time history (left) and spectral estimation error in the identified force (right): ▬▬ true signal; ── reconstructed force using the SIMO TDM; ─ ─ identified force using the FDM. 149

Table 4.5. Summary of simulation results achieved with the expanded time domain inversion routine and the standard frequency domain inverse method for SIMO system with 5 % defective data. 151

Table 4.6. Summary of simulation results achieved with the expanded time domain inversion routine and the standard frequency domain inverse method for SIMO system with 10 % defective data. 151

Table 4.7. Summary of simulation results achieved with the expanded time domain inversion routine and the standard frequency domain inverse method for SIMO system with 25 % defective response data. 151

Figure 4.21. Principle of the generalised time domain inversion routine for multiple input multiple output (MIMO) systems: Schematic of force excited beam (a) corresponding cascaded block diagram for adaptive input reconstruction consisting of *M* MISO systems (b) and detailed schematic of one MISO block (c). (Apostrophes indicate constrained conditions; angle brackets denote the averaged error gradient; $\mathbf{h}_{m:}(i)$ denotes the set of impulse response functions between all force input locations $s = [1, 2, \ldots, S]$ and a single response position m.) 154

Table 4.8. Time domain inversion routine for identification of forces in multiple input multiple output systems. 156

Figure 4.22. Housing of EPSapa PL2 steering gear with assumed sources (S_u) and response positions (P_m). 157

Table 4.9. Overview of the different MIMO systems. 158

Figure 4.23. Numerical results for noise free (2x9) MIMO system. Time signatures of structural responses (a) and reconstructed force signatures in full-length (b,d) and as close-up

(c,e); spectral estimation error in reconstructed responses (f) and identified forces (g): ▬▬ true signal; ── reconstructed signal using TDM. Relative mean prediction error (E-RMPE) as performance measure of the adaptive inversion routine (h). 159

Figure 4.24. Comparison of the generalised time domain inverse method (TDM) with the standard frequency domain inverse method (FDM) for the noise free (2x9) MIMO system. Time signatures of reconstructed forces (a,c) and spectral estimation error in the identified force (b,d): ▬▬ true signal; ── reconstructed force using the MIMO TDM; ─ ─ identified force using the FDM. 161

Table 4.10. Summary of simulation results achieved with the generalised time domain inversion routine and the standard frequency domain inverse method for all investigated noise free MIMO system. 161

Figure 4.25. Numerical results for (2x9) MIMO system with 10 % noise added to all acceleration responses. Time signatures of structural responses (a) and reconstructed force signatures in full-length (b,d) and as close-up (c,e); spectral estimation error in reconstructed responses (f) and identified forces (g): ▬▬ true signal; ── reconstructed signal using TDM. Relative mean prediction error (E-RMPE) as performance measure of the adaptive inversion routine (h). 162

Figure 4.26. Comparison of the generalised time domain inverse method (TDM) with the standard frequency domain inverse method (FDM) for the (2x9) MIMO system with 10 % noise added to all responses. Time signatures of reconstructed forces (a,c) and spectral estimation error in the identified force (b,d): ▬▬ true signal; ── reconstructed force using the MIMO TDM; ─ ─ identified force using the FDM. 164

Table 4.11. Summary of simulation results achieved with the generalised time domain inversion routine and the standard frequency domain inverse method for all MIMO systems with 10 % noise corrupted responses. 164

Figure 4.27. Influence of the degree of overdetermination on the estimation accuracy. Spectral estimation error $\Delta X(\omega)$ in the reconstructed force x_1 (a) and x_2 (b) obtained with the generalised TDM for the determined (2x2) and the overdetermined (2x4) and (2x9) MIMO system: ── with 10% noise added to all responses; ▪▪▪▪ without noise. 165

Figure 4.28. Numerical results for (2x9) MIMO system with 10 % errors added to all impulse response functions. Time signatures of structural responses (a) and reconstructed force

signatures in full-length (b,d) and as close-up (c,e); spectral estimation error in reconstructed responses (f) and identified forces (g): ▬▬ true signal; ── reconstructed signal using TDM. Relative mean prediction error (E-RMPE) as performance measure of the adaptive inversion routine (h). 166

Figure 4.29. Comparison of the generalised time domain inverse method (TDM) with the standard frequency domain inverse method (FDM) for the (2x9) MIMO system with 10 % errors added to all impulse response functions. Time signatures of reconstructed forces (a,c) and spectral estimation error in the identified force (b,d): ▬▬ true signal; ── reconstructed force using the MIMO TDM; ─ ─ identified force using the FDM. 167

Table 4.12. Summary of simulation results achieved with the generalised time domain inversion routine and the standard frequency domain inverse method for all MIMO systems with 10 % noise corrupted system model. 168

Figure 4.30. Influence of the degree of overdetermination on the estimation accuracy. Spectral estimation error in the reconstructed force x_1 (a) and x_2 (b) obtained with the standard FDM and corresponding errors (c) and (d) obtained with the generalised TDM for the determined (2x2) and the overdetermined (2x4) and (2x9) MIMO system: ── with 10% errors added to all impulse response functions (IRFs); ▪ ▪ ▪ without errors. 169

Figure 4.31. Sensitivity of the condition number to different degrees of over-determination (determined (2x2), double (2x4) and large over-determined (2x9) MIMO system) and different levels of disturbances (5%, 10% and 25%) included in the impulse response function measurements: ---- true system, ── noise corrupted system. 170

Table 4.13. Summary of simulation results achieved with the generalised time domain inversion routine and the standard frequency domain inverse method for the determined (2x2) and the overdetermined (2x4) and (2x9) MIMO system with 5 %, 10 % and 25 % noise added to all responses. 174

Table 4.14. Summary of simulation results achieved with the generalised time domain inversion routine and the standard frequency domain inverse method for the determined (2x2) and the overdetermined (2x4) and (2x9) MIMO system with 5 % and 10 % disturbances added to all impulse response functions. 174

Table 5.1. Assets and drawbacks of (i) vehicle and (ii) test bench measurements to provoke rattling inside (electric power) rack-and-pinion steering gears. 183

Figure 5.1. Functional principle and basic components of the standard test bench for evaluations of rattle noise originated inside steering gears due to external excitation provided by the roadway surface (EBR). 183

Figure 5.2. Information employed to detect transient events in measured acceleration time histories to evaluate rattle noise in electric power steering systems: ── acceleration measured on steering gear housing; ── sum of tie rod forces provided by the test bench. 185

Figure 5.3. Methodology involved in the calculation of eigenvalues for the proposes Eigenvalue Measure (EM): (a) Measured square mobility matrix; (b) symmetrisation using lower and upper triangular real part of the matrix and (c) partitioning of upper and lower symmetric matrices into (2x2) sub-matrices which are used to calculate two eigenvalues per sub-matrix. 198

Figure 5.4. Evaluation of accelerance measurements conducted in-situ for a steering system whilst mounted on the standard rattle test bench using (a) the Frequency Response Assurance Criterion, (b) the Phase Assurance Criterion and (c) the Conductance Assurance Criteria. Some elements of the accelerance matrix are modified to simulate (1) phase errors for a whole column as well as (2) random errors in driving-point and (3) the transfer accelerance measurements, respectively. 202

Figure 5.5. Employed data in the CAC analysis: Magnitude and phase response of the obtained mobility functions for the measured (a,c) and the simulated (b,d) FRF and corresponding eigenvalues and sign vectors of the real part of the lower (e,g) and the upper (f,h) (2x2) mobility sub-matrices. 203

Figure 5.6. Sample impulse response measured on the steering system whilst coupled to a receiver structure with corresponding truncation points (a) and squared impulse response (b) with dashed lines indicating decay slope and noise floor for evaluation of the truncation time. 206

Figure 5.7. Steering system connected to front axle carrier with sources (S_u) and response positions (P_m). 209

Figure 5.8. Simulation results for 4 different noise free SISO systems: Measured and reconstructed forces in full length (a) and close up (c), estimation error of reconstructed force spectrum (b) and approximated acceleration spectrum (d) for different points on the assembly. 212

Figure 5.9. Simulation results for SISO system considering point (P10): Estimation error of reconstructed force spectrum (a) and approximated acceleration spectrum (b) for noise free, 5 % and 10 % noise corrupted acceleration response. 213

Figure 5.10. Simulation results for over-determined (1x32) SIMO system: Measured and reconstructed forces in full length (a) and close up (c), estimation error of reconstructed force spectrum (b) and approximated acceleration spectrum (d) for noise free, 5 % and 10 % noise corrupted acceleration responses. 214

Figure 5.11. Effect of overdetermination (OD) on the force estimation accuracy for 10% noise corrupted response data. Original and reconstructed force signature in full length (a), close-up (b) and spectral estimation error (c): ── true force; ─ ─ reconstructed from overdetermined system; ▪▪▪▪▪ reconstructed from single response position (P10). 215

Figure 5.12. Experimental results for large (1x32) over-determined system: Measured (▬▬) and reconstructed (▬▬) force time history in full length (a) and close up (c), estimation error of reconstructed force spectrum (b) and approximated acceleration spectra (d) for all 32 response positions. 216

Figure 5.13. Numerical result for (4x9) over-determined MIMO system. Time signatures of structural responses (a) and in-situ blocked forces in full length (b)-(e) and as close-up (f)-(i): ▬▬ exact; ▬ ▬ ▬recovered from noisy responses. Spectral estimation error in identified forces (j) and reconstructed responses (k). Relative mean estimation error as performance measure of the adaptive inversion routine (l). 219

Figure 5.14. Experimental result for (3x9) over-determined MIMO system. Dynamic force signatures in full length (a,b,c) and close-up (d,e,f): measured ▬▬ ; recovered from structural responses ─ ─ ─. Spectral estimation error of identified forces (g) and reconstructed responses (h). 220

Figure 5.15. Relating transient events in the measured operational responses to the internal sources: Transient event caused by ─ ─ ─ source (S_1(z)); ─ ─ ─ source (S_2(z)) and ─ ─ ─ source (S_3(z2)). 222

Figure 5.16. Steering system mounted on the standard rattle test bench with known source (S_1), assumed internal sources (S_2 - S_6), external tie rod excitation (S_{tr1}) - (S_{tr1}) and response positions (P_m). 224

Figure 5.17. Experimental result using test bench rattle excitation: Time signatures of structural responses (a) and in-situ blocked forces in full length and as close-up for the known external force (d) and the 5 internal sources (e)-(i): ▬▬ exact; ▬▬ recovered from noisy responses. Spectral estimation error in the identified known forces (c) and the reconstructed responses (b). The red triangle indicate one external force impulse as magnified in the right diagrams. 226

Figure 5.18. Normalised blocked force energy signals of the external (d) and the 5 internal sources (e)-(i). Times at which a signal exceeds the defined threshold are denoted by coloured triangles. 228

Figure 5.19. Relation between zero-crossings of the sum of the tie rod forces and the reconstructed blocked force signatures..... 229

Figure 5.20. Simulation results for (3x9) MIMO system when tie rod forces are not considered in the inverse model. Exact and reconstructed internal source forces (a)-(c), additional unconsidered tie rod force (d) and (e), measured and reconstructed structural responses (f): ▬▬ exact signal; ── reconstructed signal..... 234

Figure 5.21. Spectral estimation error in the reconstructed accelerations for all 9 response positions when tie rod forces are not considered in the inverse model. 235

Figure 5.22. Simulation results for (3x9) MIMO system when measured responses are corrected (strategy 1). Exact and reconstructed internal source forces (a)-(c), applied tie rod force (d) and (e), measured and reconstructed structural responses (f): ▬▬ exact signal; ── reconstructed signal. 237

Figure 5.23. Simulation results for (5x9) MIMO system when all applied forces are considered in the inverse model (strategy 2). Exact and reconstructed internal source forces (a)-(c), applied tie rod force (d) and (e), measured and reconstructed structural responses (f): ▬▬ exact signal; ── reconstructed signal. 239

Figure 5.24. Normalised misalignment (a) and spectral estimation errors (b) for both external tie rod forces. 240

Figure A.3. Numerical result for SISO system with 5% noise added to the impulse response function. Representation of signals in time domain (a, d, g, j), representation of signals in frequency domain (b, e, h,) and different estimation errors (c, f, i): ▬▬ true signal; ──

reconstructed response using TDM; – – reconstructed force using TDM; —— identified force using FDM. 280

Figure A.4. Numerical result for SIMO system with 5% noise added to the acceleration responses. Representation of signals in time domain (a, d, g, j), representation of signals in frequency domain (b, e, h,) and different estimation errors (c, f, i): Quantities indicated by $\nabla\xi_m$ are obtained by the SISO recursion from Table 4.1 whereas $\langle\nabla\xi\rangle$ indicates that the SIMO recursion from Table 4.3 is used. 281

Figure A.5. Comparison of the time domain inverse method (TDM) with the standard frequency domain inverse method (FDM) for SIMO system with 5% noise added to the responses. Reconstructed force time history (left) and spectral estimation error in the identified force (right): ▬▬ true signal; —— reconstructed force using the SIMO TDM; – – identified force using the FDM. 281

Figure A.6. Numerical result for SIMO system with 25% noise added to the acceleration responses. Representation of signals in time domain (a, d, g, j), representation of signals in frequency domain (b, e, h,) and different estimation errors (c, f, i): Quantities indicated by $\nabla\xi_m$ are obtained by the SISO recursion from Table 4.1 whereas $\langle\nabla\xi\rangle$ indicates that the SIMO recursion from Table 4.3 is used. 282

Figure A.7. Comparison of the time domain inverse method (TDM) with the standard frequency domain inverse method (FDM) for SIMO system with 25% noise added to the responses. Reconstructed force time history (left) and spectral estimation error in the identified force (right): ▬▬ true signal; —— reconstructed force using the SIMO TDM; – – identified force using the FDM. 282

FigureA.8. Numerical result for SIMO system with 5% noise added impulse response functions. Representation of signals in time domain (a, d, g, j), representation of signals in frequency domain (b, e, h,) and different estimation errors (c, f, i): Quantities indicated by $\nabla\xi_m$ are obtained by the SISO recursion from Table 4.1 whereas $\langle\nabla\xi\rangle$ indicates that the SIMO recursion from Table 4.3 is used. 283

Figure A.9. Comparison of the time domain inverse method (TDM) with the standard frequency domain inverse method (FDM) for SIMO system with 5% noise added to system model. Reconstructed force time history (left) and spectral estimation error in the identified

force (right): ▬▬ true signal; ── reconstructed force using the SIMO TDM; ─ ─ identified force using the FDM. 283

Figure A.10. Numerical results for noise free (2x2) MIMO system. Time signatures of structural responses (a) and reconstructed force signatures in full-length (b,d) and as close-up (c,e); spectral estimation error in reconstructed responses (f) and identified forces (g): ▬▬ true signal; ── reconstructed signal using TDM. Relative mean prediction error (E-RMPE) as performance measure of the adaptive inversion routine (h). 284

Figure A.11. Comparison of the generalised time domain inverse method (TDM) with the standard frequency domain inverse method (FDM) for the noise free (2x2) MIMO system. Time signatures of reconstructed forces (a,c) and spectral estimation error in the identified force (b,d): ▬▬ true signal; ── reconstructed force using the MIMO TDM; ─ ─ identified force using the FDM. 284

Figure A.12. Numerical results for noise free (2x4) MIMO system. Time signatures of structural responses (a) and reconstructed force signatures in full-length (b,d) and as close-up (c,e); spectral estimation error in reconstructed responses (f) and identified forces (g): ▬▬ true signal; ── reconstructed signal using TDM. Relative mean prediction error (E-RMPE) as performance measure of the adaptive inversion routine (h). 285

Figure A.13. Comparison of the generalised time domain inverse method (TDM) with the standard frequency domain inverse method (FDM) for the noise free (2x4) MIMO system. Time signatures of reconstructed forces (a,c) and spectral estimation error in the identified force (b,d): ▬▬ true signal; ── reconstructed force using the MIMO TDM; ─ ─ identified force using the FDM. 285

Figure A.14. Numerical results for (2x2) MIMO system with 5 % noise added to all acceleration responses. Time signatures of structural responses (a) and reconstructed force signatures in full-length (b,d) and as close-up (c,e); spectral estimation error in reconstructed responses (f) and identified forces (g): ▬▬ true signal; ── reconstructed signal using TDM. Relative mean prediction error (E-RMPE) as performance measure of the adaptive inversion routine (h). 286

Figure A.15. Comparison of the generalised time domain inverse method (TDM) with the standard frequency domain inverse method (FDM) for the (2x2) MIMO system with 5 % noise added to all responses. Time signatures of reconstructed forces (a,c) and spectral

estimation error in the identified force (b,d): ▬▬ true signal; ── reconstructed force using the MIMO TDM; ─ ─ identified force using the FDM.....286

Figure A.16. Numerical results for (2x2) MIMO system with 10 % noise added to all acceleration responses. Time signatures of structural responses (a) and reconstructed force signatures in full-length (b,d) and as close-up (c,e); spectral estimation error in reconstructed responses (f) and identified forces (g): ▬▬ true signal; ── reconstructed signal using TDM. Relative mean prediction error (E-RMPE) as performance measure of the adaptive inversion routine (h). 287

Figure A.17. Comparison of the generalised time domain inverse method (TDM) with the standard frequency domain inverse method (FDM) for the (2x2) MIMO system with 10 % noise added to all responses. Time signatures of reconstructed forces (a,c) and spectral estimation error in the identified force (b,d): ▬▬ true signal; ── reconstructed force using the MIMO TDM; ─ ─ identified force using the FDM.....287

Figure A.18. Numerical results for (2x2) MIMO system with 25 % noise added to all acceleration responses. Time signatures of structural responses (a) and reconstructed force signatures in full-length (b,d) and as close-up (c,e); spectral estimation error in reconstructed responses (f) and identified forces (g): ▬▬ true signal; ── reconstructed signal using TDM. Relative mean prediction error (E-RMPE) as performance measure of the adaptive inversion routine (h). 288

Figure A.19. Comparison of the generalised time domain inverse method (TDM) with the standard frequency domain inverse method (FDM) for the (2x2) MIMO system with 25 % noise added to all responses. Time signatures of reconstructed forces (a,c) and spectral estimation error in the identified force (b,d): ▬▬ true signal; ── reconstructed force using the MIMO TDM; ─ ─ identified force using the FDM.....288

Figure A.20. Numerical results for (2x4) MIMO system with 5 % noise added to all acceleration responses. Time signatures of structural responses (a) and reconstructed force signatures in full-length (b,d) and as close-up (c,e); spectral estimation error in reconstructed responses (f) and identified forces (g): ▬▬ true signal; ── reconstructed signal using TDM. Relative mean prediction error (E-RMPE) as performance measure of the adaptive inversion routine (h). 289

Figure A.21. Comparison of the generalised time domain inverse method (TDM) with the standard frequency domain inverse method (FDM) for the (2x4) MIMO system with 5 %

noise added to all responses. Time signatures of reconstructed forces (a,c) and spectral estimation error in the identified force (b,d): ▬▬ true signal; ── reconstructed force using the MIMO TDM; ─ ─ identified force using the FDM.....289

Figure A.22. Numerical results for (2x4) MIMO system with 10 % noise added to all acceleration responses. Time signatures of structural responses (a) and reconstructed force signatures in full-length (b,d) and as close-up (c,e); spectral estimation error in reconstructed responses (f) and identified forces (g): ▬▬ true signal; ── reconstructed signal using TDM. Relative mean prediction error (E-RMPE) as performance measure of the adaptive inversion routine (h). 290

Figure A.23. Comparison of the generalised time domain inverse method (TDM) with the standard frequency domain inverse method (FDM) for the (2x4) MIMO system with 10 % noise added to all responses. Time signatures of reconstructed forces (a,c) and spectral estimation error in the identified force (b,d): ▬▬ true signal; ── reconstructed force using the MIMO TDM; ─ ─ identified force using the FDM.....290

Figure A24. Numerical results for (2x4) MIMO system with 25 % noise added to all acceleration responses. Time signatures of structural responses (a) and reconstructed force signatures in full-length (b,d) and as close-up (c,e); spectral estimation error in reconstructed responses (f) and identified forces (g): ▬▬ true signal; ── reconstructed signal using TDM. Relative mean prediction error (E-RMPE) as performance measure of the adaptive inversion routine (h). 291

Figure A.25. Comparison of the generalised time domain inverse method (TDM) with the standard frequency domain inverse method (FDM) for the (2x4) MIMO system with 25 % noise added to all responses. Time signatures of reconstructed forces (a,c) and spectral estimation error in the identified force (b,d): ▬▬ true signal; ── reconstructed force using the MIMO TDM; ─ ─ identified force using the FDM.....291

Figure A.26. Numerical results for (2x9) MIMO system with 5 % noise added to all acceleration responses. Time signatures of structural responses (a) and reconstructed force signatures in full-length (b,d) and as close-up (c,e); spectral estimation error in reconstructed responses (f) and identified forces (g): ▬▬ true signal; ── reconstructed signal using TDM. Relative mean prediction error (E-RMPE) as performance measure of the adaptive inversion routine (h). 292

Figure A.27. Comparison of the generalised time domain inverse method (TDM) with the standard frequency domain inverse method (FDM) for the (2x9) MIMO system with 5 % noise added to all responses. Time signatures of reconstructed forces (a,c) and spectral estimation error in the identified force (b,d): ▬▬ true signal; ── reconstructed force using the MIMO TDM; ─ ─ identified force using the FDM. 292

Figure A.28. Numerical results for (2x9) MIMO system with 25 % noise added to all acceleration responses. Time signatures of structural responses (a) and reconstructed force signatures in full-length (b,d) and as close-up (c,e); spectral estimation error in reconstructed responses (f) and identified forces (g): ▬▬ true signal; ── reconstructed signal using TDM. Relative mean prediction error (E-RMPE) as performance measure of the adaptive inversion routine (h). 293

Figure A.29. Comparison of the generalised time domain inverse method (TDM) with the standard frequency domain inverse method (FDM) for the (2x9) MIMO system with 25 % noise added to all responses. Time signatures of reconstructed forces (a,c) and spectral estimation error in the identified force (b,d): ▬▬ true signal; ── reconstructed force using the MIMO TDM; ─ ─ identified force using the FDM. 293

Figure A.30. Numerical results for (2x2) MIMO system with 5 % errors added to all impulse response functions. Time signatures of structural responses (a) and reconstructed force signatures in full-length (b,d) and as close-up (c,e); spectral estimation error in reconstructed responses (f) and identified forces (g): ▬▬ true signal; ── reconstructed signal using TDM. Relative mean prediction error (E-RMPE) as performance measure of the adaptive inversion routine (h). 294

Figure A.31. Comparison of the generalised time domain inverse method (TDM) with the standard frequency domain inverse method (FDM) for the (2x2) MIMO system with 5 % errors added to all impulse response functions. Time signatures of reconstructed forces (a,c) and spectral estimation error in the identified force (b,d): ▬▬ true signal; ── reconstructed force using the MIMO TDM; ─ ─ identified force using the FDM. 294

Figure A.32. Numerical results for (2x2) MIMO system with 10 % errors added to all impulse response functions. Time signatures of structural responses (a) and reconstructed force signatures in full-length (b,d) and as close-up (c,e); spectral estimation error in reconstructed responses (f) and identified forces (g): ▬▬ true signal; ── reconstructed signal using TDM.

Relative mean prediction error (E-RMPE) as performance measure of the adaptive inversion routine (h). 295

Figure A.33. Comparison of the generalised time domain inverse method (TDM) with the standard frequency domain inverse method (FDM) for the (2x2) MIMO system with 10 % errors added to all impulse response functions. Time signatures of reconstructed forces (a,c) and spectral estimation error in the identified force (b,d): ▬▬ true signal; ── reconstructed force using the MIMO TDM; ─ ─ identified force using the FDM. 295

Figure A.34. Numerical results for (2x4) MIMO system with 5 % errors added to all impulse response functions. Time signatures of structural responses (a) and reconstructed force signatures in full-length (b,d) and as close-up (c,e); spectral estimation error in reconstructed responses (f) and identified forces (g): ▬▬ true signal; ── reconstructed signal using TDM. Relative mean prediction error (E-RMPE) as performance measure of the adaptive inversion routine (h). 296

Figure A.35. Comparison of the generalised time domain inverse method (TDM) with the standard frequency domain inverse method (FDM) for the (2x4) MIMO system with 5 % errors added to all impulse response functions. Time signatures of reconstructed forces (a,c) and spectral estimation error in the identified force (b,d): ▬▬ true signal; ── reconstructed force using the MIMO TDM; ─ ─ identified force using the FDM. 296

Figure A.36. Numerical results for (2x4) MIMO system with 10 % errors added to all impulse response functions. Time signatures of structural responses (a) and reconstructed force signatures in full-length (b,d) and as close-up (c,e); spectral estimation error in reconstructed responses (f) and identified forces (g): ▬▬ true signal; ── reconstructed signal using TDM. Relative mean prediction error (E-RMPE) as performance measure of the adaptive inversion routine (h). 297

Figure A.37. Comparison of the generalised time domain inverse method (TDM) with the standard frequency domain inverse method (FDM) for the (2x4) MIMO system with 10 % errors added to all impulse response functions. Time signatures of reconstructed forces (a,c) and spectral estimation error in the identified force (b,d): ▬▬ true signal; ── reconstructed force using the MIMO TDM; ─ ─ identified force using the FDM. 297

Figure A.38. Numerical results for (2x9) MIMO system with 5 % errors added to all impulse response functions. Time signatures of structural responses (a) and reconstructed force signatures in full-length (b,d) and as close-up (c,e); spectral estimation error in reconstructed

responses (f) and identified forces (g): ▬▬ true signal; ── reconstructed signal using TDM. Relative mean prediction error (E-RMPE) as performance measure of the adaptive inversion routine (h). 298

Figure A.39. Comparison of the generalised time domain inverse method (TDM) with the standard frequency domain inverse method (FDM) for the (2x9) MIMO system with 5 % errors added to all impulse response functions. Time signatures of reconstructed forces (a,c) and spectral estimation error in the identified force (b,d): ▬▬ true signal; ── reconstructed force using the MIMO TDM; ─ ─ identified force using the FDM. 298

Acknowledgements

Primarily, Andy Moorhouse, Francis Li, Thomas Alber and Gerd Speidel must be acknowledged as their novel ideas were fundamental to the work. Credit is also due to all at the Acoustics Research Centre of the University of Salford and those at ZF Lenksysteme GmbH where I have carried out my studies.

The research was funded by industry through ZF Lenksysteme GmbH. This support is also gratefully acknowledged.

On a more personal note I would first like to thank Andy Moorhouse for his continual input and support. I feel very fortunate to have had such a committed and inspiring supervisor. I would also like to thank all my colleagues at the Acoustics Research Centre of the University of Salford for their generous help and support.

Finally I would like to thank my parents, Heidemarie and Winfried Sturm, my beloved brother, Tobias Sturm, and my friends for their help and encouragement throughout, but most of all I would like to thank my fiancée Chia-Chun Lai who constantly encourages me whilst writing the thesis.

Nomenclature

List of operators

a	Scalar
$\mathbf{a}$	Vector
$\mathbf{a}_{m:}$	Set of vectors between m-th response and all excitation locations
$\mathbf{A}$	Matrix
$\dot{x}$	Integration in time domain
x'	Constrained quantity
$[\cdot]^T$	Transpose of vector or matrix
$[\cdot]^+$	Moor-Penrose pseudo-inverse (e.g. $\mathbf{H}^+ = [\mathbf{H}^T\mathbf{H}]^{-1}\mathbf{H}^T$)
$[\cdot]^{-1}$	Inverse of square matrix
$[\cdot]^\#$	Regularised Moor-Penrose pseudo-inverse
$\hat{\cdot}$	Estimated value
$\tilde{\cdot}$	Noise corrupted value
$\langle\cdot\rangle$	Averaged error gradient
cond(·)	Condition number
sgn(·)	Signum function extracting sign of quantity
$\nabla[\cdot]$	Gradient of a quantity
$\partial[\cdot]$	Partial derivative of a quantity
$E[\cdot]$	Statistical expectation operator
$\mathcal{F}\{\cdot\}$	Fourier transform
$\mathcal{F}^{-1}\{\cdot\}$	Inverse Fourier transform
$\Re e\{\cdot\}$	Real part of complex quantity
$\Im m\{\cdot\}$	Imaginary part of complex quantity
j	Complex variable ($j = \sqrt{-1}$)

List of symbols

$a(n)$	Acceleration response in (discrete) time domain [ms^{-2}]
$A_{ik}(\omega)$	Accelerance function (excitation at *k*; response at *i*) [$mN^{-1}s^{-2}$]
ACF	Assembly Conductivity Function [response/unit excitation]
$B(\omega)$	Susceptance (imaginary part of mobility) [$mN^{-1}s^{-1}$]
CSS	Component Source Strength [response/unit excitation]
$CV(Y_{ii})$	Conductance value
$e(n)$	Estimation error in (discrete) time domain for SISO system [ms^{-2}]
$e_m(n)$	Individual estimation error for SIMO and MIMO system [ms^{-2}]
$EM(\lambda)$	Eigenvalue measure
$d_m(n)$	Desired m-th response in (discrete) time domain [ms^{-2}]
$d_{op,m}(n)$	Measured operational desired m-th response [ms^{-2}]
$d_{rattle,m}(n)$	Fraction of measured desired m-th response caused by rattling [ms^{-2}]
$f_{bl}(\omega)$	Blocked force at source interface [N]
$f_C(\omega)$	Operational contact force at source/receiver interface [N]
$f_S(\omega)$	Force applied external to the source interface [N]
F	Force [N]
F_K	Kinetic frictional resistance [N]
F_N	Normal force [N]
F_S	Static frictional resistance [N]
F_T	Tension force of spring [N]
$h_{mk}(n)$	Impulse response function (response at *m*; excitation at *k*) [$mN^{-1}s^{-2}$]
$H(\omega)$	Frequency response function [response/unit excitation]
$H(s)$	Transfer function in Laplace domain
H_1	Noise-on-output estimator
H_2	Noise-on-input estimator
H_{IMP}	Inverse structure Markov parameter
H_{MP}	Markov parameter

I	Length of finite impulse response
k	Integer counting number of iteration cycles
l	Logical integer
m	Mass [kg]
n	Discrete time step [s]
N	Length of input vector
N_g	Length of vector g
N_{rel}	Length of reliable part of a vector
NP	Specified noise level [%]
p	Sound pressure [Pa]
s	(Force) source signal within the steering system [N]
$S_{aa}(\omega)$	Auto power spectrum of response signal *a*
$S_{af}(\omega)$	Cross power spectrum (response at *a*; excitation at *f*)
$S_{ff}(\omega)$	Auto power spectrum of excitation signal *f*
Δt^{-1}	Sampling frequency [Hz]
u_i	Component of i-th left singular vector
v	Velocity [ms^{-1}]
$v_{C,bo}(\omega)$	Operational velocity measured in-situ on coupled structure C [ms^{-1}]
v_i	Component of i-th right singular vector
$v_S(\omega)$	Operational velocity at source interface [ms^{-1}]
$v_{Sf}(\omega)$	Free velocity [ms^{-1}]
$x(n)$	(Blocked) force in (discrete) time domain [N]
$x_{ex}(n)$	External (blocked) tie rod force signal [N]
$x_{int}(n)$	Internal (blocked) force source signal [N]
$x_{FD}(n)$	Force in (discrete) time domain obtained by FDM [N]
$x_{TD}(n)$	Force in (discrete) time domain obtained by TDM [N]
$X(\omega)$	(Blocked) force in frequency domain [N]
$\Delta X(\omega)$	Spectral estimation error in reconstructed input [dB(N)]
$y_m(n)$	(Reconstructed) m-th response in (discrete) time domain [ms^{-2}]
$y_{FD}(n)$	Response in (discrete) time domain obtained by FDM [ms^{-2}]

$y_{TD}(n)$	Response in (discrete) time domain obtained by TDM [ms^{-2}]
$Y(\omega)$	Response in frequency domain [ms^{-2}]
$Y_{B,bc}(\omega)$	Receiver mobility (excitation at *c*; response at *b*) [$mN^{-1}s^{-1}$]
$Y_{C,bc}(\omega)$	Generalised transfer mobility of coupled structure [$mN^{-1}s^{-1}$]
$Y_{ik}(\omega)$	Mobility function (excitation at *k*; response at *i*) [$mN^{-1}s^{-1}$]
$Y_S(\omega)$	Source mobility [$mN^{-1}s^{-1}$]
$\Delta Y(\omega)$	Spectral estimation error in reconstructed output [$dB(ms^{-2})$]
α	Kinetic variable (excitation)
α_{reg}	Regularisation parameter
β	Kinematic variable (response)
$\varepsilon_d(n)$	Unknown (blocked) force disturbance [N]
$\varepsilon_{x,\%RMS}$	Root mean square (RMS) estimation error of input $x(n)$ [%]
$\varepsilon_{y,\%RMS}$	Root mean square (RMS) estimation error of output $y(n)$ [%]
φ_i	Filter factor
Φ	Modal matrix
$\gamma^2_{af}(\omega)$	Ordinary coherence function (response at *a*; excitation at *f*)
$\eta(k)$	Relative mean prediction error (SISO system) [%]
$\eta_m(k)$	Expanded relative mean prediction error (SIMO, MIMO system) [%]
$\hat{\eta}$	Modal response (vector)
$\kappa(\omega)$	Condition number
$\lambda(\omega)$	Eigenvalue at specific frequency ω
μ	Step-size parameter (SISO and SIMO system)
μ_s	Step-size parameter for s-th force input (MIMO system)
$\nu_r(k)$	Normalised misalignment of r-th external tie rod force [dB(N)]
ω	Radian frequency [rad^{-1}]
σ_i	i-th singular value
ρ_{xy}	Correlation coefficient
$\xi(n)$	Mean square prediction error / performance surface [$(ms^{-2})^2$]
Ψ	Mode shape (matrix)

List of abbreviations

AB	Airborne Sound
ABS	Antilock braking system
ACF	Assembly Conductivity Function
AWIE	Adaptive weighting input estimation algorithm
BNA	Ball nut assembly
CAC	Conductance assurance criteria
CGM	Conjugate gradient mathod
CSS	Component Source Strength
DFT	Discrete Fourier transform
DMISF	Delayed, multi-step inverse structural filter
DOF	Degree of freedom
EBO	Excitation provided by the operator
EBR	Excitation provided by the roadway surface
ECU	Electronic control unit
EPS	Electric Power Steering
EPS	Electric power steering system
EPS	Electronic stability program
EPSapa	EPS with paraxial servo unit
EPSc	EPS with servo unit mounted on steering column
EPSdp	EPS with servo unit mounted on second pinion
ERA	Eigensystem realisation algorithm
E-RMPE	Expanded relative mean prediction error
FB	Fluid-borne Sound
FD	Frequency domain
FDM	Frequency domain inverse method
FEM	Finite element method
FIR	Finite impulse response function

FRAC	Frequency response assurance criterion
FRF	Frequency response function
GCV	Generalised cross validation
HPS	Hydraulic power steering system
IDFT	Inverse discrete Fourier transform
IRF	Impulse response function
ISF	Inverse structural filter
KF	Simple Kalman filter
LMS	Least mean square algorithm
LTI	Linear and time invariant system
MIMO	Multiple input multiple output system
NVH	Noise Vibration Harshness
OCV	Ordinary cross validation
PAC	Phase assurance criterion
PF	Perception of a fault
PY	Pinion – Yoke (interface)
RLSE	Recursive least-square estimator
RMPE	Relative mean prediction error
RMS	Root mean square
SB	Structure-borne Sound
SIMO	Single input multiple output system
SISO	Single input single output system
SNR	Signal-to-noise ratio
StSys	Steering system
SWAT	Sum of weighted acceleration technique
SWAT-CAL	SWAT using calibrated force input
SWAT-Max-Flat	SWAT using FRF data
SWAT-TEEM	SWAT using time eliminated elastic modes
TD	Time domain
TDM	Time domain inverse method

TPA	Transfer paths analysis
VAP	Virtual Acoustic Prototype
VB	Vehicle body including air space inside the cabin
ZFLS	ZF Lenksysteme GmbH

Abstract

During driving on rough roads, rattle noise may emanate from (electric power) rack-and-pinion steering gears as a result of reverse feedback from the road. This project is in collaboration with a German steering system manufacturer and aims to develop a methodology facilitating identification and quantification of transient structure-borne sound sources within electrical steering systems. To achieve this aim, a conceptual source-path-receiver model has been developed that discloses the theoretical locations and associated mechanisms of all possible transient sound sources inside the steering gear. This information forms the basis for a subsequent measurement step which is required to experimentally quantify the strength of each individual source. The measurement approach is based on a time domain equivalent of the in-situ blocked force method; thus facilitating independent source characterisation on the fully assembled structure. The time domain (TD) approach relies on a robust inversion routine that uses an adaptive algorithm to simultaneously reconstruct multi-channel (blocked) force signatures from operational responses and the corresponding impulse response functions both measured (in-situ) on the (assembled) structure. The TD inversion routine is derived from the least mean square (LMS) algorithm which is widely used in adaptive filter design. The accuracy and sensitivity of the TD inversion routine is elaborated and compared to the standard frequency domain inverse method using simple numerical examples. Its general applicability for sophisticated technical structures is evaluated by example of an electric powered steering system being subjected to artificial excitation. The use of the TD approach for characterisation of transient structure-borne sound sources based on the blocked force method is discussed and different procedures to improve the force estimation accuracy are proposed. These procedures can be classified into methods that (i) help to evaluate the quality of pre-measured frequency response functions (FRFs) which are required to set up the (inverse) system model, (ii) measurement routines that may help to improve future FRF measurements conducted in-situ, i.e. whilst the steering gear is connected to a special rattling test bench, (iii) correction strategies to separate contributions from known (external) structure-borne sound sources different from the desired (internal) rattling sources and (iv) criteria that in theory allow for monitoring the performance of the iterative TD inversion routine precisely. Finally, the developed methodology is used to identify and quantify rattle sources within a steering system under realistic testing conditions.

Chapter 1

Introduction

1.1. Background

Today's car manufacturers have to establish brand identities around customer expectations which are not purely based on functional or pragmatic considerations but rather depend on impressions and emotions. Vehicle acoustics and vibration comfort make significant contribution towards these subjective quality aspects and have increasingly become important sales arguments in international automotive industries. Intensive research and development effort has been directed to all kind of sound engineering and Noise, Vibration and Harshness (NVH) issues in order to design vehicles being consistent with the steadily increasing quality and comfort awareness of the customers. However, spanning the physical as well as the psychological domain, engineering NVH quality is a challenging and often iterative process.

Since the late 1990s, a rigorous reduction of engine, tyre-road and aerodynamic induced noise has been achieved [1]. Though, this improvement has also given rise to lower masking of previously less prominent air-, fluid- and structure-borne sound sources, such as ancillary units like fans, compressors or pumps for instance [2]. Their contributions to the overall interior vehicle sound and vibrations have in turn gained significance with respect to subjective assessment of the quality and comfort of vehicles. In the face of future hybrid and electric powered vehicles, where the interior noise levels caused by the power-train will most likely drop further, significant efforts have to be directed to assuring high NVH standards for all automotive components.

In vehicles, steering systems play a fundamental role since they give distinction to the passenger's overall driving experience and hence are strongly involved in subjective quality assessments. Furthermore, steering systems need to achieve high power density, i.e. high performance combined with lightweight design requiring little space, which, in some respects, is contradictory to low-noise NVH targets [2],[3]. To make things worse, secondary actions to reduce vibro-acoustic transmission from the steering system into the adjacent vehicle structure, e.g. by installing isolators at the fastening points or decoupling of steering gear and steering column, are not necessarily possible due to safety, handling and vehicle dynamic specifications. Considering these arguments, it is obvious that NVH design and optimisation is of particular interest for the development process of steering systems; likewise it poses significant challenges to the engineers responsible.

ZF Lenksysteme GmbH (ZFLS) is one of the major manufacturers of steering systems which enjoys worldwide recognition. In order to cope with the continuous social and technological changes, ZFLS has a policy of developing innovative high quality products in every respect. For this reason, intensive research is done in various fields of engineering.

Regarding NVH, a major part of the research is driven by the necessity of providing the engineers with appropriate tools for assessing, controlling and designing NVH behaviour in early development stages. Ideally, these tools should consider both, objective and subjective factors in order to account for the complete 'cause-effect-chain' involved in the development process. Here, 'causes' are thought of as physical parameters which are accessible as measureable (objective) quantities to the engineer, whereas 'effects' reflect the customer's (subjective) degree of satisfaction with respect to individual NVH demands. Grasping these psychological aspects from an engineering point of view is already sophisticated. This, however, becomes even more challenging with respect to engineering NVH quality for steering systems since the acoustical targets need to match the expectations of passengers inside the compartment. Especially at early development stages component suppliers like ZFLS do not have access to vehicles with representative vibro-acoustic characteristics since these may only exist as laboratory prototypes or even as numerical models.

Nevertheless, in the course of developing steering systems it is of great interest whether a structural modification will affect the NVH behaviour inside the cabin. The method of 'virtual acoustic prototyping' [4],[5],[6] offers powerful tools capable of answering these and many other NVH related questions. For this reason, a Virtual Acoustic Prototype (VAP) for electric power steering systems (EPS) was recently developed in the scope of an earlier PhD project at ZFLS [7]. This VAP constitutes a computer representation of a steering system installed in a passenger car that allows prediction and auralisation of the steering induced sound inside the compartment. Although the applicability of the VAP has successfully been tested for different types of electrical steering systems, using specific steering manoeuvres [8], its general use is limited to cases where the steering system is considered as one entire vibro-acoustic source in the vehicle. Certainly, treating the steering system as a collective of all inherent sub-sources yields important information about its overall vibro-acoustic behaviour. However, in many situations designers and engineers strive towards higher levels of detail. Identification, quantification (characterisation) and rank ordering of the underlying source and transmission mechanisms is often thought of as the bases for effective NVH design [1]. Having this information on hand, designers and engineers are able to decide whether specific sub-sources

and transmission paths respectively have to be optimised in order to reach distinct NVH targets.

One recent field of research at ZFLS in which this level of sophistication is essential deals with the occurrence of ‘transient sounds’ in electrical steering system and its perceptibility by passengers inside the car. The aim is to identify the transient sound sources within the steering system and to develop robust methods to quantify the initiating dynamic excitation forces acting inside the steering system. Based on the knowledge of the internal excitations more detailed VAPs of electrical steering systems could be achieved which has been the motivation for ZFLS to set up the research project presented in this thesis.

Before elaborating the exact motives and related objectives of the thesis (section 1.6) the idea of Virtual Acoustic Prototyping (section 1.2) , some fundamental thoughts on the generation and the assessment of steering induced sound in vehicles (section 1.3), as well as a more exact statement of the physical problem (section 1.4) and how it can be best addressed (section 1.5) will briefly be reviewed.

1.2. The general approach of Virtual acoustic Prototyping

For the purpose of this thesis, a ‘Virtual Acoustic Prototype’ (VAP) will be considered pursuant to the definition given by Moorhouse in [6]. Accordingly, a Virtual Acoustic Prototype (VAP) is “...a computer representation of a machine, e.g. a washing machine, fridge, lawnmower etc., such that its sound can be heard without it necessarily having to exist as a physical machine”. Explained in a more comprehensive way, a VAP constitutes a numerical tool to synthesis and auralise the sound of a virtually assembled machine which is constructed from elementary vibro-acoustic sources and transmitting elements that best represent the generating mechanisms inside the real machine. The latter explanation is preferred at this stage since it discloses one of the most basic principles of virtual acoustic prototyping, namely: sub-structuring an assembled machine into its most basic vibro-acoustic ‘active’ and ‘passive’ components.

Active components are those that initially generate acoustic disturbances, e.g. electric motors, compressors etc., while all remaining parts of the machine that transmit or radiate excitations from the active components, such as housings or air spaces, are considered as being ‘passive’ [4]. Each individual source is characterised by a ‘Component Source Strength’ (CSS) accounting for the elementary vibro-acoustic generating mechanism taking place within the

machine while transmission and radiation processes of the passive structure are characterised by 'Assembly Conductivity Functions' (ACF), using narrow band frequency domain metric in each case.

In order to allow for 'virtually' combining and exchanging active and passive components in a non-reactive way, an essential requirement of the VAP is that sources can be characterised independently of the remaining passive structure and vice versa [6]. Accordingly, the CSS must constitute an intrinsic property of the source itself [5].

Hypothetically, all data could be obtained from either measurements or numerical calculations. Yet, it is stressed that auralisation requires adequate description of all internal source mechanisms as well as the sound transmission and radiation processes over the entire audible frequency range. For sophisticated technical configurations, e.g. a steering system assembled in a vehicle, these demands make it impracticable to obtain reliable VAPs purely by employing numerical methods. Especially source modelling is still insufficiently developed to handle most active components [6]. Consequently, the source strengths (CSS) generally have to be measured. By contrast, experimental characterisation of the active sources is particularly difficult since meaningful measurements can only be obtained whilst the source is operated under realistic load and mounting conditions. However, applying advanced measurement techniques, as mentioned in [5] or more recent developed methods such as [9], have proved sufficient to yield reliable VAPs even for sophisticated industrial applications, as discussed in [4]-[6] and [10] respectively. In the framework of this study it is assumed that characteristic data for both, active and passive, components can only be obtained from experimental measurements.

Having determined all essential characteristics, the active and passive data sets can be combined in order to synthesise the noise output of the virtually assembled machine. The sum of all M excitations (CSS) weighted by the appropriate transfer functions (ACF) yield the total output of the machine (usually sound pressure p) at a defined external receiver point, R, and a given frequency, ω, [4]

$$p_R(\omega) = \sum_{m=1}^{M} CSS_{Rm}(\omega)\, ACF_{Rm}(\omega)\,. \tag{1.1}$$

Note, equation (1.1) is written in the most general form and does not specifically distinguish whether an active component comprises airborne (AB), fluid- (FB) or structure-borne (SB) excitations. In general, each elementary vibro-acoustic mechanism requires a separate CSS

and the appropriate ACF. Furthermore, the terms may be based on different physical quantities accounting for AB, FB or SB excitations.

The synthesised spectrum of the noise output, in the following considered to be sound pressure, is only an intermediate result. To satisfy the postulated audibility requirement of the VAP, the spectrum has to be converted into a perceived sound by auralisation [4]. Various problems to achieve audible sound of sufficient length for an operating machine have to be overcome. Different solutions to this issue can be found in literature, see amongst others [6],[7],[8] and a brief discussion on general drawbacks of the frequency domain VAP approach is given in section 1.5.

Regardless which method is used for conversion, the outcome of the VAP is always an auralisation of the sound pressure at discrete spatial points in the virtual environment. The auralised sound provides a more or less accurate impression of how the assembled machine would sound if it were operated under the same conditions in reality. In [6], Moorhouse refers to this substantial feature of a VAP as ‘listening to machines that don’t exist’.

To sum up, the following steps are essential to build a VAP:

- Sub-structuring of the complete machine into active and passive components.
- Independent characterisation of all active sources using measurement techniques that allow quantifying the source strengths, while the respective sources are operated under real conditions.
- Independent characterisation of the remaining passive structure using measurement techniques that account for all transmission, propagation and radiation processes.
- Virtually assembling active and passive data sets in order to achieve spectral and temporal signals that can be (objectively and subjectively) analysed and heard by experts and non-experts respectively.

Note, the first three steps are of particular interest for the presented research project.

Having understood the general approach of virtual acoustic prototyping, one could argue whether all the efforts required to construct a VAP are proportional to its advantages. If measurements on the physical components are still needed, why not assembling the whole machine and simply capture the temporal structure of its sound output? The answer to this question purely depends on the specific purpose for which a VAP is used. To discuss this question in detail in the context of using VAPs for electrical steering systems, some basic

understanding of the generation and assessment of steering induced sound in vehicles is required, as provided in the following.

1.3. On the generation and assessment of steering induced sound

While driving a car, multiple sound sources are acting in parallel. According to their particular strengths and the corresponding fluxes of vibro-acoustic energy, a mixture of all contributions from each source can be perceived by passengers inside the cabin (cf. equation (1.1)). Aside from the well-known sources of driving noise, such as engine, drive line, tyre-road interactions or wind [11] many other air-, fluid- or structure-borne sound sources are present in vehicles. According to Brass [1], in modern cars up to 200 ancillary components pose possible vibro-acoustic sources, amongst them electric powered steering systems.

Under normal driving conditions, the contribution of steering induced sound on the overall interior sound is insignificant. Contributions from dominant driving noise sources, such as engine, tire-road rolling contact or wind, are known to be orders of magnitudes higher so that they typically mask steering sounds [12]. In this case, passengers inside the car cannot perceive the steering system as a sound source in the vehicle.

As soon as the dominant driving noises drop out, e.g. when parking the car or performing standstill steering, electrical steering systems can make substantial contribution towards the overall interior vehicle sound. However, even if the steering system becomes noticeable as a sound source in the vehicle, most passengers will relate the perceived sound to the function of the steering system. Hence, the annoyance for passengers experiencing this or a similar situation is typically judged as low, if a mode of operation according to the specifications of the EPS can be assumed. In the following, the term ‘functional sound’ will refer to this kind of steering induced sound.

In other driving situations, e.g. rapid steering or driving on poorly conditioned road , transient forces at random times can be originated inside the steering system. These forces result in unintended acoustical phenomena with likewise transient sound patterns that often stand out the accustomed driving sounds. Such stochastic phenomena can emerge as ‘rattling’ [3],[13],[14], ‘klonk’ [13],[12], ‘groaning’ [11],[13] or other sound patterns, depending on the underlying excitation and driving conditions respectively. In this report, the generic term ‘transient sound’ will be used to describe these phenomena. The main interest of the presented research is devoted to the generation of rattling sound.

Whenever transient sounds are excited, the chance is that passengers inside the cabin will perceive the disturbance and judge it as a defect, even though no mechanical faults are present or the functionality of the steering system is affected. This so-called `perception of a fault´ (PF) is purely dependent on the subjective judgement of the passenger and poses a high risk for complaints [1],[15], for which reason ZFLS aims to minimise PF by design.

No matter if functional or transient sound is subject to noise control, difficulties always result from the fact that assessing NVH quality comprises the individual perception of each passenger (perceptual domain) whereas the parameters within the control of designers and engineers are restricted to physical parameters only (physical domain).

As discussed prior to this section, VAPs could help to link both domains, the physical and the psychological. Doing so, designers and engineers would be able to perform design optimisation in the physical domain while evaluating the improvement of a certain design modification in the psychological domain by listening to and rating of the auralised interior vehicle sound. Yet, this approach will only be sufficient if the VAP comprises a detailed description of the physical domain. Regarding the aim to minimize PF by design, this means that all internal transient sound sources need to be considered when modelling the physical problem in a VAP.

1.4. The physical problem

Electric powered steering systems (EPS) are considered as predominant structure-borne sound sources in vehicles [2],[3], for which reason airborne contributions are negligible regarding their audible perception in vehicles [7]. By definition [16], structure-borne sound is originated due to internal dynamic forces acting within a vibrating solid body, e.g. the steering system. Physical connections between this source and the adjoining passive structure allow for transmission of vibrational energy from the vibrating source into that passive receiver, e.g. the vehicle body. The injected energy is propagated within the receiver, forcing it to vibrate. Due to vibro-acoustical coupling, e.g. between the air inside the cabin and the shell of the compartment, audible sound may be radiated which is called ‘structure-borne sound’. All interrelated processes of generation, transmission, propagation and radiation of structure-borne sound span the physical domain of steering induced noise in vehicles and are to be considered when modelling the problem, as shown in Figure 1.1.

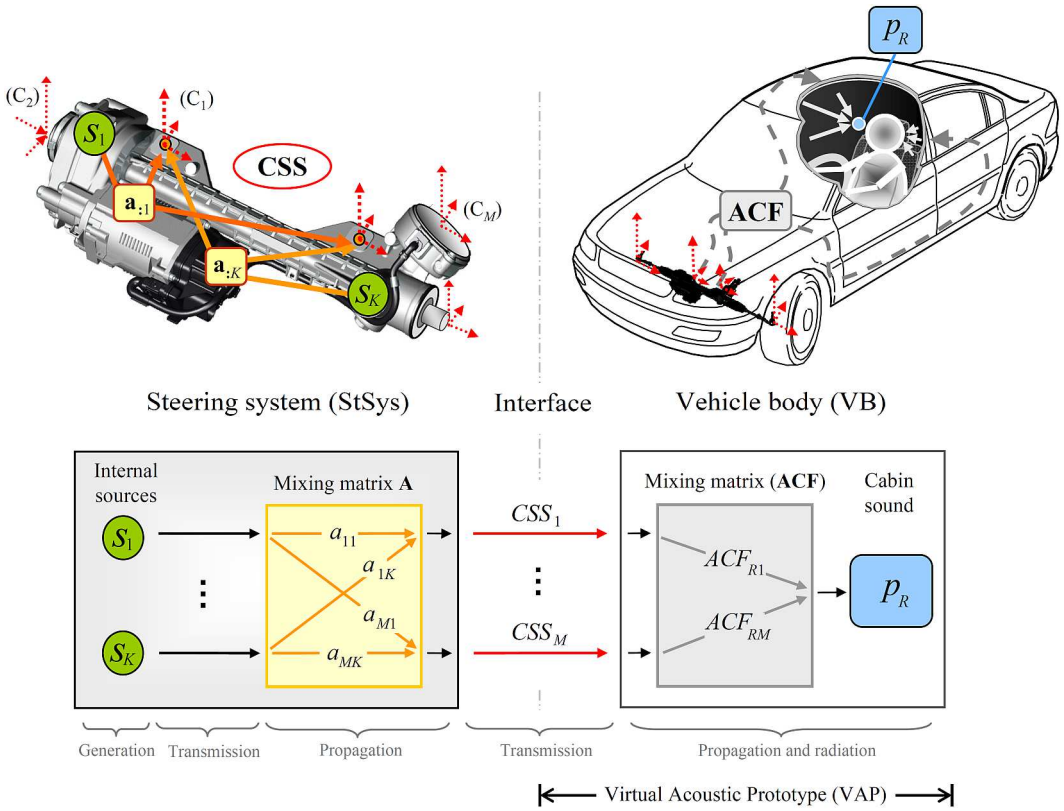

Figure 1.1: The physical problem behind steering induced noise in vehicles

The physical domain can be modelled as a multiple input single output (MISO) system: Several different source mechanism, s_k ($k = 1...K$), act as inputs of the system and, according to the mixing and filtering matrices **A** and **ACF** accounting for related transmission, propagation and radiation processes within the steering system and the vehicle body respectively, contribute in varying degree to the single sound at the driver's ear, p_R. Note, the system model in Figure 1.1 is depicted in most general form to allow approaching the problem in time domain as well as in frequency domain. In time domain the matrices **A** and **ACF** perform convolutive mixing to their respective input signals whereas linear mixing is assumed in frequency domain.

From an engineering point of view it makes sense to separate the physical domain into two sub-domains, the steering system (StSys) and the vehicle body including the air space inside the cabin (VB). Both parts are coupled through several physical links. Physical links in this respect only account for mechanical but not for acoustical or vibro-acoustical coupling. In reality, such links are usually formed by rigid connections between the steering system and the remaining vehicle structure, e.g. bolting of StSys and sub frame (Figure 1.1-(C_1)), connections between StSys and tie rods (C_2) or coupling of StSys and steering column (C_M) respectively. The entity of all mechanical connections represents the interface through which

vibrational energy can be transmitted from the steering system into the vehicle body. At the same time, this interface separates the part of the physical domain that is in the range of control for designers and engineers at ZFLS (StSys) from the non-controllable part (VB). Although the design targets for engineers at ZFLS are defined only for the steering system, both parts have to be considered in order to achieve auralisation of the interior sound which is required to judge NVH quality.

In Bauer's aforementioned VAP [7], the steering system is assumed as 'black box' which is characterised by its 'external properties' at the interface to the vehicle. Doing so, no detailed information about the structure-borne sound processes inside this box is necessary. A VAP is achieved by relating the external dynamic properties of the steering system (CSS) and the properties of the conducting vehicle body (ACF) to the cabin sound (p), using equation (1.1). It has been shown [7] that the external properties of a steering system can be characterised independently of a receiver structure, allowing to measure its source strength in arbitrary physical assemblies, e.g. when connected to a test bench. For this purpose, the component source strengths (CSS) has to be expressed in terms of blocked forces obtained in-situ by employing frequency domain inverse techniques [17],[18]. Transmission, propagation and radiation processes taking place inside the conducting vehicle body are accounted for by using vibro-acoustic transfer functions (ACF), measured in a real vehicle between the connection points of the StSys and a point inside the compartment coinciding with the head position of the driver. Although auralisation can be achieved in this way, the usability of this VAP for noise control engineers with respect to minimizing 'perception of a fault' (PF) by design is limited. The major shortcoming of this approach is, that neither the internal source mechanisms ($\boldsymbol{s}_k$) nor the internal mixing and filtering processes (**A**) inside the steering system are considered.

Gaining this information is the aim of the presented research project. Concerning the source mechanisms ($\boldsymbol{s}_k$), the internal transient sound sources within electrical steering systems are to be identified and suitable methods have to be developed in order to quantify their strengths. The source strengths have to be intrinsic quantities of the internal sources to make them independent of receivers coupled externally to the steering system, e.g. test bench or vehicle body. This requirement allows considering transient sound sources in future VAPs. Transmission and propagation processes within the StSys are to be characterised as well, yielding the mixing and filtering matrix **A**. This matrix directly relates the contributions of the independent internal sources ($\boldsymbol{s}_k$), to the external quantities of the steering system (CSS), e.g.

blocked forces at the interface to the vehicle. The external quantities (CSS) composed of $\boldsymbol{s}_k$ and **A** then could be auralised using Bauer's VAP [7].

Providing such a detailed VAP, noise control engineers were able to rank order the internal transient sound sources according to their partial contribution to the perceived interior vehicle sound. In this way, dominating internal sources could be identified and optimised first, before focussing on weak contributing sources that may influence PF only moderate. Applying a detailed VAP of a steering system would further provide essential insight into the internal generation, transmission and propagation processes of transient structure-borne sound in electrical steering systems. This comprehension could help engineers to evaluate whether primary modifications on the active sources or secondary actions on the conducting passive structure are necessary for minimizing PF. Clearly, such a sophisticated VAP, allowing users to figuratively 'look into the steering system' instead of studying the overall vibro-acoustic behaviour of the entire assembly, would be innovative and could offer many other advantages for various noise control tasks, too.

1.5. Time domain representation of electrical steering systems

Having disclosed the physical problem of steering induced transient sound in vehicles, the question of how best to address it remains. As elaborated, sources and transfer paths are to be characterised independently of each other and auralisation based on the combination of these characteristics should be possible. Each of these issues is challenging and various solutions of different level of sophistication to each matter can be found in literature. Most of them employ techniques in which the physical problem is represented either in frequency domain or time domain. Favouring one representation over the other depends on the specific application and the particular motivation.

It is believed that the problem of transient sound in vehicles originated within electrical steering systems can be best approached in time domain. The motivation for this hypothesis is explained in the following.

First, it is noted that the temporal structure of the involved signals should generally be taken into account when choosing between frequency domain and time domain representation. For example, impulsive, irregular or modulated signals are generally hard to catch in frequency domain [19]. Regarding transient sounds in steering systems, e.g. rattling, the internal originating forces, aimed to be identified within this study, are caused by some transient

mechanical phenomena, such as colliding assemblies for instance. Hence, structural and acoustic responses provoked by the internal forces also carry transient features, so that tackling the problem in time domain is favoured.

Second, the source characterisation issue poses an inverse problem since neither the transient excitation forces inside the steering system ($\boldsymbol{s}_k$) nor the external dynamic (blocked) forces acting at the interface to the vehicle connections (CSS) can be measured directly. Commonly, such ill-posed inverse problems are addressed in frequency domain where matrices containing measured frequency response functions (FRFs) have to be inverted. Yet, these methods are well known to suffer from poor conditioning and to be highly sensitive to measurement noise. Although the robustness of the solutions may be improved with some form of regularisation (see amongst many examples [20],[21]), usually significant effort and expertise is to be directed to obtaining satisfying results. Regarding possible applications of VAPs for NVH engineers, this special know-how cannot be expected.

Third, the transfer paths between the internal transient sound sources and the external connection points of the steering system are to be characterised. Although the structural dynamic properties at the external interface to the vehicle have proved to be invariant on the steering angle [7],[8], it is not known if the internal transfer path may vary in time due to dynamic steering. If so, employing time domain modelling techniques could be advantageous to account for the time-varying nature of the internal dynamic properties. It is noted that dynamic steering will not be considered within this research project.

Considering the VAP issue, one of the main objectives of Virtual Acoustic Prototyping is to synthesise and auralise the sound of a virtual assembly. As discussed in section 1.2, the general approach of virtual acousting prototyping is based on representing the active (CSS) and passive components (ACF) in the form of narrow band spectra. A spectrum of the machine's sound output can be synthesised by combining both data sets according to equation (1.1) and auralisation is achieved by converting this spectrum into time domain. However, directly employing inverse Fourier transformation to the obtained sound pressure spectrum does not necessarily yield sufficient time signals for auralisation. Time signals gained in this way may suffer from missing phase information, e.g. as a result of spectral averaging which is sometimes required to determine equivalent source strengths (CSS), or from bandwidth limitations in frequency domain yielding insufficient numbers of data points so that only very short time samples can be processed [6]. Solutions to overcome these hurdles can be found in

literature, e.g. by artificially increasing the number of data points of the synthesised spectrum by spectral interpolation [6] or adopting computationally intensive hybrid approaches in which frequency domain methods are used to gain transfer functions of the passive components (ACF) that first are transformed into time domain FIR filters before synthesis and auralisation is carried out by convolution with recorded source strength time histories (CSS) ([7], [8]). However, it is argued that a VAP directly represented as time domain model in this context would be more straightforward. First, it is believed that auralisation carried out solely with time domain data could avoid most of the above mentioned problems. Audible sounds of any length could simply be generated by directly convolving the temporal data of the passive structure (ACF) with the time data of the active sources, the latter representing time dependent CSSs captured for an arbitrary operating time. In this way, general problems due to converting data from frequency domain into time domain could be avoided completely. Second, time domain VAP models would possibly better allow for relating time dependent passive data (ACF), e.g. steering angle dependent transfer functions, to specific causative events in the captured source data (CSS).

Finally, since perception is generally dependent on the time signature of a noticed sound [1], capturing a signal's temporal waveform throughout all evolutionary stages, i.e. generation, transmission, propagation and radiation, may provide additional important information to noise control engineers.

1.6. Thesis objectives

To provide useful guidance for addressing the problem of transient structure-borne sound originated within electrical steering systems and the associated problem of perception of a fault, the following aims have to be achieved:

- Identification of internal transient sound sources:

  The most crucial phenomena responsible for the generation of transient sound within electrical steering systems and their corresponding operating conditions have to be identified. A methodology needs to be developed, which allows the source locations inside electric powered steering systems (EPS) to be determined. The underlying physical mechanisms are to be characterised as well. In order to provide better insight in transient sound issues to engineers and designers at ZFLS, a simple and clear model of the theoretical structure-borne sound processes within EPS shall be achieved.

- Development of a measurement strategy:

  In order to provoke internal transient generating forces, external excitations need to be applied to the steering system. Therefore, a strategy has to be evaluated that allows applying controlled external excitation forces to the steering system. The concept needs to consider that all measurements have to be carried out while the steering system is coupled to another structure, e.g. a test bench, which is required to provide this external excitation. Thus, in-situ measurement techniques have to be used.

- Independent characterisation of the internal sources:

  To independently characterise the transient sound sources within real steering systems a concept and a practicable approach have to be developed that allow the individual strength of each structure-borne sound source to be quantified, ideally in terms of time domain blocked forces obtained from measurements carried out in-situ. This task poses several challenges. First, a general time domain routine being able to provide robust and accurate solutions to the associated inverse problem has to be established. The method should allow for simultaneously reconstructing multi-channel (blocked) force time signatures based on measured data so that it is applicable even for sophisticated technical structures, such as steering systems. Second, since the time domain routine is used to quantify the individual strengths of each internal transient sound source from measured data, numerical tools shall be achieved that can be employed to evaluate the quality of this measured data. In this way, defective data can be detected before carrying out the inversion algorithm. Theoretical and practicable feasibility are to be tested in both cases.

- Relating internal transient sources to external properties:

  The contributions from all independent internal sources have to be related to external properties (blocked forces) determinable at the connection points of the steering system. As can be seen from Figure 1.1, this relationship is given by the mixing and filtering matrix **A**. A philosophy and a practicable approach are to be developed allowing for quantifying the mixing coefficients of this matrix. If both, the internal sources ($\mathbf{s}_k$) and the mixing matrix (**A**) are identified, a model of the physical system can be built directly relating the internal transient sound sources to the external properties of the steering system. If this objective is achieved, Bauer's VAP [7] could

be employed in order to investigate the influence of each internal transient sound source on the perceived sound inside the vehicle cabin.

- Validation of the obtained methodology based on test bench measurements.

The methodology as well as all theoretical and practical approaches developed within this research project shall be feasible for any type of electric powered steering system produced by ZFLS. By way of example an EPSapa PL2 steering system is used within this study.

Chapter 2

Literature review and theory

2.1. Introduction

In the previous chapter the problem of transient structure-borne sound and the associated phenomenon of perception of a fault (PF) within electrical steering systems were discussed. In this respect, independent characterisation of the transient sound sources inside the steering system was stressed to be one of the most fundamental tasks to be achieved within this study. Being able to quantify the activity of the internal sources as well as the respective transmission paths between each source and the connection points at which the steering system is coupled to a supporting structure, e.g. a vehicle body or a test bench, would provide important information to designers and engineers and may serve as initial guidance in order to reduce PF by design.

Unfortunately, structure-borne sound source characterisation in general is complicated due to the highly individualistic nature of each source-receiver system and the required balance between accuracy and simplification [22]. Typically, structure-borne sound is originated within the source due to internal dynamic forces resulting from one or more sound generation mechanisms, e.g. stick-slip, impact, unbalances etc. [23] that make the source vibrationally active. Activity, in this respect, is defined as the combination of all internal processes which give rise to the vibrations [24]. Source activity can be expressed as the free velocity, the velocity of the freely suspended source, or the blocked force, the force at the contact with an inert receiver [25]. If the active source is connected to a receiver both structures exert forces and moments on each other so that vibrational energy can be transmitted at the connections between the source and the receiver; the latter of which may ultimately radiate audible structure-borne sound [16]. The interfacial forces and moments as well as the vibrational responses (e.g. velocities) acting at both structures, however, dependent on the structural dynamic coupling of source and receiver, conventionally expressed as mechanical mobilities or related frequency response functions [26], as well as the activity of the vibration source. In most engineering structures, like machinery, coupling between active components (sources) and the connected passive receiver is possible through various very different types of physical links and, at each connection, translational forces along three mutually perpendicular axes as well as three moments about these orthogonal axes can act at the interface. As a consequence of this, the power transmission at a contact point can be influenced by vibration induced by forces and moments acting in all degree of freedom (DOF) at adjacent mounts on the source-receiver interface [27]. Thus, rigorous source characterisation and determination of power

transmission theoretically requires consideration of all kinds of coupling between the different contact points, i.e. transfer, cross and cross-transfer mobilities are to be considered [24].

Moreover, to fully quantify structure-borne sound transmission from the source into the receiver in theory all of the causative forces and moments have to be considered. However, on account of several practical limitations direct measuring the interfacial forces and particularly the moments is rarely possible. Instead, inverse methods may be employed that allow inferring the causative quantities from more accessible quantities, like structural responses, which are representative for the effects of the physical problem [28]. Since the source characterisation problem in this way may emerge as an ill-posed inverse problem, severe numerical difficulties have to be dealt with in order to obtain robust solutions [28],[29] required to achieve reliable quantification of the respective source activities. Additional challenges inherent in the source characterisation problem result from the need to quantify active sources independently of a connected receiver structure. In the context of transient structure-borne sound, as in the case of electrical steering systems, the ambition to achieve a description of the source activity in time domain (see section 1.5) further increases the complexity of the general source characterisation problem.

In this chapter some of the existing methods to tackle the general problem of structure-borne sound source characterisation will be overviewed. The most basic relationships and state-of-the art methods regarding structure-borne sound characterisation will be reconsidered in section 2.3. Particular attention will be devoted to mobility based methods since these allow sub-structuring, i.e. calculation of the properties of an assembled structure using the properties of its parts, as well as utilising measured input data with reference to repeatable boundary conditions which is favourable with respect to independent source characterisation [22],[26],[17]. Furthermore, basic aspects of the general inverse problem in structural dynamics, as inherent in some of the presented techniques, will be discussed. A number of different approaches for solving the inverse problem in the context of indirect force identification will be presented in section 2.4, followed by a discussion on their applicability for sophisticated structure-borne sound problems. A summary and some concluding remarks on the source characterisation problem as relevant for this study will be reasoned in section 2.5.

Since all of the presented techniques invoke concepts relying on linear and time invariant (LTI) system theory a brief discussion on the assumption of LTI behaviour for electrical steering systems subjected to internal transient sound generation is provided in the following.

2.2. Assumption of linear and time-invariant system behaviour

All methods presented and used in this study invoke principles and concepts based upon linear and time invariant (LTI) system theory. In the context of steering induced transient structure-borne sound assuming LTI behaviour may however be controversial. The generation of transient structure-borne sound is caused by some form of mechanical excitation inside the steering system (StSys) which sometimes may be construed as being related to time varying or even nonlinear system behaviour. Considering the phenomenon of rattling for example, transient forces are provoked inside the steering gear by impacting assemblies due to load-dependent short-time lifting and abrupt equalising movements between adjacent components (see section 3.3.3). The associated non-deterministic processes of interfacial movement, occurrence of clearance as well as possible transitory changes in the local physical properties of the structure (i.e. dynamic mass, stiffness and damping) point towards nonlinear, rather than linear, system behaviour [30]. If furthermore dynamic steering is considered, the transmission paths between the internal source regions and any point on the coupled source-receiver system, e.g. StSys connected to a test bench or a vehicle body, may vary with time so that again the strict LTI assumption is violated.

On the other hand, considering the StSys explicitly as a nonlinear and time-varying dynamic system is believed to be over-constrained and, moreover, would exceedingly exacerbate tackling the problem of steering induced transient sound. This is due to the fact that no unique analytical or experimental approach to deal with nonlinear system identification is available [30],[31],[32] and modelling of time-varying system properties for sophisticated technical structures is generally difficult, in particular when non-deterministic and fast varying mechanisms are to be dealt with.

In practice, almost all complex technical structures are nonlinear to some extent or show some form of time variant behaviour [32],[33]. However, in the vast majority of engineering applications concepts and methods based on linear system theory have satisfactorily been employed to analyse the structural dynamics and to perform system identification, provided that (i) the original system can be assumed to take an approximate time-invariant state at the

time when analysis or system identification is performed and (ii) some check of linearity is carried out to ascertain that the degree of nonlinearity for the prevailing testing conditions is sufficiently small [33]. In this respect, test procedures based on the evaluation of homogeneity, distortion and reciprocity of pre-measured frequency response functions or evaluation of the system's linear input-output relationship by means of the coherence function are most commonly used [30],[32],[33].

The problem of impact excited structure-borne sound occurring within mechanical structures has been studied by numerous researchers, as reviewed, for example, by Dobson and Rider [34], Inoue [35] or Hundhausen et al. [36]. Most of the published approaches favour the reasonable compromise of invoking concepts and principles based on LTI system theory. For example, in agreement with premise (ii), Inoue et al. [35] place emphasis on assuming linear system behaviour when the deformation of a mechanical structure being subject to impact excitation can be considered to be small enough to neglect geometric nonlinearity. In [37] and [1] Steinberg explicitly stresses that the vast majority of impact provoked rattling phenomena perceivable inside passengers cars can be considered as linear and approximate time invariant problems if a mode of operation according to the design specification can be assumed and under the assumption that premise (i) is met.

Within this research project, it is assumed that both premises, (i) and (ii), can consistently be met for which reason approximate LTI system behaviour will be assumed for electrical steering systems with regard to internal transient sound generation. However, all fundamental assumptions as well as actions or test procedures undertaken to justify this hypothesis will be discussed in the relevant sections of the thesis. Yet, at this point, it is re-emphasised that LTI system behaviour constitutes the most basic assumption of the presented research project. As a corollary of this, all concepts, theories and methods based on the linear superposition principle can be invoked, including

- Convolution integrals
- The theory of linear integral transforms, such as Fourier transformation and its inverse
- Frequency response functions (FRFs) for vibration analysis in frequency domain
- The theory of linear operators and spectral theory,

amongst others [33]. This enables one to address the problem of source characterisation in the context of steering induced transient structure-borne sound in either time domain or frequency

domain, since approaches may be transformed from one domain into the other without losing generality.

As discussed in section 1.5 it is beneficial to perform identification and quantification of transient sound sources within electrical StSys in time domain. However, all source characterisation approaches that will be employed in this study represent time domain duals of established frequency domain techniques; some of which are widely used in the realm of vibration. In the following, the most promising frequency domain source characterisation methods for the given application case are reviewed. It is noted that most of these methods have rarely been employed in time domain mainly due to the fact that the computational task for deconvolution, as typically required to solve (inverse) source characterisation problems, in frequency domain is far less than that for deconvolution in time domain [35]. However, it will be shown (chapter 4 and 5) that a novel time domain inversion routine can be used to overcome most difficulties inherent in the general source characterisation problem.

2.3. Characterisation of structure-borne sound sources

To predict structure-borne sound in assembled structures such as vehicles, machinery and many other situations two essential problems in the realm of vibration are to be dealt with. First, a description of the source's vibration activity is required. Second, the ability of the source to transmit vibrational energy to connected structures (receiver) has to be quantified. A combination of both quantities can eventually be used to characterise the power transmission. Difficulties associated with the related disciplines of source characterisation and determination of power transmission result partly from the inherent complexity of the interaction between structure-borne sound sources and their connected receivers and partly from the different objectives that motivate research in these fields, e.g. formulation of source strength as an independent property of the source or the trade-off between simplicity and accuracy of an approach.

In literature, the expression 'structure-borne sound source characterisation' has been used as a synonym for a wide range of approaches describing in some way the vibro-acoustic behaviour of a source based on an ensemble of physical quantities with respect to internal excitation mechanisms, dynamic properties, time dependence, dependence on the operation conditions, etc [23]. For the sake of clarity, 'structure-borne sound source characterisation' in this study will refer to a unique description of the source's ability to deliver structure-borne sound power

expressed as a set of measured data. Ideally, the source characterisation must be a property solely of the source, i.e. it has to be insensitive to changes in the receiver structure. In this way, characterisation of a vibrational active source invariant to a given installation case or the dynamic coupling between the source and the receiver onto which it is mounted can be achieved. This is what will be called 'independent' characterisation of structure-borne sound sources in the following. Some other desirable features of such an approach would be to express source strength as a single (frequency dependent) value and to achieve a characterisation that forms a basis to calculate the power transmitted when the source is installed [38].

Source characterisation and vibrational power transmission has been under intensive research. In 1987 ten Wolde and Gadefelt [39] suggested a number of possible characterisation approaches and it became apparent that different structure-borne sound problems may require different source descriptions and associated methods for characterisation. Since then significant effort has been directed to addressing the general problem of structure-borne sound characterisation and prediction. There have been reviews and comprehensive introductions in papers, for example by ten Wolde and Gadefelt [39], Bodén [40], Olhrich [41],[27], Verheij [42],[43], Fulford and Gibbs [44],[45],[46], Moorhouse and Gibbs [47], Petersson and Gibbs [24], Moorhouse [38], Hynnä [22], Elliott [17], Evans [48], Bauer [7], Pavić and Elliott [49],[50], Moorhouse et al. [9],[51], Bonhoff [52],[53] or most recently by Alber et al. [38]. The various concepts and approaches proposed are motivated by different objectives according to which different classification between the methods can be made. However, it is noted that no consistent categorisation can be found in literature. In the following, distinction is made between measurement approaches and prediction approaches. There is, however, a certain overlapping of these categories and some methods may be classified differently according to the particular purpose of use.

Measurement approaches:

Measurement approaches are mainly concerned with the acquisition of the required data such as the source activity or the structural dynamic properties of the involved structures. Examples are the direct measurement of the **free velocity** of resiliently mounted machines as issued in the international standard ISO 9611 [54], the **direct measurement of blocked forces** e.g. [55], different approaches to measure the **operational forces** (and moments) acting at the source-receiver interface although these are not invariant to the receiver structure, e.g.

indirect methods by Thite and Thompson in [20],[21], Pavić and Elliott's **in-situ techniques to indirectly measure mobility and free velocity** when the source is coupled to a receiver by elastic mounts [49],[50] or indirect methods proposed by Elliott and Moorhouse et al. [9],[51],[17] allowing for **in-situ measurement of the blocked force and the mobility** for arbitrary coupling conditions between source and receiver. However, none of these measured quantities can be collapsed to a single value if both translational and rotational degrees of freedom (DOFs) are present, because of their dimensional incompatibility. Furthermore, considering that up to 6 DOFs at each connection between source and receiver may be relevant for characterisation, the measurement effort as well as the comparability of different sources on the basis of so much data can be seen as disadvantageous. Usually, simplifications can be achieved by (i) neglecting cross-coupling between local and global transmission coordinates, and (ii) reducing the number of transmission paths taken into account by ignoring contributions in the occasional troublesome rotational coordinates, which are often of negligible influence [27]. Note that measurement approaches will be discussed in more detail in the subsections 2.3.1 to 2.3.4.

Prediction approaches:

Prediction approaches facilitate simplified comparison of vibrational sources by processing (measured) data in order to calculate, for example, the transmitted power when the source is connected to a receiver structure. Examples are the **reception plate method**, e.g. Späh and Gibbs et al. [56],[57],[25], where the vibration source is attached to a standardised receiver structure and the transmitted power is calculated based on the averaged velocity response as well as the knowledge of the receiver's loss factor and its mass. Unfortunately, the characterisation is not independent of the receiver and does not generally allow the subsequent prediction of transmitted sound when installed [38]. However, velocity source (source mobility much lower than the one of the receiver) and force source (source mobility much higher than receiver mobility) approximations can be achieved by choosing receivers that constitute light-weight [58] or heavy weight [59] structures, respectively. The reception plate method has been developed to become an European Standard as issued in EN 15657-1 [60] and EN 12354-5 [61]. The method reduces the complete complex power description to a single equivalent value which can be seen as detrimental with respect to physical transparency [62].

Mondot and Petersson [63] propose characterisation of a single-point and single-component source-receiver installation based on the **source descriptor and the coupling function.** Both expressions can be derived by manipulation of the exact equation of the complex power (i.e. half the dot product of the force applied to the receiver by the operational source and the coupled velocity at the source-receiver interface). The source descriptor characterises the ability of the source to deliver power independently of the connected receiver while the coupling function represents a ’filter’ (ratio of the source and receiver mobilities at their common interface) determining how much power is manifested. Together, as a product, the two functions establish the power delivered [46]. Due to using a power basis to describe the source strength translational and rotational contributions are dimensionally compatible and can be collapsed to a single frequency dependent value [53],[38]. Although this method allows rigorous characterisation of the source independently of the receiver as well as determination of the transmitted power, it is of limited practical use regarding multi-point and multi-component systems.

To overcome this problem the methodology of the source descriptor and the coupling function can be combined with Petersson and Plunt’s concept of the **effective mobility** [64],[65]. The concept is based upon the premise that any point in a multi-point-connected system can be considered individually if the effects on that point of all other points and components of motion are taken into account [44]. If this premise holds, the concept of effective mobility can be used to reduce a multi-point and multi-component source-receiver coupling to an equivalent single-point and single-component case expressed as a linear combination of point, transfer, point-cross and transfer-cross mobilities involving force (and moment) ratios [53]. As shown by Petersson, Gibbs and Fulford in [66] and [44], respectively, the effective mobility can be used in the source descriptor for source characterisation. However, due to the force (and moment) ratios which are inherently dependent upon both the source and the receiver structures, the source descriptor is no longer an invariant property of the source [44]. By assuming or statistically estimating these ratios [46], the independency of the source descriptor can however be retained [62].

The source descriptor concept was further developed by Moorhouse in [38] where multiple-point-connected systems can be dealt with using the **characteristic power** which represents the equivalent to the source descriptor for single points. In analogy to Mondot and Petersson‘s coupling function Moorhouse introduces the coupling factor which is defined as the constant

of proportionality between the complex power (emission) passing through the source-receiver interface to a receiver structure and the magnitude of the characteristic power. Thus, the characteristic power together with the coupling factor can be used to determine the emission of machines. Furthermore, Moorhouse [38] introduces the **maximum available power** (mobility of receiver is complex conjugate to the source mobility) and the **mirror power** (source and receiver mobility are equal in magnitude and phase) which can be considered to represent the 'worst case scenario' and the 'matched source-receiver scenario', respectively. However, experimental investigations of the characteristic, mirror and maximum available powers showed that the power transmission from a source attached at multiple points to different receiver structures was best described by the characteristic power [17]. All three descriptors, the characteristic, maximum available and mirror power are theoretically rigorous results since (i) they are purely based on independent properties of the source, (ii) they characterise the source's ability to transmit structure-borne sound power accounting for all mechanisms such as forces and moments and (iii) they facilitate useful comparisons between different sources based on single frequency-dependent quantities [38]. However, since no simplification is included in the formulation of the characteristic power the characterisation effort is generally high. Furthermore, the approach is based on a formulation requiring inversion of a possible ill-conditioned matrix so that obtaining the characteristic power purely by measurement is likely to be problematic. These practical difficulties are, however, inherent in any attempt to characterise structure-borne sound sources and do not devalue the theoretical importance of the characteristic power [38]. In order to reduce the measurement effort and to circumvent amplification of measurement errors due to the inherent matrix inversion [62], Moorhouse and Gibbs in [67] introduce some simplifications for measuring the characteristic power. Based on Moorhouse's characteristic power the simplified ‚characteristic structure-borne sound power level' has been issued in the European Standard EN 12354-5 [61].

Verheij et al. [23],[42] introduce a characterisation method based on so-called '**pseudo forces**'. Note that a similar approach, termed 'equivalent forces', is presented by Laugesen and Ohlrich in [68] as well as by Janssens et al. in [69]. Pseudo forces represent a number of fictitious forces that are assumed to be fully equivalent to the actual internal excitation so that they produce exactly the same vibrational response on the source's outer surface and the entire receiver structure. The measurement method represents a variant of indirect force identification (cf. section 2.4) in which the pseudo forces are measured in-situ, i.e. while the

source is coupled to the receiver. In this way the method respects the multi-dimensional interactions between source and receiver structure. The pseudo force method has been used successfully for rank ordering of transmission paths [43] or for a comparison of the activity of different machines [70]. An advantage of the method is the flexibility in choice of pseudo-force excitation positions due to which no great practical restrictions or limitations with respect to performing the necessary measurements will appear [23]. At the same time, the flexibility of the method has a drawback as well. Since the choice of pseudo-force positions is arbitrary, sets of pseudo-forces are not unique for which reason comparisons of different experiments may be cumbersome, and need additional modelling and/or measurements [70]. Furthermore, pseudo-forces are in general dependent on the receiver structure and therefore are not a truly independent property of the source [38].

A similar approach to Verheij's pseudo forces was presented by Lai in [71]. Based on in-situ measurements of the mobility and the operational velocity at the source-receiver interface whilst both source and receiver are coupled, the method yields the so-called '**synthesised force approximation**' from the product of the inverted mobility and the operational velocity. As stressed by Elliott and Moorhouse in [18] the synthesised force turns out to be the blocked force. The method as formulated in [71] is valid for a single point only. Since the excitation and response points are defined at the contact interface the method allows for prediction of structure-borne sound power transmission at this point. For sources with multiple excitations, the total input power can be approximated by summing the input powers from all components at all contact points. However, the method requires measurement of the driving-point mobility at the contact between source and receiver whilst both structures are coupled. Applying excitation to measure the mobility in most cases is not practical.

Simplified characterisation of the structure-borne sound excitation and determination of the transmitted power of operating machinery can also be achieved by measurement of the **equivalent force** on the source-receiver installation using direct or reciprocal substitution methods, as outlined by ten Wolde in [39] and discussed in Janssens et al. [69]. Here, a single equivalent force is used to describe the overall vibro-acoustic behaviour of the source. Further application of the equivalent force technique are referenced in Bonnhoff and Petersson [62]. They also stress that the approach is promising in its simplicity but, considering multi-point and multi-component systems, it is rather unlikely that a single fictitious excitation force will characterise the source sufficiently well.

Other advanced and elaborate techniques for determining power transmission have been developed that provide helpful physical insight with respect to design and optimisation of the source or the complete installation. In [72],[73] Pinnington et al. achieve useful simplification by employing a **multipole expansion** for predicting low frequency power transmission. This is done by expanding the acting forces and velocities into a number of poles, e.g. monopole, dipole, quadrupole etc. The power transmitted from the operating source to the connected receiver is approximated as the sum of the powers transmitted by these poles. However, the receiver structure must be geometrically symmetrical or the source is a set of uncorrelated outputs [74].

Moorhouse and Gibbs et al. [75],[76] use **eigenvalue expansion** of the mobility matrix for characterising multi-point transmission. The transmitted power is expressed as the sum of orthogonal power modes based on the eigenvalues and eigenvectors of the real part of the receiver mobility matrix. This approach can be considered as a generalisation of the multipole approach [27] and for structures featuring two perpendicular axes of symmetry the gained eigenvectors correspond to physically highly comprehensible excitation modes such as monopoles or dipoles etc. [62]. However, without symmetry a physical interpretation of the eigenvectors is difficult. In Ji et al. [74] this method is referred to as the '**power mode approach**' and further approximations are developed for the maximum possible, the minimum possible and the mean value of the transmitted power.

Recently, Bonhoff and Petersson in [77],[78] have examined a characterisation method based on '**interface mobilities**' that can be used for multi-point transmission problems involving parallel source–receiver interfaces of either discrete or continuous form [27]. Instead of treating each contact point between the source and the receiver separately, a single interface comprising all contact points is considered. Within a closed contour, the velocities, forces and mobilities at the source –receiver interface are decomposed into orders by means of Fourier series [79]. As shown in [77] the interface mobilities can be used to reformulate the source descriptor concept [63] so that source-receiver assemblies with multi-point or continous connections can be investigated. The applicability of interface mobilities for source characterisation relies upon the admissibility of neglecting a possible coupling between different orders. In [80] the coupling between different orders is found to be negligible. However, the practicability of the concept of interface mobilities is primarily determined by the number of orders required to achieve a proper resolution in the intermediate and upper

frequency range. At the moment there exist no general clarification of the influence and significance of higher-order terms [62].

In **summary**, rigorous characterisation of structure-borne sound sources and determination of the transmitted power for multipoint connected source-receiver installations is extremely complicated. Research in these fields has been driven by different objectives and various approaches of different level of sophistication have been developed. At the present, there exists no general applicable method for the prediction of structure borne sound or the characterisation of structure borne sound sources. However, despite the different points of view the general consensus tends to favour an independent source characterisation with simplifications made where possible and appropriate [17]. The focus within this research project is on applying and establishing measurement methods that facilitate accurate acquisition of the data required for structure-borne sound source characterisation which may form the basis for rigorous prediction of the transmitted power in future studies. In the following the most promising measurement approaches and basic principles with respect to characterisation of structure-borne sound sources in electrical steering systems are elaborated.

2.3.1. Mechanical mobility and related frequency response functions

The dynamic characteristics of a linear and time invariant structure can be described by the frequency response function (FRF) *H* according to

$$H(\omega) = \frac{\beta(\omega)}{\alpha(\omega)} = \frac{\beta e^{j\omega t}}{\alpha e^{j\omega t}} \tag{2.1}$$

where β is a kinematic variable used to describe the response of the system to an excitation acting at its input described by the kinetic variable α, ω is the circular frequency, *t* denotes time and $j = \sqrt{-1}$.

For mechanical structures the kinetic variable can constitute an excitation either by a rectilinear force or a moment. The kinematic variable can be a translational or rotational response expressed in terms of displacement, velocity or acceleration [81],[26]. Thus, FRFs given as per Eq. (2.1), i.e. the ratio (kinematic variable / kinetic variable), defines the willingness of a structure to vibrate in response to a forced disturbance [82]. Note that for each FRF a reciprocal (inverse) function exists, which is also a FRF (kinetic variable / kinematic variable), describing the resistance of a structure to vibrate to a given

excitation. Depending on the choice of the kinematic variable (response) different standard definitions of the FRF and the equivalent inverse function have evolved [26].

The FRF formed by the phasor ratio of the acceleration response $a_i(\omega)$ at a point *i* on the structure to a force $f_k(\omega)$ applied at point *k* is called 'accelerance' or sometimes 'inertance'. Under the condition that the structure is allowed to respond freely without any constraining forces acting on it other than the intended excitation at *k*, the accelerance is formally defined as

$$A_{ik}(\omega) = \left.\frac{a_i(\omega)}{f_k(\omega)}\right|_{f_{j\neq k}=0}. \tag{2.2}$$

Note that 'point' in this context is used to mean both a location and a direction. When the point of excitation collocates with the response point ($i = k$) the FRF is called 'direct','driving point' or 'point' accelerance. Otherwise ($i \neq k$) it is termed 'transfer' accelerance. Other FRFs can be obtained in a similar way by relating the velocity response $v_i(\omega)$ or the displacement response $x_i(\omega)$ to an input force yielding FRFs defined as the 'mobility'

$$Y_{ik}(\omega) = \left.\frac{v_i(\omega)}{f_k(\omega)}\right|_{f_{j\neq k}=0} \tag{2.3}$$

and the 'receptance' (also termed 'admittance', 'compliance' or 'dynamic flexibility' [26])

$$R_{ik}(\omega) = \left.\frac{x_i(\omega)}{f_k(\omega)}\right|_{f_{j\neq k}=0}, \tag{2.4}$$

respectively. The corresponding reciprocal FRFs are usually termed 'apparent mass' ($M = 1/A$), 'mechanical impedance' ($Z = 1/Y$) and 'dynamic stiffness' ($K = 1/R$) respectively [26]. In engineering vibration problems, structural responses are commonly measured in terms of accelerations for which reason accelerances are directly measureable using a dual channel analyser, an accelerometer and a force transducer [17]. Measuring mobilities requires knowledge of the velocities which corresponds to an integration of the acceleration time histories. Integration in time domain is equivalent to a multiplication by $(1/j\omega)$ in frequency domain so that the mobility can conveniently be obtained from the accelerance by

$$Y_{ik}(\omega) = \frac{A_{ik}(\omega)}{j\omega}. \tag{2.5}$$

Similar relationships can be found for all other FRF types [81]. The mobility and impedance representation is most widely employed in structure-borne sound source characterisation since it is more convenient in describing mechanical power transmission in contrast to accelerance or receptance and their inverses, respectively [17].

To describe the dynamic characteristics of multi degree of freedom (MDOF) systems mobility functions between several input and response DOFs have to be measured. A convenient formulation can be achieved by stacking all mobility functions up in one big frequency dependent mobility matrix **Y**, according to

$$\mathbf{Y}(\omega) = \begin{bmatrix} Y_{11} & Y_{12} & \cdots & Y_{1n} \\ Y_{21} & Y_{22} & \cdots & Y_{2n} \\ \vdots & \vdots & \ddots & \vdots \\ Y_{m1} & Y_{m2} & \cdots & Y_{mn} \end{bmatrix} \tag{2.6}$$

where *m* denotes the total number of response DOFs and *n* the number of excitation DOFs. Note that for convenience the frequency dependency (ω) of the mobility elements Y_{ij} is dropped in Eq. (2.6).

In practice, the elements of the mobility matrix can be measured by applying one force at a time to each DOF of interest allowing the structure to respond freely, and the individual elements are obtained as the complex ratio of the particular velocity response to the single induced excitation [81]. Thus, considering another input DOF of the mechanical structure results in adding another column for the excitation to **Y**, whereas considering an additional response DOF requires expanding **Y** by another row. Generally, the mobility matrix **Y** is not necessarily square, allowing more responses to be considered than induced forces and vice versa.

For LTI systems the principle of vibro-acoustic reciprocity [43] holds so that the transfer mobility between any pair of DOFs *i* and *j* remain unchanged if the response and excitation DOF are reversed, and thus $Y_{ij}(\omega) = Y_{ji}(\omega)$. As a consequence of this, an ideal mobility matrix has to be symmetrical along the main diagonal; a feature that will be discussed in more detail in chapter 4.

Furthermore, the imposed boundary conditions (absence of further forces) ensure that individual elements of the mobility matrix remain unaffected if additional rows or columns are added or eliminated so that they are invariant to each other [7]. This means that a certain mobility element Y_{ik} remains the same although measurements are made at other points [81],

which allows structures to be subdivided into different parts and each part can be characterised separately. Instead, elements of the corresponding impedance matrix, i.e. $\mathbf{Z}(\omega) = \mathbf{Y}^{-1}(\omega)$ where the inverse is assumed to exist, are not invariant of each other making experimental determination of the impedance matrix almost impossible (see e.g. [26] for further explanation).

However, different techniques to measure mobility have been established (see e.g. references in [82],[83]) so that the mobility concept can sufficiently be used to describe the dynamic characteristics of even sophisticated MDOF systems based on experimental data only. Hence, it allows sub-structuring but does not suffer from modelling inaccuracies as, for example, imposed by high-frequency limitations when the finite element method is utilised [26].

In the following the mobility concept is used to describe the dynamic properties of the passive source-receiver system which is required to obtain an independent characterisation of structure-borne sound sources.

2.3.2. Direct measurement of free velocity and blocked force

Independent characterisation of structure-borne sound sources is possible in terms of the source's active properties. Parameters typically used are the free velocity [39],[84],[45] and the blocked force [85].

The velocity of the source when operating with no external forces acting is defined as the **free velocity** of the source

$$\mathbf{v}_{Sf}(\omega) = \mathbf{v}_S(\omega)\big|_{\mathbf{f}_S(\omega)=\mathbf{0}} \tag{2.7}$$

where $\mathbf{v}_S$ is the vector of operational velocities at the interface at which the source *S* is connected to a receiver structure in normal operation, $\mathbf{f}_S$ is the vector of forces applied external to the source and ω denotes radian frequency [17]. The boundary conditions of no external forces limit approaches to measure free velocities to situations where (i) a constant velocity source idealisation can be assumed [16] so that free velocities can theoretically be obtained from in-situ measurements or (ii) the source can be separated from the receiver structure to conduct operational measurements under conformable boundary conditions. In the more prevalent latter case, the separated source has to be mounted resiliently, e.g. by means of elastic bands, foam or suitable isolators, in such a way that free boundary conditions can be assumed. As a rule of thumb, in practice the source mobility has to be much smaller than the

mobility of the required mounting and the surrounding media. Commonly a mobility mismatch of more than 10 dB within the interesting frequency range is considered as sufficient [7]. Although these conditions most often can be met sufficiently and the free velocity approach is widely accepted in principle to the extent that it has been standardised [54], severe difficulties prohibit the general usability of the method for many engineering vibration problems.

The major downside of the free velocity concept results from the need to separate the source from any rigid support which is not practical for many machines and active components [51]. In practice, this requirement prohibits characterisation of sources running under load or rather to account for internal excitation mechanisms inside active components that may vary with the external loading, e.g. transient sound sources in electrical steering systems which are caused due to interactions of the StSys and external dynamic forces. Hence, the assumption of ordinary operation conditions without load is not generally valid for engineering applications as machines may be designed to work against load, such as motors or pumps, for instance.

To circumvent difficulties with free mounting or load-less operating conditions blocked forces may be used for independent source characterisation. The **blocked force** is defined as the force that is required to counter the operational source velocity at the interface at which the source is connected to a receiver to zero

$$\mathbf{f}_{bl}(\omega) = -\mathbf{f}_S(\omega)\big|_{\mathbf{v}_S(\omega)=\mathbf{0}}. \tag{2.8}$$

The blocked force vector is directly related to the free velocity vector (Eq. (2.7)) by the source mobility matrix $\mathbf{Y}_S$ as follows

$$\mathbf{v}_{Sf}(\omega) = \mathbf{Y}_S(\omega)\mathbf{f}_{bl}(\omega). \tag{2.9}$$

Note, since the source mobility is a structural property invariant of the receiver and the free velocity is an independent characteristic of the source, the blocked force must also be invariant of the receiver.

In theory, true blocked terminations, i.e. $\mathbf{v}_S(\omega) = \mathbf{0}$, can be achieved by connecting the source to an infinite rigid receiver structure. In practice these conditions can only be approximated over a limited frequency range requiring large and rigid test rigs [51]. As a rule of thumb, the mobility mismatch between source and receiver must be opposite to the one of the free velocity concept so as to ensure approximate blocked terminations. However, even if the boundary conditions can sufficiently be met, measurement of the blocked forces is not always

straightforward. Blocked forces cannot be measured inversely while the source is blocked as the velocity downstream to the source-receiver interface need to be zero according to the definition in Eq. (2.8). Therefore, the only way to measure blocked forces is directly using force transducers which have to be inserted between the source and the (purpose-built) receiver. Difficulties result from the fact that, at each point where source and receiver connect, up to three orthogonal forces and three moments about these axes exist so that direct measurement of all interfacial blocked quantities may not be practical for sophisticated multi-point-connected structures. Design and functionality issues of the source or potential alteration of the interfacial conditions may further prohibit non-reactive instrumentation into the flux of forces (A detailed discussion can be found in section 2.4).

Hence, the free velocity and the blocked force approach yield independent source characterisation if the mounting and operational conditions are fulfilled in theory. However, the fact that these conditions differ from the realistic conditions and practical difficulties with experimental measurements limit the usability of these approaches, in particular for sophisticated engineering problems as in the case of electrical steering systems, for example.

2.3.3. Measurement of operational contact force

An alternative method to the free velocity and blocked force approach is to measure operational forces. From the earlier discussions it is clear that for source characterisation the transmission process between the source and the receiver is crucial. The transmission is governed by the interfacial dynamic forces, the so-called contact forces, acting between the active source and the passive receiver. Hence, the contact force can be interpreted as a representative quantity of the source activity for a specific source-receiver installation. Source characterisation based on contact forces is advantageous in the sense that measurements can be conducted in-situ, i.e. when the source is connected to the receiver; thus ensuring realistic operating and mounting conditions.

Since direct measurement of the contact forces suffers from the same difficulties as discussed previously for the direct blocked force method, indirect measurement techniques have to be conducted using inverse methods. Inverse methods have been widely and successfully applied, particularly in transfer paths analysis (TPA) (see for example [19],[86],[87]). Sometimes these methods are referred to as ‘inverse force synthesis’. The basic idea of applying inverse force synthesis is to infer the sought forces from structural responses

observed in-situ at some points on the receiver-site which can be related to the actual excitations utilising the corresponding FRFs which are measured on the separated receiver structure between the assumed force input locations and the response locations. Conventionally, operational velocities and mobilities are used as response and FRF quantities, respectively. The relationship is illustrated in Figure 2.1.

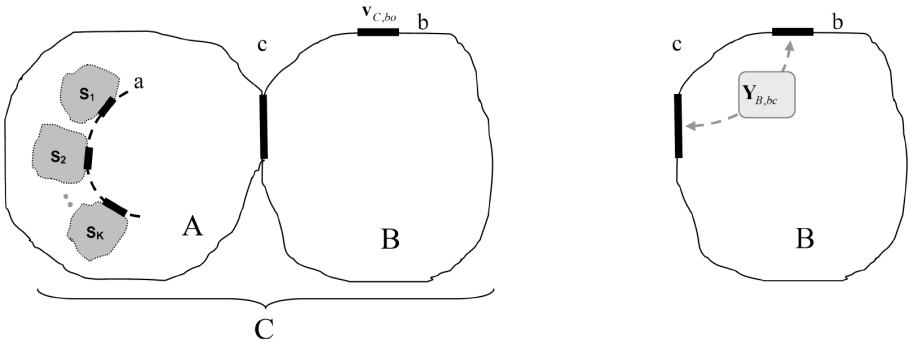

Figure 2.1: Two-stage measurement approach for determination of contact forces in-situ. Assembled structure *C* comprising the source *A* which is active due to some internal source mechanisms s_k and the passive receiver *B*; *a*,*b* and *c* represent all degree of freedom on the corresponding interfaces of structures *A*, *B* and *C*, respectively; *o* indicates that operational measurements are conducted.

Accordingly, a two-stage measurement approach is required from which the true operational contact forces $\mathbf{f}_{C,c}$ can be synthesised as follows

$$\hat{\mathbf{f}}_{C,c}(\omega) = \mathbf{Y}_{B,bc}^{-1}(\omega)\,\mathbf{v}_{C,bo}(\omega) \tag{2.10}$$

where ^ indicates that the contact force is estimated rather than directly measured, $\mathbf{Y}_{B,bc}$ denotes the mobility matrix of the separated receiver structure *B* containing the mobilities measured between all DOFs on the contact interface *c* and the reference DOFs on the receiver-interface *b* (see Figure 2.1-right), $\mathbf{v}_{C,bo}$ is the vector of operational velocities measured in-situ on the coupled structures *C* whilst the source is active (see Figure 2.1-left) and the inverse of the mobility matrix is assumed to exist. To improve the force estimation process the number of considered response locations at the receiver interface *b* should increase the number of force input locations at interface *c*, so as to overdetermine the set of linear equations in Eq. (2.10). The inverse in this case is replaced by a pseudo-inverse. Note that inverse methods and associated difficulties will explicitly be discussed in section 2.4.

The disadvantage of this approach is that the coupled mobility as well as the obtained dynamic contact force is dependent upon the properties of both the source and the receiver. Thus, measured contact forces are only valid for a certain source-receiver installation and so

are generally not suitable for independent source characterisation. From a practical point of view separation of the sub-structures for measurements of receiver FRFs is not ideal since dismantling is time consuming and is not always possible. However, it is re-emphasised that the operational measurements are conducted in-situ so that realistic operation and mounting conditions can be achieved. Furthermore, no instrumentation within the sensitive contact zone between source and receiver is required.

2.3.4. The in-situ blocked force approach

A relatively new approach, known as the in-situ blocked force method, was published by Elliott and Moorhouse et al., see for example [88],[18],[17],[9] or [51]. The measurement approach of blocked forces in-situ is very similar in many respects to the measurement of operational forces by inverse force synthesis [89], thus combining practical merits of the in-situ measurement techniques with the merits of independent source characterisation by the blocked force approach. In the following the in-situ blocked force method is introduced with reference to its application for characterisation of transient sound sources in steering systems.

As discussed in chapter 1, the generation of transient sounds in steering system is caused by external excitations (EBO and EBR). Thus, the steering system needs to be coupled with either the vehicle body or a test bench in order to excite internal transient sources. To characterise the steering system at its connection points or the internal source locations independently of a receiver structure the in-situ blocked force method is essential. The basic principle of the method is illustrated in Figure 2.2.

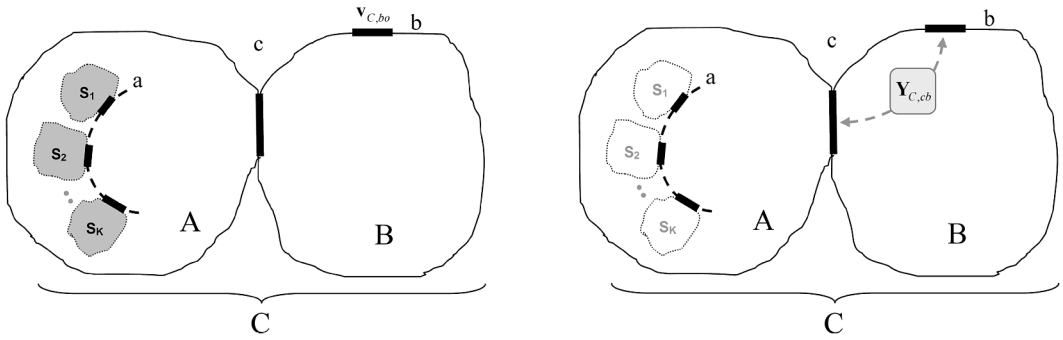

Figure 2.2: Two-stage measurement approach for determination of blocked forces in-situ. Assembled structure *C* comprising the source *A* which is active due to some internal source mechanisms s_k and the passive receiver *B*; *a*,*b* and *c* represent all degree of freedom on the corresponding interfaces of structures *A*, *B* and *C*, respectively; *o* indicates that operational measurements are conducted

Considering an assembly *C* consists of a source *A*, e.g. the steering system, and a receiver *B*, e.g. a test bench. In this assembly the source is connected to the receiver structure at the given subset *c* of co-ordinates. Furthermore, it is assumed that the source can only be operated in the given assembly since the internal source mechanisms s_k can only be excited if *A* and *B* are coupled. The resulting challenge is to characterise the source structure *A* at interface *c* independently of the receiver structure *B*. As investigated by Elliott in [17] this can be achieved by the blocked force $\mathbf{f}_{bl,c}$ measured in-situ, defined as

$$\mathbf{v}_{C,bo}(\omega) = \mathbf{Y}_{C,bc}(\omega)\mathbf{f}_{bl,c}(\omega). \tag{2.11}$$

Equation (2.11) reveals that for the determination of blocked forces $\mathbf{f}_{bl,c}$ at interface *c* a two-stage measurement is required. First, the operational velocities $\mathbf{v}_{C,bo}$ have to be measured at the receiver interface *b* when the source mechanisms inside structure *A* are active (Figure 2.2-left). Note that this measurement is essentially the same as in the previous mentioned inverse force synthesis approach, thus realistic mounting and operation conditions are retained. Second, the generalised transfer mobilities of the coupled structure $\mathbf{Y}_{C,bc}$ are measured. This quantity describes the passive properties of the assembly *C* by relating the degrees of freedom at interface *c* to those at interface *b* on the receiver structure. Note that the degrees of freedom at interface *b* are the same as used in conventional inverse force synthesis methods; the significant difference, however, is that the mobilities are of the coupled structure *C* rather than of the receiver structure *B* as used conventionally [90]. This is illustrated in Figure 2.2-right, where the internal source mechanisms of structure *A* are inactive. As mentioned in [51], the reciprocity principle could be invoked and $\mathbf{Y}_{C,cb}$ measured instead of $\mathbf{Y}_{C,bc}$ since the number and location of the degrees of freedom at interface *b* can be specifically selected for ease of applying an excitation. Invoking the reciprocity principle requires modifying Eq. (2.11) as follows

$$\mathbf{v}_{C,bo}(\omega) = \mathbf{Y}^{T}_{C,cb}(\omega)\mathbf{f}_{bl,c}(\omega) \tag{2.12}$$

where *T* denotes matrix transpose. Note that Eq. (2.12) has profound implications with respect to practical applications of the in-situ blocked force method [88]. The relationship has been validated numerically and by measurement in [9] and has also been discussed in [51] and [18]. It can also be inferred as a special case of the relationships given by Bobrovnitskii in [91]. Furthermore, Elliott and Moorhouse in [18] note that the ‘synthesised force

approximation' of a single degree of freedom system derived by Lai in [92] (cf. 'prediction approaches' in section 2.3) is a special case of Eq. (2.12).

Assuming the inverse (or pseudo-inverse if overdetermination is used) of the generalised transfer mobility matrix exists, Eq. (2.12) can be solved for the sought blocked force vector

$$\mathbf{f}_{bl,c}(\omega) = \mathbf{Y}_{C,cb}^{-T}(\omega)\,\mathbf{v}_{C,bo}(\omega), \tag{2.13}$$

facilitating independent characterisation of source *A* at its contact interface *c* based on measurements thoroughly conducted in-situ. Assuming further, that interface *c* may be moved towards the internal interface *a*, the same procedure can also be applied for independent source characterisation of the internal sources s_k at interface *a*. Both characterisation purposes are of high relevance for addressing the issue of transient sound generation in electrical steering systems.

The in-situ blocked force method has proved sufficient for simplified structures and conditions in test labs, see for example [88],[18],[93], but also for a number of sophisticated engineering applications ranging from prediction of structure-borne sound from building-mounted wind turbines [94],[95],[96],[89] and automotive components [97],[10], through Virtual Acoustic Prototyping [10], to TPA in vehicles [98],[99]. With reference to engineering vibration problems the advantageous of the in-situ blocked force method can be summarised as follows. The in-situ measurement approach ensures

- better accessibility to measurement sites which can be selected arbitrarily
- non-reactive instrumentation remote from the sensitive contact interface
- realistic mounting and operation conditions of the source
- consideration of all contributions including moment and in-plane excitations
- time saving since dismantling is not required at all
- possibility to improve the mathematical conditioning of (FRF) matrices by overdetermination

while independent source characterisation based on the blocked force

- avoids the need for special test rigs so that standard test benches can be used, which e.g. is required to provoke rattling in electrical steering systems

- enables operation of the source in different installations without affecting the characteristic source activity so that results are generally valid and may be transferred to predict structure-borne sound in other installations, e.g. internal transient sound sources in steering systems can be characterised on a test bench but may ultimately be used for sound prediction in the real vehicle (cf. VAP concept in section 1.2), and
- allows for experimental validation of the source characterisation by measuring in-situ blocked forces when source *A* is connected to a certain receiver B_1 and utilising these dynamic forces to predict the operational velocities in a different installation, i.e. when *A* is connected to a receiver B_2. For validation the operational velocities on the installation '*A*-B_2' have to be measured which is possible without expecting difficulties.

Note that all these merits are required to fulfil the objectives of the thesis as discussed in section 1.6. For this reason the in-situ blocked force method has been found to be the most promising source characterisation approach and will be used in the remainder of the thesis to quantify transient structure-borne sound sources within electrical steering systems.

However, as with inverse force synthesis the in-situ blocked force method employs inverse methods in frequency domain, in which measured structural responses are propagated back to the assumed known source regions by inverting matrices containing pre-measured FRFs. This, however, can be disadvantageous in some respects as discussed with reference to inverse force identification in the following section.

2.4. Inverse force identification

Knowledge of the dynamic forces experienced by mechanical structures is a critical aspect to many engineering applications, ranging from general design tasks [100] to structural reliability analysis [101], health monitoring [102] or impact and collision engineering applications [34]. Regardless of the actual application or the underlying physics, the actual dynamic forces and moments will play a significant role in the determination of adequate systems properties or parameters [103]. For the research presented in this thesis, identification of the time-varying forces at sub-system interfaces, i.e. the in-situ excitations acting between the active source and the passive receiver structure, is crucial in order to achieve meaningful structure-borne sound source characterisation.

A trivial solution to this problem is to measure the desired interfacial quantities directly by placing force transducer(s) between source and receiver into the load paths at the point of force application. However, in many real-life situations, non-reactive implementation of the required transducer(s) is impractical, if not impossible, due to restrictions imposed by the physical design, the functionality of the assembly, possible impacts on the load and mounting conditions or potential alterations of the interfacial conditions (unless there is significant mobility mismatch over a particular frequency regime) [104],[105],[106]. In cases where direct force measurement cannot be conducted, indirect measurement techniques may be employed in which the unknown dynamic input forces (and moments) are determined utilising a model of the dynamic system and measured structural responses, e.g. displacement, velocity, acceleration or strains. For continuous time, the response $a_i(t)$ of a linear dynamic system observed at a point i is related to an impact load $f_j(t)$ applied at point j by a linear convolution integral as

$$a_i(t) = \int_0^t h_{ij}(t-\tau)\, f_j(\tau)\, d\tau \tag{2.14}$$

where $h_{ij}(t)$ is the corresponding time impulse response Kernel. Some situations may allow measuring these responses directly at the excitation locations, i.e. the response positions coincide with the one of the applied force ($i = j$). This kind of vibration problem is usually referred to as a '**collocated**' problem and is associated with **minimum phase systems**. In many engineering vibration problems, however, placement of response sensors directly at the force input locations is prohibited due to the above mentioned practical issues or not intended due to some consideration on conducting response measurements at locations away from the excitation points. As a consequence of this, '**non-collocated**' sensor placement ($i \neq j$) has to be used causing severe difficulties when attempting to directly solve Eq. (2.14) for the input force based on the knowledge of the (measured) response data and a model of the system which, in this case, has **non-minimum phase**.

In essence, the fundamental idea behind indirect force measurement is to use the instrumented structure as its own force transducer [107],[108]. In literature, this approach is often referred to as 'indirect' or 'inverse force identification', 'inverse force reconstruction', 'inverse input estimation' or 'inverse analysis of input force' since the solution is based on one or more inverse problems to infer causes (the excitations) from effects or results (the measured

structural responses) [34]. The two associated inverse identification problems in structural dynamics are diagrammed in Figure 2.3.

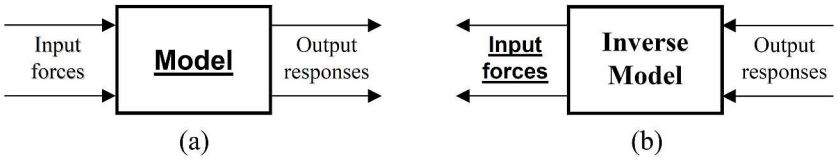

Figure 2.3. Schemes of two inverse problems in structural dynamics: (a) inverse system identification, (b) inverse force identification. Problem solutions are underlined.

The Figure 2.3-(a), consists of finding a mathematical model of a dynamic system based on the knowledge of the input forces, the structural responses and the boundary conditions. This problem has been widely studied in literature and different approaches depending on the nature of the structure (linear time-invariant, non-linear and time-variant systems) or the type of the applied signals (transient, periodic, random etc.) have been published, see amongst many examples [109]. Although system identification techniques are employed within this thesis, it is stressed that the inverse system identification problem is not the major concern. Thus, unless stated differently, established experimental methods guaranteeing well-defined boundary conditions will be used to identify dynamic properties of the structures under test. These properties are required to build inverse system models which are ultimately used to perform inverse force identification.

The challenge of the **inverse force identification problem**, illustrated in Figure 2.3-(b), is to find the unknown dynamic input forces, based upon the knowledge of the (measured) structural responses, the boundary conditions as well as a sufficient inverse system model. Referring to Eq. (2.14) the problem to be solved is a deconvolution one. To do so, the convolution integral in (2.14) first has to be discretised into algebraic equations in time domain as

$$\mathbf{a} = \mathbf{H}\mathbf{f} \tag{2.15}$$

where $\mathbf{a} = \left[a_i(\Delta t), \ldots, a_i(n\Delta t) \right]^T$ and $\mathbf{f} = \left[f_j(0), \ldots, f_j((n-1)\Delta t) \right]^T$ are vectors composed of discrete values of the response and the force, respectively,

$$\mathbf{H} = \begin{bmatrix} h_{ij}(\Delta t) & 0 & \cdots & \cdots & 0 \\ h_{ij}(2\Delta t) & h_{ij}(\Delta t) & \ddots & & 0 \\ h_{ij}(3\Delta t) & h_{ij}(2\Delta t) & \ddots & \ddots & \vdots \\ \vdots & \vdots & \ddots & \ddots & \vdots \\ h_{ij}(n\Delta t) & h_{ij}((n-1)\Delta t) & \cdots & \cdots & h_{ij}(\Delta t) \end{bmatrix} \tag{2.16}$$

is the transfer (convolution) matrix consisting of the discrete values of the system impulse response function $\mathbf{h} = \left[h_{ij}(\Delta t), \ldots, h_{ij}(n\Delta t) \right]^T$, $1/\Delta t$ is the sampling frequency and T denotes transpose of a vector or matrix. In theory, the time history of the sought impact force can be estimated by solving Eq. (2.15) for

$$\hat{\mathbf{f}} = \mathbf{H}^{+}\mathbf{a} \tag{2.17}$$

where ^ indicates estimated values and $\mathbf{H}^{+}$ denotes the inverse (or Moor-Penrose pseudo-inverse, i.e. $\mathbf{H}^{+} = [\mathbf{H}^T\mathbf{H}]^{-1}\mathbf{H}^T$) of the discrete-time transfer matrix. However, this inverse problem is **ill-posed in the sense of Hadamard**, which means that one of the following conditions is violated: (i) the existence of the solution (ii) the uniqueness of the solution or (iii) the continuous dependence of the solution on the data (stability condition) [110],[35]. With respect to inverse force identification, commonly the second and third condition cannot be met causing severe difficulties in obtaining good reconstruction results of the sought input forces. The uniqueness of the solution is generally violated due to the availability of, in a mathematical sense, only incomplete data. Restrictions in this respect result from practical issues. First, only a limited number of response data can be observed (measured) although the actual system response is generally a continuous function of the spatial coordinates [110]. Second, placing sensors at spatially discretized and assumed point-like locations can result in spatial aliasing if there are poorly placed or too few sensors [110]. Third, when dealing with non-collocated problems, in which at least one of the unknown input forces does not permanently have distinguishable influence on any of the used sensors, the effect of spatial aliasing and the general incompleteness of the response data may be increased further [111]. Note, time delays between an excitation event and the corresponding remote response, inherent in all non-collocated problems, will cause the first row(s) of the transfer matrix **H** (Eq.(2.16)) to become zero so that the convolution matrix drops rank. Besides, the inverse problem is well-known to be **ill-conditioned** which means that small perturbations in the response data or the modelling excite large excursion in the estimated input forces [110],[112]. The instability refers to the inherent sensitivity of the solutions to noise and measurement errors [101] so that the stability condition is generally violated. In a nutshell, if one of Hadamard's criteria is not met, the 'naïve' solution of the inverse force identification problem, as performed in Eq. (2.17), will never give a satisfactory solution.

Therefore, the general consensus on accurately solving the inverse force identification problem is to **relax the ill-posedness of the problem** by incorporating appropriate additional information about the solution sought. Such information may be based on (i) physical conditions, e.g. non-negativity as often used when recovering impact forces [113] or additional time delays when dealing with non-collocated problems in time domain [114], or (ii) incorporating non-physical information such as compromises between the residual norm and the smoothness on the solution [113]. In the field of inverse force identification, the most widely used approach to involve the additional information is to employ mathematical methods, classed as **regularisation techniques** [35], based on the minimisation of an assumed objective function subjected to the additional conditions. Typically, the least square error, i.e. the distance between the predicted ($\hat{\mathbf{a}} = \mathbf{H}\hat{\mathbf{f}}$) and the desired (measured) system responses **a**, is utilised as objective function in order to achieve stable solutions. The regularisation problem then consists of identifying the force vector $\hat{\mathbf{f}}$ in such a way that the general functional

$$\min_{\hat{\mathbf{f}}} \left\| [\mathbf{H}\hat{\mathbf{f}}] - \mathbf{a} \right\|_2 \text{ subject to } \textit{further conditions} \tag{2.18}$$

is satisfied [113]. Several systematic approaches to obtain '**regularised solutions**' to the inverse force identification problem have been proposed.

For relatively **small least-squares problems** the use of direct parameter-based regularisation methods is common. These techniques usually employ the Singular Value Decomposition (SVD) of the transfer matrix. For the general case, the SVD of a real-valued matrix $\mathbf{H} \in \mathbb{R}^{m \times n}$ with $m \geq n$ is defined as

$$\mathbf{H} = \mathbf{U}\boldsymbol{\Sigma}\mathbf{V}^T = \sum_{i=1}^{n} \mathbf{u}_i \sigma_i \mathbf{v}_i^T \tag{2.19}$$

where $\mathbf{U} = [\mathbf{u}_1, \ldots, \mathbf{u}_n] \in \mathbb{R}^{m \times n}$ and $\mathbf{V} = [\mathbf{v}_1, \ldots, \mathbf{v}_n] \in \mathbb{R}^{n \times n}$ are unitary matrices ($\mathbf{U}^T\mathbf{U} = \mathbf{V}^T\mathbf{V} = \mathbf{I}_n$) composed of the left and right singular vectors of **H**, respectively, and $\boldsymbol{\Sigma} = diag(\sigma_1, \ldots, \sigma_n)$ is a diagonal matrix containing non-negative real numbers, the so-called singular values of **H**, which are arranged in non-increasing order ($\sigma_1 \geq \sigma_2 \geq \ldots \geq \sigma_n \geq 0$), the so-called 'singular value spectrum' [29]. Note that as σ_i decreases, i.e. *i* tends to *n*, the associated left and right singular vectors $\mathbf{u}_i$ and $\mathbf{v}_i$ become more and more oscillatory so that high index terms can be associated with noise. The number of non-zero singular values determines the rank of the

coefficient matrix **H**. Utilising the SVD (Eq. (2.19)) allows to re-formulate the problem in Eq. (2.17) based on a least-squares scheme as follows

$$\hat{\mathbf{f}} = \underbrace{[\mathbf{V}\boldsymbol{\Sigma}^{-1}\mathbf{U}^T]}_{\mathbf{H}^+}\mathbf{a} = \sum_{i=1}^{n}\frac{\mathbf{u}_i^T\mathbf{a}}{\sigma_i}\mathbf{v}_i \ . \tag{2.20}$$

From Eq. (2.20) it is obvious that the high index terms are responsible for the ill-conditioning of the problem. For example, when *i* tends to *n*, the factor $1/\sigma_i$ tends to infinity so that $\mathbf{u}_i^T\mathbf{a}$ has to tend to zero faster than σ_i in order to achieve a stable solution. Furthermore, when *i* tends to *n*, $\mathbf{v}_i$ becomes more oscillating so that the solution becomes strongly oscillating if $\mathbf{u}_i^T\mathbf{a}/\sigma_i$ does not tend to zero as quickly [113]. Thus, the ability to solve the inverse problem depends on the singular values and singular vectors of the transfer matrix **H**. The nature of the ill-conditioned inverse problem can be characterised according to the spectrum of singular values σ_i. If the singular values decay gradually to zero without a distinct gap in the singular value spectrum, the problem is a discrete ill-posed one. Instead, if there is a well-determined gap in the spectrum of the singular values the problem is said to be ill-posed and 'rank-deficient' [29]. In the latter case, the 'pseudo-rank' of matrix **H** can be determined by the number of singular values which appear before the gap. Jacquelin et al. [113] note that for solely ill-posed inverse problems the unknown impact forces can be recovered by directly solving the discrete convolution problem stated in Eq. (2.15) by employing either Eq. (2.17) or (2.20). If the problem is ill-posed and rank-deficient this solution will fail, yielding unstable and highly erroneous force estimations. It is noted that in Eq. (2.20) the division by small singular values ($i \to n$) amplifies the high-frequency (noise) components in **a**. Therefore, the sensitivity of the solution to relative errors in the measured responses and the transfer matrix depends on the conditioning of **H**. The ratio of the largest and smallest non-zero singular value, i.e. the condition number $\kappa = \sigma_1/\sigma_n$, can be used to quantify the conditioning. Low condition numbers are related to well-conditioned problems whereas problems with large condition numbers are said to be ill-conditioned.

To improve the conditioning of the problem, SVD-based regularisation techniques can be achieved by including some parameter φ_i in Eq. (2.20), the so-called filter factors, yielding

$$\hat{\mathbf{f}} = \sum_{i=1}^{n}\varphi_i\frac{\mathbf{u}_i^T\mathbf{a}}{\sigma_i}\mathbf{v}_i = \underbrace{[\mathbf{V}\boldsymbol{\Gamma}\boldsymbol{\Sigma}^{-1}\mathbf{U}^T]}_{\mathbf{H}^\#}\mathbf{a} \tag{2.21}$$

where $\mathbf{\Gamma} = diag(\varphi_1,\ldots,\varphi_n)$ is the diagonal filter matrix and $\mathbf{H}^{\#}$ denotes the regularised pseudo-inverse of **H**. The filter factors φ_i are incorporated with the aim to minimise the negative influence of the high index (noise) terms. Note that the filter factors are commonly chosen between 0, i.e. the contribution of the *i*-th term is completely suppressed, or 1, i.e. the contribution of the *i*-th term is completely passed through. Thus, one may either damp the high index terms by choosing the filter factors according to Eq. (2.22), which in conjunction with Eq. (2.21) results in a **Tikhonov regularisation scheme** in which the regularisation parameter α has to be determined, or one may completely reject terms higher than a certain rank $n = r$, according to Eq. (2.23), which together with Eq. (2.21) results in the **Truncated Singular Value Decomposition (TSVD)** scheme

$$\varphi_i = \frac{\sigma_i^2}{\sigma_i^2 + \alpha_{reg}} \quad \text{Tikhonov filter factors} \tag{2.22}$$

$$\varphi_i = \begin{cases} 1 & \forall \quad i \le r \\ 0 & \forall \quad i > r \end{cases} \quad \text{TSVD filter factors}. \tag{2.23}$$

Note that the index r in the TSVD method assumes the same role as the regularisation parameter α_{reg} in the Tikhonov method [113]. To specify the filter factors the associated regularisation parameters (α and r) have to be determined in order to achieve a physical meaningful solution to the inverse force identification problem. This can be done by employing so-called parameter-choice methods, such as the L-curve criterion, ordinary cross validation (OCV), generalised cross validation (GCV) or Morozov's discrepancy principle [115],[29].

For **large least-squares problems**, as often posed when performing inverse force analysis in time domain, the functional in Eq. (2.18) can be solved utilising iterative regularisation methods, such as the conjugate gradient method (CGM) [101],[112],[116],[117], or non-iterative recurrence algorithms, e.g. dynamic programming [111],[118],[119],[120],[121]. Detailed research monographs on numerical regularisation techniques to solve general inverse problems have been published, for example, by Hansen [29] or Engl et al. [28].

However, there is an ongoing research effort in the field of inverse force identification. A diversity of methods motivated by different objectives and incorporating various regularisation strategies have been developed over the years. Some **classical reviews** often referred to in literature have been published by Hillary and Ewins (1984) [122], Stevens

(1987) [123], Starkey and Merrill (1989) [124], Dobson and Rider (1990) [34] or Doyle (1993) [125]. Relatively **recent reviews** and comprehensive introductions in papers summarising emerging advances in different fields of inverse force analysis can be found, for example, in Ma et al. (1998) [126], Inoue et al. (2001) [35], Jacquelin et al. (2003) [113], Hundhausen et al. (2005) [36], Gunawan et al. (2006) [101], Uhl (2007) [111], Nordström and Larsson (2007) [103], Jankowski (2008) [117], Mao et al. (2010) [127] or Zhang et al. 2010 [102].

Usually, (i) the properties of the involved structure (e.g. linear time-invariant or non-linear and time-variant parameters), (ii) the a priori information of the applied load profile (e.g. number of input forces, pointwise or distributed forces, steady or moving forces) as well as (iii) the type and number of the unknown load characteristics to be identified (e.g. location, direction, magnitude, evolution, duration etc.) determine which of the various force identification techniques may be best suited for a specific application case.

The different inverse force analysis methods can be classified into three main groups [111], namely stochastic methods (e.g. based on regression-model inversion [111]), methods based on computational intelligence (e.g. artificial neural network (ANN) [35],[128], case-based reasoning [102] or methods based on statistical learning theory, e.g. [100]) and deterministic methods. The latter are most widely studied in literature. In essence, **deterministic approaches** address the inverse force identification problem by deconvolution of a limited number of measured structural responses utilising system models that are estimated analytically, numerically or experimentally in advance to the force identification process. Note that some deterministic input identification techniques have been developed that do not require system models, e.g. blind deconvolution methods as discussed in [129], for instance. According to the employed signal analysis procedures used for data processing and modelling the various deterministic approaches can roughly be subdivided into frequency domain (FD) methods and time domain (TD) methods, disregarding a few hybrid techniques, such as frequency-time domain (FTD) methods for moving force identification [130],[131], for instance.

The aim of the following sections is to briefly review and categorise some of the most widely used deterministic FD and TD force identification techniques. Advantages, difficulties as well as some typical applications of the different methods are discussed. To deliver insight into various fields of inverse force identification a diversity of methods is touched, although the

focus of this study is on linear problems where the load locations are known a priori and the corresponding force time signatures (magnitude) are to be identified. Although most of the presented approaches have rigorous mathematical foundations, these are not elaborated in the following. Instead appropriate references are provided (see also the overview given in APPENDIX A.1).

2.4.1. Frequency domain inverse methods and related approaches

FD inverse methods involve transformation of the signals and the underlying differential equations into the frequency domain for which reason they are most suited for linear time-invariant systems [103]. Using spectral analysis, the original TD deconvolution problem can be solved by pre-multiplying the vector of measured response spectra $\mathbf{a}(\omega) \in \mathbb{C}^{M\times 1}$ at each frequency ω by the inverse (or the least-square Moore-Penrose pseudoinverse) of the corresponding FRF matrix $\mathbf{H}(\omega) \in \mathbb{C}^{M\times N}$ at that frequency, according to the relation $\hat{\mathbf{f}}(\omega) = \mathbf{H}^{+}(\omega)\mathbf{a}(\omega)$, where N and M $(M>N)$ refers to the number of excitation and response DOFs, respectively. Inverse discrete Fourier transform may be applied to the estimated spectral force vector $\hat{\mathbf{f}}(\omega) \in \mathbb{C}^{N\times 1}$ in order to gain the time signatures of the dynamic input forces.

Unfortunately, due to poor conditioning of the FRF matrix, particularly at frequencies associated with the natural frequencies of the structure [132], the robustness of the solutions usually needs to be improved by applying some form of **regularisation**. It is stressed that invoking the regularisation techniques touched in the previous section is straightforward in FD if the matrix transpose operator T is replaced by the Hermitian transpose so as to account for the complex-valued double-sided frequency spectrum of the respective quantities. Regularisation techniques are, for example, utilised by Inoue et al. [133] where Tikhonov regularisation (cf. Eq. (2.21) with (2.22)) in conjunction with the L-curve parameter-choice method is employed to calculate impact forces. Liu and Shepard [134] utilise the TSVD filter (cf. Eq. (2.21), (2.22)) as well as the Tikhonov filter method (cf. Eq. (2.21), (2.23)), respectively, in conjunction with a parameter-choice method based on Morozov's discrepancy principle to reconstruct the time signatures of multiple harmonic forces applied to a beam structure. Further applications and comprehensive reviews of conventional FD inverse force reconstruction methods can be found, for example, in Inoue [35], Thite and Thompson [20],[21], Choi et al. [135] or Hundhausen et al. [36].

A specific problem of all FD inverse techniques is caused by averaging the measured data in frequency domain and the necessity to provide steady phase relationship between different response channels; the latter is crucial for yielding reliable force reconstruction. However, for structures subjected to multiple simultaneous excitations the operational responses may only be partially correlated, if at all, so that a steady phase relationship between them may not necessarily exist. To overcome these problems, advanced FD inverse methods have been developed that utilise decomposition methods, such as Principal Component Analysis (PCA), to condition the measured operational responses by referencing them to virtual inputs (sources), the so-called principal components [98]. Note that PCA is used to decompose the response cross-spectral matrix into a set of incoherent responses 'produced' by a corresponding set of incoherent virtual sources, although the physical sources are possibly partially correlated [136]. In literature, this method is sometimes referred to as '**virtual coherence method**' and has successfully been applied for transfer paths analysis (TPA), see amongst others [137],[98]. Leclére et al. [136] employs a FD inverse method in conjunction with the virtual coherence principle to identify multiple main bearing loads in operating diesel engines.

The **modal model method** is another indirect FD force identification method [138], which is different to the direct FD inverse method discussed so far. In modal modelling the FRF matrix is somehow reduced to a parametric model that can directly be obtained from conventionally (measured) FRFs. To reconstruct the actual FD input forces, a set of (measured) structural (displacement) responses $\mathbf{x}(\omega)$ is (i) transformed into modal responses $\hat{\boldsymbol{\eta}}(\omega)=\boldsymbol{\Phi}^{+}\mathbf{x}(\omega)$ and then (ii) pre-multiplied by the inverse of the mode shape matrix $\boldsymbol{\Psi}$ yielding a set of modal excitations $\hat{\mathbf{f}}_{\eta}(\omega)=\boldsymbol{\Psi}^{-1}\hat{\boldsymbol{\eta}}(\omega)$ which eventually (iii) is transformed back into physical excitation $\hat{\mathbf{f}}(\omega)=\boldsymbol{\Phi}'^{T+}\hat{\mathbf{f}}_{\eta}(\omega)$ [139], where $\boldsymbol{\Phi}$, $\boldsymbol{\Phi}'$ denote the modal matrix and the truncated modal matrix, respectively. Y.-R. Kim and K.-J. Kim [139] compare different extensions to the modal model method in which discrete multi-channel modal filters are used to identify multiple input forces based on numerical examples. A very recent review on classical and operational FD modal filtering methods including several examples and references related to indirect load identification has been published by Mendrok and Kurowski (2013) [140].

Other indirect force identification techniques which are closely related to inverse FD methods have also been published. The following two are possibly the most popular approaches.

Instead of using spectral analysis, Doyle [141] employs a **wavelet deconvolution method** in conjunction with a finite element modelling method to identify impact forces applied to a numerical plate model. The time history of the estimated forces can be obtained by performing an inverse wavelet transform to the forces calculated in wavelet domain. To reconstruct diesel engine cylinder pressures Gao and Randall [142] use **cepstral analysis** which can be thought of as an extension of the conventional FD inverse method in which the division is replaced by subtraction [113].

The different FD approaches has been demonstrated to yield satisfying force identification results for specific application cases. However, in literature the general **use of FD inverse force analysis methods is controversial** due to inherent limitations which have been found to be primarily introduced by the need to invert frequency-dependent matrices [34]. Particular difficulties arise from the severe ill-conditioning at frequencies associated with the natural frequencies causing highly unstable solutions if errors and noise are included in the measurements. Several researchers have studied the ill-conditioned nature of the problem and possible remedy by means of regularisation techniques, see e.g. Lee and Park [143] or the discussion and literature provided above. In some situations the use of FD deconvolution may also not be favoured due to signal processing issues, e.g. when the available data is of such short duration (early time problems) that leakage renders FD processing inaccurate [113],[144], when real-time force estimation is required [132],[108], or due to other practical considerations as it has been elaborated in section 1.5, for instance. Also, for transient input forces, it is natural to use time domain methods [114]. Since transient forces play a major role in the presented study, the most widely used time domain force identification methods are reviewed in the following.

2.4.2. Direct deconvolution methods in time domain

A great deal of research has been devoted to solving the inverse force identification in time domain. Especially, the seismic and signal processing communities have developed deconvolution methods that directly solve the time domain convolution matrix equation (Eq. (2.15)) using methods such as least-squares, Wiener filtering or minimum-variance deconvolution [107]. Unfortunately, most techniques developed in these fields are prohibitively memory intensive for which reason they cannot straightforwardly be applied for force identification in structural dynamics.

Vibration problems in structural dynamics usually involve multiple in- and outputs and commonly require consideration of thousands of data points [107]. Thus, the direct TD deconvolution approach and the regularisation techniques introduced previously (Introduction of section 2.4) can only be applied for ‘small’ inverse input identification problems. With ‘small’ it is meant that the inverse force analysis is restricted to cases in which short-duration force histories are to be identified for structures with a small number of excitation and response positions. Note, that for vibration problems with multiple responses and possibly multiple excitations (MIMO) the convolution matrix equation (Eq. (2.15)) and all subsequent relations, in theory, can be extended to partitioned block matrix without loosing generality.

Due to the limitation to only small vibration problems direct TD deconvolution methods have mainly been studied with respect to impact engineering problems, e.g. foreign object impact identification in aerospace [36] or ground vehicles [113], as these typically involve reconstruction of a single transient load from only a few structural responses. Numerous researchers have applied direct TD deconvolution techniques for impact force reconstruction. Reviews and different applications can be found, for example, in Hinoue et al. (2001) [35] or Hundhausen et al. (2005) [36]. Jacquelin et al. (2003) [113] elaborate general difficulties of TD devonvolution methods and provide comprehensive mathematical understanding and examples with focus on different SVD-based regularisation techniques.

For engineering applications in which the vibration problem cannot be considered as ‘small’, i.e. for force excited structures with many in- and outputs and long or even progressional response data, the use of other time domain methods is more straightforward. In the following some of the most widely used linear TD inverse methods are presented. Basically, these methods can be subdivided into modal filtering methods, state-space methods including inverse filters and Kalman filters, sensitivity methods and a number of other advanced techniques.

2.4.3. Time domain modal filtering

Reconstruction of dynamic forces in time domain is also possible by employing TD modal filtering. Using measurements of the structural responses and a modal model of the structure these methods isolate the portion of the responses caused by certain modes which can be mapped to the physical excitations. Note that the basic principle of TD modal filtering is very similar to the one of the FD modal matrix approach (section 2.4.1).

The most widely known time domain modal filtering approach is named ‘Sum of Weighted Acceleration Technique’ (SWAT). The basic principle of SWAT is to reconstruct the sum of all forces applied externally to a free elastic structure from measured acceleration time responses by (i) isolating and summing the rigid body accelerations using modal decomposition, i.e. elastic vibration responses due to the dynamic force input are removed (filtered out) from the measured responses, and (ii) simply multiplying this ‘sum of weighted accelerations’, which is acting at the centre-of-mass, by the structure’s mass according to Newton’s second law [145]. The SWAT algorithm is capable of estimating the forces acting on a structure in real time, e.g. as required for system control purposes, or when time data is available over such a short duration that frequency domain methods (FD) cannot be applied effectively [108]. Using SWAT, the spatial force distribution is implicitly integrated over the structure, so that only the sum of all externally applied forces and the sum of all moments about the centre-of-gravity can be obtained for the chosen bandwidths [146]. In some applications this lack of spatial information may be disadvantageous. In other situations where no spatial information of the exciting forces is required, e.g. structures excited by a single force with known excitation location, the summing of data in time domain makes the technique more robust and generally insensitive to noise that normally affects FRF measurements made at distributed locations on the structure [146]. By demanding less information, the SWAT technique avoids ill-conditioning problems that have affected other inverse force identification techniques [147].

The major difficulty of the SWAT approach is to calculate the scalar weights required for isolating the rigid-body accelerations from the measured structural responses. Various ways to determine these weights have been developed according to which distinction between different variants of SWAT can be made.

The fundamental principles of the ‘**traditional’ SWAT** approach were first explored analytically and experimentally by Gregory, Priddy and Smallwood [148],[149] where it was shown that for linear systems the required weighting coefficients can be determined from the mode shapes of the structure with free boundary conditions by inverting the modal matrix. Depending upon the locations at which the mode-shapes are measured and the accuracy of the measurements, this matrix can easily be inverted to produce estimates of the weights [147]. Thus, the number and placement of sensors is very important for reconstructing the time signatures of forces acting on a structure. Theoretically, the traditional SWAT algorithm requires one acceleration measurement for every mode of the structure that affects its motion

in the frequency band of interest. In [150] the strategic placement of accelerometers with respect to force reconstruction based on the traditional SWAT approach was discussed. For cases where the structure under test is equipped with additional sensors, Mayes [145] proposed a systematic sensor selection method that minimises the condition number of the mode shape matrix in order to find the optimal number and the best locations of sensors on the basis of initial laboratory tests. Wang and Kreitinger [151] extended the traditional method by providing an analytical procedure to determine the weighting coefficients based on finite elements which may be used for simple structures. In [152] they applied the SWAT method to nonlinear structures. Kreitinger [153] provides an extensive review of the basic developments of the SWAT algorithm until 1990. Bateman et al. [146] used the 'traditional' SWAT algorithm to determine the dynamic impact force experienced by a bomb during full scale dynamic tests based on acceleration measurements and initial experimental modal tests.

However, for sophisticated technical structures performing experimental modal tests is laborious and the use of finite element procedures is restricted to very simple structures. To facilitate force reconstruction for structure's whose mode shapes are not available or measurable, Mayes et.al. [154],[145],[147] present various extensions to the traditional SWAT approach. The so-called **SWAT-CAL** (SWAT using a calibrated force input) approach [154] utilises the measured force input and the acceleration responses with the rigid body mode shapes obtained from an initial calibration test to calculate the scalar weighting vector. The obtained weight vector can then be used to determine the dynamic forces from a second acceleration measurement carried out whilst the structure is exposed to the 'operational' external forces. The method has successfully been demonstrated for a lumped mass beam. The **SWAT TEEM** (SWAT using time eliminated elastic modes) algorithm [145] also employs an initial laboratory test in which the structure is impacted and allowed to decay freely. The scalar weighting factors can be calculated only from the free-decay time response of the structure with the rigid body mode shapes by utilising a constraint least square solution. As shown in [145], the SWAT TEEM algorithm requires more sensors than modes to achieve satisfactory results within the considered bandwidths. Carne, Mayes and Bateman in [147] describe an alternative approach, the so-called **SWAT Max-Flat procedure** in which measured FRF data is employed to assemble a set of highly over-determined equations which is solved for the weighting coefficients in a least squares sense. Problems associated with estimating the mode-shapes, as required for the traditional approach, and the inaccuracy that

may be generated in that process can be avoided. Possible errors in the measured FRFs may of course affect the determination of the weight vector but the Max-Flat procedure is relatively insensitive to measurement errors since it is not a deconvolution technique in the sense of inverting a FRF matrix as a function of frequency. Instead, the technique stacks up the FRF data into one large matrix with each new frequency representing an equation in this matrix which is used to determine the weights [147]. Weights determined by the SWAT Max-Flat algorithm would be equivalent to weights obtained by inversion of the mode-shape matrix in the traditional approach if both the used mode-shapes and the FRF data could be perfectly determined. In an experimental study [147], in which the SWAT Max-Flat approach was used to reconstruct the transient force experienced by a weapon impacting a rigid barrier, the method performed very well. In comparison with the traditional approach the Max-Flat variant showed similar accuracy but the data acquisition effort seems to be less.

The effectiveness of the different variants of SWAT have successfully been demonstrated for a variety of different engineering applications, e.g. [155],[156],[153],[154],[145],[147], mostly with respect to reconstructing forces of impact or collision events, and SWAT has become one of the most widely known TD force identification methods [100]. Since elegant theory exists for predicting its performance SWAT is sometimes used as a benchmark technique to evaluate the accuracy of other less popular TD force reconstruction approaches, see e.g. [144] or [108]. However, some **fundamental limitations inherent in the SWAT approach** restrict its more general utilisation. First, the method only allows reconstructing the sum of the external forces (and moments) acting on the structure's centre-of-mass, while the spatial distribution of the individual applied forces remains unknown. Second, since only the rigid body modes are considered by the modal filtration, the SWAT algorithm can only be applied to structures featuring free boundary conditions.

To overcome these hurdles Genaro and Rade [157] developed a more advanced method based on an extension to SWAT. Nordström and Larsson [103] refer to this extension as the '**partial modal matrix approach**'. The basic principle of this method still relies on applying modal filtering to structural time responses measured whilst the structure is exited by the external loading to be identified. The major difference is that Genaro and Rade's method considers both rigid body and elastic modes for which reason it can be applied to either free or constrained structures. Furthermore, it allows recovering multiple forces simultaneously so that the spatial distribution of the external forces can be retained [157]. In order to solve the

equations of motion for the unknown input forces, Genaro and Rade's technique requires (i) integration of the structural acceleration time signatures so as to generate corresponding velocity and displacement time responses as well as (ii) inversion of a partial modal matrix, which is generally well-conditioned if a convenient set of sensor locations is chosen. The effectiveness of the method and the effects of errors in the used data have been demonstrated for a simple test structure using numerical data only [157]. However, this application is to be considered as feasibility study and it does appear that no experimental application of Genaros and Rade's SWAT extension has been published yet. One essential limitation that may prohibit the general use of the method for experimental exercise is the number of required sensors which needs to be equal to or greater than the number of modes responding [132]. In particular, for complex or large structures with many closely spaced modes this constraint may be difficult to achieve.

2.4.4. Inverse filtering using state-space methods

A different way to address inverse force identification is to invoke multi-channel inverse filters in state-space form. These filters constitute mathematical models of the inverse structure in the sense that a set of responses observed on the physical structure, when applied to the inputs of the inverse filter, will produce an estimate of the associated actual exciting forces at the filter's outputs. State-space representation is used in order to collapse the continuous-time governing equations of motion for causal LTI MIMO systems into a more convenient and simple mathematical form. The differential equations can generally be reduced to a set of first-order differential equations in terms of input, output and state variables [35]. To avoid difficulties with integrating or differentiating measured (response) data to achieve state-space model representation, in most cases discrete-time state-space from is preferred to its continuous-time dual [108], as follows:

$$\begin{aligned} \mathbf{x}(k+1) &= \mathbf{A}\mathbf{x}(k) + \mathbf{B}\mathbf{u}(k) \\ \mathbf{y}(k) &= \mathbf{C}\mathbf{x}(k) + \mathbf{D}\mathbf{u}(k) \end{aligned} \tag{2.24}$$

where $\mathbf{x} \in \mathbb{R}^n$ is the state vector for the *n*-state system, $\mathbf{u} \in \mathbb{R}^s$ is the input vector considering *s* input forces, $\mathbf{y} \in \mathbb{R}^m$ is the output vector considering *m* structural responses and $\mathbf{A} \in \mathbb{R}^{n \times n}$, $\mathbf{B} \in \mathbb{R}^{n \times s}$, $\mathbf{C} \in \mathbb{R}^{m \times n}$ and $\mathbf{D} \in \mathbb{R}^{m \times s}$ are the state, the input, the output and the direct throughput matrices, respectively, which are determined by the properties of the physical (forward) system. Assuming zero initial conditions, the state-space representation in Eq. (2.24) can also

be stepped forward in time to write an expression for the pulse response of the forward structure

$$\mathbf{y}(k) = \sum_{i=0}^{k} \mathbf{H}_{MP}(i)\mathbf{u}(k-i) \tag{2.25}$$

where the Markov parameters $\mathbf{H}_{MP} \in \mathbb{R}^{m\times s}$ have the form [132],[114]

$$\mathbf{H}_{MP}(i) = \begin{cases} \mathbf{D} & i = 0 \\ \mathbf{C}\mathbf{A}^{i-1}\mathbf{B} & i = 1,2,\ldots,N \end{cases}. \tag{2.26}$$

From Eq (2.25) and (2.26) it is obvious that the Markov parameters represent the response of the discrete system to unit force pulses at the input locations; thus containing the dynamic properties of the (forward) structure which can be obtained from analysis or experiments [107]. It is further noted that Eq. (2.25) is in the form of a moving average representation which at each time step *k* provides the system output to an arbitrary input sequence $\{\mathbf{u}(k)\}_{k=0}^{N}$. Alternatively, this can be expressed in block matrix form

$$\begin{bmatrix} \mathbf{y}(N) \\ \mathbf{y}(N-1) \\ \vdots \\ \mathbf{y}(0) \end{bmatrix} = \underbrace{\begin{bmatrix} \mathbf{H}_{MP}(0) & \mathbf{H}_{MP}(1) & \cdots & \mathbf{H}_{MP}(N) \\ \mathbf{0} & \mathbf{H}_{MP}(0) & \cdots & \mathbf{H}_{MP}(N-1) \\ \vdots & \vdots & \ddots & \vdots \\ \mathbf{0} & \mathbf{0} & \cdots & \mathbf{H}_{MP}(0) \end{bmatrix}}_{\underline{\mathbf{H}}_{MP}} \begin{bmatrix} \mathbf{u}(N) \\ \mathbf{u}(N-1) \\ \vdots \\ \mathbf{u}(0) \end{bmatrix} \tag{2.27}$$

where the coefficient matrix $\underline{\mathbf{H}}_{MP}$ is in upper-block-triangular Toeplitz form and consists of $(N+1)\times(N+1)$ Markov parameter blocks, each of dimension $(m\times s)$.

In order to solve this deconvolution problem so as to estimate the time signatures of the input forces, two basic inverse filter approaches have been established. The first approach, pursued e.g. by Kammer [107], Steltzner et al. [158],[132] or Allen and Carne [144],[108], is known as the 'inverse structural filter' (ISF) method. In essence, the ISF approach is based on a manipulation of the forward state-space model in Eq. (2.24) in which the role of the input and output vectors are interchanged. This yields a state-space model of the inverse structural system in which the system dynamics are represented by the inverse system Markov parameters. The second approach tackles the deconvolution problem by solving the (forward) state-space form in Eq. (2.27) for the unknown input sequence which is achieved by inversion of the forward system Markov parameter block matrix $\underline{\mathbf{H}}_{MP}$. Both TD inverse filtering methods are discussed in more detail in the following.

The idea of time domain **inverse structural filtering (ISF)** in the context of indirect force identification was first presented by Kammer [107] who derived the basic ISF algorithm for MIMO structures with **collocated** force input and response measurement locations so that minimum phase forward system are maintained. By manipulating the linear discrete-time state space representation of the forward system (Eq. (2.24)) in such a way that the system's in- and output are interchanged, a causal MIMO moving average approximation of the input/output relationship for the inverse structural system can be found

$$\mathbf{u}(k) = \sum_{i=0}^{k} \mathbf{H}_{IMP}(i)\mathbf{y}(k-i) \tag{2.28}$$

where $\mathbf{H}_{IMP} \in \mathbb{R}^{s \times m}$ are the inverse structure Markov parameters. This can also be construed as a discrete filter that acts on the sampled response time data for which reason the term 'Inverse Structural Filter' (ISF) was suggested by Kammer [107]. The **causal finite length ISF** consist of the inverse system Markov parameters which can be thought of as a compressed generalized pulse response for the inverse structural system [159] representing the dynamic properties of the inverse system. To obtain the ISF, Kammer [107] uses a computationally intensive linear predictive scheme to estimate the corresponding inverse system Markov parameters from the associated forward system Markov parameters. In order to stabilise the computation of the inverse Markov parameters, which is sensitive to noise included in the forward Markov parameters, a Tikhonov regularisation technique is employed. The forward system Markov parameters are identified using force input data and response data from standard vibration tests of the physical structure. The obtained ISF then can be used to perform near real-time force estimation by simply convolving the operational response time histories measured on the physical structure with the obtained inverse system parameters. In [107], Kammer demonstrates the proposed ISF force reconstruction technique for a simple numerical model of a communication satellite for which the time signatures of six simulated input forces are successfully recovered from the same number of acceleration responses whilst noisy measurement conditions for the standard vibration test and the structural operation are assumed. However, the general use of the basic ISF force identification approach has shown to be limited due to the highly intensive computational effort, the sensitivity to noise of computing the inverse Markov parameters and, moreover, the requirement of collocation of the system's in- and outputs [107].

A **generalisation of the basic ISF** approach for MIMO systems with **non-collocated input/output pairs** is given by Steltzner and Kammer et al. in [158] and [132]. The method only requires as many response measurements as force input locations. Due to the non-collocation there is always a delay between impulses applied to the inputs of the physical system and their resulting responses measured by the remotely positioned sensors. As a consequence of this, at least one of the inputs does not have instant influence on any of the sensors causing at least the first Markov parameters ($\mathbf{H}_{MP}(i=0)$) of the non-minimum phase forward system to be rank deficient [114]. Thus, for non-collocated problems, the according inverse structural system is generally unstable [158]. To overcome this hurdle, Steltzner and Kammer et al. [132],[158] construct a non-causal '*l*-lead' inverse state-space model in which the time lead '*l*' is used to omit the contributions from the first *l*-1 Markov parameters to the output of the forward state-space model. The corresponding **non-causal finite length ISF** can be found from the modified inverse model as

$$\mathbf{u}(k) = \sum_{i=0}^{k} \mathbf{H}_{IMP}(i)\mathbf{y}(k-i+l)\,. \tag{2.29}$$

In practice, however, the computation of the non-causal ISF is not straightforward since (i) the measured and possibly ill-conditioned forward Markov parameters have to be inverted and (ii) the optimum non-causal lead, which is related to the wave travel times between the force input locations and the sensors, is problem dependent and thus has to be estimated for each structure. To solve these difficulties, Steltzner and Kammer et al. [132],[158] propose an empirical method to compute the non-causal ISF with optimum lead from the forward Markov parameters in which (i) the pseudo-inverse of the possibly ill-conditioned forward Markov parameters are calculated by a TSVD method and (ii) the resulting pseudo-inverse is pre-multiplied by a unit pulse sequence with a precedent *l*-length lag. While step (i) has to be performed only once for a structure, various ISFs each with a different non-causal lead *l* must be calculated by performing step (ii). The different ISFs (comprising different leads) then are evaluated using vibration test input / output data to generate force estimations for a known broadband input force. The ISF which performs best at reconstructing the vibration test force input sequence is chosen to be optimum and is ultimately used for the reconstruction of operational forces when the actual structure is placed in service [132]. The non-causal ISF force reconstruction approach was successfully tested by Steltzner and Kammer et al. [132], [158] for numerical simulated vibration tests of a SISO spring/mass chain in which a remote

accelerometer is used to estimate an input force and a MIMO FEM model to estimate six docking forces and moments between the Space Shuttle and the Russian MIR Space Station during a numerical simulation of a docking event. For the spring/mass chain Steltzner and Kammer et al. [132],[158] illustrate the ISF-dependent estimation error as a function of the non-causal lead *l*. As discussed by Nordström and Nordberg in [114], the large estimation errors apparent for either very small or very large time leads can be traced back to ill-conditioning of the first used Markov parameter and most likely to truncation effects associated with disregarding too many Markov parameters, respectively. Thus, the choice of the optimum ISF is very critical and requires extensive study of a variety of different non-causal leads. The usability of the method for experimental applications is investigated by Allen and Carne in [144],[108] where inverse structural filtering is employed to reconstruct the time signature of a single impact force applied to a free-free aluminium beam equipped with multiple non-collocated accelerometers. Although different non-causal leads were investigated, according to Steltzner and Kammer's empirical method, the force prediction only shows satisfying accuracy for the short duration of the transient impact event whilst the prediction contains a spurious, large amplitude ringing after the force impulse had ceased.

A slightly different formulation of the non-causal ISF force reconstruction algorithm is given by Allen and Carne in [144],[108]. They present an extension to the non-causal ISF, dubbed the **delayed, multi-step inverse structural filter** (DMISF), that utilises data from multiple time steps simultaneously to improve the accuracy and robustness of the ISF. Instead of deriving the ISF directly from experimental data using the proscribed technique [108] as suggested by Steltzner and Kammer in [158], the inverse structural filter in the DMISF approach is created from a forward system model that can be identified by any standard modal analysis algorithm [144]. In a comparison, based on Allen and Carne's beam experiment mentioned in the previous paragraph, the DMISF algorithm is shown to yield more robust reconstruction of the transient input force than Steltzner and Kammer's original ISF technique, although it is shown that the DMISF generally suffers from high sensitivity at its pole frequencies [108]. Although observed empirically, it is stressed in [108] that no general proof exists that the DMISF produces a more stable inverse system than the original ISF approach in every case. Furthermore, at the time, no other experimental application of either the original ISF or the DMISF algorithm seems to exist in literature, for which reason the general practicability of TD inverse structural filtering for sophisticated engineering

applications is arguable. Moreover, both methods will fail if some collocated and some non-collocated senor/force input pairs are used together so that the general applicability is further narrowed.

Nordström and Nordberg in [114] investigate a **time delay method to solve non-collocated input estimation problems**. The method uses essentially the same basic principle as the ISF or DMISF technique, i.e. the introduction of a *l*-step time delay in order to ignore the contributions from the first *l*-1 Markov parameters to the output of the forward state-space model so as to improve the conditioning of the structural parameters. Due to this conditioning it is possible to invert the modified upper-triangular-block Toeplitz matrix $\underline{\mathbf{H}}_{LMP}$ in the forward state-space model (cf. Eq. (2.27)) which now only consists of (full-rank) Markov parameters of the form $\mathbf{H}_{LMP}(i) = \left\{ \mathbf{C}\mathbf{A}^{i-1}\mathbf{B} \quad \forall\, i = l, \ldots, N \right\}$. In theory, the time-delay procedure can be used to recast the originally ill-posed deconvolution problem into a problem with a unique solution [114]. Unlike the original ISF approach or its DMISF variant Nordström and Nordberg's method utilises an independent time delay for each individual sensor which can help to improve the input estimation considerably. The time delay method is effectually demonstrated using different numerical examples of a one-dimensional spring/mass chain excited by two identical transient forces whilst response data is calculated for either collocated or non-collacated sensor set-ups. However, the choice of the individual sensor time delays is generally complicated and requires extensive calculations in order to find the best combination of time delays. With respect to the empirical method proposed by Steltzner and Kammer [158], which is seen to be the only possibility to evaluate the optimum combination, utilising individual time delays for force predictions for sophisticated structure-borne sound problems with a large number of non-collocated sensors seems to be impractical. Furthermore, no experimental example is shown in which the method is tested for noisy measurement data.

Nordberg and Gustafsson in [121] present a **block inversion algorithm** based on a modified dynamic programming approach to invert the forward Markov parameters, which are represented in upper block triangular Toeplitz matrix form (see Eq. (2.27)). For regularisation, the block inversion algorithm is combined with a damped least-square approach. The obtained regularisation procedure is called '**dynamic Tikhonov regularisation**'. The inversion routine can be employed to reconstruct input forces for large least square problems in the sense of inverse structural filtering. In [121] this block inversion algorithm is successfully employed to

recover dynamic forces from noisy responses based on a numerical spring/mass model with collocated in- and outputs. Note that the first Markov parameters of the forward system drop rank if non-collocated problems are treated so that inversion of the upper block triangular Toeplitz matrix is generally not possible. To overcome this difficulty, for non-collocated problems, the forward Markov parameters can be reformulated according to Nordström and Nordberg's time delay method [114]; incorporating all shortcomings of the time delay method, unfortunately. In exchange, dynamic Tikhonov reguralisation may then be applied to the conditioned full-rank Markov parameter matrix.

Irrespective of the variant used to perform indirect force identification based on TD state-space inverse filtering, the estimation accuracy in general depends on the proper choice of the Markov parameters considered by the inverse system. Both the correct choice of the non-causal lead(s) and the number of terms, i.e. the number of Markov parameters considered by the finite term approximation to the inverse model, influence the force reconstruction process. Considering first the **number of terms** used, it should be as great as is computationally feasible, although experience has shown that improvements in force estimates diminish as ISF size or generally the number of Markov parameters gets very large and numerical errors, matrix conditioning and other factors begin to dominate [132]. The other way round, incorporating not enough terms amounts to truncating the generalised impulse response of the state-space model too early so that important contributions may be missing in the force reconstruction when using the associated truncated inverse model. Regarding the choice of the **non-causal lead(s)**, finding an acceptable value may not be possible if the wave travel times between the force input locations and the sensors differ significantly. For the ISF and the DMISF approach the single (global) lead need to be chosen with respect to the longest signal transfer time from any input to its nearest sensor and the time delay method has been shown to fail for inappropriate sensor placements [114]. In general, overestimating the non-causal lead(s) will introduce truncation errors whereas underestimation will result in an unstable inversion process; each of which yielding erroneous force identification [108],[114],[158]. The general advice for using any of these methods is to position the sensors as near to the input locations as possible, partly to minimise the distortion of the signal from input to sensor, and partly to ensure that the signal from each input will reach a specific sensor ahead of the signals from all other input sources [114]. Yet, this advice seems to limit the general applicability of inverse structural filtering for many real-life situations. Furthermore, the

optimal size of the inverse filter, as employed by any of the reviewed methods, can be a function of the number of inputs and outputs, the number of modes and their damping, the bandwidth of the frequency range of interest or the noise characteristics, amongst others [132]. Thus, finding the optimal size of the inverse structural filter is a problem specific issue which, in practice, can only be solved by trial and error.

2.4.5. Kalman filtering

A different line of research to solve the inverse force identification problem in time domain has evolved from Kalman filter theory. The Kalman filter is based on the state-space analysis method. The underlying discrete-time state-space model of the system dynamics incorporate additive noise terms to model possible errors and uncertainties as follows [160]:

$$\begin{aligned} \mathbf{x}(k+1) &= \mathbf{\Lambda}\mathbf{x}(k) + \mathbf{\Gamma}\left[\mathbf{u}(k) + \mathbf{w}(k)\right] \\ \mathbf{z}(k+1) &= \mathbf{\Theta}\mathbf{x}(k) + \mathbf{v}(k) \end{aligned} \tag{2.30}$$

where $\mathbf{x} \in \mathbb{R}^n$ is the state vector for the *n*-state system, $\mathbf{u} \in \mathbb{R}^s$ is the input vector considering *s* input forces, $\mathbf{w} \in \mathbb{R}^s$ is the process noise vector, $\mathbf{z} \in \mathbb{R}^m$ is the observation vector, $\mathbf{v} \in \mathbb{R}^n$ is the measurement noise vector and $\mathbf{\Lambda} \in \mathbb{R}^{n \times n}$, $\mathbf{\Gamma} \in \mathbb{R}^{n \times s}$ and $\mathbf{\Theta} = \mathbf{I} \in \mathbb{R}^{n \times n}$ are the state transition, the input and the measurement matrices, respectively. Note that Eq. (2.30) is expressed in the form as it is used with respect to inverse force analysis by several researchers (see the references given below). Furthermore it is noted that the state transition and the input matrices are dependent on the properties of the physical system and that the Kalman filter requires knowledge of the process noise and the measurement noise vectors.

Based on this model the Kalman filter (KF) produces a statistically optimal estimate of the system's underlying state from a series of noisy measurements. The KF constitutes a recursive data-processing algorithm in the sense that it estimates the new system state by processing measurements as they arrive incorporating only the last estimate of the state rather than requiring the entire state history (opposed to batch processing where all data need to be available). The recursive nature of the KF allows for real-time state estimation, which makes it highly appealing for online time series analysis in various fields of engineering and control theory.

With respect to solving the inverse force identification problem, Ma et al. (1998) [126] implement the **simple Kalman filter (KF)** in conjunction with **a recursive least-square estimator (RLSE)** for online reconstruction of dynamic input forces acting on structural

systems. At each time step, the KF generates the residual innovation sequence (i.e. the prediction error in the observation signal, the Kalman gain and the innovation covariance) which is subsequently utilised by the RLSE algorithm to compute the onset time histories of the sought excitation forces [126],[161]. Note that Ma et al. adopted the KF-RLSE inverse routine from the earlier work of Tuan et al. (1996) [162] where the method was derived in order to solve two-dimensional inverse heat conduction problems.

In [126] Ma et al. employ the proposed KF-RLSE state-space method to identify impulsive loads for SDOF and MDOF lumped-mass structural systems with motion along a single axis. A different application of the KF-RLSE approach for a numerical model of a cantilever beam with a lumped mass on its free end is investigated in [161]. In both studies [126] and [161] the finite element method **(FEM) was used to construct the state equations** of the dynamic systems before the inverse force estimation scheme was employed. Furthermore, it is noted that both studies only deal with **collocated vibration problems**. Thus, only minimum phase systems are considered. Both feasibility studies [126],[161] demonstrate that the KF-RLSE inverse method can successfully be used to recover single and multiple input forces (featuring sinusoidal, rectangular, triangular or random signals, as well as, a series of impulses composed of these signal types) from (noisy) structural responses. For the presented applications the estimation accuracy is generally satisfying although some of the achieved results show constant time delays between the exact and the reconstructed force signatures. Unfortunately, no discussion on the suspected causes or possible remedy for these delays is provided. In the presence of large process and measurement noise ($\mathbf{w}$ and $\mathbf{v}$ in Eq. (2.30)) to which the Kalman filter is sensitive [163], the recursive inversion routine was found to be able to track changes in the applied input forces. However, the additional noise caused severe degradation of the estimation accuracy [161]. In [126] Ma et al. conclude that the inverse method generally requires high precision measurement data.

In [164] Ma et al. presented an experimental apparatus and conducted a series of **experiments on a physical cantilever beam** to identify steady-state periodic and random excitation forces applied at a single point on the beam. The estimation results have demonstrated the validity of the recursive inverse method for this specific experimental test. However, the state-space model of the beam employed was simplified to a single-degree-of-freedom lumped-mass system. Such a simplification cannot be made for sophisticated technical structures.

Another experimental application of the KS-RLSE approach is given by Liu et al. in [165].

They investigate the feasibility of the inverse method for on-line identification of **input forces** (sinusoidal and rectangular) **applied experimentally** at a single point **to a physical cantilever plate**. Besides addressing the collocated SISO vibration problem the inverse method is also demonstrated for inferring the time history of the unknown input force from a structural response measured at a **single non-collocated sensor position**. In order to obtain a discrete-time state-space model, Liu et al. employ a realisation based upon a linear time-domain identification technique with Markov parameters and Eigensystem Realization Algorithm (ERA) [166] yielding the unknown system dynamics based on experimental vibration tests. The KF-RLSE method is then adopted to reconstruct the unknown input force from the identified state matrices and measured operational response data. For both the collocated and the non-collocated vibration problem the time signature of the respective excitation force has been recovered accurately.

In [160] Ma et al. analyse the noise sensitivity and the tracking ability of the KF-RLSE technique for time-varying input events. Based on the regression model provided by the simple Kalman filter, a constant fading factor is used in the conventional RLSE formulation to estimate on-line the input loads involving measurement noise and modelling errors. This fading factor directly influences the convergence of the force estimation process. A small fading factor ensures fast tracking ability of transient input events at the expense of more noise in the estimation process whereas large values bring disturbances about being filtered out while the transient performance is slow. Thus, the correct choice of the fading factor is essential. In the conventional RLSE, this choice is performed heuristically based on an estimation of the transient status of the unknown input data. This procedure, however, requires a priori information about the sought input forces which in real-life applications is not available. It is noted that the fading factors in all previous studies [126],[164],[165],[161] are possibly tuned in such a way that the time history of the reconstructed input forces best approximates the original (known) excitations, although this fact is not explicitly discussed in the related literature. Hwang et al. [167] adumbrate the intricacy of finding the optimal fading factor and stress that laborious parametric studies are required when dealing with real-life force identification problems. To overcome these hurdles and to ensure a robust and efficient weighting input estimation algorithm, Ma et al. [160] introduce an adaptive fading factor which is controlled according to the residual innovation sequence provided at each time step by the simple Kalman filer. The Kalman filter in conjunction with the adaptive weighted

recursive least-square scheme is referred to as '**adaptive weighting input estimation' (AWIE)** algorithm. In a numerical feasibility study Ma et al. [160] utilise the AWIE algorithm to identify single and multiple impulsive forces for two lumped-mass systems with collocated response locations. In both cases the unknown input forces have been reconstructed satisfactorily. In an additional example the AWIE is employed to identify the impulsive input force applied to a cantilever beam with a single collocated input/output pair. FEM was used to construct the discrete-time state-space model of the dynamic system. For all tested excitations, i.e. a sinusoidal periodic load and single impulses of either rectangular or triangular shape, the estimation results show severe fluctuations. In [160] this phenomenon is interpreted to result from the complexity of the mathematical beam model and the small order of magnitudes of the input loads. With reference to an earlier study of Ma et al. [161], in which (i) the same finite element beam model, (ii) identical parameterisation (covariance matrix of measurement noise $\mathbf{v}$ and process noise $\mathbf{w}$, respectively) and (iii) almost identical force signatures with equal magnitudes are used, the AWIE results contain more noise than equivalent results obtained with the conventional KF-RLSE approach in which the fading factor was set to its optimum (tuned) value. Therefore, the merit of AWIE for general application cases seems not unambiguously be clarified. By all means, it can be argued that most real-life engineering applications likely require system models that outrun the complexity of the cantilever beam model by far.

Based upon the conventional KS-RLSE method Hwang et al. (2009) [167] developed an analytical (closed-form) procedure which facilitates identification of external modal loads using a limited number of structural responses. The **modal space force identification approach** may be reasonable in situations in which the mass, stiffness and damping matrices of the system are not fully known and the responses can be assumed to be dominated by the first fundamental structural mode only, e.g. in applications to wind excited buildings or slender structures. The method is evaluated through numerical analysis for SDOF and MDOF systems subjected to sinusoidal as well as vortex shedding induced (random) loads. The presented results show that the sensitivity of the identification method to measurement noise and errors in the estimated structural dynamic properties (damping and natural frequency) depends on the type of the sought input force. While the reconstruction of random input forces is relatively insensitive to these disturbances, identifications of sinusoidal loads are subject to high estimation errors. However, application of the modal space Kalman filtering

technique is restricted to very limited applications and is not practical for structure-borne sound problems where many modes are excited.

For completeness it is noted that some applications of the **Kalman filtering scheme for nonlinear inverse force identification problems** have also been published. An extended Kalman filter in conjunction with a tire model is utilised by Ray (1995) [168] to reconstruct nonlinear states and tyre forces for advanced vehicle control. Ma and Ho (2004) [169] and later Lin (2010) [170] generalise the previous work of Ma et al. [126],[116] for nonlinear force vibration problems. In essence, an extended Kalman filter in conjunction with the recursive least-square estimator (RLSE) is used for online estimation of the exciting forces in non-linear spring-mass-damper systems.

Although all presented inverse routines based on the Kalman filtering scheme have been proved to yield sufficient accurate force estimations for specific vibration problems, **inherent limitations prohibit the general applicability** of these methods for practical structure-borne sound problems.

First, a prerequisite for employing the Kalman filter is to **provide an accurate discrete-time state-space representation**, i.e. detailed state variable equations including the system dynamics [165], which poses major difficulties in practice. For relatively simple vibration problems, e.g. low frequency dynamic problems or beam- and plate-like structures with preferably low modal density and well separated modes, it may be feasible to obtain sufficient accurate mathematical models using **FEM methods** (Ma et al. [126],[161],[160]) or **analytical approaches** (Hwang et al. [167]), as discussed above. Unfortunately, the complexity of vibration problems involved in many practical engineering applications is too high to achieve reliable models in this way, in particular for structure-borne sound problems where many modes are excited and multiple input forces are applied to the physical structure. To overcome these hurdles, state-space system realisation algorithms may be employed to obtain discrete-time state space models from experimental vibration test data, as demonstrated by Liu et al. [165]. However, it is well-known that even modern and established **state-space system realisation methods**, such as the ERA technique as utilised by Liu et al. [165], which have shown to work very well for numerical simulations and experimental data for ‘simple’ structure-borne sound problems with well separated modes in frequency, may fail to identify adequate state-space models for complex engineering problems [171]. If not impractical, the identified models only represent approximations of the true systems and their validity depends

on numerous factors, such as the chosen model order, the length of the available and computational processible experimental data, the noise included in the measurements, the number of system in- and outputs as well as the modal density, overlap and damping of the physical system. Discussions and appropriate references concerning modern state-space system identification methods can be found in [109],[171] and [172], for instance.

Second, in all the above references the feasibility of Kalman filter state-space methods for inverse force identification has only be studied for vibration problems in which the number of considered response 'measurements' equals the number of input forces. According to the author's best knowledge, no application has been discussed for overdetermined structure-borne sound problems in which the number of responses exceeds the one of the unknown excitations. More important than this, within all studies satisfying force identification results have been achieved when considering response measurements from either collocated or non-collocated sensor positions. Yet, no study seems to exist in which multiple input forces are recovered from a set of responses which are recorded simultaneously at **collocated and non-collocated sensor positions**, as well. This problem, however, has been found to limit the applicability of other inverse state-space methods, such as the ISF [107][132], DMISF [108] or the time delay method [114]; all relying on sufficient state-space modelling and estimation of the system Markov parameters. For this reason, it is presumed that similar difficulties as discussed in section 2.4.4 may also limit the usability of Kalman filter state-space methods for general force identification problems.

Third, both the Kalman filter implementation and the associated recursive least-square algorithm rely on **optimal parameterisation** making the application for practical engineering problems difficult. On the one hand, the Kalman filter requires exact knowledge of the **process noise** covariance matrix and the **measurement noise** covariance matrix, each of which is generally not easy to determine in real engineering problems [160]. Furthermore, the measurement noise covariance matrix normally depends on the accuracy of the used instrumentation [126]. On the other hand, the sequential least-squares approach demands optimal choice of the **fading factor** in order to ensure good estimation accuracy while still being able to sufficiently track transient events in the input data [160]. To achieve good convergence in real engineering problems, the optimal choice of the fading factor involves an extensive parametric study [167], unless the adaptive weighting input estimation (AWIE) algorithm [160] is used. However, since only a few applications of the AWIE algorithm for

simple numerical vibration tests have been published so far, the feasibility of AWIE for real-life force identification problems is not clarified, yet.

In a nutshell, state-space methods based on Kalman filter theory are theoretically able to perform real-time inverse force analysis for multi-excited structures. However, due to several inherent limitations these methods have been found to be of limited use for inverse force identification in real-life engineering vibration problems. In essence, application of these inverse approaches, if practical at all, is cumbersome partly due to the requirement of providing an accurate system model in state-space form and partly due to parameterisation issues; both of which highly affect the convergence behaviour and the accuracy of the force identification process.

2.4.6. Sensitivity methods

Lu and Law in [173] present a TD inverse method that allows reconstructing the time signatures of multiple input forces from a single dynamic structural response assuming the force input and response locations are known. The input forces are approximated by Fourier series in which the higher orders are neglected so that only a finite number of parameters, i.e. the force magnitude and its circular frequency for each of the considered low order oscillations, are to be identified. In this way the inverse force identification problem can be thought of as a parameter identification problem. To identify these parameters, Liu and Law utilise a sensitivity-based method implemented in an iterative procedure. Starting with an initial guess of the unknown force parameters, the governing equations of the structure, expressed in finite element form, are employed to calculate the sensitivities of the dynamic response with respect to the unknown input force parameters. The obtained sensitivity matrix is then inverted employing a Tikhonov regularisation method before the pseudo-inverse is used to update the current parameter estimates by minimizing the difference between the dynamic response measured on the real structure and its reconstructed equivalent calculated from the latest update of the force parameters and the dynamic model of the structure.

A feasibility study of the proposed force identification method is given by Liu and Law in [173]. Using different numerical examples of a simple spring/mass chain excited by a single sinusoidal or alternatively a transient input force and a finite element model of a plane truss structure excited at two nodes by periodic forces, the accuracy and robustness of the sensitivity method has been demonstrated. The applicability of the method is further

investigated for a laboratory experiment in which measured structural responses from a steel beam under sinusoidal excitation and a dynamic model based on Euler–Bernoulli beam theory is used to identify the input force time signature. In all presented examples, the time domain sensitivity approach is found to yield satisfactory results even when the structural model contains initial model error and/or the measured data is polluted with noise. However, the general use of the method is restricted to situations in which a sufficient accurate dynamic model of the structure is available. This might be the case for low frequency dynamics problems but for structure-borne sound problems where many modes are excited application of the sensitivity method is not practical.

2.4.7. Adaptive method based on the LMS algorithm

In [174] Kropp and Larsson introduce a TD force identification technique based on an adaptive algorithm that seems to be less restrictive than most of the aforementioned methods. The main idea of the TD inverse routine is based on the Least Mean Square (LMS) algorithm which is widely used in adaptive filter theory due to its simplicity, flexibility and robustness [175]. The adaptive algorithm does not rely on inversion of a possibly ill-conditioned FRF matrix nor does it require extensive regularisation techniques to improve the solution as often required in FD inverse methods. Issues with finding appropriate regularisation parameters in this way can be avoided. Avoiding matrix inversion is further advantageous since ‘weak’ paths that bring about dominant contributions after inversion, which are highly susceptible to noise, can be circumvented. Instead, it is always the measurement point with the strongest signal that dominates the adaptive TD inversion process at a certain frequency. This, in general, makes the choice of appropriate measurement positions on the physical structure less crucial than in most of the aforementioned inverse force reconstruction techniques. Also, the adaptive TD inversion routine has been demonstrated suitable for dealing with collocated and non-collocated vibration problems or a mixture of these two [174]. Furthermore, the physical system is modelled by means of measured impulse response functions (IRF) which can easily be obtained from vibration tests utilising conventional system identification methods. This facilitates the use of the method for engineering applications dealing with even sophisticated structure-borne sound problems for which most of the abovementioned force identification techniques would fail.

In essence, the adaptive inversion routine can be thought of as a successive adjustment of a forward system model in which the measured IRFs assume the role of the inputs to the

system, the structural responses are the respective outputs and a set of adjustable system parameters account for a finite number of unknown coefficients that form the time signature of the input force to be identified. Starting with an arbitrary initial guess of the unknown input force time signature, the pre-measured IRFs are used to filter the predicted input forces so as to predict a set of estimated responses. The error between the estimated and true responses is then used to update the input force estimation recursively.

The validity of the adaptive force identification technique has been demonstrated in a couple of numerical and experimental examples for a freely suspended steel beam in [174]. The method has proved sufficient to yield robust and accurate reconstruction for both transient and stationary force signatures applied to structures with single degree of freedom excitation. However, a generalisation of the method facilitating simultaneous identification of force time histories for MDOF excited structures has not been published yet. Thus, achieving a generalisation of the adaptive TD inversion routine for MIMO systems is one of the main objectives of this thesis. The detailed derivation and a comprehensive validation of the MIMO inversion routine is presented in chapter 4 before its application is tested in chapter 5 for independent characterisation of transient structure-borne sound sources within electrical steering systems.

2.5. Summary and concluding remarks

Accurate characterisation of structure-borne sound sources, i.e. structures with some form of internal excitation, is crucial for predicting sound and vibration in assembled structures such as machinery, vehicles or for the specific purpose of transient sound source characterisation in electrical steering systems. Since source modelling is still insufficiently developed to handle such sophisticated structure-borne sound problems, independent source characterisation is only possible by utilising **experimental approaches**. In general, theses techniques require the measurement of **passive properties**, normally characterised by FRFs, such as mobility, impedance, receptance, admittance, dynamic stiffness and compliance, apparent mass and a variety of vibro-acoustic transfer functions, as well as **active properties** [51]. Different techniques to determine the activity of structure-borne sound sources based on measured data have been published. One line of research focuses on source characterisation in terms of power, using prediction approaches of which the source descriptor [63], the characteristic power, the mirror power or the maximum power [38] are most promising. A second line of research employs measurement approaches which commonly characterise the source activity

in terms of the free velocity [39],[84],[45] as standardised in [54] and the blocked force [85]. Unfortunately, measuring free velocity and blocked forces is not always straightforward due to several practical limitations [9],[51],[104]. Concerning first the **free velocity**, a major drawback of the method is that measurements on the operating source are to be carried out whilst it is separated from any rigid support structure [51]. In practice, this requirement prohibits characterisation of sources running under load or rather to account for internal excitation mechanisms inside active components that may vary with the external loading, e.g. the transient source mechanisms in electrical StSys. Employing the **blocked force** approach theoretically allows operating vibration sources under load, but large and rigid test rigs are required to approximate true blocked terminations over the entire frequency range of interest [9]. Difficulties also result from the fact that, at each point where source and receiver connect, up to three orthogonal forces and three moments about these axes exist so that direct measurement of all interfacial blocked quantities may not be practical for sophisticated multi-point-connected systems. Design and functionality issues of the source or potential alteration of the interfacial conditions may further prohibit non-reactive instrumentation into the flux of forces [105]. To overcome these hurdles, **operational forces** can be measured at the source receiver interface using inverse force synthesis [34]. Since the measurements are partially conducted in-situ, i.e. when source and receiver are coupled, realistic operation and mounting conditions can be achieved. Furthermore, no instrumentation within the sensitive contact zone of source and receiver is required. Yet, forces obtained in this way are not an independent property of the source but also depend on the structural dynamic properties of the connected receiver so that source characterisation is only possible for a specific installation [51]. A relatively new approach, known as the **in-situ blocked force method**, has the advantage that blocked forces can be obtained from measurements conducted in-situ on assembled machines, thus facilitating both practicability and independent source characterisation [9]. The method has proved successful for even complex technical applications [89],[94],[95],[96],[97],[10], [98],[99]. As with inverse force synthesis, the in-situ blocked force method employs inverse methods in frequency domain, in which measured structural responses are propagated back to the assumed known source regions by inverting matrices containing pre-measured FRFs. This, however, can be disadvantageous in some respects.

First, the **inversion problem** is well known to be ill-posed and solutions based on frequency domain methods have been shown to suffer from numerical ill-conditioning at frequencies

associated with the natural frequencies of the structures. Furthermore, the inversion process is sensitive to measurement noise [132]. Usually, the robustness of such solutions has to be improved artificially by applying some form of regularisation (see amongst many examples [20]). Second, tackling source characterisation in frequency domain could lead to **obscuring some essential features** of the originating source mechanisms, such as excitations carrying impulsive, irregular or modulated temporal structures, as these are generally hard to catch in frequency domain [19]. Finally, characterisation of sources **which are operated under non-stationary conditions** like engine run-ups/run-downs turns out not to be straightforward in frequency domain [86].

On the contrary, the challenges in the inverse problem are manifested differently in time domain so that more accurate and robust solutions may be found by formulating the problem in the time domain. Besides, **time domain methods** could possibly account for all types of source mechanisms in equal measure, e.g. periodic, random or transient excitation, and would make handling of non-stationary operation conditions easy. Furthermore, time domain source characterisation would yield continuous time signatures of arbitrary length allowing all sorts of post-processing for each particular source which is an attractive prospect for many industrial demands, such as time domain TPA [19],[86], auralisation purposes [6] or condition monitoring [176] amongst others.

A number of **time-domain approaches** for solving the inverse problem associated with indirect force measurement can be found in literature including direct **deconvolution techniques** (see references in section 2.4.2), **modal filtering** (section 2.4.3), **inverse filtering** (section. 2.4.4) and **Kalman filtering** (section 2.4.5) both of which are based on state-space methods, as well as **sensitivity methods** (section 2.4.6). However, most of them lack generality with respect to the underlying assumptions, the way they describe the physical system or the need for additional information to parameterise the algorithms. Thus, these inverse force identification methods are not practicable for sophisticated structure-borne sound problems. Kropp and Larsson [174] introduced a time domain inversion routine based on an adaptive algorithm that seems to be less restrictive (section 2.4.7). However, so far the method has only been studied for relatively simple structures with single-degree of freedom excitation.

Given the above discussion, there could be significant potential advantages in developing a robust time domain inversion routine based on an expansion of Kropp and Larsson's adaptive

algorithm that is capable of calculating simultaneous multi-channel blocked force signatures from measurement made in-situ. One of the main objectives of this thesis is to derive such a generalisation and to demonstrate its applicability for independent source characterisation using a time domain representation of the in-situ blocked force method with respect to transient sound generation in electrical steering systems. Both issues, the generalisation of the time domain inversion routine (see chapter 4) and its application in independent source characterisation (see chapter 5) are believed to be original.

Chapter 3

Identification of internal source locations

3.1. Introduction

As outlined in chapter 1, rigorous reduction of the overall driving noises, such as powertrain, tyre-road and aerodynamic induced noise, has been achieved within the last two decades. In this way, some air-, fluid- and structure-borne sound sources which were formerly less important, such as electric powered steering systems (EPS), have become relatively more important for NVH design.

In this chapter the role of electrical steering system as structure-borne sound sources in vehicles is discussed. Based on the EPSapa PL2 steering system, which will invariably be used within this study, emphasis is placed on the basic design and functional principle of electric powered steering systems in section 3.2. The fundamental mechanisms and the associated sound phenomena of steering induced structure-borne sound are elaborated in section 3.3. A methodology and a conceptual model for identifying possible transient sound sources within electrical steering systems is discussed in section 3.4 before a summary of the most important findings is given in section 3.5.

3.2. Electric power steering systems

One major characteristic of power-driven vehicles is the ability to change lane or more generally to steer independently of external lane restrictions as in the case of rail transport for instance. To guide and direct a vehicle steering systems (StSys) are required which are understood as the entire mechanism consisting of the steering wheel, steering column, steering gear and tie rods (see Figure 3.2 - (a)). As part of the chassis suspension the steering system constitutes a major subsystem for vehicle operation which transmits dynamic forces between the vehicle superstructure and the road. Typically, the suspension system is designed to handle all vertical, longitudinal and lateral dynamics of the vehicle superstructure. However, the lateral dynamics, i.e. rotation about the vertical axis passing through the car’s centre of gravity (yaw) and movements in lateral direction, are essentially governed by the StSys in combination with the wheel suspensions and the wheels [177].

In general, one can distinguish between mechanical steering systems which are operated manually by the driver and power steering systems that assist the driver in turning the steering wheel in situations where considerable steering effort is required, e.g. in large vehicles

particularly when the vehicle is stopped or moving slowly [178]. Within the last few decades, rotary valve hydraulic power steering systems have been most widely used for passengers cars. However, since these conventional hydraulic power steering systems (HPS) are permanently powered by the engine, HPS systems decrease the engine efficiency and further require additional space-consuming hydraulic components like pumps, drive belts and hoses for operation [179]

Electric powered steering systems (EPS) are more recent developments and are superior to conventional HPS systems, in many respects. EPS systems use compact electronic controlled and engine-independent electrical motors which only consume energy while power steering is performed. Due to the functional principle and the compact design EPS systems have distinct advantages with respect to energy-consumption (90% less than HPS [180]) and emission, ease of installation and modular design, maintenance considerations, ease of integration in modern electronic control systems (e.g. Antilock Braking System (ABS), Electronic Stability Program (ESP), Automatic Parking Assistant, Lane Keeping Assistant etc.) as well as improved response characteristics to vehicle dynamics and handling [178],[179],[180],[181],[14]. For these reasons, EPS systems have become very popular in recent years, especially with respect to passengers cars since here the required steering forces (from 3 kN for subcompact cars up to 16 kN for upper-class cars and vans [180]) can sufficiently be provided by electric motors in combination with different types of gear systems. The electric motor together with the respective gear system constitutes the so-called servo unit. According to the position of the servo unit distinction between three basic types of EPS systems is common (see Figure 3.1).

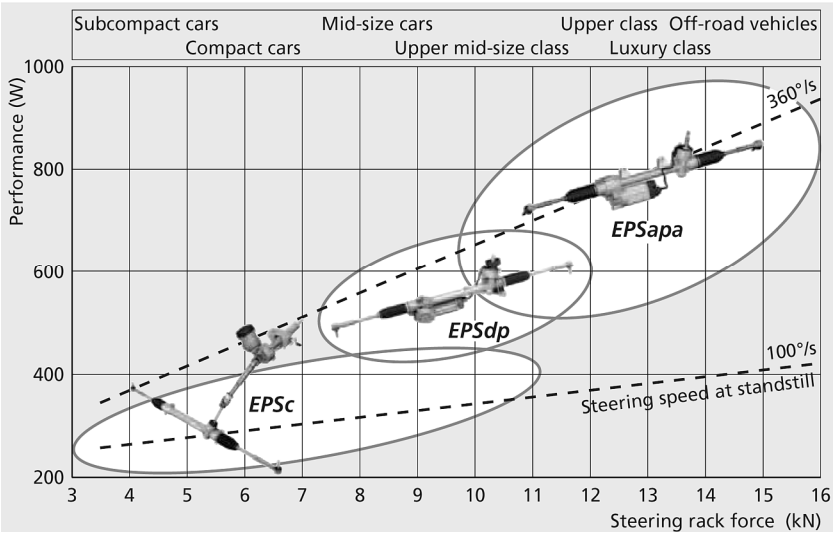

Figure 3.1. Application areas of different EPS systems according to standard values of steering rack force and mechanical performance for all vehicle classes [180].

Dependent on the installation space available and the steering rack forces required, the servo unit can be mounted on the steering column (EPSc), on a second pinion (EPSdp) or in parallel to the steering rack (EPSapa) [180]. Although each type of EPS system features a different design they are all based on the same functional principle. As this thesis invariably deals with EPSapa systems the design and the fundamental functional principle of electrical steering systems is explained using the example of an electrical steering system with paraxial servo unit, in the following. However, it is emphasised that all general approaches presented in this thesis are valid for any other type of electric steering system or other structure-borne sound sources as well.

3.2.1. The functional principle

Within this research project an electric powered steering system with paraxial servo unit (EPSapa) is used. The chosen EPSapa system is in mass production at ZFLS and embedded in a BMW (platform 2- PL2) compact class vehicle. A typical schematic diagram and an illustration of the physical assembly of the EPSapa PL2 system is given in Figure 3.2.

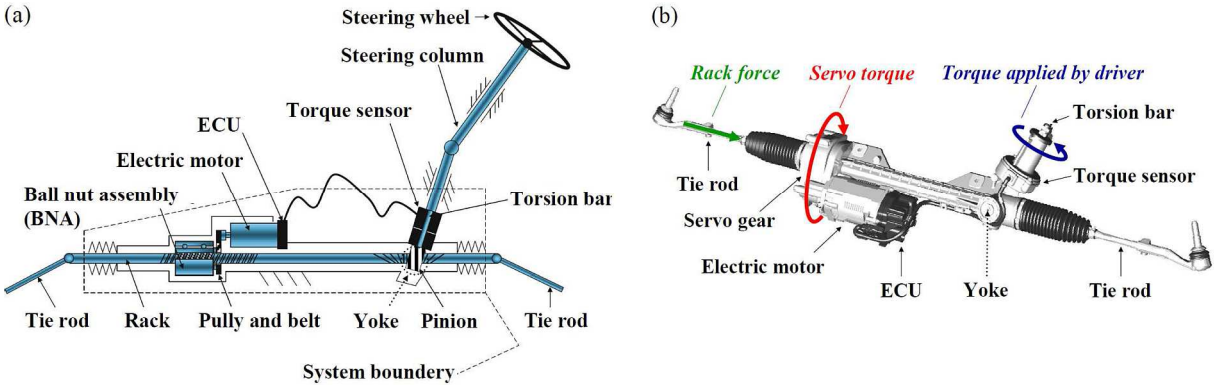

Figure 3.2. The electrical steering system EPSapa PL2: Schematic diagram [2] (a) and illustration of the physical assembly of the steering gear including the acting loads (b).

The EPSapa system is based on the rack and pinion principle which is known as the most advanced steering solution to date [178],[180],[2]. Neglecting first any mechanism powering the steering process, rack and pinion systems are essentially based on the following principle: The steering wheel is connected via the steering column to a round gear, the so-called pinion. If the driver turns the steering wheel the pinion is rotated and in turn drives a straight bar with gear teeth, the so-called rack, that meshes with the pinion. In this way the rotatory motion of the pinion is transformed into a translatory (side-to-side) motion of the rack so that the wheels, which are connected to the rack via the tie rods, are turned. In order to ensure zero-

play tooth meshing between pinion and rack whilst serving as zero-play sliding contact bearing for the translatory moving rack at the same time, a spring-loaded pressure piece, the so-called yoke, is used to push rack and pinion together. Hence, conventional rack and pinion steering systems rely on a very simple construction comprising only a very few moving parts. For this reason they generally tend to be light weight, very precise, highly responsive, easy to control and further provide direct feedback from the road [2].

EPS systems supplement the fundamental rack and pinion principle with an electromechanical servo unit providing power assistance to move the steering rack according to the instantaneous driving conditions. To do so, the electronic control unit (ECU) registers and processes a wide range of parameters like road speed, steering angle, steering torque and steering speed for instance. Parameters related to the steering process which are induced by the driver are measured by sensors directly built in the steering system such as the torque sensor in combination with the torsion bar. As soon as the driver turns the steering wheel the data is registered and processed on-line by the ECU in order to calculate the required steering assistance. Based on the calculated control commands the electric motor is operated and the servo gear system transmits the optimum servo torque and transforms it into a lateral force which is then superposed to the steering force applied by the driver so as to assist the driver moving the rack in lateral direction. The functional principle of electric power assisted steering is summarised by the block diagram in Figure 3.3.

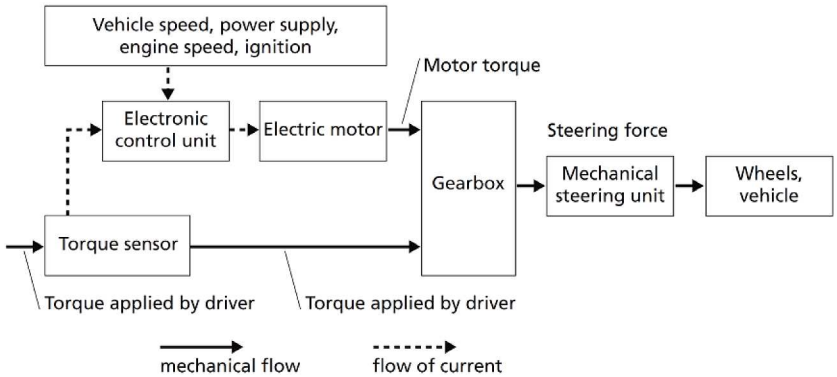

Figure 3.3. Functional block diagram of electric power assisted steering [180]

As illustrated, under normal conditions the torque applied by the driver to the gear is superposed by the motor torque. In case that the vehicle power supply fails or the flow of current is interrupted the mechanical connection between the steering wheel and the steered wheels still enables the driver to continue steering the vehicle (see also Figure 3.2). Accordingly, the mechanical flow, as indicated by solid lines, in the latter case is identical to

the one in conventional rack and pinion steering systems that do not feature mechanisms to perform power assisted steering.

In case of electric power steering systems with paraxial servo unit (EPSapa) the servo gear system consists of a two stage drive concept, as illustrated in Figure 3.4. The first stage is constructed as a slip-free toothed belt drive, i.e. the electrical motor powers a small toothed disc (3) meshing with the toothed belt (2) that drives the big toothed disc (4) to which the second transmission gear is connected. The second drive stage consists of a recirculating ball gear in which the ball chain is returned through a channel (7) integrated in the steering nut (5) [180]. Forces and moments induced by the steering nut in and about axial as well as radial directions, respectively, are supported via the ball screw bearing (6) by the housing of the steering system. By contrast, the rack (1) is able to move freely in its longitudinal direction so that the resultant forces induced by the rotating steering nut finally drives the rack. In this way the original rotational movement of the electric motor is transformed into a linear movement of the steering rack.

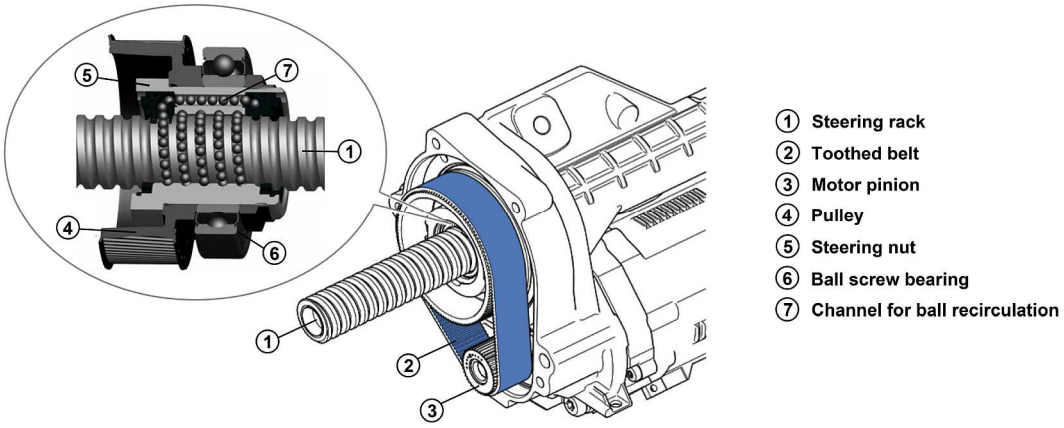

Figure 3.4. Configuration of servo gear system in EPS with paraxial servo unit.

The EPSapa two-stage servo gear system allows efficiently transmitting high torques while consuming minimum space in the physical assembly. Another advantage of this concept is that low noise performance during operation of the overall servo unit can be achieved [180],[2]. Note that low noise performance in this respect is purely related to functional steering sound (see section 3.3.1). However, the low noise generation of the servo unit legitimates connecting the entire steering gear rigidly to the subframe of the vehicle which is aimed so as to ensure a direct steering feel and road feedback, respectively [180]. Unfortunately, connecting the steering gear rigidly to the subframe or to any other part of the vehicle, such as the wheel suspension via the tie rods or the vehicle body through the steering

column as explained in section 1.4 can become problematic if structure-borne sound is originated inside the steering gear due to some unforeseen phenomena which are independent on the functional principle or rather the operation of the steering gear. Elaborating the specific mechanisms and the associated sound phenomena as well as the respective conditions under which structure-borne sound may be originated within electrical steering systems is task of the following sections.

3.3. Sound phenomena induced by electrical steering systems

A diversity of subjective factors affects the passenger's perception and assessment of steering induced structure-borne sound which, under certain conditions, can become audible inside the passenger compartment. The individual degree of satisfaction in this context is strongly related to whether a specific sound phenomenon is seen to be caused by a steering manoeuvre or not. Therefore, subdividing steering induced structure-borne sound into two classes is worthwhile, as discussed in the following.

3.3.1. Functional steering sound

The first class of steering induced sound phenomena comprises all structure-borne sound phenomena that are provoked by deterministic internal dynamic forces due to the expected operation of the steering system. The term 'expected operation' is used to signify that sound immission in the cabin correlates with the actual steering manoeuvre performed by the driver. The underlying mechanisms for the origination of structure-borne sound inside the steering system in this case depend on the inherent functional principles of the steering system. Thus, all sound phenomena associated with this type of steering induced sound are referred to as 'functional steering sound'. It is noted that external loading, e.g. tie rod forces induced by dynamic steering, may influence the intensity of the perceived functional steering.

The most significant source mechanisms of functional steering sound can be traced back to oscillating forces excited inside the steering system in consequence of rotating components or component assemblies. These forces may either be caused by mechanical or electro-magnetic effects and feature rotation speed-dependent characteristics. Typical phenomena of functional steering sounds in electric powered steering systems are

- noise caused by electro-magnetic forces within the electric motor [2],[182],[183]
- engagement noise caused by the meshing of pinion and gear rack [2],[12],[184]

- noise caused by the belt drive due to interactions between pulley and belt [2],[185],[186]
- noise caused by imperfect ball-bearings [2]

The distinct dependency of these phenomena on the rotation speed can effectively be used to identify dominant sources of functional steering sound inside electrical steering systems. Since the steering system can be considered as a linear system (section 2.2), periodic excitation provoked by a distinct source mechanism inside the steering system always yields a periodic response at the same frequency. This response may either constitute a perceivable sound at the driver's ear, e.g. when the steering system is operated in the car, or a vibration response measured on the housing, e.g. when the steering system is operated on a test bench. Considering the gear transmission ratios between each rotating component and the motor shaft as well as the actual rotation speed of the electric motor to be known, dominant internal sources of functional steering sound can be identified by applying spectral analysis or order tracking analysis to the measured responses. By way of example, Figure 3.5 illustrates the typical characteristics of steering induced sound immission in vehicles for standstill steering manoeuvres.

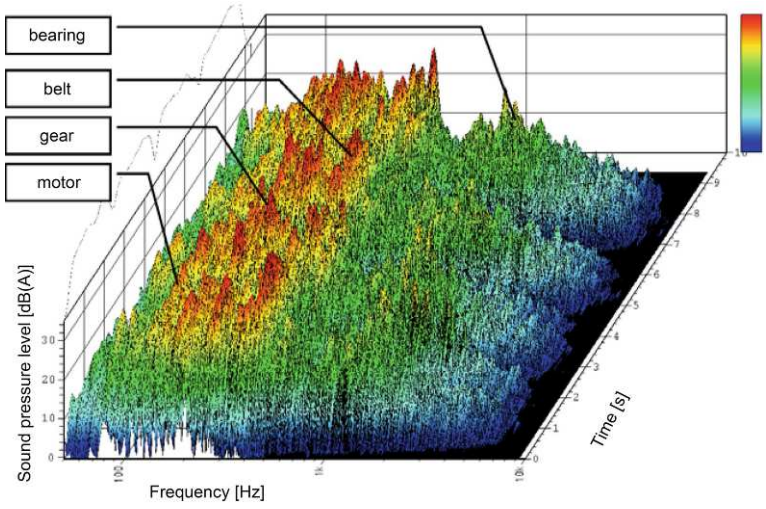

Figure 3.5. Spectogram (frequency vs. time) of sound pressure level measured inside the passenger compartment and order contributions from associated functional steering sound sources [2].

Clearly, the most significant sources of functional steering sound (motor, gear, belt, bearings) can distinctively be identified from the measured interior sound pressure level. As a corollary of this, the descriptive order contribution from each particular sound source can be utilized as performance criterion to review NVH specifications of assembled steering systems. Thus, at ZFLS specially designed test procedures based on end-of-line testing are employed to monitor quality and functionality of each produced steering system.

Recalling section (section 1.3) one can summarize that functional steering sound typically does not pose high risk for complaints, as contributions from the associated internal sources to the overall cabin sound are insignificant under normal driving conditions and if functional steering sound is perceived by the passenger, e.g. when performing standstill steering or parking manoeuvres, its occurrence can directly be related to the actual mode of operation of the steering system. However, it is stressed that all theoretical and practical approaches presented in this thesis are generally valid for any structure-borne sound problem irrespective of its origin.

3.3.2. Interfering steering sound

All structure-borne sound phenomena perceivable inside the passenger compartment that are not directly related to an actual steering manoeuvre, or more generally, that do not correlate with the physical mode of operation of the steering system are classified as ‘interfering steering sound’ in the following. Since sound phenomena of this category are not expected by passengers inside the car they are most likely to be perceived as unpleasant, disturbing or interfering [37]. Usually their perception is assessed as an annoyance; thus posing high risk for complaints. Once a disturbance is perceived it is believed that this can draw attention and increase annoyance further [177]. However, the way an unexpected disturbance is perceived and assessed by a passenger depends on a diversity of factors, such as the probability of occurrence, the intensity, the characteristics, the time duration or the personal association of the perceived sound phenomenon [1],[2],[177].

In the context of sound emission from electric power steering systems, different physical mechanisms exist that can give rise to structure-borne sound phenomena associated with interfering steering sound. By way of example, distinct tonal disturbances can result from self-excited transversal belt vibration when passing through critical steering speeds so that the tooth engagement frequency coincides with the resonance frequency of the belt strand [187]. However, as with functional steering sound such tonal phenomena can readily be addressed, e.g. by employing spectral analysis to identify the respective structure-borne sound sources inside the steering system, since the natural frequency of the installed belts are known. Furthermore, the underlying excitation mechanisms as well as the critical operation conditions of the steering system are well understood and various physical parameters in the control of

designers and engineers allow the risk of provoking such steering induced noise to be minimised.

By contrast, addressing the problem of steering induced ‘contact noise’ is much more difficult. For example, unique determination of the operation conditions under which contact noise is provoked within electrical steering systems is not possible since a diversity of uncontrollable factors influence the internal excitation mechanisms. In addition, sound phenomena associated with contact noise can exhibit a wide range of different characteristics, including high intensity transient and impulsive sound characteristics which are known to have substantial disruption potential [2]. Hence, the occurrence of steering induced contact noise is generally critical. In the following the most important source mechanisms and influencing factors responsible for the generation of contact noise in electrical steering systems are discussed.

3.3.3. Contact noise

The fundamental generation mechanisms of contact noise originated inside electrical steering systems can be attributed to internal time-varying forces provoked at the contact interface between two adjacent components due to unpredictable relative movement between one and the other. Thus, contact noise can only be originated if the following two conditions are fulfilled at the same time: (i) adjoining components or component assemblies inside the steering system have to physically contact each other and (ii) relative movement between these components has to be enforced by some form of primary excitation in order to provoke secondary reactive forces at their contact interface that ultimately generate structure-borne sound. It is stressed that the locations of primary excitation are not collocated with the source regions inside the steering system at which contact noise is originated.

According to Zeller [177] and Steinberg [1],[37], two fundamental physical mechanisms are known that provoke structure-borne contact noise within mechanical structures; namely stick-slip vibrations induced by dry friction and vibrations excited by impacting assemblies. Both phenomena emerge as non-stationary or transient sound events at random times, as elaborated below with respect to the generation of steering induced contact noise.

Stick-slip phenomenon

The phenomenon of stick-slip describes self-sustained vibrations induced by dry friction between two contacting surfaces that are alternately at rest (stick mode) and in sliding motion

(slip mode) with respect to each other. The abrupt transition from one mode to the other induces time-varying frictional forces within the contact zone [188],[189]. Depending on the structural dynamic properties of the interfacing structures, these dynamic contact forces ultimately give rise to structure-borne sound, i.e. stick-slip noise. The physical principle and the interrelated internal forces are schematised in Figure 3.6 - (a).

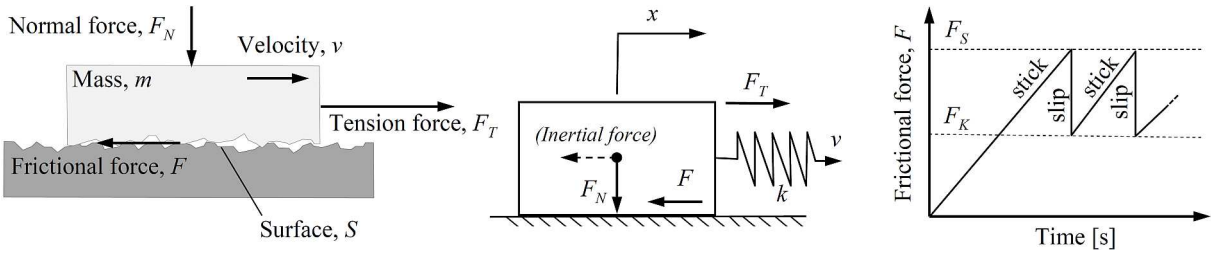

(a) (b) (c)

Figure 3.6. (a) Stick-slip phenomenon: Schematic illustration of the physical relationship between interfacing solids ; (b) simple mass-spring-model of interfacial relationship and (c) schematic of oscillating friction forces responsible for the generation of stick-slip noise.

The most simple model for explaining the fundamental mechanism of stick-slip vibration is given by the single degree of freedom mass-spring system depicted in Figure 3.6 - (b). A mass (m) attached to a spring (k) is pulled by an external tension force (F_T) over a solid surface (S) so as to move the spring at a constant velocity (v). It is noted that the spring accounts for elastic deformation occurring in real structures at the contact between two interacting surfaces.

In equilibrium, the mass is stationary on the surface and the contact between them results from the normal force F_N acting perpendicular to the surface. As soon as the external driving mechanism starts pulling the spring, dry friction appears as a resistance against the beginning of the motion so that the mass remains stationary on the surface (stick mode) [188]. The associated constraining force, the so-called static frictional resistance F_S, is given by

$$F_S = \mu_S \cdot F_N \tag{3.1}$$

where μ_s is the coefficient of static friction at the contact area and F_N is the normal force. As a result of the mass sticking to the surface and the ongoing driving mechanism, the spring is loaded and its tension (F_T) increases until the static frictional resistance F_S is not able to hold the mass at rest anymore. When the mass starts sliding over the surface (slip mode) the frictional resistance decreases abruptly due to the transition from static to dynamic friction behaviour. Since the kinematic friction is far less than the static friction, the spring powers the

mass by releasing energy stored in the stressed spring so as to accelerate the mass which, as a result, moves at a velocity ($\dot{x}$) faster than that of the spring. Note that the relative velocity between the mass and the spring is defined as the slip velocity ($v - \dot{x}$). Accordingly, sliding of the mass over the surface brings the spring about decreasing its tension until the restoring force is insufficient to counterbalance the prevailing kinematic frictional resistance, which is considered as an applied force in the slip mode [188]. However, due to the kinematic friction resistance F_K, given by

$$F_K = \mu_K \cdot F_N \tag{3.2}$$

where μ_K is the kinematic friction coefficient satisfying the condition $\mu_K < \mu_S$, exceeding the driving tension force, the mass is decelerated and again comes to rest (stick-mode). Hence, a single stick-slip cycle, represented by the mentioned processes, involves a stick state associated with elastic loading of the system followed by an abrupt slip corresponding to stress relaxation [189].

Assuming that constant velocity traction applied to the mass is maintained by the external driving mechanism both phenomena stick and slip take place successively, resulting in stick-slip oscillations. In Figure 3.6 - (c) the characteristic sawtooth evolution of the associated frictional contact force is illustrated for two complete stick-slip cycles. The distinct impulsive behaviour results from the significant different friction characteristics related to the stick and the slip mode, respectively. As a result, the interfacial friction force can only take values between the limiting values given by the corresponding friction resistances as defined in equation (3.1) and (3.2).

If the interfacial oscillations are sufficient to excite neighbouring structures, the impulsive nature of the friction force emerges as likewise transient structure-borne sound phenomena. However, the ultimate characteristics of this so-called stick-slip noise are influenced by a variety of factors, such as the normal force (F_N), the relative (slip) velocity between the sliding surfaces ($v - \dot{x}$) and the interfacial friction behaviour (μ_S and μ_K) which again depends on the nature of the surfaces in contact, i.e. material properties, geometry or roughness. Some of these parameters may even be functions of external factors such as temperature or time [190]. Moreover, the dynamic properties of the corresponding transmission paths as well as the nature of the external driving mechanism, which is required to initiate stick-slip vibration, essentially govern the characteristic of the emitted structure-borne sound phenomena.

Due to the diversity of factors influencing stick-slip phenomena the emitted sounds can exhibit a multitude of different characteristics which, according to their temporal signal structure and frequency content amongst others, are known as ‘creaking’, ’grinding’, ‘cracking’ or ‘squeaking’ [1],[177]. In the context of steering induced contact noise stick-slip noise is usually referred to as ‘groaning’. Note that the sound phenomenon of groaning is often said to sound similar to the noise one hears when opening an old wooden door [177]. Groaning mostly results from insufficient or partial lubrication between adjacent assemblies, such as

- yoke and housing [191],[2]
- sliding film of the yoke and rack [2]
- the peripheral surface of the bearing ring and housing [191], [192]
- motor and motor flange [193].

By way of example, a stick-slip excited structural response measured on the housing of an EPSapa steering system is depicted in Figure 3.7. Note that the acceleration response is plotted in which the characteristic sawtooth evolution of the contact force cannot be seen.

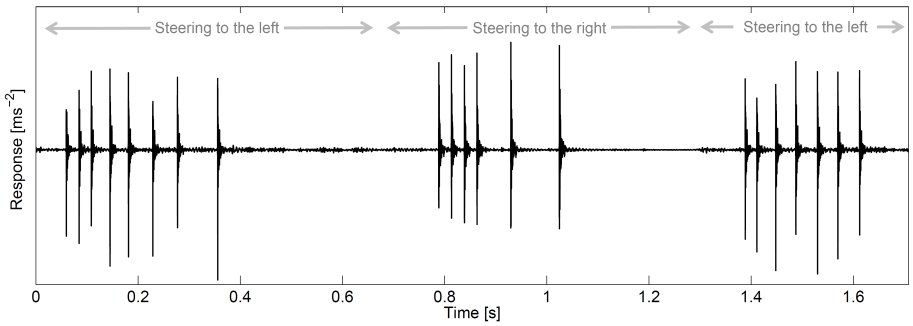

Figure 3.7. Groaning in EPS systems: Impulsive structural response (measured on the steering housing) resulting from stick-slip between bearing ring and housing while alternating left-right-steering is performed.

As a result of dynamic loading, provoked inside the steering gear by alternating left-right steering around the straight-ahead position, the bearing ring is moved relative to the contacting housing so that stick-slip can occur at its peripheral surface in the case of insufficient or partial lubrication of their interface. The impulsive response signal is characteristic for steering induced stick-slip vibration and the associated groaning noise.

Impact phenomenon

The interrelated processes of adjacent structures colliding with each other and the associated emission of interfering sound, the so-called ‘impact noise’, is referred to as ‘impact

phenomenon'. Harnemik and Hsueh [194] describe impact noise as noise transients provoked by impacts between objects which are essentially the result of a rapid release of energy through primarily mechanical mechanisms. In this context, Steinberg in [1] and [37] distinguishes between the following two mechanisms: First, the colliding structures induce transient forces that can excite structure-borne sound in one or both of the interacting structures. Audible sound in this case results from radiation of sound by vibrating surfaces that do not necessarily have to coincide with the location of impact within the contact zone. Second, the temporary contact between the objects causes impulsive air displacement from the contact zone resulting in density fluctuations in the surrounding air which ultimately provoke emission of airborne sound. However, in the context of interfering steering system sound the contribution of airborne impact noise to the interior vehicle sound is insignificant so that only sources of structure-borne impact noise will be considered in this study.

In order to provoke impact between objects two conditions need to be satisfied. First, the interacting structures need to be separated from each other prior to the impact. A characteristic of this state is the initial separation gap between the structures which in mechanical structures may be understood as clearance between two neighbouring assemblies. Second, some form of driving mechanism need to be present in order to provide energy for initiating the impact. This energy may either be required to separate adjacent structures from each other, which under normal operation conditions are in contact by design, e.g. preloaded assembly groups like pinion, rack and pressure piece in EPS (see Figure 3.10 and Figure 3.11 – PY domain), or to overcome an already existing gap between the structures, e.g. clearance between balls and ball nut (see Figure 3.10 and Figure 3.11 – BNA domain).

In [1] and [37] Steinberg stresses that the vast majority of impact phenomena occurring within mechanical structures can be considered as linear and time invariant problems if a mode of operation according to the design specification can be assumed. Thus, only elastic deformation in the contact zone is considered. This assumption is invariably adopted throughout this study. Based on this assumption Steinberg exemplifies the complex impact phenomenon utilising simple linear spring-mass systems with viscous damping, as depicted in Figure 3.8.

Accordingly, the fundamental principles of the impact phenomenon occurring within mechanical structures can be best described by dividing the problem into two interlinked

models accounting for the different states (separation and contact) that can be adopted by the interacting structures.

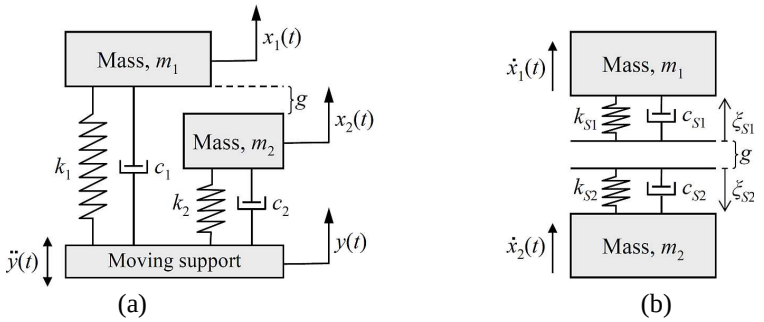

Figure 3.8. Impact phenomenon: (a) Exemplary model of driving mechanism forcing two neighbouring ‘inactive’ objects to vibrate; (b) Contact model descriptive for the duration of the impact between ‘active’ components.

The first model (Figure 3.8 - (a)) is to describe the underlying driving mechanism (here: support excitation with acceleration $\ddot{y}(t)$) which forces the neighbouring uncoupled bodies to vibrate while they are considered to be ‘inactive’, i.e. the moving bodies do not exert forces on each other. The variables *m*, *k* and *c* refer to mass, stiffness and damping of the corresponding structures respectively. Note that in this example both bodies are separated from each other prior to the impact, indicated by the gap (*g*). However similar models can be found for pre-loaded assembly groups, as discussed above, or for force excitation.

As soon as contact between both bodies is detected the ‘contact model’ (Figure 3.8 - (b)) can be used to describe the relationship governing the impact event. During contact both systems from Figure 3.8 - (a) are coupled; thus a two degree of freedom system is given. The input of the contact model is given by the output of the first model that is the kinetic energy of both bodies (mass *m* and velocity $\dot{x}(t)$). Elastic deformation within the contact zone is considered by utilising Kelvin-Voigt models, i.e. an elastic spring and a purely viscous damper connected in parallel. Their function with regard to Figure 3.8 - (b) can be explained as follows: The springs (k_{S1} and k_{S2}), describing the stiffness of each surface, are assumed only to support compressive but not tensile forces. The parallel dampers (c_{S1} and c_{S2}) account for energy dissipation during the impact. The depth of penetration of both bodies is considered by the parameters ξ_{S1} and ξ_{S2}, respectively.

From the contact model (Figure 3.8 – (b)) it is obvious that impacts between rigid bodies characterised by surfaces with high stiffness and low damping yield high restoring forces featuring severe impulsive forces. These impulsive forces, acting at the contact between both

bodies, are considered as the generation mechanism of structure-borne sound causing impact noise. The ultimate characteristics of the perceived sounds, however, do not only depend on the characteristics of the impulses, e.g. duration and energy, but also are affected by the resonance and damping characteristics of the corresponding transmission paths.

As mentioned earlier, some form of external driving mechanisms is required to provoke impact noise. With regard to electric steering systems such mechanisms result from interactions between the steering system and the vehicle structure to which it is connected. One can distinguish between two primary excitations causing interactions between steering system and the vehicle, each of which results in a distinctive transient sound pattern, namely ‘clunk’ and ‘rattling’ noise as described in the following.

‘Clunk noise’ is induced when the driver (operator) excites the steering system via the steering column. This excitation is denoted as ‘excitation provided by the operator’ (EBO). EBO involves cyclic loading within the steering system caused by rapid changes of the steering direction. Mechanical inertia combined with the steering induced loading give rise to temporary clearance between adjacent components resulting in short-time lifting and abrupt equalising movements between these assemblies. Clunk noise is ultimately generated due to impacts between assemblies returning to their initial positions. In general, clunk can occur at very low driving speeds or mainly when the car is parked and the driver moves the steering wheel rapidly from one side to the other. The phenomenon of clunk can be perceived at the same time as, or shortly after the change of the steering direction. As a rule of thumb, the intensity of clunk noise is proportional to the steering speed and the steering angle [195]. Furthermore it depends on the influencing factors mentioned prior to this in the context of impact noise.

Driving a vehicle on bumpy irregular roads such as cobblestones can cause ‘rattling noise’ inside the passenger compartment that may be perceived as transient self-excited vibration [14]. However, the primary mechanism responsible for the generation of rattling can be traced back to stochastic excitations provided by the road surface (EBR). EBR results in impulsive tie rod forces applied externally to the steering system at both sides of the rack [13]. These, in turn, induce dynamic loads (forces and moments) inside the steering system that can ultimately force adjacent components to collide with each other according to the principles mentioned above in the context of clunk noise [196]. Since rattling is caused by EBR the axle kinematics governs the generation of this type of impact noise to a high degree, for which

reason source mechanisms inside the steering system are highly dependent on the actual steering angle and the (dynamic) horizontal plane angles between the tie rods and the rack [13]. Furthermore, the instantaneous driving speed and the nature of the roadway surface directly influences the characteristics of the provoked rattling noise. In this respect Verkoyen [3] differentiates between rattle noise and impact noise that is characterised by a single noise transient caused by an isolated excitation impulse, e.g. due to driving over an obstacle such as a kerb stone edge. Rattle noise prevails if the system is excited again before previous vibration transients have decayed completely. In industrial practice this differentiation is not made and all impact noises in the wake of EBR are defined as rattling.

3.3.4. Relevance ranking of steering induced (transient) sounds

Recalling the different mechanisms involved in the generation of structure-borne sound within electrical steering systems a classification of steering induced sound has been achieved for EPS systems, as illustrated in Figure 3.9. Note that comparable classifications exist for sound generation within general mechanical structures; see amongst others [1],[177] but have not previously been applied to steering systems.

The classification considers the dominant mechanisms of functional and interfering steering system sounds as perceived inside the vehicle, as discussed in the previous sections. Hypothetically, the interior sound may represent a mixture of several different sound phenomena. In reality, however, costumers will perceive a nuisance as soon as one of these sound phenomena exceeds the individual subjective threshold of acceptance. Thus, complaints are normally based on the perception of a single sound phenomenon.

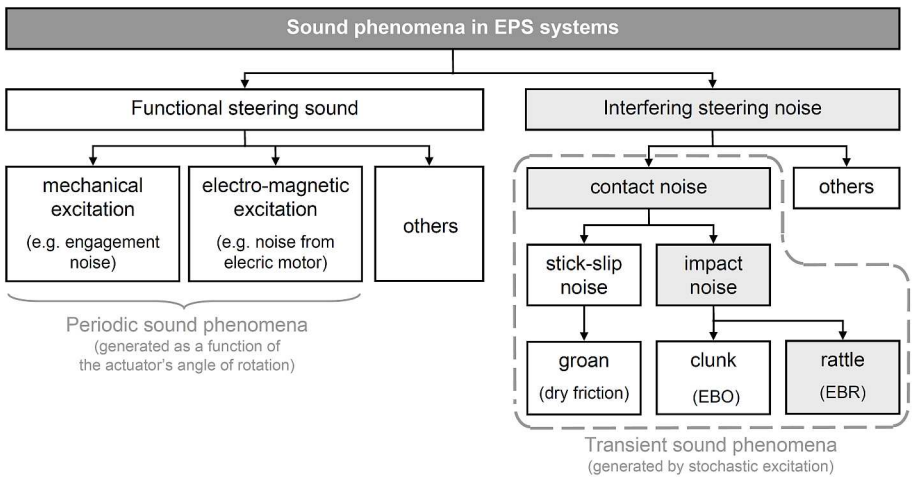

Figure 3.9. Classification of sound phenomena in electric powered steering systems (EPS)

As discussed in section 1.3, functional steering sounds pose far less risk for complaints than sounds associated with interfering steering noise. Due to the transient nature and the randomness of its occurrence, contact noise is considered as critical in this respect. In general, the more instantaneous and unanticipated the occurrence of a noise is, the more stressful is the human reaction [37]. In the context of steering induced contact noise the abstract term ‘perception of a fault’ (PF) has been established (section 1.3) to refer to the negative association passengers may have when perceiving such transient steering sound phenomena. Note that the general term ‘transient sound’ is used interchangeably to refer to all kind of contact noise emerging as groan, clunk and rattle noise (see Figure 3.9). However, the significance of these sound phenomena in the context of PF within electrical steering systems is judged differently.

In general, groaning noise seldom occurs in electrical steering systems. If so, its emitted sound pattern is unique and in most cases can unambiguously be identified as stick-slip induced noise. Since only a few locations exists within electrical steering systems at which stick-slip mechanisms can arise (see section 3.3.3), detection of the possible sources is usually not very difficult. Moreover, the occurrence of stick-slip is highly affected by the dynamic friction forces acting between contacting assemblies while moving relative to one another. As elaborated earlier, the friction forces are governed by the static and kinetic friction coefficients. These, however, can relatively easy be influenced. In practice, increasing the lubrication between assemblies being suspected of causing stick-slip noise in steering systems in most cases will solve the problem. For this reason, groaning noise is usually regarded as of minor importance with respect to interfering steering noise. Consequently, stick-slip excited groaning noise will not specifically be considered within this study.

As pointed out in section 1.3, impact noises like rattle and clunk can lead to perception of a fault for which reason their occurrence in electric powered steering systems needs to be prevented. Basically, the underlying internal mechanisms for both types of transient sound are similar [3],[12] even though the external excitations, i.e. excitation provided by the operator (EBO) and excitation provided by the roadway surface (EBR), are not (Figure 3.9). Furthermore, the internal source locations are considered to be identical [2], [13],[196],[197],[198]. As a corollary of this, the physical problem, which has to be characterised in order to address the problem of transient sound in EPS systems (section 1.4), is essentially the same for both clunk and rattle generation. Due to the influence of the axle

kinematics on the internal excitation mechanisms, rattling phenomena are known to be much more sophisticated than clunk phenomena. Furthermore, since rattle noise is caused by EBR the range of operating conditions under which rattling can be perceived as an annoyance is wide-ranging. On this account, routines for vehicle and test bench measurements to address the problem of clunk noise have been established to become a standard at ZFLS. On the other hand no consistent procedures have so far been implemented to handle rattling phenomena in electrical steering systems. However, neither clunk nor rattle noise routines allow for sufficient localisation of the corresponding internal structure-borne sound sources or for satisfactory quantification of the underlying physical mechanisms, i.e. the internal transient forces. Instead, state-of-the-art tests at ZFLS mainly strive to quantify the amount of generated transient sound in order to rate the vibro-acoustic quality based on predefined limits for structural responses readily measurable on the steering housing. Approaches to identify the internal source locations are usually based on extensive experimental tests which mostly involve mechanical modifications on the affected steering system, such as alteration of internal clearances [199], mechanical blocking of degrees of freedom (e.g. bearings) and replacement of components or entire component assemblies [191].

In summary, the diversity of causes and conditions provoking rattling inside electrical steering systems is far beyond the one related to clunk noise, even though the same internal mechanisms and source locations are involved. Furthermore, no sufficient approaches to relate internal transient structure-borne sound sources to the emitted clunk or rattle noises are available. In order to provide practical techniques allowing for sufficient localisation and quantification of the most crucial internal transient source mechanisms this study mainly deals with rattling noise phenomena caused by excitations provided by the roadway surface (EBR). However, it is stressed that the methodology and all approaches as presented in this study can generally be applied to any active structure-borne sound source comprised within electric steering systems and indeed within other such equipment. Notwithstanding this, the theoretical locations of all possible sources need to be known in advance so as to model the entire physical problem of steering induced structure-borne sound (see section 1.4). Once, the theoretical locations of all concerning sources are determined the approach will allow the physically active sources to be distinguished from the inactive ones thus providing important information to designers and engineers. To achieve this aim in the context of steering induced

rattling noise, in the following a concept is presented which can be utilized to identify the theoretical locations of transient sound sources within electrical steering systems.

3.4. The conceptual source-path-receiver model

This section aims to identify the possible locations of transient sound sources within electrical steering systems. In section 3.4.1 the basic concept of the developed methodology is introduced. This concept allows obtaining a simple source-path-receiver model for electrical steering systems. The most essential step to achieve such a model is based on a sub-structuring approach as elaborated in section 3.4.2. In section 3.4.3 the source-path-receiver model derived for an EPSapa PL2 steering system is presented and the identified possible source locations responsible for the generation of transient structure-borne sound are established. Finally, a brief discussion on the usability of the model is given in section 3.4.4.

3.4.1. The concept

As discussed prior to this, transient interfacial forces acting inside the steering system between adjacent assemblies are responsible for the emission of transient interfering steering noise. In order to minimise the risk of generating transient sound by design, the first task is to identify the theoretical locations inside the steering system at which those interfacial dynamic forces are induced. Consequently, the interfaces between vibrationally active and passive components need to be identified. To find these interfaces the relative movement of the components inside the steering system have been studied so as to substructure the steering system into different layers. Each layer corresponds to a certain movement. Components belonging to the same layer physically cannot move relative to each other. Instead, relative movement can only occur between adjacent components located on different layers. Accordingly, the interfaces at which dynamic excitations could generate transient sound are restricted to the intersections of neighbouring layers. These intersections represent the desired contact zones at which transient sound sources may be located.

One major advantage of sub-structuring the steering system into active and passive components and grouping these components to layers according to their relative movement is that potential source locations can even be spotted between components which under normal driving conditions can be assumed as passive. This for example is the case for pre-loaded component assemblies (e.g. pinion, rack and yoke - see Figure 3.10) where, due to external

excitation (EBO and EBR), the components may lift from each other if the loading inside the steering system rapidly increases. Furthermore, since the active sources are assumed to be located inbetween two neighbouring layers, components located on the layers can readily be considered as vibro-acoustically passive structures. In this way, unambiguous sub-structuring is possible and a simplified source-path-receiver model of the complex mechanical structure of the steering system can be achieved, as described in the next section.

The idea of sub-structuring a complex technical structure into active and passive subsystems is of course not new, (see for example [5]), but it is believed the systematic breakdown of a sophisticated mechanical structure into passive and temporally active components in the context of transient contact noise does not appear to have been published.. Furthermore, the idea of gaining a simplified source-path-receiver model of an electric power steering system is novel and is considered to represent a significant contribution towards understanding the internal processes of transient structure-borne sound phenomena leading to perception of a fault.

3.4.2. Sub-structuring into active and passive parts

Constructing a meaningful source-path-receiver model of an electrical steering system subject to internal transient sound generation requires accurate separation of the potential active sources and the remaining passive parts. However, since the external driving mechanisms (e.g. EBO or EBR) are not sufficient to constantly provoke transient contact noise within the steering system, sources in this respect are presumed to be ‘temporarily active’. Only under certain driving conditions is short-time force excitation between neighbouring components possible during which their contact interface constitutes an active structure-borne sound source; otherwise this region is assumed to be passive.

Sub-structuring is achieved in subsequent steps. First, two major domains on both sides of the steering system are defined, as illustrated in Figure 3.10.
According to the location of each domain on the steering system they are denoted as `domain gearbox´ (BNA), i.e. BNA signifies the component group ball nut assembly located inside the gearbox, and `domain pinion/yoke´ (PY), respectively. Next, both domains are sub-structured conforming to the methodology described above. Figure 3.11 illustrates the sub-structuring approach for both domains (BNA and PY).

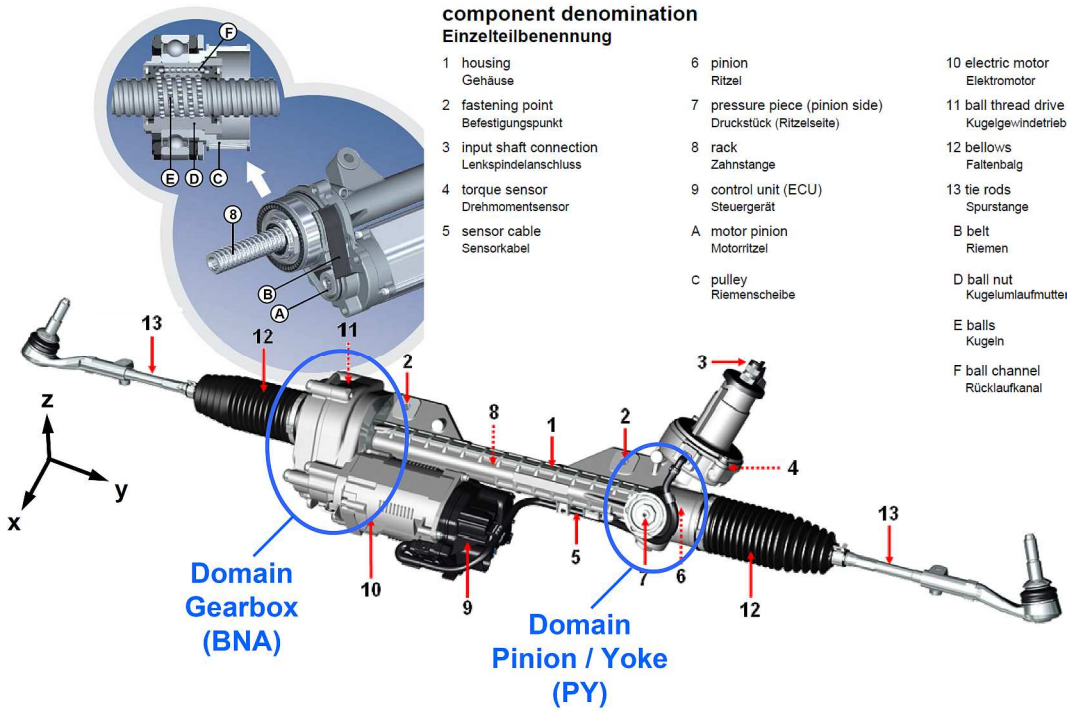

Figure 3.10. Domains and components of the EPSapa PL2 steering system.

The housing of the steering system is considered to be static and thus can be defined as a reference for identifying all remaining interfaces. Furthermore, the housing constitutes a part that links both domains. All components that are directly connected to the housing are classified as static components. Those components are highlighted in red in Figure 3.11. One assumption that has been made is that the bearing ring (5) in the gearbox domain is considered to be fixed to the housing. In the mechanical assembly the bearing ring is supported by a rubber coating and therefore can slightly move radial and axial.

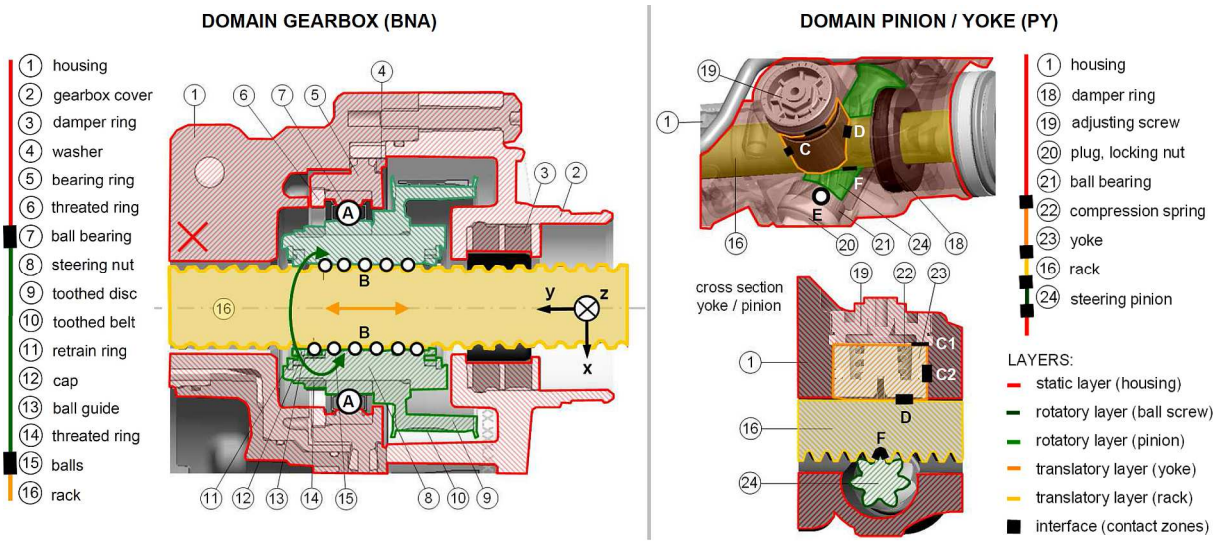

Figure 3.11. Layers within gearbox and pinion/yoke domain of EPSapa PL2 steering system

Nevertheless, due to the high damping of the rubber coating this contact zone does not cause any trouble with regard to impact noise excitation. Note that, as mentioned in section 3.3.3, the bearing ring is sometimes involved in generating groan noise due to sliding contact between its peripheral surface and the housing. However, since the focus of this study is on transient impact sound sources the bearing ring is regarded as quasi-static part, for which reason it is accounted for as part of the housing.

Layers highlighted in green specify rotating layers, such as the ball screw nut unit ((8)-(14)) in the BNA domain or the steering pinion (24) in the PY domain. Rotating layers are always mounted by means of ball bearings to the static housing. According to the definition given above, intersections of two adjoining layers define the contact zone (marked in black in Figure 3.11) at which possible transient structure-borne sound sources are located. In this way, the surfaces of the balls in the ball bearings in both domains are identified as possible rattle and clunk sources. The corresponding interfaces are denoted as (A) and (E) in Figure 3.11.

In the gearbox domain (BNA) the rack (16) is driven by the steering nut (8) in either left (+y) or right (-y) direction. For this reason, the whole rack is considered as translational moving component. The corresponding layer is coloured in yellow. The interface (B) that separates the rotatory layer of the ball screw unit from the translatory layer of the rack runs through the balls of the ball screw drive (15) so that these balls represent possible sources for impact noise excitation as well.

The rack connects the gearbox domain with the pinion/yoke domain as translatory layer. In the pinion/yoke domain the rack (16) is in contact with the rotatory layer of the steering pinion (24), so that the tooth engagement of the pinion with the rack is considered as possible transient sound source. The corresponding interface is referred to as (F) in Figure 3.11.

To avoid lifting of the steering pinion from the rack during operation, the yoke (23) presses the rack towards the pinion axes by means of a compression spring (23). Consequently, a new interface (D) can be drawn between the front end of the yoke and the back side of the rack. The resulting contact zone can be assumed as a further source location for impact sound.

The yoke itself performs a translatory motion, for which reason it is highlighted as second translational layer in orange. The yoke is supported by the static housing (1) yielding further interfaces between the static and translatory layer. Possible impact sources due to impacts between the back side of the yoke and the adjusting screw (19) are located at the interface (C1), whereas impact sources at the contact of the lateral area of the yoke and the housing are

located at interface (C2). The latter contact area may play an important role if the yoke performs tilting movement along the y-axis. However, since both interfaces (C1) and (C2) separate the same layers, i.e. the yoke and the static housing, at different locations they are summarised as one mutual interface, denoted as (C). This helps to decrease the complexity of the system once again. Nevertheless, as the different underlying impact mechanisms have been spotted, they can be considered later on. This is also valid for stick-slip mechanisms, which might appear at the interfaces (C) and (D), as discussed in section 3.3.3.

Another rotatory layer that has not been discussed yet is given by the toothed belt (10) and the electrical motor of the steering systems. As pointed out in section 3.3.1, both components are known as sources for functional noises and thus do not need to be regarded within the impact sound model. However, the belt connects the steering nut (8) with the electrical motor which is again coupled with the housing. For this reason, the belt can be considered as an additional transmission path of vibro-acoustic energy through the gearbox domain. Furthermore, as the belt is pre-stressed, it affects the clearance between the steering nut and the rack as well as the backlash within the ball bearing (7). As a result, this rotatory layer will be accounted for in the source-path-receiver model solely as a passive structure.

3.4.3. The source-path-receiver model

In general, the mechanical assembly can be sub-structured, i.e. active sources and passive receiver structures can clearly be separated from each other. The outcome is the source-path-receiver model, shown in Figure 3.12. The obtained layers (static, rotatory, translatory) are considered as passive receiver structures which can be excited by transient excitation forces at the expected source locations (A to F) between these layers. The type of coupling at the contact zone, e.g. engagement of pinion and rack or sliding fit, is indicated by means of symbols as explained in the legend. This allows considering additional excitation mechanisms beside impact excitation, such as stick-slip mechanisms in consequence of sliding fits (C and D) or functional excitations due to engagement mechanisms (F and G).

The model is consistent with current industry thinking [196],[197],[198],[199],[200] and has been endorsed by engineers working in the field of testing/research and numerical simulation of vibrating structures. Some of the identified source locations are also mentioned in literature [177],[14] although it is emphasised that no systematic approach comparable to the derived source-path-receiver model has been utilised to detect internal noise sources. It is further

noted that no such comprehensive mapping of sound sources inside of (electrical) steering systems has been published to date.

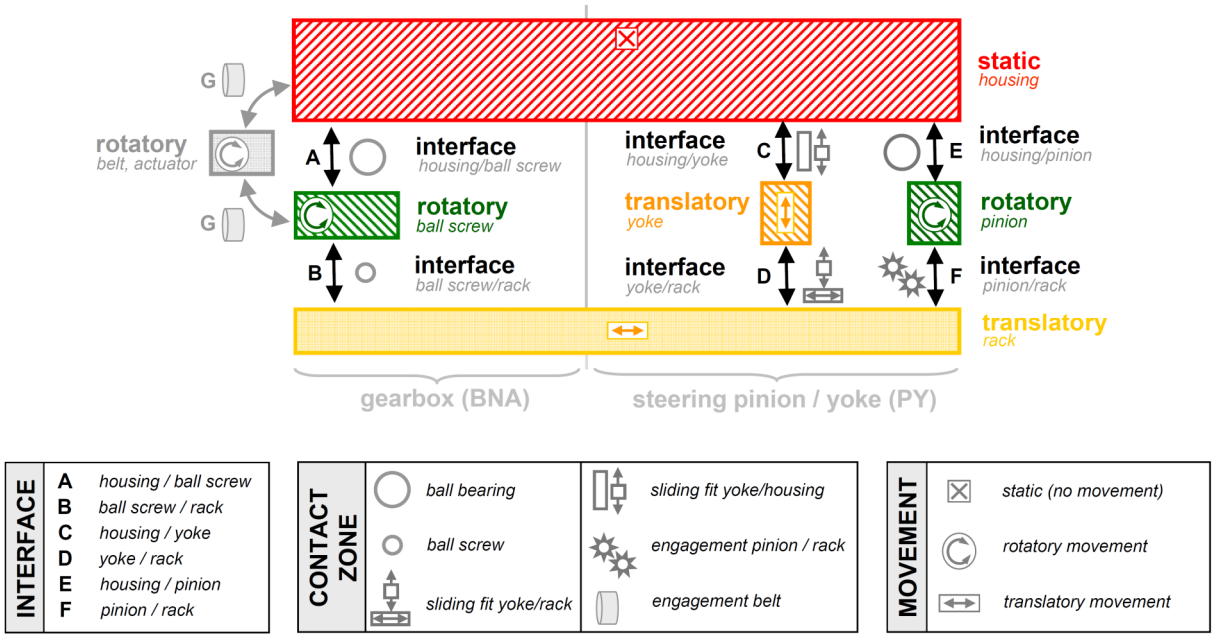

Figure 3.12. Source-path-receiver model of the EPSapa PL2 steering system.

Since the proposed source-path-receiver (SPR) model is dependent on the functional principles and the physical assembly of the steering system it is generally valid for all types of electrical steering systems invoking the same functional principles. In this respect the systematic SPR approach as illustrated in Figure 3.11 and Figure 3.12 has been found to be a very effective tool with respect to mapping possible sound sources in electrical steering systems.

3.4.4. Discussion

The obtained source-path-receiver model (Figure 3.12) already reveals some fundamental information for designers and engineers at ZFLS regarding potential actions to be taken in order to reduce the risk of perception of a fault (PF) within electrical steering systems. Since the most crucial transient sound phenomenon with respect to PF (see section 3.3.4) is based on impact excitation between adjacent assemblies inside the steering system a minimisation of the clearances within the respective contact zones will reduce the excitation [13],[200]. Under this assumption the presented model highlights the corresponding locations at which clearances significant for PF can occur. In this respect the following proposal can be made:

i. Impact noise sources within the gearbox domain (BNA), i.e. sources located at the interfaces (A) and (B), can be positively influenced by:
   - decreasing the clearance in the ball bearing of the steering nut (A)
   - decreasing the clearance between the balls of the steering nut and the rack (B)
   - decreasing the tilting clearance within the ball screw drive (B)
   - increasing the tipping of the ball nut assembly with regard to the rack which will affect the clearance at both interfaces (A) and (B)
   - increasing the belt tension which will affect the clearance in (A) and (B).

ii. Impact noise sources within the pinion/yoke domain (PY), i.e. sources located at the interfaces (C),(D),(E) and (F), can be positively influenced by:
   - decreasing the tilting clearance between yoke and housing (C)
   - decreasing the clearance within the ball bearing of the steering pinion (E)
   - increasing the stiffness of the compression spring which will decrease the clearance in (C),(D) and (F)

Not all of these suggestions are realisable within real physical assemblies since a multitude of factors involving safety and comfort issues of the steering system have to be considered. However, it is emphasised that the suggestions in combination with the simplified source-path-receiver model are potentially helpful to evaluate possible influencing factors of transient sound generation that may improve the overall noise performance.

The SPR model further discloses how the assumed active sources interact with the adjoining passive (receiver) structure inside the steering gear. This may be of particular interest when examining how the axle kinematics and the external excitation mechanisms (EBO, EBR) affect the internal source mechanisms and the dynamic properties of the passive structure as soon as dynamic steering is performed.

Considering first the dynamic properties of the passive structure, moving the rack from the middle position towards one end position will most likely affect the structural dynamic properties between points on the housing (A,C,E) less than the dynamic characteristics between points interacting with the rack (B,D,F). As proven by Bauer in [7] the dynamic properties of the passive structure measured between different points on the steering housing can be assumed to be invariant to the axle kinematics and the steering angle, respectively.

However, the transfer paths between the assumed internal transient sound sources and external receiver points on the housing may be affected.

Considering next possible influences of the axle kinematics and the steering angle on the generation of transient sound, the SPR model unfolds that the internal source mechanisms may significantly be affected by the actual position of the rack and the instantaneous forces applied externally to both sides of the rack and tie rods, respectively. For instance, assuming an external excitation force is acting on the extended end of the rack, the induced internal forces and moments will vary according to the lever principle. Furthermore, the elastic deflexion of the rack depends on the external loading and the rack position which again affects the clearances, the loading as well as the overall generation mechanisms of transient structure-borne sound inside the steering system. The influence of the axle kinematics and the external loading, or more general the current driving condition, on the noise performance of steering systems is generally known as significant [177],[191],[3].

As can be seen from Figure 3.12, due to the rigid coupling via the static housing and the moving rack any source located in either the gear box domain or the pinion/yoke domain can strictly contribute to all receiver points on the steering housing. The simple SPR model in this respect schematises the existing transmission paths within the complex mechanical assembly of electrical steering systems. Information about the rough transmission paths is often of interest when test purposes require performing mechanical modifications on the physical assembly. Mechanical modifications may be instrumental in experimental detecting existing transient sound sources based on methods of elimination in which degree of freedom of specific components are successively blocked so as to deliberately activate or deactivate the expected sources of transient sound. Thus, it is believed that the derived SPR model constitutes a simple tool to roughly evaluate if a mechanical modification will affect certain internal transmission paths.

3.5. Summary

The underlying generation mechanisms of steering induced structure-borne sound have been elaborated. According to psychological criteria a general classification system of steering induced sound has been achieved comprising two main groups, namely functional steering sounds and interfering steering noise. Most important in the latter category is steering induced transient sound. The fundamental generation mechanisms of transient sound within electrical

steering systems have been found to be transient forces induced by stick-slip and impact phenomena resulting from relative movements between contacting assemblies. Rattling has been ranked as the most relevant transient noise phenomenon which is caused as a consequence of excitations provided by the roadway surface (EBR). It has been found that the range of operation conditions under which rattle noise may be provoked cannot exactly be specified due to the diversity of influencing factors including the indeterminacy of the road surface and the time variance of the axle kinematics amongst others.

A methodology has been presented that facilitates determining the possible source locations of transient sound within electric power steering systems. Following this methodology, a simplified model of the EPSapa PL2 steering system has been derived by gradually sub-structuring the mechanical assembly. Sub-structuring has been achieved by grouping components inside the steering system according to their relative movement. In this way different component layers with either static, rotational or translational motion have been identified. Intersections of adjacent layers with different movements have been used to define the contact zones at which transient sound sources inside the physical assembly can be expected. The identified source locations have been found to affirm the experience of specialists at ZFLS and to be consistent with the available literature. Based on a plain schematic, the so-called source-paths-receiver model has been derived which is believed to constitute a significant contribution towards ascertaining the causes of steering induced structure-borne sound within electrical steering systems and the associated phenomenon of perception of a fault. Besides visualising the expected source locations and the related generation mechanisms of steering induced transient sound the explanatory model allows for theoretical studies of the vibro-acoustic processes inside the steering system.

Chapter 4

Force reconstruction in time domain using an adaptive algorithm

4.1. Introduction

It was established in previous chapters that independent characterisation of transient structure-borne sound sources in electrical steering systems requires the use of inverse force identification methods that are applicable to sophisticated technical structures with multiple inputs and multiple outputs, allow for robust and accurate force identification even if the available data comprise considerable errors and should preferably be capable of addressing the inverse force identification problem in time domain. Although a number of time-domain inverse force identification approaches exist an intensive literature research showed that most of these methods lack generality so that they are not practicable for sophisticated structure-borne sound problems. From all reviewed techniques an iterative time domain inversion routine [174] employing an adaptive algorithm to perform inverse identification was found to be less restrictive than most other methods. However, the adaptive inversion routine still cannot be used for inverse force identification in sophisticated technical structures since (i) it has only been studied for relatively simple structures with single-degree of freedom excitation and (ii) it requires a-priori information on the force input location.

Considering issues with the required knowledge of the force input location (ii), the conceptual source-path-receiver model, developed in the last chapter, is able to disclose all theoretical locations and associated mechanisms of possible transient sound sources acting inside the steering gear. Thus all force input locations can be assumed known and fixed with respect to applications of the time domain inverse routine for independent characterisation of transient structure-borne sound sources in electrical steering systems. Moreover, to facilitate a broader applicability of the time domain inverse routine than only for single-degree of freedom excited structures, this chapter is devoted to the derivation of a generalisation of the adaptive algorithm invoked in the time domain inversion routine that facilitates simultaneous reconstruction of multi-channel force signatures for sophisticated multiple input multiple output (MIMO) systems.

The fundamentals of the time domain inverse routine are reviewed in section 4.2. In section 4.3 a methodology is introduced that will be employed to obtain system and noise models for numerical simulations. Additionally, a strategy is proposed that will be used to evaluate the performance of the derived time domain inverse method (TDM) and allows for fair

comparison of the TDM with the standard frequency domain inverse method (FDM). Later sections (4.4 to 4.6) are devoted to study the sensitivity of the iterative process to noise and errors in the used data and to derive several expansions of the basic inverse routine with the aim to achieve a generalised adaptive algorithm that enables robust reconstruction of multi-channel force signatures for sophisticated structures in the presence of potential defective data sets. Finally, the most important findings and some concluding remarks are summarised in section 4.7.

4.2. Fundamentals of the time domain inverse routine

The main idea of the presented time domain inverse routine is based on the conventional Least Mean Square (LMS) algorithm, devised by Widrow and Hoff [201]. An application of the conventional LMS algorithm, which may be readily thought of, is the problem of single-input single-output (SISO) system identification in the context of adaptive filtering. Using this example a derivation of the conventional LMS algorithm will be recalled in section 4.2.1. Based on this, the fundamental mathematical relations will be modified in section 4.2.2 in such a way that the algorithm can be used for reconstructing the time history of unknown dynamic forces acting on technical structures. It will be shown that the inverse routine is built around a cyclic iterative routine in which several interrelated steps have to be processed subsequently. Section 4.2.3 is devoted to elaborate the different steps involved in the iterative process and to provide the reader with profound information of how the inverse routine processes the data before the basic approach is demonstrated for an ideal numerical system.

4.2.1. The conventional Least Mean Square algorithm

Consider the problem of single input single output (SISO) system identification in the context of adaptive filtering, depicted in Figure 4.1 (a). An adaptive filter is used to provide a linear model of an unknown system to be identified. Let their respective impulse responses be denoted by $\mathbf{h}(n)$ and $\mathbf{h}_u$ where n indicates discrete time. Both systems are driven by the same (real-valued) input data $x(n)$, in the following considered to be a dynamic force applied to a mechanical structure.

The adaptive modelling scheme is built of a transversal filter structure (i), depicted in Figure 4.1 (b) which consists of a finite number I of adjustable coefficients , $h_i(n)$ for i=[0, 1,…, I-1], that are controlled by the adaption algorithm (ii).

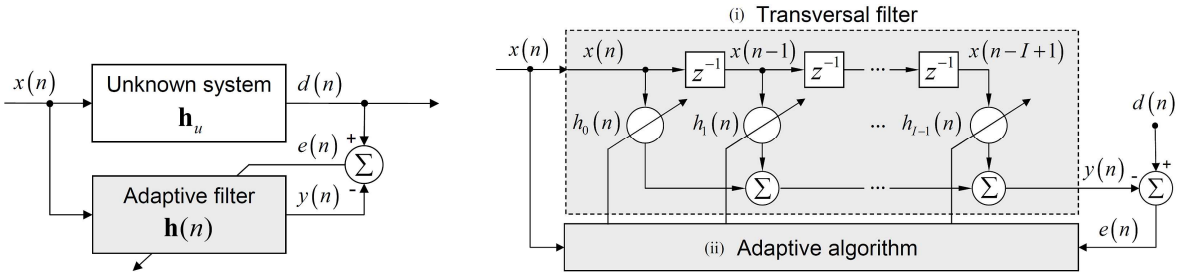

Figure 4.1. Block diagram of adaptive system modelling (a) and detailed structure of the adaptive filter (b)

At each time n the output sample $y(n)$ of the adaptive filter is computed by a weighted sum of the current input sample $x(n)$ and delayed input samples $x(n\text{-}1)$, $x(n\text{-}2)$…

$$y(n)=\sum_{i=0}^{I-1}h_i(n)x(n-i)=\mathbf{h}^T(n)\mathbf{x}(n) \tag{4.1}$$

$$\mathbf{x}(n)=\left[x(n),x(n-1),\ldots,x(n-I+1)\right]^T \tag{4.2}$$

$$\mathbf{h}(n)=\left[h_0(n),h_1(n),\ldots,h_{I-1}(n)\right]^T, \tag{4.3}$$

where I is the length of the finite impulse response (FIR) of the filter, $\mathbf{x}(n)$ is the tap-input vector at time n and $\mathbf{h}(n)$ is the adjustable coefficient vector at time n. The superscript T denotes transpose of the vector. The error signal $e(n)$ required for adaption is defined as the difference between the desired response $d(n)$ and the output $y(n)$ of the adaptive filter

$$e(n)=d(n)-\mathbf{h}^T(n)\mathbf{x}(n). \tag{4.4}$$

Note that the estimation error is the sample value of a random variable. The aim is to minimise the error with respect to the tap-weight vector $\mathbf{h}(n)$ so as to achieve a set of FIR filter coefficients that best approximates the impulse response function $\mathbf{h}_u$ of the true system. To optimise the filter design, a cost function based on this error is to be minimised with respect to the coefficient vector $\mathbf{h}(n)$. The mean square error

$$MSE \triangleq \xi(n)=E\left[e^2(n)\right] \tag{4.5}$$

where $E[\cdot]$ denotes statistical expectation, has turned out to be an advantageous criterion for minimisation [202],[203]. Using (4.4) in (4.5) gives the MSE or the performance surface $\xi(n)$,

$$\xi(n)=E\left[e^2(n)\right]=E\left[d^2(n)\right]-2\mathbf{h}^T(n)E\left[d(n)\mathbf{x}(n)\right]+\mathbf{h}^T(n)E\left[\mathbf{x}(n)\mathbf{x}^T(n)\right]\mathbf{h}(n) \tag{4.6}$$

where $\mathbf{h}(n)$ is shifted out of the expectation operator $E[\cdot]$ since it is not a statistical variable. It is clear that the performance surface $\xi(n)$ is a quadratic function of the coefficient vector $\mathbf{h}(n)$.

For real physical systems $\xi(n)$ must be concave upward [204] with a single global minimum at which the coefficient vector assumes its optimum value, the so-called Wiener solution [202]. Hence, starting at an arbitrary point on the performance surface and moving down into the direction of the steepest descent, i.e. the direction of the negative gradient of the surface with respect to the coefficient vector, will lead to the optimum solution $\mathbf{h}_0$. Note that at the bottom of the error-performance surface the gradient is identically zero so that the gradient-based search method always ends in the minimum of the performance surface (cf. Figure 4.2). The gradient at any point on the performance surface is obtained by differentiating (4.6) with respect to the coefficient vector $\mathbf{h}(n)$ which, expressed in terms of the error in (4.4), can be written as

$$\nabla\xi(n)=\frac{\partial\xi(n)}{\partial\mathbf{h}(n)}=2E\left[e(n)\left[\frac{\partial e(n)}{\partial h_0(n)},\ldots,\frac{\partial e(n)}{\partial h_{I-1}(n)}\right]^T\right]=-2E\left[e(n)\mathbf{x}(n)\right]. \tag{4.7}$$

Based on the strategy mentioned above, a simple iterative search method, referred to as the steepest descent (SD) algorithm can be derived. Starting with an initial value $\mathbf{h}(0)$, the current coefficient vector $\mathbf{h}(n)$ is adjusted at each time step n by an amount μ proportional to the negative of the current gradient vector

$$\mathbf{h}(n+1)=\mathbf{h}(n)-\mu\nabla\xi(n)=\mathbf{h}(n)+2\mu E\left[e(n)\mathbf{x}(n)\right]. \tag{4.8}$$

A schematic of the SD algorithm for searching the optimum value of a single-tap transversal filter is given in Figure 4.2.

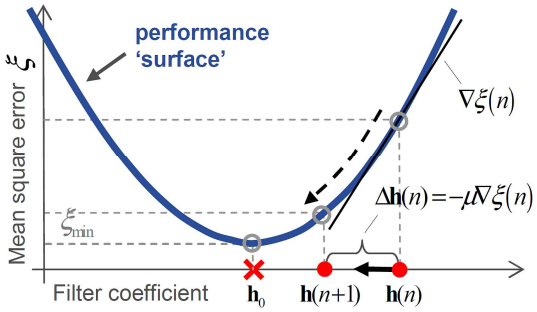

Figure 4.2. Schematic of the steepest descent rule applied to the performance surface of a single-tap transversal filter with optimum value $\mathbf{h}_0$.

It is noted that the performance surface for this simple case is given by a 2nd degree polynomial. For real physical structures the adaptive filter considers a finite number I of filter coefficients so that the performance surface of the transversal filter is a bowl-shaped (I+1)-

dimensional surface with I degrees of freedom represented by the tap weights of the filter [202].

The coefficient vector computed by the SD algorithm (4.8) would theoretically converge to the optimum Wiener solution if the step-size parameter μ is suitably chosen and the gradient vector were determined exactly at each time n. However, the gradient is expressed as the ensemble average of the product between the error and the tap-input vector and, in practise, must be estimated from the data available at each time n. (For a more detailed discussion see, e.g., [202], [203], [204]). As shown by Widrow and Hoff [201], a simple estimator for the gradient can be achieved by replacing the cost function $\xi(n) = E[e^2(n)]$ in (4.5) by its instantaneous coarse estimate $\hat{\xi}(n) \approx e^2(n)$ that is simply the instantaneous squared error. Replacing the ensemble average in (4.8) by the instantaneous sample values of the error and the tap-input vector is straightforward and results in the widely known least-mean square (LMS) algorithm

$$\mathbf{h}(n+1) = \mathbf{h}(n) - \mu \nabla \hat{\xi} = \mathbf{h}(n) + 2\mu e(n)\mathbf{x}(n). \tag{4.9}$$

Since the LMS algorithm is recursive in nature the imperfect gradient estimates are averaged so that their inherent noise is attenuated with increasing time, i.e. when n tends to infinity, by the adaptive process. The step-size parameter μ is a convergence factor that controls stability and rate of adaption. In order to ensure convergence, the step-size parameter, in practice, needs to be chosen according to the stability bound [204],[205]

$$0 < \mu < \frac{1}{E\left[x^2(n)\right] I}. \tag{4.10}$$

Referring to the identification problem stated at the beginning this means that the impulse response function of an unknown system can be adaptively reconstructed (approximated) as an FIR of defined length I by (i) sequentially performing the LMS algorithm steps for filtering (4.1), error estimation (4.4) and adaption of the filter coefficients (4.9) with respect to the bound in (4.10) and (ii) if sufficiently long signals for the input and the desired response are available so that the iterative process can be carried out often enough.

4.2.2. Adaptive algorithm for the reconstruction of forces in time domain

In the following, it is aimed to modify the conventional LMS algorithm in such a way that it allows for reconstructing the input signal instead of adjusting the system's finite impulse

response (FIR). The former system identification problem thus turns into the challenging problem of identifying the time history of a dynamic force applied to a mechanical structure with known and time-invariant FIR.

Revisiting the filtering process in equation (4.1), it has been shown that the convolution, at each time step *n*, processes a set of *I* FIR coefficients with a subset of *I* sample values of the input signal. Since the convolution operation satisfies algebraic commutativity, the FIR coefficient vector and the tap-input vector in (4.1) can be interchanged. Accordingly, the block diagram from Figure 4.1 (a), which is closely related to the filtering process, may also be rearranged and depicted as the block schematic in Figure 4.3.

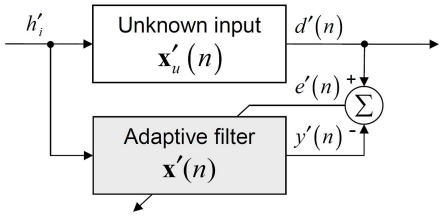

Figure 4.3. Block diagram for adaptive input reconstruction (Apostrophes indicate constrained conditions)

Clearly, the FIR now assumes the role of an input signal, h_i for i=[0, 1,…, I-1], which, at each time n, is applied to the adaptive filter in order to adjust the values of the current tap-input vector, $\mathbf{x}(n)$. Note, in order to derive a convergent adaption algorithm, further constraints need to be put on the involved signals. Constraints are indicated by an apostrophe and will be explained later on. However, most important at this point is that the block diagram in Figure 4.3 is essentially the same as the one of the conventional LMS algorithm and so are the basic mathematical relations. As a consequence of this the error signal in Eq. (4.4) also remains unchanged. The only difference is now that the error signal need to be minimised with respect to the unknown input force $x(n)$. Interestingly, when reconsidering the cost function $\xi(n)$ in (4.6), one can also find a second-order dependence of the performance surface on the input signal $x(n)$ to be adjusted. Thus, following the previously discussed strategy the recursive SD algorithm from (4.8) can be reformulated with respect to the sought input vector, $\mathbf{x}$(n),

$$\mathbf{x}(n+1) = \mathbf{x}(n) - \mu\nabla\xi(n) = \mathbf{x}(n) + 2\mu E\left[e(n)\mathbf{h}\right]. \tag{4.11}$$

In a further step the ensemble average of the gradient, here expressed by the rightmost term of equation (4.11), can be replaced by the instantaneous sample values. This procedure has been shown to be satisfactory for the conventional LMS algorithm where convergence in the mean square can be achieved by averaging over the corrections at each time step for a sufficiently

long input signal ($n \mapsto \infty$). However, for the problem on hand, the ensemble average cannot be reached in the same manner. First, the system's (finite) impulse response h_i, which assumes the role of the input to the adaptive filter, is only of restricted length $i = [0,1,\ldots,I-1]$. Second, at each time step *n* a different subset of the unknown input signal $x(n)$ is considered by the adaptive filter. At time *n*, the values $[x(n), x(n-1), \ldots, x(n-I+1)]$ of the vector $\mathbf{x}(n)$ are adjusted. At the next time step $n+1$, the subset is first modified by shifting forward by one sample before its most recent values, $[x(n+1), x(n), \ldots, x(n-I+2)]$, are updated. In consequence of the shifting process each value of the unknown input signal can at most be updated *I* times.

Since this is not sufficient to bring the input signal $x(n)$ about converging towards its optimum values, Kropp and Larsson [174] introduce two constraints for the sequences involved in the iterative adaptive process:

i. By considering only *N* values of the unknown input signal $x(n)$ and the desired response $d(n)$ the progressional shifting process is restricted to a finite number $(N-I+1)$ of modifications (shifts).

ii. The required ensemble average is then achieved by applying a synthesised (created) arbitrarily long input signal to the adaptive algorithm. For this purpose, the sequence h_i for i=[0, 1,…, *I*-1], i.e. the series of the known FIR coefficients, is assumed to be repeated periodically with period length *N*. As a consequence of this, the desired signal $d(n)$ also needs to be repeated periodically with period length *N*.

Note that periodic repetition of the signals (constraint (ii)) is achieved by carrying out the iterative process in a cyclic manner, as explained next. To indicate that the adaptive algorithm relies on a cyclic iterative process the time variable *n* will be indexed by the integer *k* in the following. It is further noted that Figure 4.4 (b) and Figure 4.5 together with the explanations provided in section 4.2.3 may help to better comprehend the role of the additional constraints.

Considering the constraints (i) and (ii) the final recursion can be derived from Eq. (4.11) as

$$\mathbf{x}(n_{k+1}) = \mathbf{x}(n_k) + 2\mu e(n_k)\mathbf{h}(n_k) \qquad \text{for } I \le n_k \le N \;\; \forall \;\; N \ge 2 \cdot I \tag{4.12}$$

where the integer *k* counts the number of iteration cycles. The analogy to the conventional LMS algorithm is given by the mathematical steps (4.1), (4.4) and (4.12) which, in this order,

are required to complete each iteration cycle *k*. When n_k reaches *N* the next iteration cycle $k = k+1$ is started and the process is repeated again from $n_{k+1} = I$.

In order to achieve convergence in the mean square the step size parameter μ needs to satisfy a stability bound. For the conventional LMS algorithm the bound given by Eq. (4.10) depends on the sequence applied to the input of the adaptive filter. Here, the known periodic FIR assumes this role so that the stability bound is defined in terms of its signal power [206]

$$0 < \mu < \left(\sum_{i=0}^{I-1} \left| h(i) \right|^2 \right)^{-1}. \tag{4.13}$$

The condition $N \geq 2 \cdot I$ in Eq. (4.12) is required as the first *I* values of the desired signal *d*(*n*) are influenced by values of the input signal outside of the observation window $[1, \ldots, N]$. As a corollary of this, reliable reconstruction of the input signal is only possible for values at times $n_k \geq I+1$ [174],[206],[207], [208].

Table 4.1 summarises an implication of the achieved time domain inversion routine facilitating reconstruction of the time signature of a dynamic force applied to single input single output (SISO) systems.

Table 4.1. Time domain inversion routine for identification of forces in single input single output systems.

Parameters:	n… time step k… iteration cycle N… length of input vector I… length of finite impulse response	
Initialisation:	$\mathbf{x}(n_{k=0}) = \mathbf{0}$	
Computation:	for $I \leq n_k \leq N \quad \forall \quad N \geq 2 \cdot I \qquad k = k+1$	{1}
Filtering:	$y(n_k) = \sum_{i=0}^{I-1} x(n_k - i)\, h(i)$	{2}
Error:	$e(n_k) = d(n_k) - y(n_k)$	{3}
Update:	$\mathbf{x}(n_k+1) = \mathbf{x}(n_k) + 2\mu\, e(n_k)\mathbf{h}(n_k)$	{4}
Stability bound:	$0 < \mu < \left(\sum_{i=0}^{I-1} \left| h(i) \right|^2 \right)^{-1}$	{5}

According to the numbering given in the curly brackets in Table 4.1 the algorithm can be summarised as follows: Starting with an initial guess of the unknown input force, at each time step, n_k, the pre-measured impulse response function (IRF) *h* of finite length *I*, is used to filter the current force estimate, $x(n_k)$, so as to predict the response of the adaptive filter, $y(n_k)$ {2}. An error, $e(n_k)$, between the estimated filter output and the desired response, $d(n_k)$, is calculated {3}. This error is then weighted with the corresponding IRF and is used to update the current force estimate recursively {4}. In order to achieve an iterative procedure these

steps are to be repeated at each iteration cycle k according to the constraints given in {1}. To ensure convergence the step size parameters, μ, need to be chosen according to the stability bound in equation {5}.

4.2.3. The iterative adaptive process

In the previous section the most basic mathematical relations of the time domain inversion routine have been derived for single input single output (SISO) systems. As discussed, the inversion routine is based on an adaptive algorithm that is implemented in an iterative recursive scheme. Before the algorithm can be studied in more detail, understanding the underlying data-processing steps is essential. To provide the reader with a detailed background, the functionality of the time domain inversion routine is demonstrated for an elementary numerical model in the following.

Assuming a single input single output system, e.g. a force excited beam as depicted in Figure 4.4 (a), it is aimed to identify the unknown excitation force $x(n)$ under the assumption that the dynamic properties of the passive structure can fully be described by the known (pre-measured) time invariant finite impulse response function **h** and under the assumption that the corresponding structural response $d(n)$ can be measured at each discrete time n.

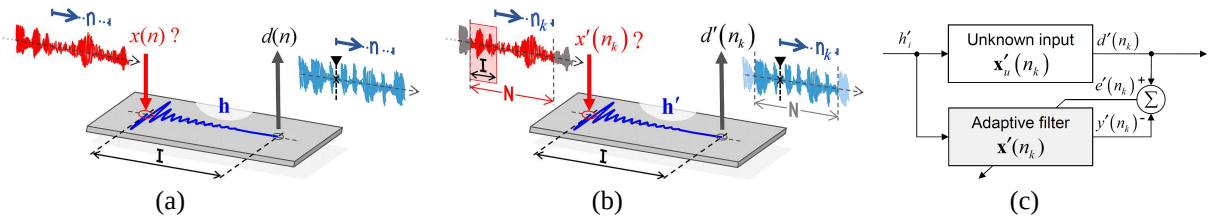

Figure 4.4. SISO system - force excited beam: Schematic of physical input identification problem (a), principle of cyclic iterative process achieved by consideration of additional constraints (b) and corresponding block diagram of adaptive input reconstruction algorithm (c). (Apostrophes indicate constrained conditions.)

According to the derivation of the time domain inverse method two constraints are required, i.e. (i) consideration of only a part of the input and the desired response signals both of which are assumed to be of length N and (ii) cyclic operation of the iterative process by repeating the FIR and the desired signal periodically with period length N so as to achieve a convergent adaptive algorithm in the mean square sense. Considering these constraints the basic data-processing principle of the inverse routine can be schematised for the given SISO force reconstruction problem as depicted in Figure 4.4 (b). The ambition of the following paragraphs is to deliver insight into the basic data-processing principle of the cyclic iterative

routine. For the sake of completeness the associated block diagram is visualised in Figure 4.4 (c).

To demonstrate the basic data-processing principle of the time domain inversion routine (Figure 4.4 (b)) an elementary numerical model was set up. An arbitrary input signal of length $N = 5$ samples simulates the time signature of a dynamic force $x_u(n) = [0, 2, 3, -3, -1]^T$ to be identified in the following. The excitation is applied to a structure which is fully represented by the two-tap ($I = 2$ samples) impulse response function $h_i = [-10, 2]^T$. The corresponding desired response was calculated using linear convolution, denoted as $d(n) = x_u(n) * h_i$ where '$*$' is the convolution operation. According to constraint (i) only the first $N = 5$ samples are considered in the following so that the desired response is given by $d(n) = [0, -20, -26, 36, 4]^T$ .The SISO time domain inversion routine from Table 4.1 was then used to reconstruct the assumed unknown input force $x_u(n)$ based on the knowledge of the desired response $d(n)$ and the FIR h_i of the true system. The iterative process was carried out for 10 complete iteration cycles.

Some intermediate results are plotted in Figure 4.5 (a)-(d) illustrating the different data-processing steps required to achieve an adaption of the estimated force sequence $x(n_k)$ at different time steps n_k for the first iteration cycle $k = 1$. Figure 4.5 (e) depicts the data-processing steps required after each iteration cycle is completed using the example of the final solution which was achieved after $k = 10$ full iteration cycles. For clarity, the different data-processing steps are numbered sequentially so that the corresponding processes can be identified in Figure 4.5. The different steps are:

(1) Selection of *I* sequent values from the entire force estimation sequence $x(n_k) \in \mathbb{R}^{N+1}$. These values are stored in the current force estimation vector $\mathbf{x}(n_k) \in \mathbb{R}^{I \times 1}$. Due to the recursive nature of the iterative algorithm the force estimation vector has to be initialised before the first iteration can be carried out. If a priori information of the applied force is available this information may be used for initialisation. This would reduce the total number of iterations required to achieve a convergent force reconstruction result. Since in general no a priori knowledge of the applied input force is available the force estimation vector usually is initialised as the zero input vector $\mathbf{x}(n_{k=0}) = \mathbf{0}$.

(2) The convolution between the instantaneous force estimate $\mathbf{x}(n_k)$ and the finite impulse response function $\mathbf{h} \in \mathbb{R}^{I\times 1}$ of length I is carried out (equation (4.1)). This gives an estimated sample value of the most recent filter output $y(n_k) \in \mathbb{R}^{1\times 1}$.

(3) By comparing the approximated filter output $y(n_k)$ with the sample value of the desired (true) response $d(n_k) \in \mathbb{R}^{1\times 1}$ the error $e(n_k)$ is obtained as their difference (equation (4.4)).

(4) The error is then used to adjust the selected I values of the unknown input force vector by weighting the impulse response **h** with the product of the step size parameter $\mu \in \mathbb{R}^{1\times 1}$ and the current estimation error $e(n_k)$ (Eq. (4.12)). In this manner the adjusted input vector $\mathbf{x}(n_k+1) \in \mathbb{R}^{I\times 1}$ is obtained. Note that the time index is increased by 1 so as to indicate that the values were updated. The updated values are then used to overwrite the respective older values of the entire force sequence $x(n_k)$. In Figure 4.5 (a), updated values are illustrated as black crosses in the entire force input sequence.

(5) The process is repeated for the next time step $n_k = n_k + 1$.

(6) The data-processing steps (1) to (5) are repeated sequentially for the time steps $I \le n_k \le N$ (Figure 4.5 (b)-(c)). When n_k reaches N this sequence is repeated again from $n_k = I$ (Figure 4.5 (d)) and the next iteration cycle $k = k+1$ is started until a defined criterion of interruption is reached (6'), e.g. when the error (difference) between the reconstructed and the observed output falls below a defined limit for the first time. Note that different interruption criteria will be discussed in later sections.

(7) After completing the iterative process (Figure 4.5 (e)), values for $n_k > I$ can be considered to represent reliable estimates while values to earlier times cannot be reconstructed (7'). If the iterative process is carried out sufficiently often the reconstructed force will match exactly the original one within the reliable time range, assuming that perfect data is available.

It is noted that the order in which the basic data-processing steps are carried out allows construing the fundamental principle of the time domain inverse routine as solving stepwise forward identification problems. In essence, the unknown input force is updated gradually until the predicted response, obtained by solving a forward problem (convolution of the input force with the system's known FIR), is concordant with the desired one. At no stage the data-processing needs to rely on an inverse system model nor does the iterative routine require inversion of a possibly ill-conditioned matrix. All data-processing steps are carried out in an invariable forward manner which is believed to pose one of the major advantages of the routine in contrast to other inverse methods, e.g. frequency domain inverse methods.

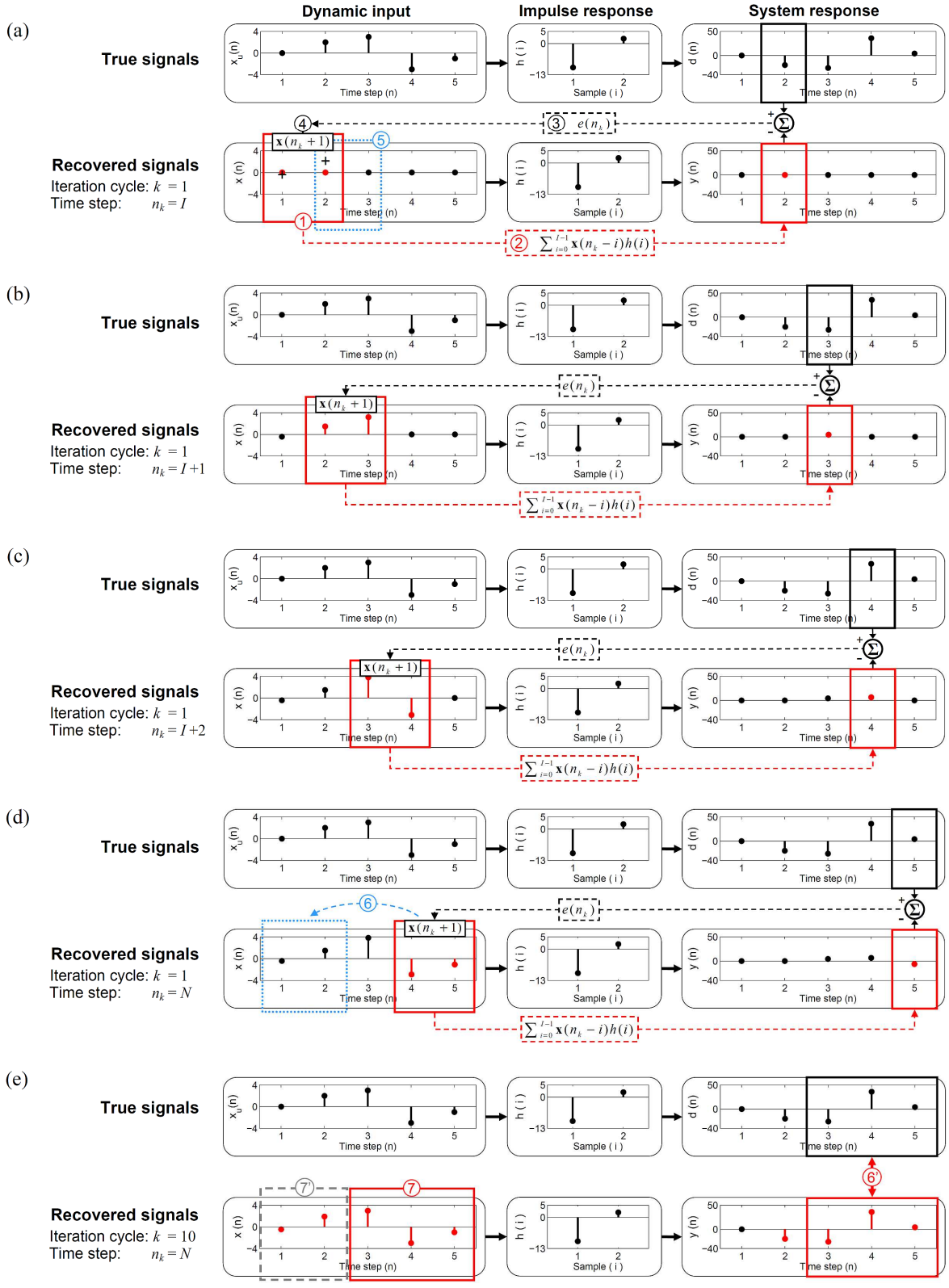

Figure 4.5. Elementary numerical model to illustrate the iterative recursive process involved in the time domain inverse routine. Steps (a)-(d) are to be processed at each time step n_k while step (e) is to be performed after each full iteration cycle k. Diagram (e) illustrates the final solution after the last iteration cycle $k = 10$ was completed.

4.2.4. Demonstration of the inversion routine for an ideal numerical model

In this section a simple numerical example is provided in order to demonstrate that the proposed method is suitable for reconstructing unknown input forces assuming the system's impulse response h_i and the desired response signal $d(n)$ are not corrupted by noise or otherwise imperfect. The unit impulse response of an underdamped second-order lowpass system with transfer function $H(s) = A_0\omega_0{}^2\left(s^2 + 2\zeta\omega_0 s + \omega_0{}^2\right)^{-1}$, DC gain $A_0 = 0.3$, natural frequency ω_0=6000 rads^{-1} and damping coefficient $\zeta = 0.03$ s^{-1} is considered to describe the relationship between a force applied to the system's input and the acceleration response observed at the system's output. The length of the impulse response function (IRF) is chosen to be $I = 512$ samples. As input force a random signal of length $5 \cdot I$ is generated. The entire force signal is convolved with the obtained IRF, although only the rearmost $N=4 \cdot I$ samples of these signals are used within the force reconstruction process. In doing so one accounts for real-life applications where the first values, according to the decay time of the system's IRF, of a sampled acceleration signal are always influenced by forces applied to the structure outside of the observation window. The force signal is then reconstructed by means of the proposed adaptive identification approach, i.e. using equations (4.1), (4.4), (4.12) and (4.13). In order to interrupt the iterative adaption process without requiring knowledge of the original force signal, [174] suggests the use of the relative mean prediction error

$$\eta(k) = \frac{\sum_{n_k=I+1}^{N} e^2(n_k)}{\sum_{n_k=I+1}^{N} d^2(n_k)} \cdot 100\% \tag{4.14}$$

which is calculated after each iteration cycle k. Note, that the relative mean error is defined only for the reliable part of the reconstructed acceleration signal, that is for values corresponding to times $I+1 \le n_k \le N$. The relative mean prediction error (RMPE) can be understood as a performance measure of the iterative process and monitors the discrepancy between the reference acceleration signal (desired response) and its reconstructed counterpart. As interruption criterion a value of $\eta = 0.1\%$ is used in [174], i.e. the iterative process is stopped when the relative mean error falls below the value of 0.1% for the first time. Here, the adaptive process is interrupted when the error underruns $\eta = 0.001\%$ since the computational effort for this simulation is fairly small and a high estimation accuracy is desired. However, the reconstructed force sequence that would be obtained when interrupting the iteration

process according to the proposed $0.1\,\%$ limit was also calculated. The simulation results are depicted in Figure 4.6.

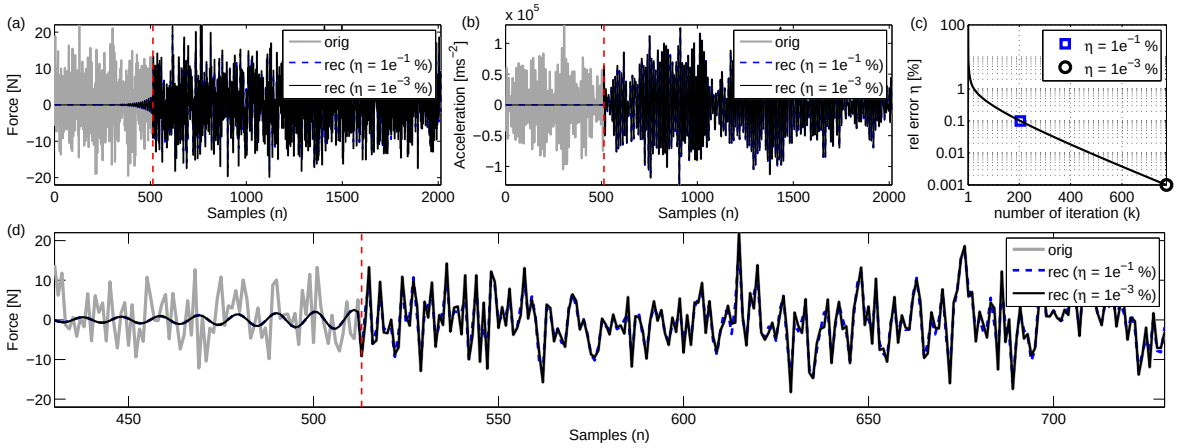

Figure 4.6. Simulation results for noise free underdamped second-order system: Original and reconstructed force time history in full length (a) and close up (d), desired and reconstructed acceleration time history (b), progression of relative mean prediction error (c). —— original signal, ---- reconstructed signal using η = 0.1 % as interruption criterion, —— reconstructed signal using η = 0.001 %

Diagrams (a) and (b) show the full length sequences of the original (grey) and reconstructed (blue for $\eta = 0.1\,\%$, black for $\eta = 0.001\,\%$) input force and acceleration, respectively. From (a) it can clearly be seen that reliable estimates for the unknown force signature can not be achieved within the first 512 samples of the sequence. This corresponds to the length *I* of the system's impulse response and is indicated by a vertical red dashed line. As mentioned before, the acceleration signal in this range is influenced by forces applied to the system outside of the observation window which cannot be recovered from the data on hand. Outside this sample range, i.e. for all times $n_k \geq I+1$, the forces can be reconstructed with satisfying accuracy, as depicted in (d) in more detail. The progression of the relative error (c) reveals that an estimation accuracy according to $\eta = 0.1\,\%$ was achieved after 204 iterations. The estimated force time history is depicted by a blue dashed line in the diagrams (a) and (d). Setting the interruption criterion to $\eta = 0.001\,\%$ causes the algorithm to stop after 773 iterations. The unknown dynamic force then is identified with high precision, as depicted by the black solid line in (a) and (d), coping with an increase in computing time. Nevertheless, with regard to identifying forces on real structures where usually much longer impulse responses and operational measurements need to be processed, the interruption criterion

$\eta = 0.1\%$ proposed by [174] has been found to be a good means to obtain rough estimates within a short calculation time. Note that other interruption criteria will be introduced later on.

Since the iterative process is governed by the used data it is of interest to which degree the convergence behaviour of the adaptive algorithm is influenced by the type of the applied input force. In order to investigate the sensitivity of the inversion routine to different input signals the previous numerical model was expanded. Three different force signatures were generated and convolved with the impulse response function to obtain the respective acceleration response of the system. The inversion routine was then applied to the noise free response so as to reconstruct the input force. As excitations a periodic load (Simulation I), a load sequence constructed of several impulses with different shapes (half-sine, rectangular and triangular) (Simulation II) and a single force transient (Simulation III) are used. It is stressed that all signals are designed to have similar range of magnitude, i.e. the distance between the maximum signal value and the modulus of the smallest value ($R(x(n)) = \max(x(n)) - |\min(x(n))| \approx 40\ N$).

Furthermore it is noted that the step size parameter μ in all simulations is identical to the one of the previous example in which a random input sequence was identified (see Figure 4.6). Also, the interruption criterion was chosen in accordance with the introduced $\eta = 0.1\%$ and $\eta = 0.001\%$ limit, respectively. In this way all results are directly comparable so that conclusions with respect to convergence speed, accuracy and stability can be drawn. The different simulation results are illustrated in Figure 4.7

Compared to the convergence speed achieved when reconstructing the random input signal in Figure 6 the iterative process performs much faster when employed to identify the periodic force signature. For the periodic input signal the $\eta = 0.1\%$ and $\eta = 0.001\%$ limit is reached already after $k = 17$ and $k = 50$ full iteration cycles, respectively. Satisfying force identification is possible when using either of the proposed interruption limits. It is noted that similar results can be achieved for periodic signals of different frequency as long as sufficient excitation of the system is possible, i.e. the excitation frequency need to lie within the frequency range in which the system can be assumed to be linear and its FRF is known with satisfying accuracy. It is believed that the good convergence behaviour results from the smoothness of the signal with respect to differentiability, meaning that the signal does not contain sudden jumps or sharp discontinuities as in the case of the random signal (Figure 4.6).

Simulation I: Periodic input force

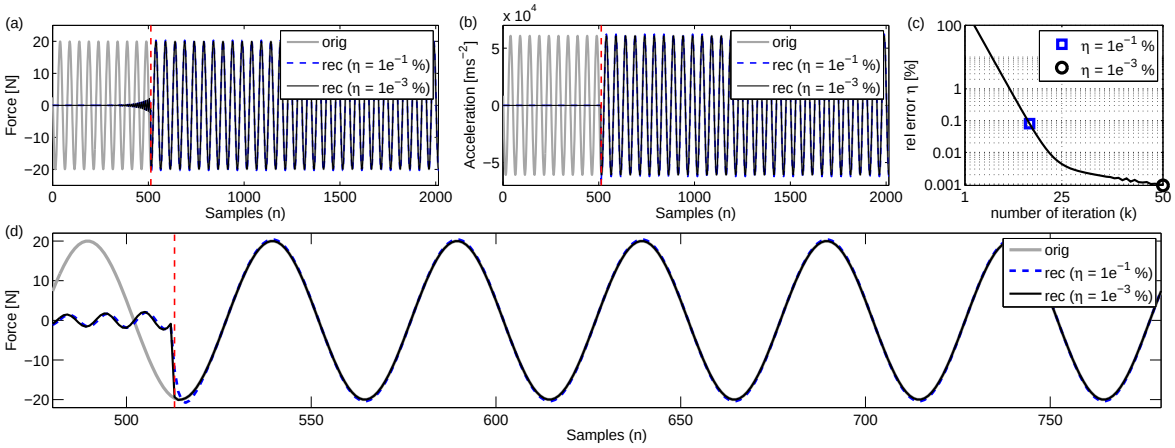

Simulation II: Input force constructed of differently shaped impulses

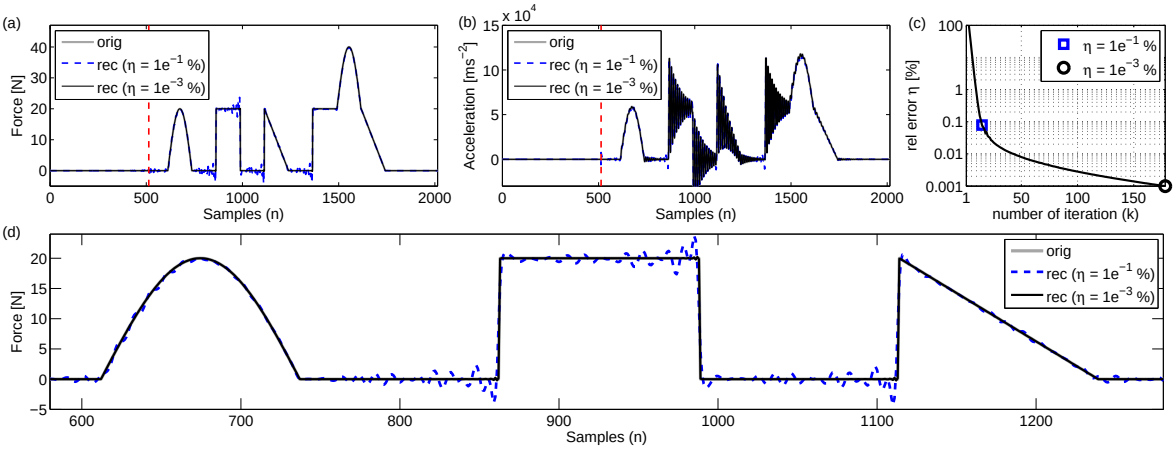

Simulation III: Transient input force (sharp impulse)

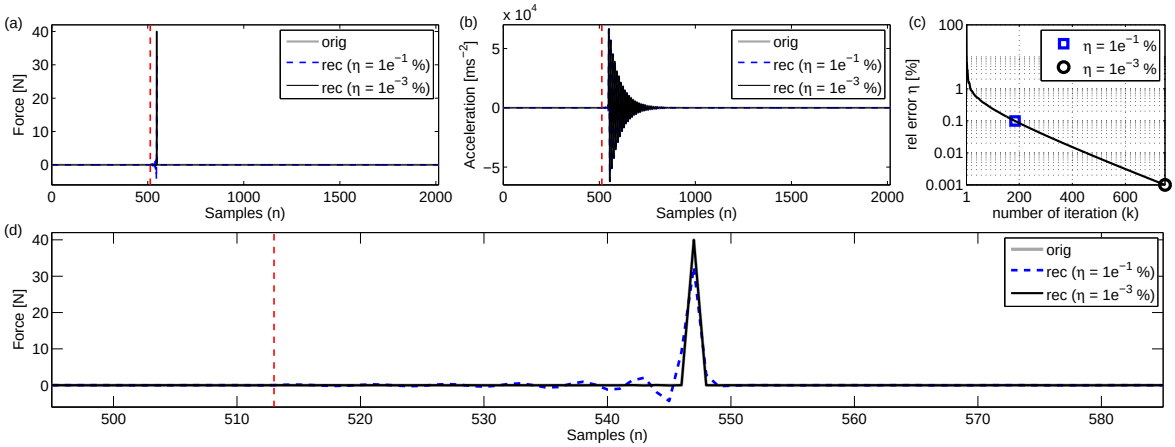

Figure 4.7. Simulation results for 3 different input force signatures (periodic - Simulation 1, constructed impulse sequence – Simulation 2, single transient –Simulation 3): Original and reconstructed force time history in full length (a) and close up (d), desired and reconstructed acceleration time history (b), progression of relative mean prediction error (c). —— original signal, ---- reconstructed signal using η = 0.1 % as interruption criterion, —— reconstructed signal using η = 0.001 %

The influence of discontinuities in the force signature on the convergence behaviour becomes apparent when employing the inversion routine to identify impulsive force signatures as illustrated in Figure 4.7 – Simulation II. It can clearly be seen that the estimation error in the vicinity of a discontinuity increases significantly if the iterative process is stopped too early, e.g. when using the $\eta = 0.1\%$ interruption criteria. It is stressed that perfect force reconstruction is possible if the iterative process is carried out sufficiently, i.e. when interrupting the iterative process according to the $\eta = 0.001\%$ limit. However, when choosing an insufficient number of iterations ($\eta = 0.1\%$) the reconstructed force generally tends to oscillate at times shortly before a discontinuity occurs in the original signal. The amplitudes of the associated 'ripples' (overshoot and undershoot of the original signal) vary with the sharpness of the local discontinuity as illustrated in diagram (d) (Figure 4.7 - Simulation II) where three differently shaped impulses are magnified. Accordingly, the best force reconstruction is achieved for the half-sine impulse which features only moderate 'jumps' between two neighbouring sample values at the roots of the impulse ($n = 612$, and $n = 738$ samples). Instead, the iterative routine struggles to approximate the sudden jumps occurring at the beginning and the end of the rectangular impulse ($n = 862$, and $n = 988$ samples) and the beginning of the triangular impulse ($n = 1112$ samples) while the end of the triangular impulse ($n = 1238$ samples) is reconstructed satisfactorily since the discontinuity is less sharp. In this example it turns out that the bound of the ripples for the sudden jumps is about 15% of the height of the discontinuity's modulus. Convergence according to the defined limits for the RMPE can be achieved after $k = 15$ ($\eta = 0.1\%$) and $k = 178$ ($\eta = 0.001\%$) iteration cycles, respectively.

In many situations identification of impact loads is of particular interest. Typically the time history of the acting impact forces can be considered as being sparse, meaning that the signal comprises a small number of nonzero samples, which for impact excitations usually take very large values, while all other values are assumed to be of negligible size. In order to evaluate the suitability of the proposed time domain inversion routine for performing inverse analysis of impact forces an additional simulation was carried out. The time history of the assumed impact load to be identified was modelled as a single force transient characterised by a single nonzero sample with a relatively high value. The simulation results are illustrated in Figure 4.7 – Simulation III. Note that the degree of sparsity of the force signal does not influence the convergence behaviour of the inversion routine. It is rather the characteristics of the nonzero

part of the force time history that affects the convergence behaviour. Since the defined impact force features closely located, sharp discontinuities at its beginning ($n = 546$), its peak ($n = 547$) and its end ($n = 548$) the inverse routine struggles to reconstruct the force transient if the iterative process is not carried out sufficiently. Thus, using the $\eta = 0.1\,\%$ limit yield to interrupting the iterative process too early causing considerable rippling prior to the force impulse (about 10% of the height of the discontinuity) while the maximum amplitude of the impulse is underestimated significantly (about 23% of the impulse's peak value). On the contrary, using the $\eta = 0.001\,\%$ limit facilitates carrying out the iterative process sufficiently and the reconstructed impact force match exactly with the original one (see black curves in diagram (a) and (d)). Convergence according to the set limits for the RMPE can be achieved after $k = 184$ ($\eta = 0.1\,\%$) and $k = 749$ ($\eta = 0.001\,\%$) iteration cycles, respectively.

At this stage it is concluded that the proposed adaptive algorithm allows for reconstruction of dynamic forces in time domain with high precision if (i) the system's IRF and the operational responses can be considered as ideal and (ii) the interruption criterion is chosen so that the iterative process can be carried out sufficiently. The inversion routine is generally suitable for any kind of sparse or non-sparse input signal including random, periodic, impulsive, transient or steady state signals. Discontinuities contained in the force time signature can generally be reconstructed exactly also they affect the convergence speed. To achieve the same estimation accuracy the iterative process has to be carried out more often if sharp discontinuities are present. Choosing the step size parameter properly (according to Eq. (4.10)) will generally yield a stable and convergent iterative process.

4.3. The modelling approach

In the previous section the fundamental principles of the derived time domain inversion routine were discussed and its functionality has been demonstrated for different force signatures. However, one basic assumption was that the used data is ideal in the sense that neither the system description nor the structural response contains any errors. The following sections are devoted to the use of the time domain identification technique for the predominant case where these assumptions do not hold, i.e. where noise in the response measurements or inconsistencies in the impulse response function are present and may degrade the reconstruction process.

4.3.1. System and noise model

As concluded in the previous section, the convergence speed is affected by discontinuities inherent in the sought input force. In this respect identification of impact excitations has been found to be most demanding. In order to achieve conservative results which are generally valid for any other force signature and with reference to the aimed application of the inversion routine for identification of transient forces in electrical steering systems, a single force pulse will be used within all following examples. Instead of investigating the effectiveness of the method for measured data, at this stage purely numerical data is preferred due to the following considerations:

1. Numerical generated models and data are free from any uncertainties. Considering again that the inversion routine is based on the error signal $e(n_k) = d(n_k) - \sum_{i=0}^{I-1} h(i)\mathbf{x}(n_k - i)$ (see Eqs. (4.4),(4.1)) it is clear that noise or errors in either the considered part of the desired response $d(n_k)$ or the impulse response function $h(i)$ could easily affect the adaptive inversion process.
2. The computational effort to sufficiently carry out the iterative process can be decreased by using short sequences for the impulse response function (IRF) and the system in- and outputs. Time efficiency is an important factor since profound study of the time domain inversion routine requires repeating simulations several times, for example, to account for different noise levels or different parameterisation of the model.
3. The iterative process requires sufficiently decayed impulse response functions so as to carry out the ensemble average by assuming periodicity of the filter and the desired signal (see section 4.2.2). Modelling IRFs guarantees that this condition is perfectly satisfied.

For the mentioned reasons relatively simple numerical models are believed to be best suited for investigating the convergence behaviour of the iterative routine under different conditions. In particular, the sensitivity of the inversion routine to noise inherent in the used data will be studied. The basic modelling procedure employed is as follows (see also Figure 4.8):

1. Definition of the I-tap impulse response vector $\mathbf{h} \in \mathbb{R}^{I\times 1}$: Impulse response functions (IRFs) are generated numerically by calculating the unit impulse response of second-order damped linear systems, according to the descriptions given in section 4.2.4. In some cases it is beneficial to build a system model based on pre-measured impulse response functions. This may be the case to generate detailed models of sophisticated technical

structures with preferably multiple in- and outputs, e.g. a model of the dynamic properties of the gear box housing of an electrical steering system (cf. section 4.6). To obtain IRFs from experiments, the measured frequency response functions are converted into time domain employing inverse Fourier transformation. Note that further actions are required to obtain impulse response functions that can satisfactorily be used within the inversion routine (see. chapter 5.6.).

2. Definition of the original assumed unknown input force sequence $x_u(n) \in \mathbb{R}^{N\times 1}$ where the condition $N \geq 2 \cdot I$ needs to be satisfied. As discussed above, impulsive force signatures are of main interest within this study.
3. Calculation of the desired response sequence $d(n) \in \mathbb{R}^{N\times 1}$ by convolving the input force $x_u(n)$ with the corresponding impulse response function $h(i)$.
4. Definition of additional noise sequences: In order to account for measurement noise and other errors in the used data random sequences of white noise are generated and added to the respective signals. In essence, noise corrupted signals are simulated according to

$$\tilde{\mathbf{g}}_{noise}(n) = \mathbf{g}_{ideal}(n) + \underbrace{\frac{NP_{\%}}{100\,\%}\left(\sqrt{\frac{\sum_{j=1}^{Nt} {g_{ideal}}^2(j)}{N_g}}\right)\mathbf{w}(n)}_{Noise} \tag{4.15}$$

where $\mathbf{g}_{ideal}$ is the N_g-length column vector of the (calculated) noise free signal, $\tilde{\mathbf{g}}_{noise}$ is the noise corrupted version of $\mathbf{g}_{ideal}$, $NP_{\%}$ is a specified noise level defined in percent and $\mathbf{w}(n) \in \mathbb{R}^{N_g \times 1}$ is the vector of normally distributed random numbers with zero mean and variance equal to 1. Employing Eq. (4.15) results in adding noise with an amplitude of $NP_{\%}$ of the RMS of the noise free (ideal) signal. The definition of the signal $g_{ideal}(n)$ depends on which data is assumed to contain additional noise. Basically, noise can be added to the desired response or the impulse response function. According to their respective length N_g needs to be chosen as $N_g = N$ when simulating noise in the desired response and $N_g = I$ when the impulse response is assumed to be noisy.

The block schematic in Figure 4.8 visualises both possibilities of how the noise model from Eq. (4.15) can be related to the different signals involved in the iterative process.

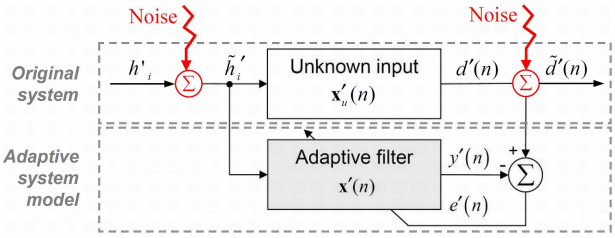

Figure 4.8. Modelling approach to account for measurement noise in different data sets

4.3.2. Performance evaluation

Rigorous evaluation of the performance of the proposed time domain (TD) inversion routine is crucial. One way to obtain a measure of the performance is to compare the identified force(s) with the exact one(s) so as to quantify their deviations. Since only numerical data will be used to validate the TD inversion routine by simulation the exact solution is always available allowing the use of normalised error measurements to evaluate the estimation accuracy without any source of uncertainty included. In detail, the root mean square (RMS) estimation error will be utilised to quantify the estimation accuracy in time domain. The RMS error is defined as the scalar

$$\varepsilon_{x,\%RMS} = \frac{\sqrt{\sum_{n_k=I+1}^{N}\left(x(n_k)-x_u(n_k)\right)^2}}{\sqrt{\sum_{n_k=I+1}^{N}\left(x_u(n_k)\right)^2}}\cdot 100\,\% \tag{4.16}$$

where $x(n_k)$ and $x_u(n_k)$ are the reconstructed force and the true one, respectively [157]. Note that only the reliable time range is considered for calculation of the estimation error. Note further that this time domain error is widely used to quantify the estimation accuracy of different force identification techniques (see e.g. [127],[161],[131],[134],[160],[157],[120]) for which reason it is also adopted in this study. An analogue error is used to evaluate the accuracy of the reconstructed response

$$\varepsilon_{y,\%RMS} = \frac{\sqrt{\sum_{n_k=I+1}^{N}\left(y(n_k)-d(n_k)\right)^2}}{\sqrt{\sum_{n_k=I+1}^{N}\left(d(n_k)\right)^2}}\cdot 100\,\% \tag{4.17}$$

where $y(n_k)$ is the estimated response and $d(n_k)$ is the desired response. As the desired response, by definition, is known at any time this error can also be used when the sought input force is unknown.

Besides solely using TD prediction errors also the according spectral errors are believed to provide important information about the performance of the proposed TD inversion routine.

For this reason, in the frequency domain, spectral estimation errors are used to quantify the accuracy of the identified forces and responses. The spectral estimation error in the reconstructed force is defined as

$$\Delta X(\omega) = 20\log\left(\left|\frac{X_{rel}(\omega)}{X_{u,rel}(\omega)}\right|\right) \tag{4.18}$$

where $X_{rel}(\omega)$ is the spectrum of the identified force which is calculated using only the reliable part of the time signal ($I+1 \le n_k \le N$) and $X_{u,rel}(\omega)$ is the corresponding spectrum of the true force. The corresponding spectral error in the reconstructed response is defined as

$$\Delta Y(\omega) = 20\log\left(\left|\frac{Y_{rel}(\omega)}{D_{rel}(\omega)}\right|\right) \tag{4.19}$$

where $Y_{rel}(\omega)$ and $D_{rel}(\omega)$ are the spectra of the reconstructed and the desired response, respectively.

The spectrum is obtained employing discrete Fourier transform (DFT) to the reliable time range of the corresponding time sequence $g(n)$, i.e. $g(n) = x(n_k)$ for the identified force, $g(n) = x_u(n_k)$ for the true force, $g(n) = y(n_k)$ and $g(n) = d(n_k)$ for the reconstructed and the desired response, respectively. The reliable part of the time signal is denoted by

$$g_{rel}(n) = g(n)\big|_{I+1 \le n \le N} \tag{4.20}$$

where *N* denotes the length of the considered part of the signal according to the constraints involved in the adaptive inversion routine (see section 4.2.2). The DFT of the reliable part of the time signal is then given as

$$G_{rel}(\omega) = G_{rel}(l) = \sum_{n=0}^{N_{rel}-1} g_{rel}(n)\, e^{-j(2\pi/N_{rel})nl} \tag{4.21}$$

where *l* is the integer frequency variable, *j* is $\sqrt{-1}$ and $N_{rel} = N - (I+1)$ is the length of the reliable part of the respective time sequence as defined above. Note that in Eq. (4.18), (4.19) and (4.21) ω is used to indicate the frequency dependence of the respective quantities and is used for either continuous or discrete frequency domain representation throughout this thesis. Note further that the transform (DFT) will be denoted by the symbol $\mathcal{F}$ in the following so that the vector containing the spectrum of the reliable range of a time sequence can conveniently be expressed as

$$\mathbf{G}_{rel}(\omega) = \mathcal{F}\left\{g(n)\big|_{I+1 \le n \le N}\right\}. \tag{4.22}$$

The inverse discrete Fourier transform (IDFT) is defined analogously as

$$g_{rel}(n) = \frac{1}{N_{rel}} \sum_{l=0}^{N_{rel}-1} G_{rel}(l)\, e^{j(2\pi/N_{rel})nl} \tag{4.23}$$

and will be denoted by the symbol $\mathcal{F}^{-1}$. In accordance to Eq. (4.22) and considering (4.20), the vector containing the sample values of the reliable part of the time sequence can be expressed as

$$\mathbf{g}_{rel}(n) = \mathcal{F}^{-1}\left\{\mathcal{F}\left\{g(n)\big|_{I+1\le n\le N}\right\}\right\} = \mathcal{F}^{-1}\left\{G_{rel}(\omega)\right\}. \tag{4.24}$$

Besides evaluating the performance of the time domain inverse method (TDM) in terms of deviations to the exact solution, one may also be interested in the performance behaviour of the novel TDM in comparison to the standard frequency domain inverse method (FDM) which is most widely used to perform inverse force identification in practice. In order to achieve comparable results in time domain (TD) and frequency domain (FD) simulations carried out with each method have to rely on equivalent models. To do so, the strategy illustrated in Figure 4.9 is invoked.

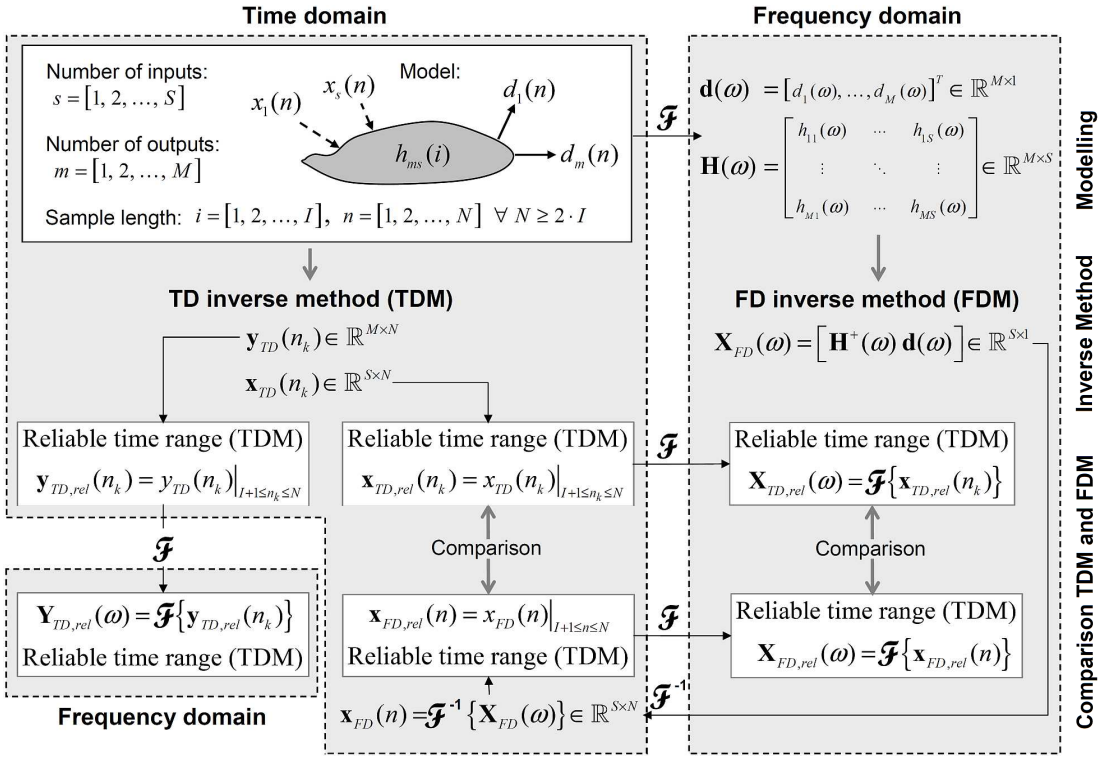

Figure 4.9. Strategy invoked for identification of dynamic input forces using the time domain inverse method (TDM) and the standard frequency domain inverse method (FDM). Both methods rely on the same data sets.

Both methods use the same fundamental data which is generated in time domain according to the modelling procedure described in the previous section. The obtained model provides all required data as time sequences, i.e. (i) numerically designed *N*-length impulsive force signatures to be identified from (ii) a set of finite impulse response functions (FIRs) of which each is of length *I* and (iii) the corresponding *N*-length time histories of the desired structural responses. Additional noise or errors in the data can be added in time domain according to Eq. (4.15).

Whereas the TDM can directly be applied to this data a pre-processing step is required for the FDM in which the full-length time data is transformed into frequency domain by means of DFT. Note that the DFT of the full-length signals is achieved according to Eq. (4.21) though the respective signal length has to be set according to the length of the signal being transformed to $N_{rel} = N$ for the forces and response time signatures or to $N_{rel} = I$ for the impulse response functions. In this way the time sequences are converted into spectra which are stacked up in frequency dependent vectors accounting for the structural responses and forces, respectively, or in matrices containing the system's frequency response functions (FRFs). It is noted that the dimensions of the vectors and matrices at each frequency ω vary with the number of unknown input forces $s = [1, 2, \ldots S]$ and the number of considered responses $m = [1, 2, \ldots M]$ as indicated in Figure 4.9. Furthermore it is stressed that no form of signal averaging is used when transforming data from time domain into frequency domain so as to ensure that errors (random noise) added to the time sequences are not reduced in the according spectra in the course of the transformation process. This is achieved by choosing a block size for the DFT of $N_{DFT} = N + I - 1$ samples and padding the corresponding time signals with zeros before DFT is carried out. This approach is believed to be essential in order to achieve an appropriate comparison between forces identified with the time domain inversion routine (TDM) and the standard frequency domain inverse method (FDM), respectively.

Simulations with each method are then carried out using the respective data sets so as to identify the assumed unknown forces. The TDM generally yields estimates for both, the structural responses and the applied input forces, denoted by the vectors $\mathbf{y}_{TD}(n_k)$ and $\mathbf{x}_{TD}(n_k)$, respectively, where the sub-script '*TD*' indicates that the time domain force identification routine was originally used to determine the accordant quantity. By definition, only values at times $n_k \geq I + 1$ can be considered as reliable estimates which in Figure 4.9 is indicated using the definition given in Eq. (4.20). Accordingly, the RMS estimation error in the identified

force and response time signatures can be calculated using Eqs. (4.16) and (4.17). To obtain the corresponding spectral estimation errors the time sequences first have to be transformed into frequency domain according to Eq. (4.21) or (4.22), as shown in Figure 4.9, before the reconstructed spectra can be compared to the true ones using Eqs. (4.18) and (4.19).

The FDM only facilitates identification of the unknown force spectrum (spectra) which is denoted by the frequency dependent vector $\mathbf{X}_{FD}(\omega)$, where the sub-script '*FD*' indicates that the identified quantity was originally calculated employing frequency domain inverse methods. However, the identified spectral force(s) contain information of the full-length time signals for which reason they cannot be compared directly with the force(s) provided by the TDM since the latter only contain(s) valid information for times $n_k \geq I+1$. In order to ensure comparability, the spectral force $\mathbf{X}_{FD}(\omega)$ is first transformed back into time domain by means of IDFT yielding the vector $\mathbf{x}_{FD}(n)$ containing the identified force time signature(s) in full-length (*N* samples). Based on this data the reliable part of the force time history ($\mathbf{x}_{FD,rel}(n)$) is selected according to Eq. (4.20) and the RMS estimation error is calculated using Eq. (4.16). The spectral estimation error is obtained by transforming only the reliable time range of the identified force signature(s) into frequency domain using DFT as defined in Eq. (4.21). The obtained spectral force(s) can finally be used to calculate the spectral estimation error according to Eq. (4.18) which now considers only the part of the identified forces which can also be predicted accurately with the TDM.

Employing this strategy facilitates conclusive comparison of estimation results achieved with both force identification techniques in time domain as well as in frequency domain. Thus, the strategy will invariably be used in the following sections to evaluate the accuracy and sensitivity of the novel TDM to noise and errors inherent in the used data in comparison to the standard FDM. Starting with the simplest case, i.e. identification of dynamic forces applied to single input single output (SISO) systems, the complexity of the time domain inversion routine and the invoked evaluation strategy will gradually be expanded in order to allow for force reconstruction for single input multiple output (SIMO) and multiple input multiple output (MIMO) systems, respectively.

4.4. Force reconstruction for single input single output systems

Aiming at future application of the derived time domain inverse method (TDM) for reconstruction of dynamic forces causing rattling in steering gears, the effectiveness of the

TDM needs to be investigated with respect to transient excitation forces. Reconsidering the findings from section 4.2.4 where a sparse load time history consisting of a single sharp force pulse has been found to be most critical with respect to the trade-off between convergence speed and estimation accuracy, the performance of the TDM will be evaluated for this assumed worst case scenario. Therefore, in the following examples, a transient input force is used which is designed as a $N = 513$ sample long signal of zero amplitude except of one sample at which the force pulse has a peak value of $x_{\max}(n = 276) = 40\,N$. The impulse response function of length $I = 256$ samples and the desired acceleration response of $N = 513$ samples are obtained as explained in section 4.3.1.

The assumed unknown input force is identified according to the TDM for SISO systems as given by the adaptive algorithm in Table 4.1. The FDM is conducted according to the explanations given in section 2.4.1. However, in the special case of identifying the input force for SISO systems, the force spectrum can be identified according to equation (4.25)

$$X_{FD}(\omega) = \left(1/H(\omega)\right) D(\omega) \tag{4.25}$$

where the spectrum of the known desired response $D(\omega)$ is pre-multiplied at each frequency ω by the reciprocal (multiplicative inverse) of the corresponding FRF. The performance evaluation and the comparison of the TDM and the FDM estimation results are carried out according to the description given in section 4.3.2.

4.4.1. Application to noise free system

A first simulation is conducted in which the used data is assumed to be free of any additional noise. The purpose of this simulation is to confirm the correctness of the strategy used to compare the different force identification results. Furthermore, the convergence behaviour, measured in terms of the relative mean estimation error (RMPE) $\eta(k)$ as introduced in Eq. (4.14), is monitored and will be used in later simulations to benchmark how additional noise added to the involved data sets may influence the convergence behaviour of the TDM. Based on the RMPE the iterative process involved in the TDM is interrupted according to the previously defined $\eta = 0.001\,\%$ criterion.

Figure 4.10 illustrates the simulation results for the identification of the impulsive input force assuming a noise free SISO system.

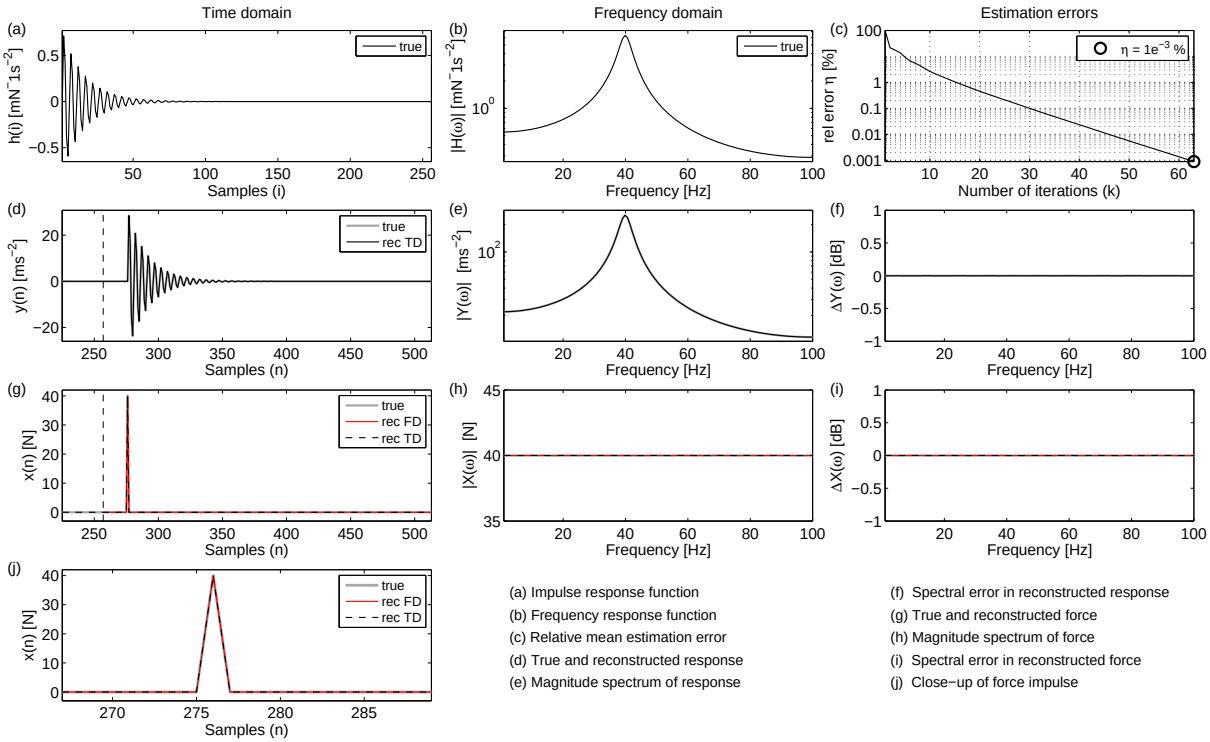

Figure 4.10. Numerical result for noise free SISO system. Representation of signals in time domain (a, d, g, j), representation of signals in frequency domain (b, e, h,) and different estimation errors (c, f, i): ▬ true signal; ── reconstructed response using TDM; ─ ─ reconstructed force using TDM; ── identified force using FDM.

Clearly, both inverse techniques, i.e. the time domain inverse method (TDM) and the standard frequency domain inverse method (FDM), perform excellently. Each of the methods is able to identify the assumed unknown force pulse with high precision. For the TDM $k = 63$ iterations are sufficient to reach perfect reconstruction of the acceleration responses, i.e. the final RMS error in the estimated response is $\varepsilon_{y,\%RMS} = 0.0\,\%$ and the according spectral estimation error is $\Delta Y(\omega) = 0.0\,\text{dB}$ (see Figure 4.10 - (d-f)). The estimation error in the reconstructed force time history is $\varepsilon_{x,\%RMS} = 0.0\,\%$ and the associated spectral estimation error is $\Delta X(\omega) = 0.0\,\text{dB}$ (see Figure 4.10 - (g-j)). The same estimation accuracy in time domain and in frequency domain is reached if the FDM is employed. Thus, for an ideally noise free SISO system it can be concluded that the TDM and the FDM perform equally. In this case the identified forces match exactly the original one(s). Further, it is stressed that the utilised system model and the invoked strategy to evaluate the performance of both force identification techniques has been proved suitable and will be used in the following to contrast both methods with each other for cases where the used data is corrupted by additional noise.

4.4.2. Sensitivity to noise in the structural response

In reality, noise will always be present in the measured response data. The time domain force identification technique is based on the error function in Eq. (4.4) which can be understood as a comparison of the output provided by the adaptive filter at each time step with the desired response. Since the adaptive filter aims to adjust its filter weights in such a way that the estimated filter output best approximates the desired response it becomes apparent that the force estimation accuracy will be negatively influenced if the adaptive algorithm tries to track a noise corrupted or otherwise defective desired response signal. To account for noisy measurement data, the previous simulation is repeated with additional noise added to the desired response according to Eq. (4.15). Different noise levels ranging from 5% over 10% to 25% of the RMS value of the noise free response are investigated resulting in signal-to-noise ratios of $SNR_{5\%} = 26\,\text{dB}$, $SNR_{10\%} = 20\,\text{dB}$ and $SNR_{25\%} = 12\,\text{dB}$, respectively. By means of example, the simulation results for the 10% noise corrupted response data are illustrated in Figure 4.11. Note that simulation results for the other noise levels can be found in Appendix A.2.

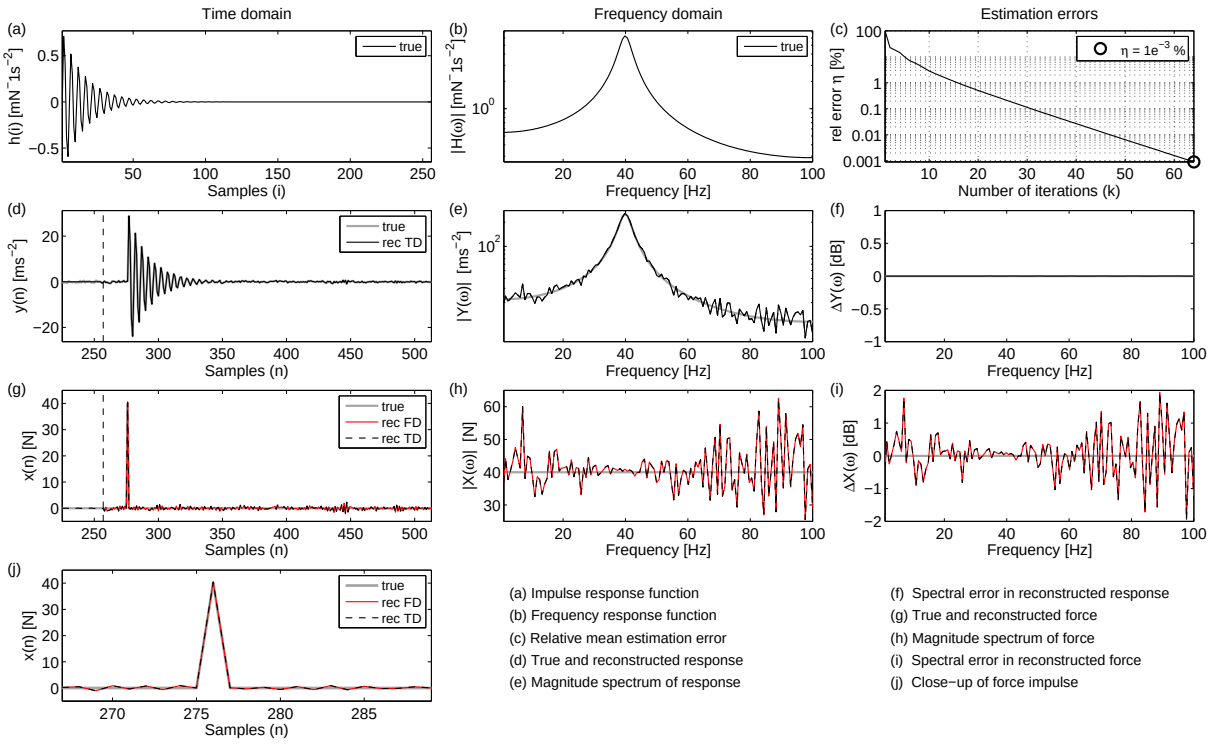

Figure 4.11. Numerical result for SISO system with 10% noise added to the acceleration response. Representation of signals in time domain (a, d, g, j), representation of signals in frequency domain (b, e, h,) and different estimation errors (c, f, i): ▬▬ true signal; ── reconstructed response using TDM; ─ ─ reconstructed force using TDM; ── identified force using FDM.

As can been seen from Figure 4.11 - (c), a convergent solution is achieved after carrying out the iterative process for $k = 64$ iterations in order to reach the predefined interruption criterion of $\eta = 0.001\,\%$. Revisiting the convergence behaviour of the TDM for the noise free SISO system in the previous example where $k = 63$ iterations are required to satisfy the interruption criterion, the convergence speed of the TDM seems to be insensitive to additional noise in the response data. Note that this conclusion is coherent with the simulation results obtained for the same SISO system with 5% and 25% noise added to the response data, respectively (cf. Appendix A.2).

The desired and reconstructed acceleration response match perfectly (Figure 4.11 - (d-f)) yielding an estimation error in time domain and in frequency domain of $\varepsilon_{y,\%RMS} = 0.0\,\%$ and $\Delta Y(\omega) = 0.0\,\mathrm{dB}$, respectively. However, as expected, the additional noise in the desired response degrades the force reconstruction process so that the applied impulsive force signature cannot be reconstructed precisely (see Figure 4.11 - (g) and (j)). Although the peak value of the force pulse can be reconstructed accurately (Figure 4.11 - (j)) the identified force signature contains considerable noise beside the force transient. This noise is reflected in the RMS estimation error which now indicates an error in the reconstructed force time history of $\varepsilon_{x,\%RMS} = 24.8\,\%$. The additional energy contained in the noisy part of the reconstructed force signature becomes apparent when investigating the corresponding magnitude spectrum, as shown in Figure 4.11 - (h), which exhibits severe deviations from the true force spectrum. It is noted that deviations in the identified force spectrum correlate well with the noise included in the spectrum of the desired response as can be seen from Figure 4.11 - (e). The spectral estimation error in the identified force can take values up to $\left|X_{TD,\max}(\omega)\right| = 2\,\mathrm{dB}$, in particular in the low and high frequency range since here the acceleration response undergoes the noise floor (see Figure 4.11 - (e)).

Using the standard frequency domain inverse method (FDM) yields exactly the same estimation accuracy as the TDM. The force signature identified by means of the FDM is indistinguishable from the one obtained with the TDM (see Figure 4.11 - (g) and (j)) and so are the according force spectra (Figure 4.11 - (h)) and the corresponding error measurements in time domain (cf. Table 4.2) and frequency domain (cf. Figure 4.11 - (i)).

It is concluded that for the investigated SISO system any amount of noise added to the response data has been found to degrade the force identification accuracy, independent of which inverse method is used. The more noise is added to the response data the more noise

will be included in the identified force, especially at frequencies at which the response spectrum is below the noise floor. In all investigated cases (see also Appendix A.2) the TDM and the FDM have performed exactly the same for which reason no advice can be given which method should preferably be used to identify forces in SISO systems under the assumption that solely the response data is defective. Important to note is, however, that the transient force pulse in all simulations has been reconstructed with high precision, which is an important finding considering future applications of the TDM for identification of impulsive force signatures, as e.g. required to characterise transient structure-borne sound sources in electrical steering systems.

With respect to the severe discrepancies in the reconstructed force (obtained with either inverse method) and considering the zero estimation error in the reconstructed response provided by the TDM, it is noted that observing solely the relative mean estimation error (RMPE) $\eta(k)$ to monitor the performance of the TDM does not implicitly guarantee accurateness of the identified forces. However, the RMPE is a very helpful means to evaluate the general convergence behaviour of the TDM and will invariably be used for this purpose. Instead, other attempts to evaluate the accuracy of the estimated force(s) if the true force(s) is not available will be discussed in chapter 5.

4.4.3. Sensitivity to errors in the system model

Errors in the (inverse) system model usually do not result from issues with noise included in the FRF measurements but are rather related to practical issues with adequate placement of sensors (cf. ‘spatial discretisation’ in section 2.4) or consistent excitation of the passive structure in the desired degrees of freedom. For these reasons, system descriptions based on pre-measured FRFs in practice can generally be considered to contain inconsistencies (errors) to some extent. In the examples presented in this chapter inconsistencies in the system model are modelled as white noise sequences added to the associated impulse response function(s) as defined in Eq. (4.15). The influence of such inconsistencies on the force identification accuracy is investigated in the following for SISO systems.

As elaborated in section 4.2, the finite impulse response function (FIR) is involved in the iterative process of the TDM twice. It is employed (i) to compute the error signal (Eq. (4.4)) before (ii) the error multiplied by a convergence determining factor (2μ) is ultimately used to weight the FIR so as to achieve an update of the reconstructed force at each time step

(Eq. (4.12)). Hence, any error included in the FIR is likely to affect the force identification process rigorously. The sensitivity of the TDM in comparison to the FDM is investigated for different levels of inconsistencies corresponding to 5% and 10% of the RMS value of the system's true impulse response function. The associated signal-to-noise ratios are $SNR_{5\%} = 26\,\text{dB}$ and $SNR_{10\%} = 20\,\text{dB}$ which are approximately the same as the ones of the noise corrupted response data from the previous examples. Figure 4.12 exemplifies the effects of inconsistencies in the impulse response function if 10% white noise is added to the true FIR. Note that the simulation results for the 5% corrupted FIR data are provided in Appendix A.2.

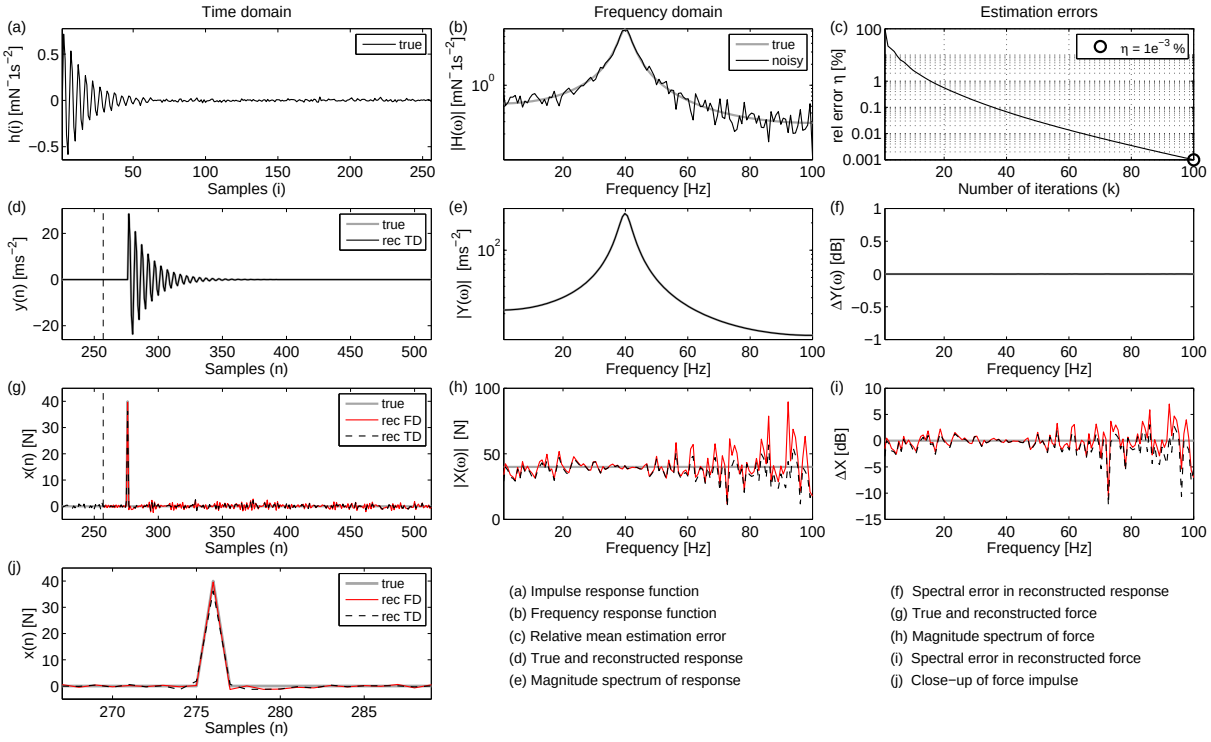

Figure 4.12. Numerical result for SISO system with 10% noise added to the impulse response function. Representation of signals in time domain (a, d, g, j), representation of signals in frequency domain (b, e, h,) and different estimation errors (c, f, i): ▬ true signal; ── reconstructed response using TDM; ─ ─ reconstructed force using TDM; ── identified force using FDM.

Investigating first the convergence behaviour of the TDM measured in terms of the RMPE (Figure 4.12 - (c)) it turns out that the additional noise in the FIR decreases the convergence speed. Compared to the simulations performed for the noise free SISO system (cf. Figure 4.10) and the SISO system with noise added to the response data (Figure 4.11 and Appendix A.2) the iterative process has to be carried out more often to reach the postulated $\eta = 0.001\,\%$ interruption criterion. In detail $k = 100$ iterations are required for the SISO system with 10% defective FIR data. In other simulations with different levels of inconsistencies in the FIR data

it has been found that the convergence speed tends to decrease if the level of inconsistencies increases, e.g. for 5% noise corrupted FIR data in average $k = 70$ iterations are required (see also Appendix A.2) while degrading the FIR to a level of 25% results in approximately $k = 215$ iterations to reach the $\eta = 0.001\,\%$ interruption criterion.

Due to the strict interruption criterion the residual error in the reconstructed response is approximately zero in the time domain ($\varepsilon_{y,\%RMS} = 0.0\,\%$) as well as in the frequency domain ($\Delta Y(\omega) = 0.0\,\text{dB}$), as can be seen from Figure 4.12 - (d-f). However, the defective FIR data causes the predicted force to contain severe errors beside the transient force pulse and the peak value of the pulse itself tends to be slightly underestimated using any of the tested inverse methods. Generally, the standard frequency domain inverse method (FDM) seems to be more sensitive to inconsistent system descriptions than the time domain inversion routine (TDM). In essence, the time history of the identified force using the FDM appears to be more 'noisy' than the one obtained with the TDM (see Figure 4.12 - (g) and (j)). This finding is reinforced by comparison of the corresponding time domain estimation errors which are $\varepsilon_{x,FD,\%RMS} = 35.7\,\%$ for the FDM and $\varepsilon_{x,TD,\%RMS} = 28.8\,\%$ for the TDM, respectively. The additional energy in the identified force signature put forth by the errors included in the FIR data results in severe discrepancies at frequencies governed by the modelled inconsistencies, as can be found by comparing the magnitude spectrum of the defective FRF in Fig.12 – (b) with the reconstructed force spectra illustrated in Fig.12 – (h).

It is noted that the FDM tends to dramatically overestimate the force spectrum at frequencies where the FRF assumes small values caused by the modelled random inconsistencies. Revisiting Eq. (4.25) where the reciprocal of the FRF is used at each frequency to estimate the force spectrum this behaviour is plausible and seems to constitute a general shortcoming of the FDM. Instead, the force spectrum calculated by means of the TDM appears to be less affected by errors in the FIR data and generally match better with the true spectrum. This is also affirmed by the corresponding spectral estimation errors provided in Fig.12 – (i). Equivalent conclusions have been drawn for simulations with different levels of inconsistencies added to the FIR data (see e.g. Appendix A.2).

4.4.4. Conclusions

It has been found that the derived time domain inversion routine (TDM) in general is suitable for reconstructing transient forces in SISO systems under the assumption that the basic

constraints are provided (i.e. sufficiently decayed impulse response function of finite length, the considered part of the desired response is at least twice of the length of the finite impulse response function (FIR), no other unaccounted external forces are acting on the structure)

- the used data is neither noise corrupted (response data) nor inconsistent (FIR data)
- and the iterative process is carried out sufficiently.

The influence of noise and inconsistencies included in the structural response and the system model, respectively, was investigated for a numerically designed SISO system. In order to achieve a fair evaluation of the TDM's sensitivity to such errors, its performance measured in terms of convergence speed and estimation accuracy was compared to the standard frequency domain inverse method (FDM). All simulations results are summarised in Table 4.2.

Table 4.2. Summary of all simulation results achieved with the novel time domain inversion routine and the standard frequency domain inverse method for force identification in single input single output (SISO) systems.

Amount of noise		Corrupted signal		TD inversion routine		FD inverse method
				Error ε_{RMS} in reconstructed response [%]	Error ε_{RMS} in reconstructed force [%]	Error ε_{RMS} in reconstructed force [%]
RMS [%]	SNR [dB]	$g(n)$	(Type)	$y(n)$	$x_{TD}(n)$	$x_{FD}(n)$
0	-	-	-	0.0	0.0	0.0
5	26	$d(n)$	(response)	0.0	11.9	11.9
		$h(i)$	(IRF)	0.0	13.8	14.6
10	20	$d(n)$	(response)	0.0	24.8	24.8
		$h(i)$	(IRF)	0.0	28.8	35.7
25	12	$d(n)$	(response)	0.0	50.7	50.7

For the conducted simulations it has been found that

- exact force identification is possible with the FDM and the TDM if neither the structural response nor the system model comprises any errors,
- both methods, the FDM and the TDM, perform exactly the same if only the structural response is corrupted by additional (white) noise. The residual error in the identified force correlates with the amount of noise added to the response, i.e. the error increases with increasing noise level. For the investigated noise levels the time range of the identified force signature corresponding to the duration of the transient force pulse is reconstructed with high precision whereas considerable noise can occasionally appear in the estimated force signature for times beside the pulse.

- the FDM seems to be more sensitive to errors in the system description than the TDM. While the FDM tends to (dramatically) overestimate the force spectrum at frequencies where the FRF assumes low values the TDM performs better and generally yields more reliable force predictions. Energy introduced due to overestimation in frequency domain may significantly degrade the estimation accuracy in time domain which is ascertained by higher RMS estimation errors in the reconstructed force signatures for the FDM compared to the ones achieved with the TDM.
- the relative mean prediction error (RMPE) is not a sufficient criterion to evaluate the residual error in the reconstructed force time history. However, it constitutes a good means to monitor the convergence behaviour of the iterative process involved in the TDM.

Furthermore, it is stressed that the iterative process involved in the TDM converged in all examples even in the presence of considerable errors in the used response data or the system model. Therefore, the iterative process is considered to be robust for noise and inconsistencies. All findings are consistent with the findings presented in [174],[206] and [207].

4.5. Force reconstruction for single input multiple output systems

In the previous section it is discussed that the derived time domain inverse method (TDM) is sensitive to noise included in the used structural responses and inconsistencies in the system model. This problem is tackled in the following and a modified version of the adaptive time domain algorithm is presented that facilitates compensating for uncorrelated errors in the used data sets. By means of numerical examples the performance of the expanded TDM and its sensitivity to errors in the utilised data is investigated and compared with the standard frequency domain inverse method (FDM). The main idea to expand the SISO time domain inversion routine is based on the concept of over-determination as elaborated in the following sections.

4.5.1. The concept of over-determination and the averaged error gradient

It is known that over-determining the system, i.e. by consideration of a larger number of structural responses than forces to be identified, can reduce the extreme sensitivity of frequency domain inverse methods (FDM) to measurement errors [20]. Sufficient over-

determination is achieved if the number of modes contributing to the considered responses at a given frequency exceeds the number of applied forces. Thus, selection of suitable measurement positions is significant in order to improve the condition of the FRF matrix. Since the proposed time domain inverse routine (TDM) does not require solution of an equation system by inversion of a possibly ill-conditioned FRF matrix, the choice of measurement positions is less crucial than for common FD inverse methods. Difficulties with (FRF) matrices near to singularity will not emerge. Still, noise in the measured impulse response functions (IRFs) or the desired structural responses will affect the instantaneous gradient of a particular measurement position resulting in erroneous force reconstructions if only one response position is considered, as done in the SISO recursion in Eq. (4.12). However, under the general assumption that measurement errors at different positions are uncorrelated, spatial averaging over the instantaneous gradients of multiple response positions will compensate for the inherent errors. The mean over all instantaneous gradients will then converge towards the gradient expected without the influence of noise, thus leading to the required minimum squared error, as suggested in [174] and proved sufficient in [206] and [207].

The principle of over-determination with respect to the adaptive algorithm involved in the expanded time domain inversion routine can be illustrated in block diagram form as shown in Figure 4.13.

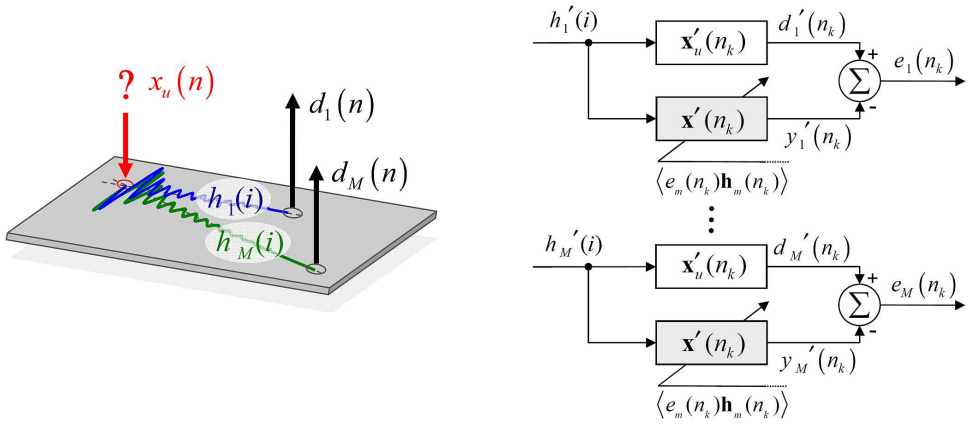

(a) (b)

Figure 4.13. Principle of over-determination for structures with single degree of freedom excitation: Schematic of force excited beam (a) and corresponding block diagram for adaptive input reconstruction in single input multiple output (SIMO) systems. (Apostrophes indicate constrained conditions; angle brackets denote the averaged error gradient used to update the estimated force at each time step.)

As can be seen from the block diagram, taking over-determination into account requires modifying the former SISO inversion routine (Eqs. (4.1), (4.4), (4.12) and (4.13)) as follows: First, an individual error for each response position is introduced. Referring to each response signal by means of the variable *m*, Eq. (4.4) expressed in terms of (4.1) gives the individual error signals

$$e_m(n_k) = d_m(n_k) - y_m(n_k) = d_m(n_k) - \sum_{i=0}^{I-1} x(n_k - i)\, h_m(i) \quad \text{for } m = [1, 2, \ldots, M] \tag{4.26}$$

where *M* denotes the total number of considered structural responses. Assuming for a moment noise free response data and a consistent system model the block diagram in Figure 4.13 could be construed as an array of *M* independent SISO systems from which *M*-1 systems would carry redundant information regarding the force identification procedure. In this case any of the structural responses could be selected to update the most recent prediction of the input force based on an estimate of the instantaneous error gradient which for SISO systems is defined as the product of a single error $e_m(n_k)$ and the corresponding impulse response function $\mathbf{h}_m(n_k)$ (see Eq. (4.12)).

However, as soon as uncorrelated noise or inconsistencies are added to the desired responses $d_m(n_k)$ or the impulse response functions $h_m(i)$ the instantaneous gradients of all measurement positions *m* are affected. This would inevitably result in unsatisfying force reconstruction if only SISO solutions were considered, as elaborated previously (see section 4.4). Considering now the principle of over-determination as depicted in Figure 4.13, averaging over several defective gradients will compensate for inherent uncorrelated errors as indicated by the angle brackets. Correspondingly, the instantaneous gradient in the SISO recursion (Eq. (4.12)) needs to be replaced by the average over all *m* instantaneous gradients, given for each response position as the error in Eq. (4.26) weighted with the respective FIR between the location of excitation and the corresponding response. The SISO recursion in this way is expanded for single input multiple output (SIMO) systems as

$$\mathbf{x}(n_{k+1}) = \mathbf{x}(n_k) + 2\mu_m \left\langle e_m(n)\mathbf{h}_m(n_k) \right\rangle \qquad \text{for } I \le n_k \le N \;\; \forall \;\; N \ge 2 \cdot I \tag{4.27}$$

where the angle brackets denote the averaged error gradient which is defined as

$$\left\langle e_m(n_k)\mathbf{h}_m(n_k) \right\rangle = \frac{1}{M}\left(\sum_{m=1}^{M} e_m(n_k) \cdot \mathbf{h}_m(n_k) \right). \tag{4.28}$$

The role of the averaged error gradient is to compensate for uncorrelated noise inherent in the used data sets, as discussed above. It is emphasised that the averaged error gradient is governed by the strongest of the *M* individual gradients. The latter is directly related to the response location to which the force contributes most (at a certain frequency) so that measurement positions with weak contributions from a force do not influence the adaptive process negatively. Instead, in frequency domain inverse methods 'weak' paths, which are highly susceptible to noise, bring about dominant contribution after inversion. For this reason the selection of additional measurement positions to achieve a sufficiently over-determined system is less crucial with the time domain inversion routine than using standard frequency domain inverse methods. Furthermore, the inversion process is likely to be more robust for noise in the used measurements. Note that this matter will be discussed in more detail in the following examples.

In order to achieve convergence in the mean-square, the step size parameter μ_m controlling stability and rate of adaption in the iterative routine also needs to be adjusted. It has been found [206],[207] that the step size parameter, in practice, needs to satisfy the stability bound

$$0 < \mu_m < M \cdot \left(\sum_{m=1}^{M} \sum_{i=0}^{I-1} \left| h_m(i) \right|^2 \right)^{-1} \tag{4.29}$$

where *M* is the total number of responses considered in the iterative process. Note that the step size parameter for all response locations is the same so that the sub-script '*m*' may be dropped. For reason of distinction between the different step size parameter used in the SISO and the (expanded) SIMO inversion routine, respectively, the sub-script, however, will be used throughout the thesis.

Table 4.3. Time domain inversion routine for identification of forces in single input multiple output systems.

Parameters:	n… time step k… iteration cycle N… length of input vector I… length of finite impulse response M… number of responses		
Initialisation:	$\mathbf{x}(n_{k=0}) = \mathbf{0}$		
Computation:	for $I \le n_k \le N \quad \forall \quad N \ge 2 \cdot I$	$k = k+1$	{1}
Filtering:	$y_m(n_k) = \sum_{i=0}^{I-1} x(n_k - i)\, h_m(i)$	for $m = [1, 2, \ldots, M]$	{2}
Error:	$e_m(n_k) = d_m(n_k) - y_m(n_k)$		{3}
Update:	$\mathbf{x}(n_{k+1}) = \mathbf{x}(n_k) + 2\mu \langle e_m(n_k)\, \mathbf{h}_m(n_k) \rangle$		{4}
Stability bound:	$0 < \mu < M \left(\sum_{m=1}^{M} \sum_{i=0}^{I-1} \left| h_m(i) \right|^2 \right)^{-1}$		{5}

In this way an expansion of the time domain inversion routine has been achieved that allows identification of dynamic forces for over-determined systems with single degree of freedom excitation. To complete one iteration cycle *k*, the mathematical steps (4.1), (4.26) and (4.27), in this order, are to be carried out, in accordance with the stability bound in (4.29). The expanded time domain inversion routine is summarised in Table 4.3.

According to the numbering given in the curly brackets the expanded time domain inversion routine can be summarised as follows: Starting with an initial guess of the unknown input force, at each time step n_k, the measured IRFs (h_m) are used to filter the current force estimate $x(n_k)$ so as to predict a response, $y_m(n_k)$, for each measurement position, m {2}. An individual error, $e_m(n_k)$, between each of the estimated filter outputs and the desired responses, $d_m(n_k)$, is calculated {3}. The average over all instantaneous errors weighted with the corresponding IRF is then used to update the current force estimate recursively {4}. In order to achieve an iterative procedure these steps are to be repeated at each iteration cycle k according to the constraints given in equation {1}. To ensure convergence the step size parameter, μ_m, needs to be chosen according to the stability bound in equation {5}.

4.5.2. Application to noise free system

Certainly, the use of the derived SIMO time domain inversion routine, as given in Table 4.3, is only advantageous if the employed response data or the system model is defective to some extent. Nevertheless, the SIMO routine is obliged to hold also for non-corrupted data sets. This requirement is used to validate the correctness of a newly designed SIMO model (see Figure 4.14) and to confirm that the strategy used to compare the time domain inverse method (TDM) with the standard frequency domain inverse method (FDM) still holds for single input multiple output systems.

Therefore, a SIMO system is set up according to the modelling approach explained in section 4.3. For this purpose the transient force pulse from section 4.4 is convolved with 4 created impulse response functions (IRFs) $h_m(i)$ for $m = [1, 2, \ldots, 4]$ (see IRFs in Figure 4.14 – (a) and the associated FRFs in (b)) in order to calculate the corresponding set of desired responses $d_m(n)$ (see true responses in TD in Figure 4.14 – (d) or in FD in (e)). To evaluate the effectiveness of the expanded TDM in relation to the original SISO algorithm all conducted simulations include force estimation results obtained by using the SISO routine from Table 4.1 as well as solutions obtained by employing the expanded SIMO algorithm from Table 4.3.

To indicate that a quantity, e.g. force or relative mean prediction error, is determined by consideration of a single error gradient using the SISO recursion the notation '$\nabla\xi m$' for $m=[1, 2, \ldots, 4]$ is used. Instead, estimation results obtained by employing the expanded SIMO algorithm are denoted by $\langle\nabla\xi\rangle$ so as to reveal that the solution is based on the use of the averaged error gradient (Eq. (4.28)).

To monitor the convergence behaviour of the TDM, the previously introduced relative mean prediction error (RMPE) $\eta(k)$ (see Eq. (4.14)) is used for all simulations conducted with the SISO algorithm. Again, a RMPE value of $\eta = 0.001\,\%$ is used to interrupt the different iterative processes. For the SIMO TDM the RMPE needs to be expanded in order to account for multiple response locations considered in the adaptive algorithm. The expanded RMPE (E-RMPE) can be formulated as

$$\eta_m(k) = \frac{1}{M}\cdot\sum_{m=1}^{M}\left(\frac{\sum_{n_k=I+1}^{N}\left[e_m(n_k)\right]^2}{\sum_{n_k=I+1}^{N}\left[d_m(n_k)\right]^2}\right)\cdot 100\%\,. \tag{4.30}$$

where *M* indicates the total number of response positions and the errors $e_m(n_k)$ are calculated according to Eq. (4.26). Note that only one prediction error exists so that the sub-script '*m*' may be dropped in the notation of the E-RMPE. However, in the remainder of this thesis the sub-script will be used to distinguish between the RMPE of the SISO TDM ($\eta(k)$) and the E-RMPE of the SIMO algorithm ($\eta_m(k)$). Unfortunately, the E-RMPE cannot be used as criterion to interrupt the iterative process involved in the SIMO TDM since the averaged error gradient can cause substantial deviations between the desired and the reconstructed response signals (see e.g. section 4.5.3 and 4.5.4) and their difference, i.e. the error $e_m(n_k)$, is involved in Eq. (4.30). Thus, the absolute value of the E-RMPE is dependent on the application case, for which reason no specific limit to interrupt the iterative process can be defined. Notwithstanding this, the progression of the E-RMPE is still very useful to observe the convergence behaviour of the SIMO TDM. Since no alternative interruption criterion is presented at this stage the iterative process of the SIMO TDM in the following examples is interrupted according to the number of iterations required by the slowest converging SISO simulation to reach the defined RMPE value of $\eta = 0.001\,\%$. Note that alternative interruption criteria will be discussed in section 5.5.

According to the given explanations a first simulation is conducted assuming that noise free structural responses and a consistent system model are present. The simulation results obtained with the SISO and SIMO time domain inversion routine, respectively, are illustrated in Figure 4.14.

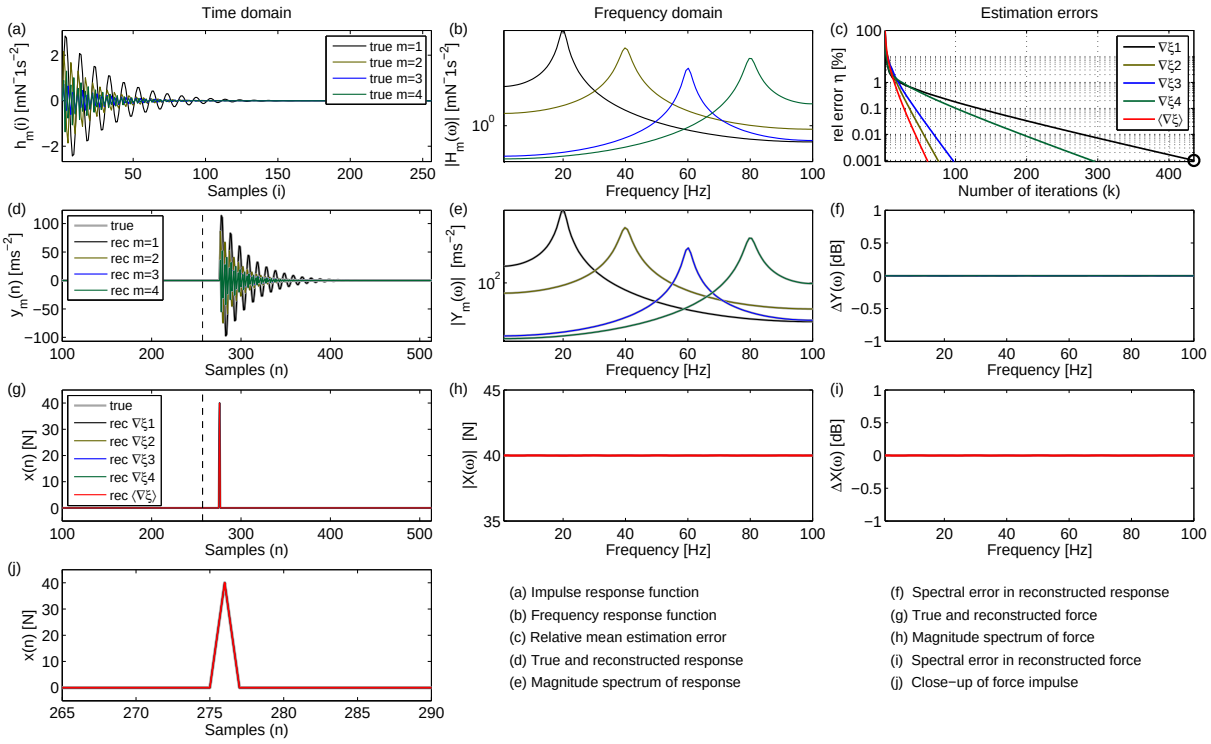

Figure 4.14. Numerical result for noise free SIMO system. Representation of signals in time domain (a, d, g, j), representation of signals in frequency domain (b, e, h,) and different estimation errors (c, f, i): Quantities indicated by $\nabla\xi m$ are obtained by the SISO recursion from Table 4.1 whereas $\langle\nabla\xi\rangle$ indicates that the SIMO recursion from Table 4.3 is used.

As can be seen from the relative mean prediction errors in Figure 4.14 – (c) all iterative processes are sufficiently carried out. It is noted that the maximum number of iterations is required when reconstructing the force by consideration of only the first response location ($m=1$) for which reason the interruption criterion for the SIMO TDM will be chosen according to the convergence behaviour of this response channel. Note further that for the special case of using perfect numerical data, as it is the case here, the E-RMPE does represent a reliable criterion to evaluate the estimation accuracy. This is due to the averaged error gradient which in the noise free case is able to reconstruct all considered responses precisely, as evidenced by the corresponding spectral estimation errors $\Delta Y_m(\omega)$ (Fig.14 – (f)) which are all approximately zero. Note that the associated RMS errors in the reconstructed response

signatures are also zero, as summarised in Table 4.4. Therefore, the absolute values of the E-RMPE determined for the SIMO simulation (indicated by $\langle \nabla \xi \rangle$ in Figure 4.14 – (c)) can directly be compared with the individual RMPEs calculated for the four different SISO simulations (see $\nabla \xi m$ in Figure 4.14 – (c)). It is clear, that for the noise free case the SIMO TDM converges fastest or, in other words, the SIMO TDM is able to achieve more reliable estimation results within the same calculation time than any of the conducted SISO simulations. Again, it is emphasised that this conclusion is only valid for the noise free state.

Considering the reconstructed force obtained when using the different TDM approaches, one can conclude that for ideally noise free numerical data perfect reconstruction of the transient force pulse is possible with any of the conducted SISO or SIMO simulations, as illustrated in Figure 4.14 – (g) and (j). All RMS force estimation errors ($\varepsilon_{x,\%,RMS}$) are approximately zero as summarised in Table 4.4. Accordingly the associated spectral estimations errors also have to be approximately zero as plotted in diagram (i).

Table 4.4. Summary of simulation results achieved with the expanded time domain inversion routine and the standard frequency domain inverse method for the noise free SIMO system.

		Noise free				
		Error ε_{RMS} in reconstructed responses [%]				Error ε_{RMS} in reconstructed force [%]
Used method		$y_1(n)$	$y_2(n)$	$y_3(n)$	$y_4(n)$	$x(n)$
TD	$\nabla \xi_1$	0.0	-	-	-	0.0
TD	$\nabla \xi_2$	-	0.0	-	-	0.0
TD	$\nabla \xi_3$	-	-	0.0	-	0.0
TD	$\nabla \xi_4$	-	-	-	0.0	0.0
TD	$\langle \nabla \xi \rangle$	0.0	0.0	0.0	0.0	0.0
FD	inverse	-	-	-	-	0.0

A comparison of the identified forces achieved with the SIMO TDM and the standard frequency domain inverse method (FDM) is given in Figure 4.15. It is noted that least-square Moore-Penrose pseudo inverse was employed in the FDM to obtain the inverse system model.

From Figure 4.15 it is clear that for an ideally noise free SIMO system the expanded TDM and the FDM perform equally. In both cases the identified forces match exactly the true one (see also the corresponding RMS force estimation error in Table 4.4). Further, it is stressed that the utilised system model and the invoked strategy to evaluate the performance of both force identification techniques has been validated. In the following, both methods are contrasted for cases where the used data is corrupted by additional noise.

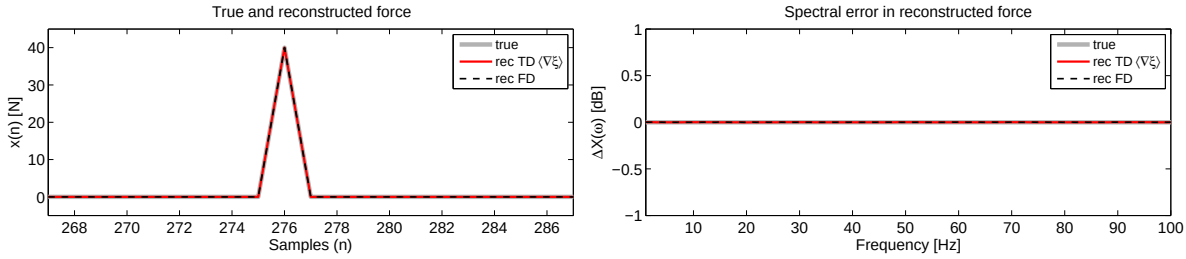

Figure 4.15. Comparison of the time domain inverse method (TDM) with the standard frequency domain inverse method (FDM) for the noise free SIMO system. Reconstructed force time history (left) and spectral estimation error in the identified force (right): ▬ true signal; ▬ reconstructed force using the SIMO TDM; ▬ ▬ identified force using the FDM.

4.5.3. Sensitivity to noise in the structural responses

The expanded SIMO TDM (see Table 4.3) becomes significant when uncorrelated disturbances corrupt either the system model or the desired responses. The latter case is investigated in the following. For this purpose, uncorrelated noise sequences are added according to Eq. (4.15) to the structural responses of the previously validated SIMO model. Different noise levels ranging from 5% over 10% to 25% of the RMS value of the respective noise free responses are investigated resulting in signal-to-noise ratios of approximately $SNR_{5\%} = 26\,\text{dB}$, $SNR_{10\%} = 20\,\text{dB}$ and $SNR_{25\%} = 12\,\text{dB}$, respectively. The simulation results obtained with the SIMO TDM assuming 10% noise corrupted response data are illustrated in Figure 4.16.

The additional noise in the desired responses in combination with the use of the averaged error gradient involved in the SIMO TDM cause severe errors in the reconstructed responses. The corresponding RMS errors in the recovered response time histories ($\varepsilon_{y,\%RMS}(\langle\nabla\xi\rangle)$) range from approximately 6.0 % to 7.5 % as can be found in Table 4.6. The magnitude spectra of the reconstructed responses ($|Y_m(\omega)|$) and the associated spectral estimation errors ($\Delta Y_m(\omega)$) displayed in Figure 4.16 – (e) and (f), respectively, illustrate how the noise corrupted response data affects the reconstruction of the true responses when using the averaged error gradient approach. At certain frequencies the error in the estimated responses can take values up to 18 dB. Note that the according errors for the SISO TDM are all zero since only a single response and the corresponding gradient is used.

The substantial deviations between the desired and the reconstructed response signals caused by the averaged error gradient in the SIMO TDM are also apparent in the associated expanded

relative mean prediction error (E-RMPE), denoted by $\eta(\langle\nabla\xi\rangle)$ in Fig.16 – (c). Clearly, a convergent iterative process is achieved already after approximately $k = 50$ iterations.

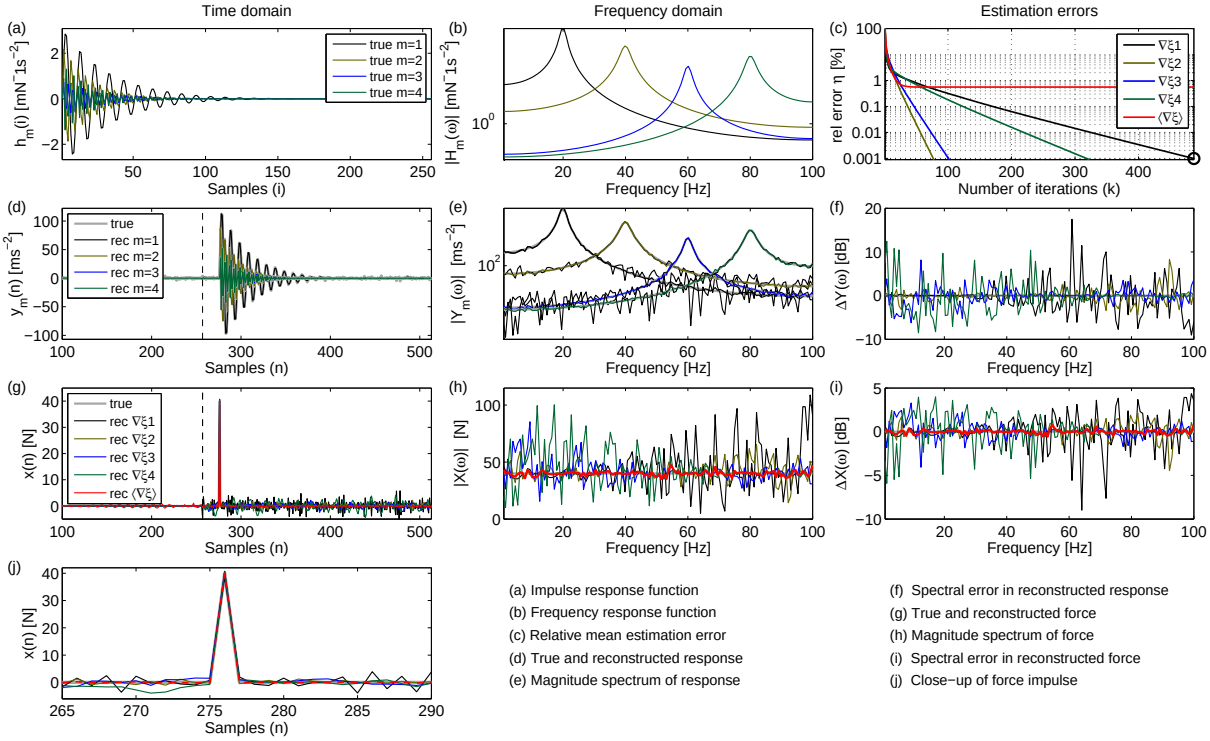

Figure 4.16. Numerical result for SIMO system with 10% noise added to the acceleration responses. Representation of signals in time domain (a, d, g, j), representation of signals in frequency domain (b, e, h,) and different estimation errors (c, f, i): Quantities indicated by $\nabla\xi m$ are obtained by the SISO recursion from Table 4.1 whereas $\langle\nabla\xi\rangle$ indicates that the SIMO recursion from Table 4.3 is used.

However, the additional noise in the structural responses hinders (fast) improvement of the reconstruction process for the chosen parameterisation of the adaptive algorithm and causes the E-RMPE to converge towards a residual value.

By comparison of simulations achieved for different amounts of noise added to the structural responses it has been found that the residual E-RMPE value varies with the noise level. Figure 4.17 illustrates different E-RMPE evolutions as a function of the noise level for the investigated SIMO system. Note that the corresponding simulations can be found in Appendix A.2. Note further that the same tendencies in the evolution of the E-RMPE can be found if, instead of noise added to the responses, errors are added to the system model.

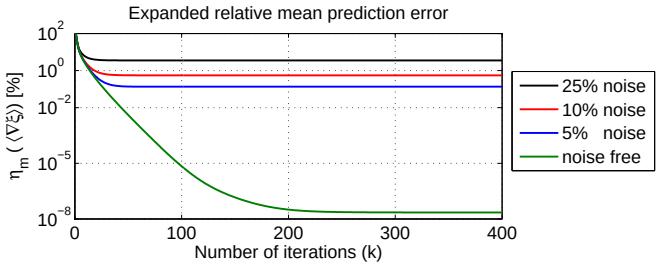

Figure 4.17. Evolution of the expanded relative mean prediction error (E-RMPE) as a function of noise added to all responses of the investigated SIMO system. The residual E-RMPE value after convergence is dependent on the noise level.

From Figure 4.17 it can be concluded that noise or other errors in the used data determine the lower bound of the (residual) E-RMPE. The more uncertainties are included in the data the higher is the residual E-RMPE.

Furthermore, it turns out that a residual E-RMPE value also exists for the noise free SIMO system although the averaged error gradient is not affected by any additional noise. This residual results from using the adaptive (stochastic) mechanism to control the weights in the basic LMS filter in place of the deterministic approach, as in the method of steepest descent (see section 4.2). Due to stochastically estimating the gradient in the adaptive filter the tap-weight vector (vector of filter coefficients) are always subject to perturbation around its optimum value so that the same effect is present in the evolution of the relative mean prediction error in the SISO TDM, although this has not been discussed in particular yet. However, as known from detailed discussions on the related excess mean-square error of the conventional LMS algorithm, see e.g. [202] or [203], the effects of this gradient noise on the tap-weights - and hence on the reconstruction accuracy - is in the designer's control. In particular, a proper choice of the step-size parameter, i.e. μ in the SISO TDM (Eq. (4.13)) and μ_m in the SIMO TDM (Eq. (4.29)), is important. By assigning a small value to the step-size parameter the adaptive process converges slowly but, in return, the effects of gradient noise are largely filtered out [202]. It is emphasised that all simulations presented in this chapter are conducted with the largest possible step-size parameter (according to the presented stability bounds in Eqs. (4.13) and (4.29)) so as to ensure fast convergence.

At this stage it is concluded that, although the E-RMPE cannot be used as an absolute measure to interrupt the iterative process in the SIMO TDM, its evolution still reveals important information about the progress of the iterative reconstruction process. As a rule of thumb, one should carry out the iterative process until the E-RMPE converges towards its

lower bound, i.e. the residual value, which can clearly be observed when plotting its evolution over the number of iterations, as illustrated in Figure 4.17. Before the E-RMPE reaches its lower bound, interrupting the iterative process could yield incomplete reconstruction processes. Instead, carrying out the iterative process after the E-RMPE has already reached its residual value results in increasing calculation times but does not improve the reconstruction accuracy further, unless the step-size parameter is reduced within the valid range (4.29). Although it has not been performed within this study, it is noted that an interruption criterion may be obtained in terms of the E-RMPE's gradient or curvature, respectively. Nevertheless, one should not forget that the E-RMPE of the SIMO TDM as well as the RMPE of the SISO TDM only monitors the accuracy in the reconstructed responses so that alternative interruption criteria that directly monitor the progress of the iterative process in terms of the identified forces would be more appropriate. This issue is discussed in more detail in section 5.5.

Notwithstanding the previous digression, although the reconstructed responses show substantial deviations from the true ones if the SIMO TDM is used, the assumed unknown force signature can be recovered with high precision from the noisy response data, as illustrated in Figure 4.16 – (g) and (j). Due to the use of the averaged error gradient in the SIMO recursion the over-determined inversion process is affected only slightly, although a considerable amount of noise is added to all responses. The RMS error in the reconstructed force time history is approximately $\varepsilon_{x,\%RMS}(\langle\nabla\xi\rangle) = 6.7\,\%$ when using the SIMO recursion, whereas the according errors achieved with the SISO routine range from $\varepsilon_{x,\%RMS}(\nabla\xi 2) = 27.2\,\%$ to $\varepsilon_{x,\%RMS}(\nabla\xi 1) = 73.6\,\%$, as summarised in Table 4.6. As can be seen from Figure 4.16 – (g) and (j), all SISO simulations yield highly noisy force estimation results ($\nabla\xi m$) while the over-determined approach is almost free of any errors ($\langle\nabla\xi\rangle$).

The advantages of using the over-determined SIMO TDM instead of the SISO recursion also become apparent in the estimated force spectrum ($|X_m(\omega)|$) and the related spectral estimation error ($\Delta X(\omega)$), as illustrated Figure 4.16 – (h) and (i), respectively. According to the findings from section 4.4, the SISO routine only allows satisfying force identification at frequencies where the response spectrum considerably exceeds the noise floor. This can be seen in the diagrams (h) and (i), e.g. for response location $m = 1$ (black solid line) at frequencies below 30 Hz or for response position $m = 4$ (dark green solid line) above 70 Hz. However, at

frequencies where the response spectrum undergoes the noise floor all SISO solutions fail and yield unacceptable errors in the estimated forces of up to $|\Delta X(\omega)| = 8.9\,dB$. Instead, the averaged error gradient invoked in the SIMO algorithm is governed at each frequency by the strongest contributing signal while weak paths do not contribute to the averaged error gradient for which reason their negative influence on the reconstruction process is suppressed. In this way, the averaged error gradient allows for very accurate force identification throughout the entire frequency range, as indicated by the red solid line in Figure 4.16 – (g) and (i). Thus, when using the averaged error gradient the maximum spectral estimation in the reconstructed force is less than $|\Delta X(\omega)| = 0.7\,dB$.

To conclude, a comparison of the SIMO TDM and the standard frequency domain inverse method (FDM) is given in Figure 4.18.

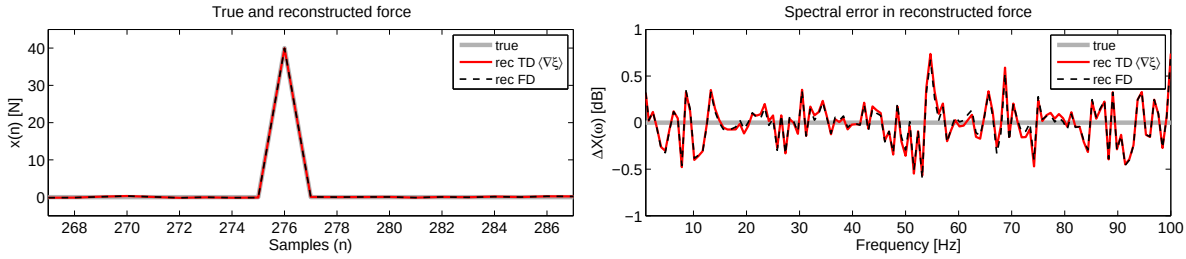

Figure 4.18. Comparison of the time domain inverse method (TDM) with the standard frequency domain inverse method (FDM) for SIMO system with 10% noise added to the responses. Reconstructed force time history (left) and spectral estimation error in the identified force (right): ——— true signal; —— reconstructed force using the SIMO TDM; – – identified force using the FDM.

In accordance with the findings from section 4.4.2 the TDM and FDM perform equally when identifying the assumed unknown input force from a set of noise corrupted responses. Both methods yield accurate reconstructions of the transient force pulse in time domain and satisfying estimation accuracy in frequency domain. Note that the corresponding estimation errors are summarised in Table 4.6. Again, there exists no objective criterion to advise the use of one force identification method over the other, although the time domain approach provides more physical insight by additionally estimating the responses and monitoring the progress of the inversion process.

4.5.4. Sensitivity to errors in the system model

In practice, the employed system model is always inconsistent to some extend. The suitability of the expanded SIMO TDM for imperfect system models is investigated in the following. For

this purpose, the impulse response functions (IRFs) of the previously used SIMO model are degraded according to Eq. (4.15). As inconsistencies white noise of a magnitude of 5% and 10% of the RMS value of the respective noise free IRF is added resulting in signal-to-noise ratios of approximately $SNR_{5\%} = 26\,\mathrm{dB}$ and $SNR_{10\%} = 20\,\mathrm{dB}$, respectively. To demonstrate the efficiency of the averaged error gradient if inconsistent system models are to be processed, the expanded SIMO TDM is compared with the basic SISO TDM, as elaborated in the previous sections. The simulation results obtained with the SISO and the SIMO TDM assuming a 10% noise corrupted system model are illustrated in Figure 4.19.

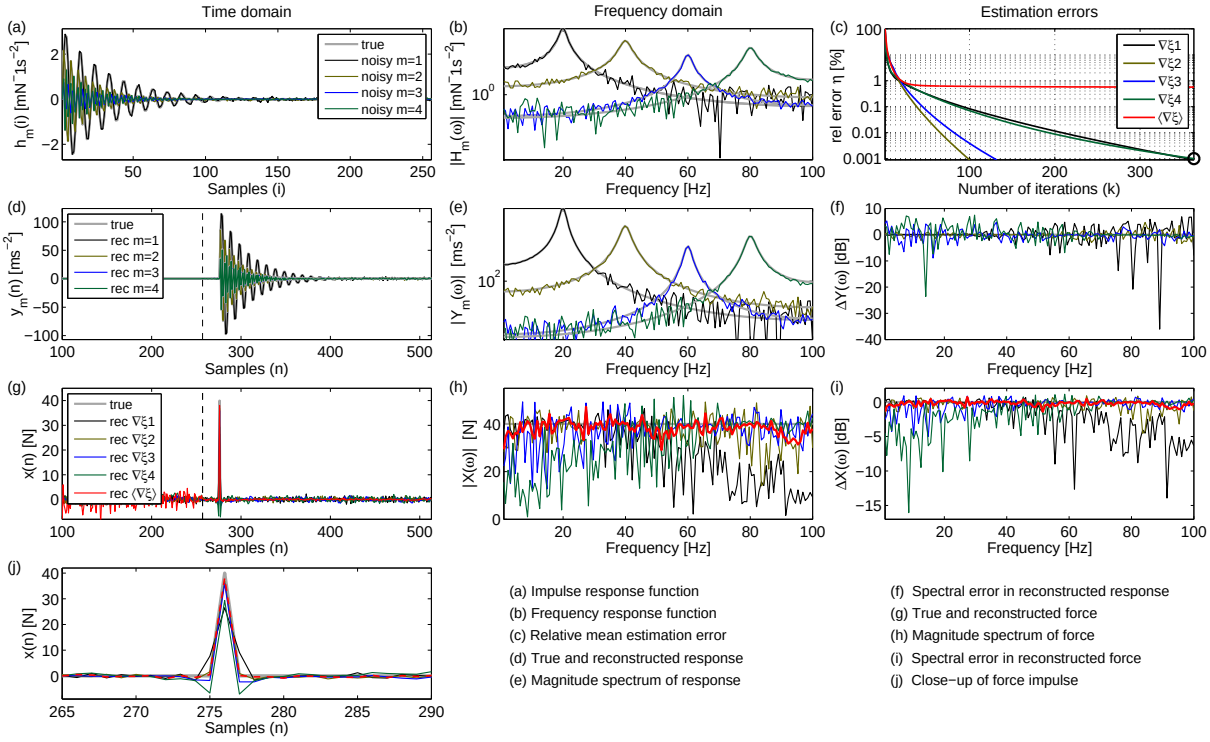

Figure 4.19. Numerical result for SIMO system with 10% noise added to impulse response functions. Representation of signals in time domain (a, d, g, j), representation of signals in frequency domain (b, e, h,) and different estimation errors (c, f, i): Quantities indicated by $\nabla\xi m$ are obtained by the SISO recursion from Table 4.1 whereas $\langle\nabla\xi\rangle$ indicates that the SIMO recursion from Table 4.3 is used.

As can be seen from the relative mean prediction errors (RMPEs) in Figure 4.19 – (c) all simulations using the SISO TDM show a convergent behaviour. In comparison to simulations for the noise free state (cf. Figure 4.14) the additional errors in the system model slow the adaptive SISO algorithm down so that the SISO TDM on average requires about 30 % more iterations to reach the pre-defined RMPE-based interruption criterion of $\eta = 0.001\,\%$. Note that this finding is consistent with the findings in section 4.4.3. However, as discussed in the

previous section, the expanded relative mean prediction error (E-RMPE) of the SIMO TDM converges towards a residual value which is influenced by the amount of errors included in the employed system model. Clearly, the iterative process for the SIMO TDM is carried out sufficiently for the chosen parameterisation since steady E-RMPE values are reached already after approximately $k = 90$ iterations. Thus, it can be assumed that the SIMO TDM yield the best possible force estimation for the chosen parameterisation and the given (defective) data set.

As elaborated previously, the SISO TDM yields perfect reconstruction of the structural responses for all response locations (see Figure 4.19 – (d) and (e)). The according time domain estimation errors and the spectral estimation errors are all approximately zero, as displayed in Table 4.6 and Figure 4.19 – (f), respectively. However, considering only a single response is at the expense of accuracy in the reconstructed forces. Inspecting the time histories of the identified forces in Figure 4.19 – (g) and (h), all SISO simulations appear to be noisy beside the force impulse while the reconstructed forces in the vicinity of the pulse lack in accuracy. Except from the force obtained by the SISO simulation that considers response position $m = 3$ (blue solid line) all identified forces tend to underestimate the peak value or misrepresent the shape of the force pulse. This results in large deviations in the identified force signatures yielding considerable RMS errors ($\varepsilon_{x\%RMS}(\nabla\xi m)$) that range from 24.7 % to 52.8 %, as given in Table 4.6. The large errors in time domain also become apparent in frequency domain as can be seen from the plot of the magnitude force spectrum in diagram (h) and the associated spectral estimation errors in diagram (i). Accordingly, the SISO TDM considering response position $m = 3$ performs best but still yields errors in the reconstructed force spectra of up to |5 dB|. The maximum errors obtained with the SISO TDM for other response locations can reach values up to |16 dB|.

Instead, the averaged error gradient involved in the SIMO TDM produces large discrepancies between the reconstructed and the true responses (Figure 4.19 – (d)-(f)). The RMS errors in the reconstructed response time histories ($\varepsilon_{y,\%RMS}(\langle\nabla\xi\rangle)$) can take values from approximately 4.4 % to 9.1 %, as provided in Table 4.6, while the associated spectral estimation errors can reach values up to $|\Delta Y(\omega)| = 36\,dB$ at certain frequencies (see Figure 4.19 – (f)). However, due to the use of the averaged error gradient the uncorrelated noise that falsifies the reconstruction of the responses is sufficiently suppressed in the identified force. Inspecting the time history of the recovered force in Figure 4.19 – (g) and (j), the SIMO TDM performs very well. The

transient force peak is reconstructed with high precision and only little noise can be found beside the force transient, yielding a RMS error in the identified force of $\varepsilon_{x,\%RMS}(\langle\nabla\xi\rangle) = 9.0\,\%$ (see Table 4.6). Satisfying estimation accuracy is also reached in frequency domain as can be seen from the corresponding magnitude force spectrum in diagram (h) and the related spectral estimation error plotted in diagram (i). Accordingly, the force can be identified with an uncertainty of less than $|\Delta X(\omega)| = 1\,dB$ throughout the entire frequency range.

The excellent performance of the SIMO TDM can also be seen from Figure 4.20 where the identified force is compared with the one obtained when using the standard frequency domain inverse method (FDM).

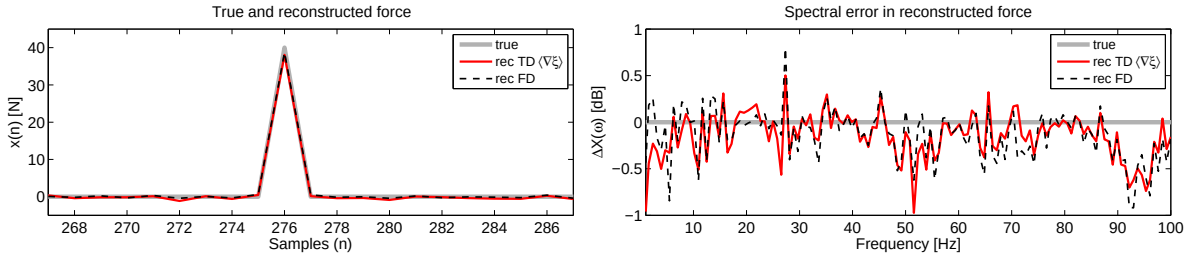

Figure 4.20. Comparison of the time domain inverse method (TDM) with the standard frequency domain inverse method (FDM) for SIMO system with 10% noise added to system model. Reconstructed force time history (left) and spectral estimation error in the identified force (right): ——— true signal; ——— reconstructed force using the SIMO TDM; — — identified force using the FDM.

In general, the SIMO TDM and the FDM perform similar although the force spectrum identified with the FDM for most frequencies shows slightly larger discrepancies to the true force (Fig.20 – (right)). The identified force signatures obtained with the SIMO TDM and the FDM, respectively, are almost indistinguishable from each other, as illustrated in Figure 4.20– (left), yielding similar RMS prediction errors as summarised in Table 4.6. Note that similar results have been achieved for the 5% noise corrupted system model, as illustrated in Appendix A.2.

4.5.5. Conclusions

Based on the principle of over-determining the system, i.e. considering more structural responses than forces to be identified, an expanded time domain inversion routine has been derived that allows for improved force identification in single input multiple output (SIMO) systems (see Table 4.3). The expansion is based on the introduction of the averaged error gradient which is used in the update equation to adjust the estimated force. Generally, the

averaged error gradient, at each frequency, is governed by the strongest signal so that ‘weak’ paths, which in frequency domain inverse methods bring about dominant contributions after inversion and are highly susceptible to noise, do not influence the force reconstruction process. Under the assumption that errors inherent in the considered responses or inconsistencies in different paths of the used system model are uncorrelated, the averaged error gradient will converge towards the gradient expected without the influence of errors. In this way, the expanded SIMO TDM is able to significantly suppress the negative influence of noise and inconsistencies in the used data and has been found to yield robust force identification for SIMO systems even if the used data is considerably defective.

In order to monitor the convergence behaviour of the SIMO TDM an expanded relative mean prediction error (E-RMPE) has been introduced. It has been found that a residual value exists for the E-RMPE which is dependent on the application case. The residual E-RMPE value after convergence is dependent on

- the number of considered responses
- the amount of noise or inconsistencies included in the employed data and
- the step-size parameter used in the basic adaptive algorithm.

For this reason the absolute value of the E-RMPE cannot serve as reliable interruption criterion to stop the iterative process. Notwithstanding this, it has been found that observing the evolution of the E-RMPE is still a good means to monitor the progress of the iterative process and it has been outlined that alternative interruption criteria in terms of the E-RMPE’s gradient or curvature may be defined in future works.

In numerical simulations the sensitivity of the expanded SIMO TDM to noise and inconsistencies included in the structural responses and the system model, respectively, was investigated. The performance of the SIMO TDM was further compared to the standard frequency domain method (FDM). The simulation results for different levels of disturbances are summarised in Table 4.5, 4.6 and 4.7 for 5 %, 10 % and 25 % corrupted data, respectively. Note that the corresponding diagrams of all simulations can be found in Appendix A.2.

Table 4.5. Summary of simulation results achieved with the expanded time domain inversion routine and the standard frequency domain inverse method for SIMO system with 5 % defective data.

		5% noise added to responses ($SNR_m \approx 26$ dB)					5% noise added to IRFs ($SNR_m \approx 26$ dB)				
		Error ε_{RMS} in reconstructed responses [%]				Error ε_{RMS} in reconstructed force [%]	Error ε_{RMS} in reconstructed responses [%]				Error ε_{RMS} in reconstructed force [%]
Used method		$y_1(n)$	$y_2(n)$	$y_3(n)$	$y_4(n)$	$x(n)$	$y_1(n)$	$y_2(n)$	$y_3(n)$	$y_4(n)$	$x(n)$
TD	$\nabla\xi_1$	0.0	-	-	-	33.4	0.0	-	-	-	40.7
TD	$\nabla\xi_2$	-	0.0	-	-	13.8	-	0.0	-	-	18.5
TD	$\nabla\xi_3$	-	-	0.0	-	16.1	-	-	0.0	-	19.1
TD	$\nabla\xi_4$	-	-	-	0.0	26.4	-	-	-	0.0	31.1
TD	$\langle\nabla\xi\rangle$	2.8	3.2	4.1	3.0	3.9	3.0	3.6	5.9	3.9	4.7
FD	inverse	-	-	-	-	3.8	-	-	-	-	4.5

Table 4.6. Summary of simulation results achieved with the expanded time domain inversion routine and the standard frequency domain inverse method for SIMO system with 10 % defective data.

		10% noise added to responses ($SNR_m \approx 20$ dB)					10% noise added to IRFs ($SNR_m \approx 20$ dB)				
		Error ε_{RMS} in reconstructed responses [%]				Error ε_{RMS} in reconstructed force [%]	Error ε_{RMS} in reconstructed responses [%]				Error ε_{RMS} in reconstructed force [%]
Used method		$y_1(n)$	$y_2(n)$	$y_3(n)$	$y_4(n)$	$x(n)$	$y_1(n)$	$y_2(n)$	$y_3(n)$	$y_4(n)$	$x(n)$
TD	$\nabla\xi_1$	0.0	-	-	-	73.6	0.0	-	-	-	52.8
TD	$\nabla\xi_2$	-	0.0	-	-	27.2	-	0.0	-	-	24.7
TD	$\nabla\xi_3$	-	-	0.0	-	32.2	-	-	0.0	-	28.1
TD	$\nabla\xi_4$	-	-	-	0.0	60.8	-	-	-	0.0	46.8
TD	$\langle\nabla\xi\rangle$	6.0	6.5	7.5	6.5	6.7	4.4	5.7	9.1	7.2	9.0
FD	inverse	-	-	-	-	6.6	-	-	-	-	8.9

Table 4.7. Summary of simulation results achieved with the expanded time domain inversion routine and the standard frequency domain inverse method for SIMO system with 25 % defective response data.

		25% noise added to responses ($SNR_m \approx 12$ dB)				
		Error ε_{RMS} in reconstructed responses [%]				Error ε_{RMS} in reconstructed force [%]
Used method		$y_1(n)$	$y_2(n)$	$y_3(n)$	$y_4(n)$	$x(n)$
TD	$\nabla\xi_1$	0.0	-	-	-	191.2
TD	$\nabla\xi_2$	-	0.0	-	-	67.2
TD	$\nabla\xi_3$	-	-	0.0	-	75.7
TD	$\nabla\xi_4$	-	-	-	0.0	177.8
TD	$\langle\nabla\xi\rangle$	14.1	15.3	19.4	18.3	19.6
FD	inverse	-	-	-	-	19.5

For the conducted simulations it has been found that

- exact force identification is possible with the FDM and the SIMO TDM if neither the structural responses nor the system model comprises any errors,
- both methods, the FDM and the SIMO TDM, perform exactly the same if only the structural responses are corrupted by additional noise. The residual error in the identified force correlates with the amount of noise added to the response, i.e. the error increases with increasing noise level. Due to the use of the averaged error gradient the transient force pulse can be reconstructed with high precision while, at the same time, errors and noise beside the force pulse are sufficiently suppressed. In comparison to the SISO TDM the over-determined approach yields much better estimation accuracy and tends to be more robust for errors included in the data.
- both methods, the FDM and the SIMO TDM, perform similarly if the used system model is assumed to be inconsistent. It is noted that the derived TDM in contrast to the FDM generally is not sensitive to the choice of the measurement position, for which reason, in practice, the FDM may require more care in order to achieve the same estimation accuracy as the TDM. However, for the numerical examples presented here the assumed unknown input force was identified accurately with either of the two methods. Negative influences of uncorrelated errors inherent in the system model are sufficiently suppressed by the averaged error gradient in the SIMO TDM. Again, the SIMO TDM has been found to be more robust to errors than the basic SISO TDM.
- as with the SISO case, the expanded relative mean prediction error (E-RMPE) is not a sufficient criterion to evaluate the residual error in the reconstructed force. However, it constitutes a good means to monitor the convergence behaviour of the iterative process involved in the SIMO TDM.

Furthermore it is noted that the averaged error gradient only reduces the negative influence of disturbances, as long as they are uncorrelated. The presence of correlated disturbances would lead an averaged gradient adapting the reconstructed responses to the garbled system responses yielding highly inaccurate force identification [206]. One reason for correlated errors in the used data is additional excitations applied to the system at locations that are not considered by the TDM. The next section will show how such additional forces can be considered in the force reconstruction process.

4.6. Force reconstruction for multiple input multiple output systems

So far the derived time domain inverse method (TDM) has proved sufficient to yield robust and accurate reconstruction for systems with single degree of freedom excitation. However, most sophisticated technical structures undergo more complex excitations caused by multiple independent forces that act in parallel. Often, all or at least a few of these forces may have to be identified simultaneously using inverse methods. A generalisation of the previously derived TDM for multiple input multiple output (MIMO) systems could offer significant advantages compared to other existing inverse methods, as concluded in section 2.5 (Literature and theory). Therefore, the following sections are devoted to derive and evaluate the suitability of a generally valid variant of the introduced TDM that facilitates simultaneous reconstruction of multi-channel force signatures based on (measured) data that can easily be obtained for any complex technical structure. Utilising numerical examples, the performance of the generalised MIMO TDM and its sensitivity to errors inherent in the employed data will be investigated and compared with the standard frequency domain inverse method (FDM).

4.6.1. The generalisation of the method

Ideally, a generalisation of the time domain inversion routine should yield a practical approach that (i) is robust for disturbances included in the used data and (ii) can be applied for structures with arbitrary numbers of in- and outputs.

Considering first (i) the issue with possibly erroneous data sets, it has been shown in the previous section that the concept of over-determination and the introduction of the associated averaged error gradient in the update recursion of the (expanded) TDM significantly improves the force reconstruction process. Since this approach has been found to be robust for noise in the available response data as well as for inconsistencies included in the system model, the same principle is to be employed in the generalised TDM. Regarding next (ii) multiple forces applied to a structure, the operational responses at any point on the structure are influenced by contributions from all acting forces. For better understanding, one may consider the beam structure depicted in Figure 4.21 – (a) which is excited by multiple unknown input forces $x_{us}(n)$, for $s=[1,2,\ldots,S]$; each of which contribute to the structural responses $d_m(n)$, for $m=[1,2,\ldots,M]$, according to the corresponding impulse response functions $h_{ms}(i)$. Since the over-determined TDM employs the averaged error gradient which requires calculation of an

error signal for each individual response location m, consideration of all forces contributing to any of the responses is crucial. Nonconsideration will inevitably cause biased force reconstruction that usually results in over-estimating the true forces due to the additionally introduced energy. As unconsidered forces theoretically contribute to several or all observed responses their contributions may be regarded as correlated disturbances corrupting the observed responses. Unfortunately, the averaged error gradient in the expanded TDM has only the ability to suppress uncorrelated disturbances for which reason it is mandatory to account for all forces possibly acting on a structure. Thus, if one is not sure whether or not a force is acting at a certain position on a structure during operation, it is advisable to rather account for an additional force location than leaving it unconsidered. Ideally, the TDM then would yield a zero force signal for the additional excitation position if in fact no force is applied to it.

Hence, taking the ideas behind over-determination and multiple excitation forces into account a block schematic for the generalised TDM can be framed, as illustrated in Figure 4.21 – (b,c).

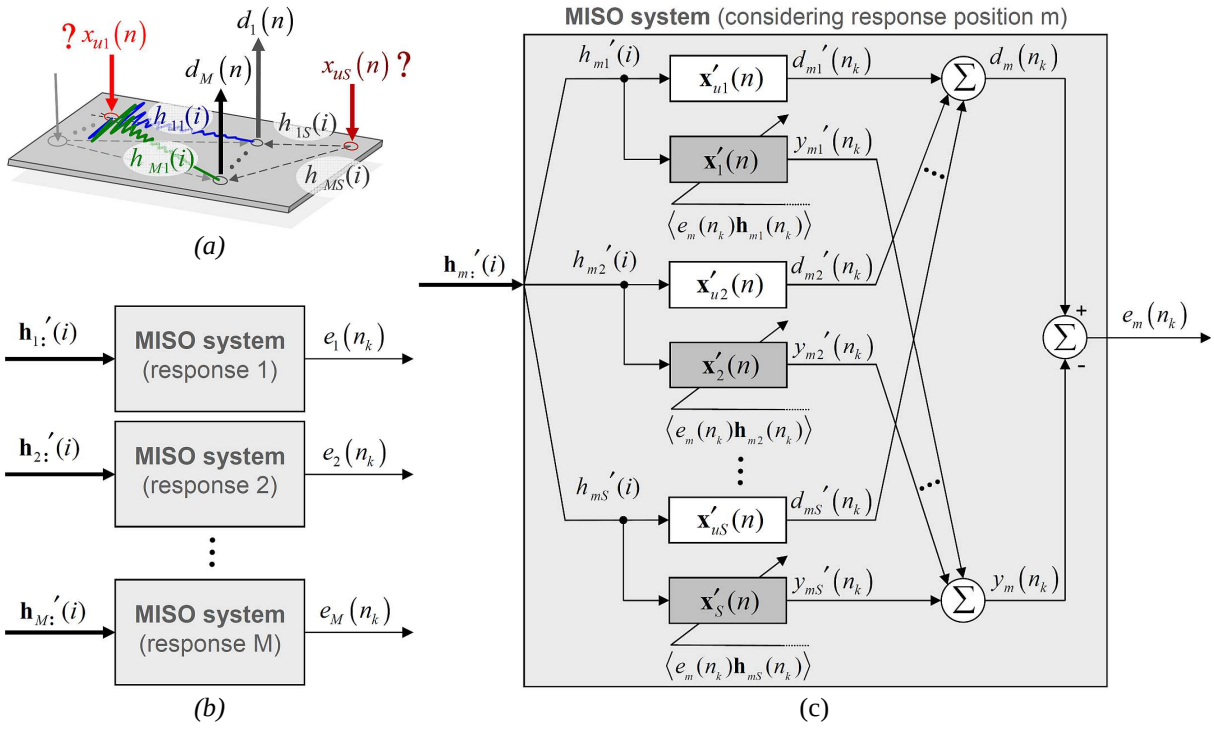

Figure 4.21. Principle of the generalised time domain inversion routine for multiple input multiple output (MIMO) systems: Schematic of force excited beam (a) corresponding cascaded block diagram for adaptive input reconstruction consisting of *M* MISO systems (b) and detailed schematic of one MISO block (c). (Apostrophes indicate constrained conditions; angle brackets denote the averaged error gradient; $\mathbf{h}_{m:}(i)$ denotes the set of impulse response functions between all force input locations $s = [1, 2, \ldots, S]$ and a single response position m.)

At each time step n_k an error signal for each of the $m=[1,2,\ldots,M]$ response positions has to be calculated as the difference between the observed (desired) response $d_m(n_k)$ and the response $y_m(n_k)$ provided by the adaptive filter (see Figure 4.21 – (c)). Since for multi-point excited structures all acting forces influence the structural responses, the total output of the adaptive scheme, at a specific response position m, is modelled as a linear superposition of the contributions from each current force estimate $x_s(n_k)$ weighted by the corresponding finite impulse response function $h_{ms}(i)$ between the assumed source location, $s=[1,2,\ldots,S]$, and the response position, *m*,

$$y_m(n_k)=\sum_{s=1}^{S}\sum_{i=0}^{I-1}h_{ms}(i)\,x_s(n_k-i) \qquad \text{for} \quad m=[1,2,\ldots,M] \tag{4.31}$$

where *M* is the total number of considered responses and *S* is the number of input forces applied to the structure. Note, over-determination requires the condition $M > S$ to be satisfied. The instantaneous error $e_m(n_k)$ for each individual response position m is obtained in accordance with Eq. (4.26) as

$$e_m(n_k)=d_m(n_k)-y_m(n_k)=d_m(n_k)-\sum_{s=1}^{S}\sum_{i=0}^{I-1}h_{ms}(i)\,x_s(n_k-i) \qquad \text{for} \quad m=[1,2,\ldots,M]. \tag{4.32}$$

For each individual response position the calculation of the error can be visualised as the MISO block schematic depicted in Figure 4.21 – (c), where the multiple inputs, denoted by $\mathbf{h}_{m:}(i)=[h_{m1}(i),h_{m2}(i),\ldots,h_{mS}(i)]^T$, represent the set of impulse response functions between all source locations $s=[1,2,\ldots,S]$ and the selected response position m, and the single output is the error signal given by Eq. (4.32). Note that a MISO block is required to calculate an error for each of the $m=[1,2,\ldots,M]$ considered responses so that the entire block diagram for the generalised MIMO TDM consists of *M* cascaded MISO blocks (see Figure 4.21 – (b)).

Based on the M error signals (Eq. (4.32)) a generalised recursion has to be defined that allows for adaptively updating the most recent time histories of the reconstructed forces $x_s(n_k)$. To account for multiple response positions the previously introduced concept of the averaged error gradient is invoked. Due to considering multiple force channels an individual averaged error gradient is to be calculated for each of the S input forces. The corresponding averaged error gradients are defined as

$$\left\langle e_m(n_k)\mathbf{h}_{ms}(n_k)\right\rangle=\frac{1}{M}\left(\sum_{m=1}^{M}e_m(n_k)\cdot\mathbf{h}_{ms}(n_k)\right) \quad \text{for} \quad s=[1,2,\ldots,S] \tag{4.33}$$

which then are ultimately employed to update each particular input force $x_s(n_k)$, for $s=[1,2,\ldots,S]$, yielding the final recursion of the generalised TDM

$$\mathbf{x}_s\left(n_{k+1}\right)=\mathbf{x}_s\left(n_k\right)+2\mu_s\left\langle e_m\left(n_k\right)\mathbf{h}_{ms}\left(n_k\right)\right\rangle \qquad \text{for } I\le n_k\le N \quad \forall \quad N\ge 2\cdot I \tag{4.34}$$

where the angle brackets indicate the averaged error gradient. As discussed above, the averaged error gradients compensate for uncorrelated disturbances inherent in the used data.

To achieve convergence in the mean-square the *S* step size parameters μ_s involved in the recursions Eq. (4.34) have to be chosen properly. It has been found that choosing the step size parameters according to the bounds

$$0<\mu_s<M\left(\sum_{m=1}^{M}\sum_{i=0}^{I-1}\left|h_{ms}\left(i\right)\right|^2\right)^{-1} \quad \text{for} \quad s=[1,2,\ldots S], \tag{4.35}$$

where *M* is the total number of considered responses and *S* is the number of input forces applied to the structure, is sufficient to achieve stable iterative processes in practice [208].

In this way a generalisation of the time domain inverse method has been achieved that facilitates simultaneous identification of multi-channel force signatures for arbitrary multiple input multiple output (MIMO) systems. To complete one iteration cycle *k*, the mathematical steps (4.31), (4.32) and (4.34), in this order, are to be carried out, in accordance with the stability bound in (4.35). The generalised TDM is summarised in Table 4.8.

Table 4.8. Time domain inversion routine for identification of forces in multiple input multiple output systems.

Parameters:	$n\ldots$ time step $k\ldots$ iteration cycle $N\ldots$ length of input vector $I\ldots$ length of finite impulse response $M\ldots$ number of responses $S\ldots$ number of unknown inputs		
Initialisation:	$\mathbf{x}_s\left(n_{k=0}\right)=\mathbf{0}$	for $s=[1,2,\ldots,S]$	
Computation:	for $I\le n_k\le N \quad \forall \quad N\ge 2\cdot I$	$k=k+1$	{1}
Filtering:	$y_m\left(n_k\right)=\sum_{s=1}^{S}\sum_{i=0}^{I-1}x_s\left(n_k-i\right)h_{ms}\left(i\right)$	for $m=[1,2,\ldots,M]$	{2}
Error:	$e_m\left(n_k\right)=d_m\left(n_k\right)-y_m\left(n_k\right)$		{3}
Update:	$\mathbf{x}_s\left(n_{k+1}\right)=\mathbf{x}_s\left(n_k\right)+2\mu_s\left\langle e_m\left(n_k\right)\mathbf{h}_{ms}\left(n_k\right)\right\rangle$	for $s=[1,2,\ldots,S]$	{4}
Stability bound:	$0<\mu_s<M\left(\sum_{m=1}^{M}\sum_{i=0}^{I-1}\left\|h_{ms}\left(i\right)\right\|^2\right)^{-1}$		{5}

According to the numbering given in curly brackets in Table 4.8 the generalised adaptive algorithm can be summarised as follows: Starting with an initial guess of the *S* unknown input

forces, at each time step, n_k, measured impulse response functions (IRFs), $h_{ms}(i)$, are used to filter the current force estimates, $x_s(n_k)$, so as to predict a response, $y_m(n_k)$, for each measurement position, m, {2}. An individual error, $e_m(n_k)$, between each of the estimated filter outputs and the desired responses, $d_m(n_k)$, is calculated {3}. The average over all instantaneous errors weighted with the corresponding IRFs is then used to update the current force estimates recursively {4}. In order to achieve an iterative procedure these steps are to be repeated at each iteration cycle k according to the constraints given in {1}. To ensure convergence the step size parameters, μ_S, need to be chosen according to the stability bound given in {5}.

4.6.2. Application to noise free system

Due to the use of the averaged error gradients in each of the S recursions (see Eq. (4.34)) the generalised TDM is expected to suppress adverse effects of inconsistent system models or noise inherent in the desired responses; assuming that inherent disturbances are uncorrelated and the system is sufficiently over-determined ($M > S$). In the following the sensitivity of the generalised TDM to disturbances included in the used data is investigated using numerical simulations.

To achieve a physical correct MIMO system all simulations are based on a system model obtained from measurements conducted on an empty housing of an EPSapa PL2 steering gear, as depicted in Figure 4.22.

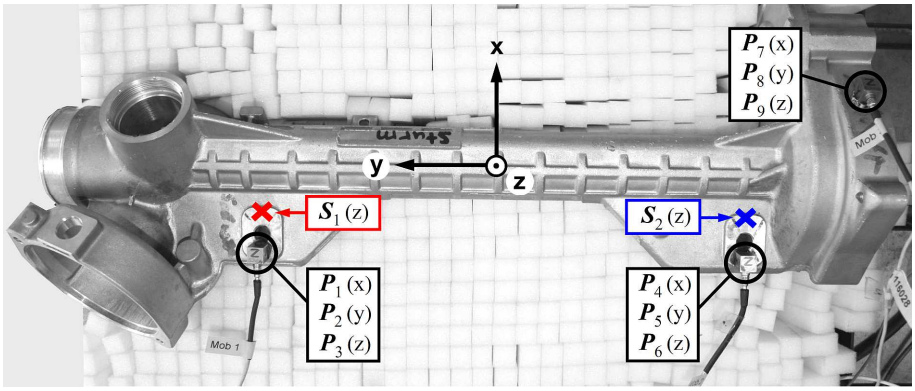

Figure 4.22. Housing of EPSapa PL2 steering gear with assumed sources (S_u) and response positions (P_m).

Frequency response functions (FRFs) between the two assumed source locations, S_1 and S_2, and the $M = 9$ response positions P_m, for $m = [1, 2, \ldots, M]$, are measured on the assumed freely

suspended structure, i.e. roving textured foam material is used to support the steering gear housing in order to achieve reasonably free conditions. Note that for each point the measurement direction (x, y and z) is indicated in round brackets in Figure 4.22. By means of inverse discrete Fourier transform (IDFT) the measured FRFs are transformed into impulse response functions (IRFs) which ultimately are used to build up a system model of the steering gear housing. In theory, this methodology allows for obtaining a MIMO model relying on a physically correct relationship between all involved IRFs disregarding possible uncorrelated errors in the FRF measurements to which the TDM has shown to be robust. With respect to the computing time required to sufficiently carry out the iterative inversion routine, IRFs of short sample length are favoured. On the contrary, the length of the IRFs has to be chosen in such a way that they have sufficiently decayed inside the chosen time window (see section 4.2). For the given example, the IRF length is chosen to be $I = 512$ samples.

Operational responses, $d_m(n)$ for $m = [1, 2, \ldots, M]$, are calculated by convolving two synthesised uncorrelated impulsive force signatures, $x_{us}(n)$ for $s = [1, 2]$, with the corresponding IRFs, $h_{ms}(i)$, according to the modelling approach in section 4.3. Inconsistencies in the measured IRFs in this way become part of the system whilst the generated responses are free from any errors. The length of the synthesised force signatures and correspondingly the length of the calculated responses is chosen to be $N = 1280$ samples which is consistent to the constraint $N > 2 \cdot I$ (see e.g. Table 4.8).

Assuming an ideal system model and noise free desired responses the generalised TDM from Table 4.8 is employed in a first simulation to validate the correctness of the newly designed system model. Further, the performance of the generalised TDM is tested for three different degrees of overdetermination.

Table 4.9. Overview of the different MIMO systems.

Degree of over-determination	Name of MIMO system	Considered response positions									Considered force locations	
		P_1 (x)	P_2 (y)	P_3 (z)	P_4 (x)	P_5 (y)	P_6 (z)	P_7 (x)	P_8 (y)	P_9 (z)	S_1 (z)	S_2 (z)
1	(2x2)	X	-	-	X	-	-	-	-	-	X	X
2	(2x4)	X	X	-	X	-	-	-	X	-	X	X
4.5	(2x9)	X	X	X	X	X	X	X	X	X	X	X

The degree of overdetermination is measured as the number of considered responses over the number of forces to be identified. An overview of the three corresponding MIMO systems is given in Table 4.9 including information about the respective degree of overdetermination, the

considered responses, the force input locations as well as the name that will be used in the following to refer to a specific MIMO system.

Simulations for each of these systems are carried out. The simulation results for the noise free (2x9) MIMO system (2 inputs, 9 outputs) are illustrated in Figure 4.23. Note that the simulation results for the determined (2x2) and the double overdetermined (2x4) MIMO system can be found in Appendix A.2.

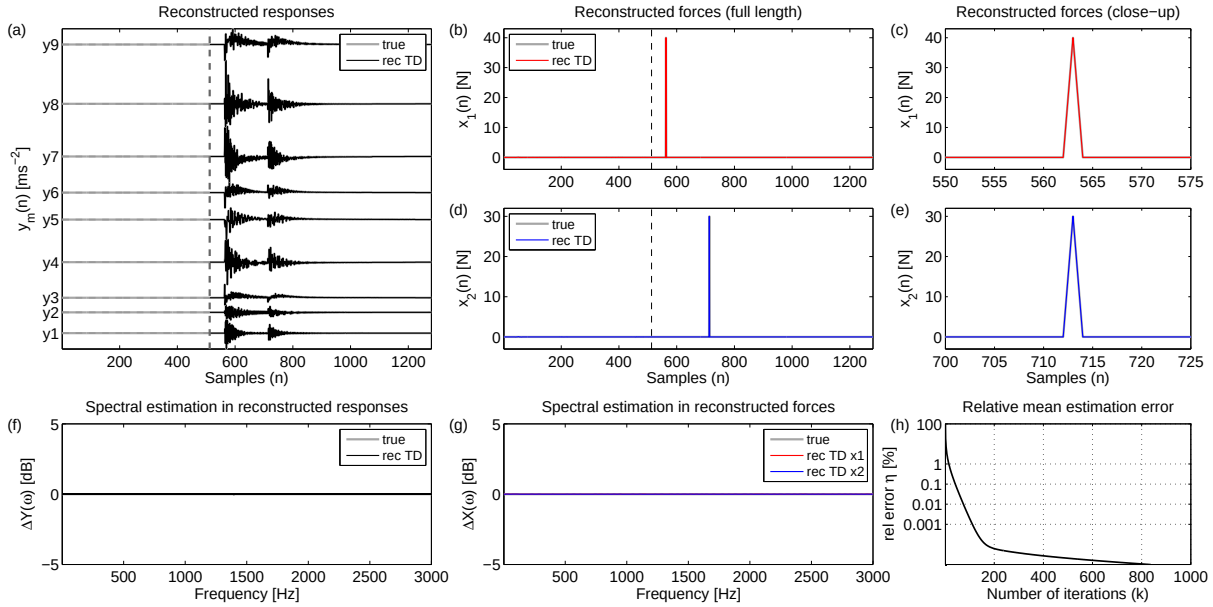

Figure 4.23. Numerical results for noise free (2x9) MIMO system. Time signatures of structural responses (a) and reconstructed force signatures in full-length (b,d) and as close-up (c,e); spectral estimation error in reconstructed responses (f) and identified forces (g): ▬▬ true signal; ── reconstructed signal using TDM. Relative mean prediction error (E-RMPE) as performance measure of the adaptive inversion routine (h).

To monitor the convergence behaviour of the iterative process the expanded relative mean prediction error (E-RMPE) from Eq. (4.30) is used. Since the absolute value of the E-RMPE cannot be used as a criterion to interrupt the iterative reconstruction process, unless for the special case of a perfect numerical model (see discussion in section 4.5.2), the interruption criterion in the following simulations is defined in terms of the iteration number. Thus, the iterative process is interrupted after completing $k = 1000$ iterations, which has been found to be sufficient for the systems under test. Based on the evolution of the E-RMPE (see Figure 4.23 - (h)) one can conclude that a convergent iterative process is achieved for the noise free (2x9) MIMO system.

Although the FRF measurements used to build the different MIMO models have been found to contain severe errors, the generalised TDM is able to accurately reconstruct all response signatures (see Figure 4.23 - (a)). This is due to the use of the averaged error gradients involved in the update recursions (Eq. (4.34)) so that uncorrelated disturbances can be filtered out if the system is sufficiently overdetermined as it is the case for the (2x9) MIMO system. Therefore, the RMS estimation errors in the reconstructed response time histories $\varepsilon_{y\%RMS}$ are all approximately zero, as summarized in Table 4.10 – (2x9). Accordingly, the spectral estimation errors in the reconstructed responses $\Delta Y_m(\omega)$ are also close to zero throughout the entire frequency range of interest, as evidenced by diagram (f).

By means of the reconstructed force time histories depicted in diagrams (b,d) and (c,e) in full-length and as close-up, respectively, one can conclude that the generalised MIMO TDM facilitates perfect identification of the transient force signatures. Again it is noted that the FRF measurements comprise considerable errors which are completely counterbalanced owing to the averaged error gradients and due to considering a sufficient over-determined system. Note that the degree of overdetermination is 4.5 for the (2x9) MIMO system, which in the following is considered as large overdetermination. The high accuracy of the force reconstruction process is also evidenced by the RMS force estimation errors $\varepsilon_{x\%RMS}$ which are approximately zero for both forces $x_1(n)$ and $x_2(n)$ (see Table 4.10 – (2x9)). Correspondingly, the spectral estimation errors in the reconstructed forces are also close to zero as plotted in diagram (g).

A comparison of the identified forces obtained with the generalised TDM and the standard frequency domain inverse method (FDM) is presented in Figure 4.24. It is noted that the FDM invokes least-square Moore-Penrose pseudo inverse to obtain the inverse system model.

As evidenced in Figure 4.24 the generalised TDM and the FDM perform equally for the noise free (2x9) MIMO system. Both methods are able to identify the transient force signatures with high precision (see also Table 4.10 for the corresponding RMS force estimation error achieved with the FDM). Note that equivalent conclusions can be drawn for the simulations obtained for the (2x2) and the (2x4) MIMO system, provided in Appendix A.2.

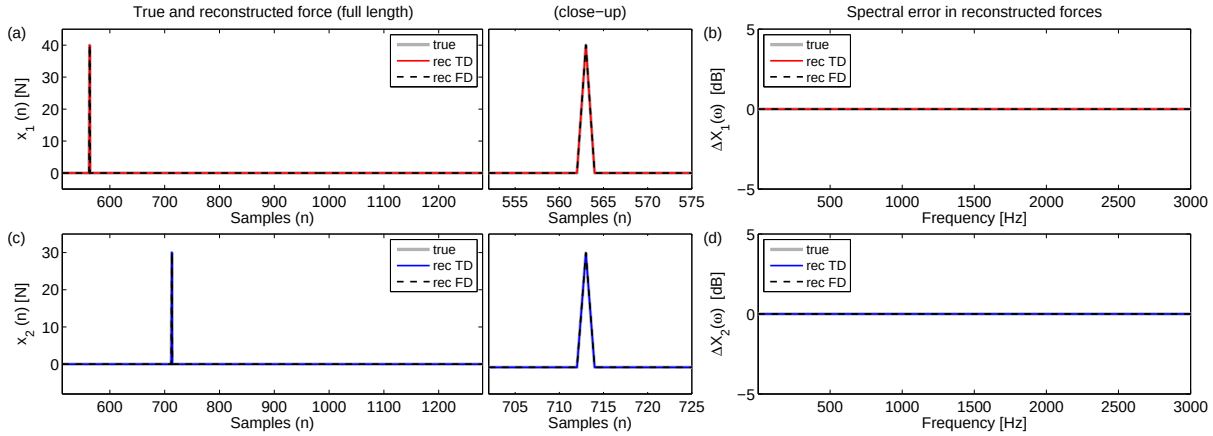

Figure 4.24. Comparison of the generalised time domain inverse method (TDM) with the standard frequency domain inverse method (FDM) for the noise free (2x9) MIMO system. Time signatures of reconstructed forces (a,c) and spectral estimation error in the identified force (b,d): ▬ true signal; — reconstructed force using the MIMO TDM; ‒ ‒ identified force using the FDM.

A summary of all time domain estimation results obtained with the generalised TDM and the FDM is given in Table 4.10 for all investigated noise free MIMO systems.

Table 4.10. Summary of simulation results achieved with the generalised time domain inversion routine and the standard frequency domain inverse method for all investigated noise free MIMO system.

		Noise free												
		TD inversion routine											FD inverse method	
Degree of over-determination (used system)		Error ε_{RMS} in reconstructed responses [%]									Error ε_{RMS} in reconstructed force [%]		Error ε_{RMS} in reconstructed force [%]	
		$y_1(n)$	$y_2(n)$	$y_3(n)$	$y_4(n)$	$y_5(n)$	$y_6(n)$	$y_7(n)$	$y_8(n)$	$y_9(n)$	$x_{1,TD}(n)$	$x_{2,TD}(n)$	$x_{1,FD}(n)$	$x_{2,FD}(n)$
1	(2x2)	0.1	-	-	0.0	-	-	-	-	-	1.9	3.2	0.0	0.0
2	(2x4)	0.0	0.0	-	0.0	-	-	-	0.0	-	0.2	0.3	0.0	0.0
4.5	(2x9)	0.0	0.0	0.0	0.0	0.0	0.0	0.0	0.0	0.0	0.0	0.0	0.0	0.0

As can be seen for the determined (2x2) and the double over-determined (2x4) MIMO system the force time histories cannot be identified exactly. This is due to inconsistencies included in the system model, originated from errors in the FRF measurements, and the lack to sufficiently over-determining the system at certain frequencies. Note that the FDM is able to reconstruct the forces exactly since the convolution routine used to build the MIMO system in Matlab for the noise free case is exactly the inverse process as employed by the FDM to identify the forces, whereas the TDM utilises an essentially different approach to reconstruct the force signatures. In a way, the MIMO model employed by the FDM thus can be considered as ideal while this is not necessarily the case for the TDM. However, as soon as uncorrelated disturbances will be added to the system model or the structural responses both

methods have to deal with imperfect data. Evaluating the performance of the TDM in comparison to the FDM in the presence of defective data is subject of the following sections.

4.6.3. Sensitivity to noise in the structural responses

In the following, the sensitivity of the generalised TDM to noise in the structural responses is investigated. To do so, uncorrelated noise sequences are added to the structural responses according to Eq. (4.15). Noise of different levels ranging from 5% over 10% to 25% of the RMS value of the respective noise free responses are simulated resulting in signal-to-noise ratios of approximately $SNR_{5\%} = 26\,\text{dB}$, $SNR_{10\%} = 20\,\text{dB}$ and $SNR_{25\%} = 12\,\text{dB}$, respectively. Simulations for the determined (2x2), the double overdetermined (2x4) and the large overdetermined (2x9) MIMO system are carried out for each noise level.

Figure 4.25 depicts the simulation results obtained with the generalised TDM for the (2x9) MIMO system considering 10% noise corrupted response data. Note that the simulation results for different noise levels and the remaining MIMO models are provided in Appendix A.2.

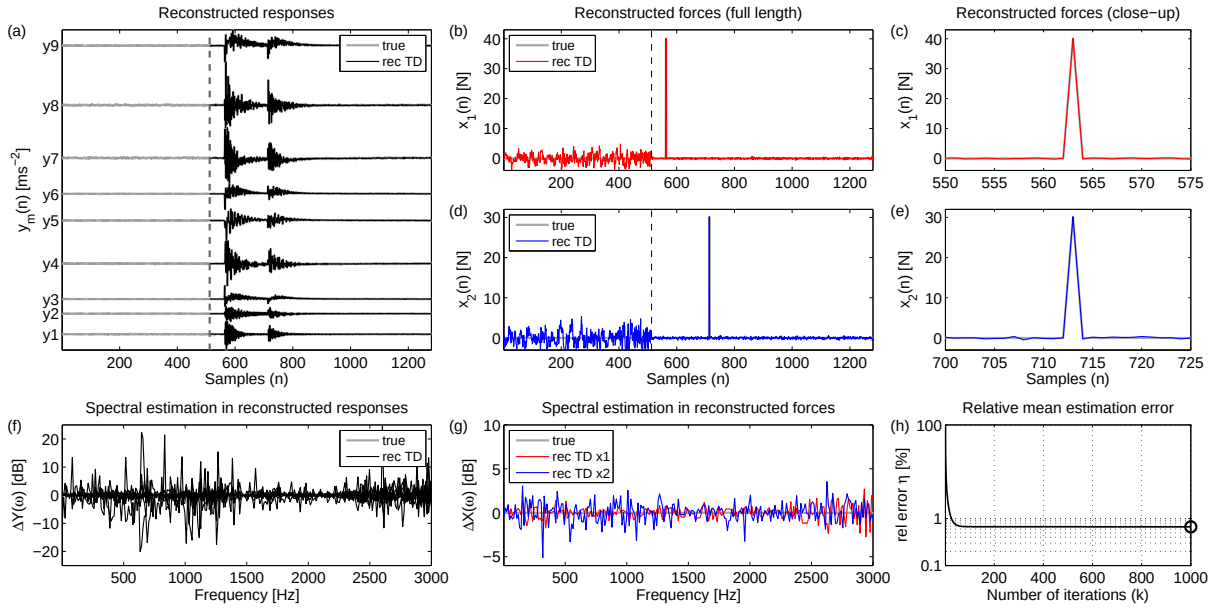

Figure 4.25. Numerical results for (2x9) MIMO system with 10 % noise added to all acceleration responses. Time signatures of structural responses (a) and reconstructed force signatures in full-length (b,d) and as close-up (c,e); spectral estimation error in reconstructed responses (f) and identified forces (g): ▬ true signal; ▬ reconstructed signal using TDM. Relative mean prediction error (E-RMPE) as performance measure of the adaptive inversion routine (h).

As expected, the additional noise in the data forces the E-RMPE to approximate towards a relative high residual value (cf. discussion in section 4.5.3). However, the evolution of the E-RMPE (Figure 4.25 - (h)) reveals that a convergent adaptive process is achieved and that the iterative process is carried out sufficiently for the chosen parameterisation of the adaptive algorithm.

Due to the additional noise and the use of the averaged error gradients the estimation errors in the reconstructed responses can reach relatively high values. In time domain the RMS error in the reconstructed responses $\varepsilon_{y,\%RMS}$ range from 5.5 % to 9.1 % (see also Table 4.11) resulting in considerable spectral estimation errors $\Delta Y_m(\omega)$ of up to $|23\,\mathrm{dB}|$ (Figure 4.25 - (f)). However, since the averaged gradients involved in the force reconstruction process at each frequency are governed by the strongest contributing signal the negative influence of the additional noise is significantly suppressed in the identified forces. The spectral estimation errors in the reconstructed forces at most frequencies are only $\Delta X_1(\omega) \le |2.7\,\mathrm{dB}|$ and $\Delta X_2(\omega) \le |3.5\,\mathrm{dB}|$, respectively (Figure 4.25 - (g)).

The efficiency of the averaged error gradients to counterbalance uncorrelated disturbances in the response data is also evidenced by the identified force time histories plotted in diagrams (b,c) for the full length sequences and in (d,e) as close-ups of the transient force peaks. For both forces the transient force pulses can be recovered from the noise corrupted responses with high precision and only little noise can be found at times beside the force peaks. The corresponding time domain RMS estimation errors $\varepsilon_{x,\%RMS}$ are 13.0 % and 19 % for force x_1 and x_2, respectively. Note that the time domain estimation results are summarised in Table 4.11.

A comparison of the identified forces obtained with the TDM and the ones calculated by means of the standard FDM is given in Figure 4.26.

It turns out that both inverse methods are able to identify the forces with the same accuracy if noise is added to the response data and overdetermination is used. Similar conclusions can be drawn for the simulations carried out with different noise levels and different degrees of overdetermination.

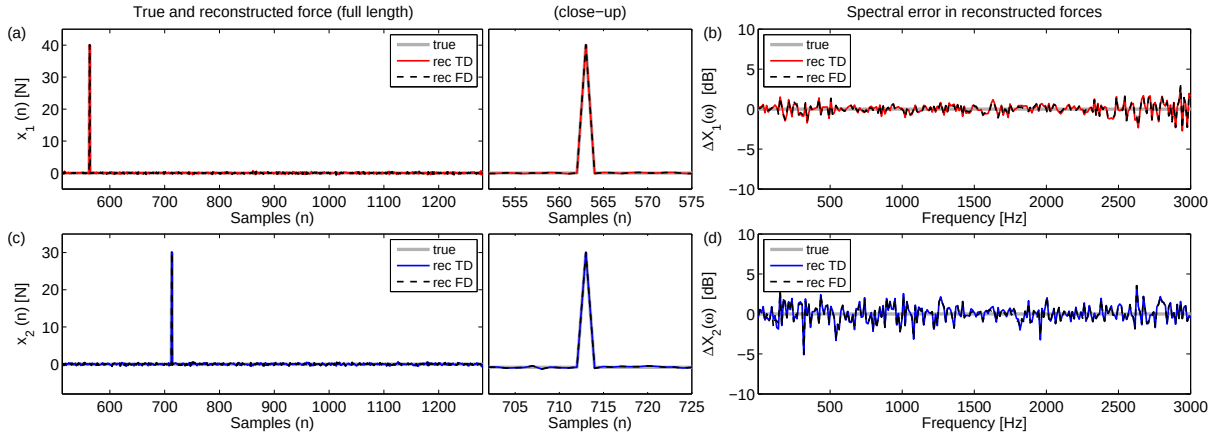

Figure 4.26. Comparison of the generalised time domain inverse method (TDM) with the standard frequency domain inverse method (FDM) for the (2x9) MIMO system with 10 % noise added to all responses. Time signatures of reconstructed forces (a,c) and spectral estimation error in the identified force (b,d): ▬ true signal; — reconstructed force using the MIMO TDM; – – identified force using the FDM.

It is stressed that for the determined (2x2) MIMO system the TDM generally performs better than the FDM (see also Appendix A.2), as can be seen e.g. from Table 4.11 where a summary of all simulation results obtained for the investigated MIMO systems in the presence of 10 % noise corrupted response data is given.

Table 4.11. Summary of simulation results achieved with the generalised time domain inversion routine and the standard frequency domain inverse method for all MIMO systems with 10 % noise corrupted responses.

		10% noise added to responses ($SNR_m \approx 20$ dB)												
		TD inversion routine											FD inverse method	
Degree of over-determination (used system)		Error ε_{RMS} in reconstructed responses [%]									Error ε_{RMS} in reconstructed force [%]		Error ε_{RMS} in reconstructed force [%]	
		$y_1(n)$	$y_2(n)$	$y_3(n)$	$y_4(n)$	$y_5(n)$	$y_6(n)$	$y_7(n)$	$y_8(n)$	$y_9(n)$	$x_{1,TD}(n)$	$x_{2,TD}(n)$	$x_{1,FD}(n)$	$x_{2,FD}(n)$
1	(2x2)	0.5	-	-	0.0	-	-	-	-	-	118.4	274.1	144.1	328.5
2	(2x4)	6.9	8.7	-	4.1	-	-	-	2.4	-	30.2	54.8	30.1	54.9
4.5	(2x9)	7.9	8.4	9.1	6.8	7.7	8.0	5.5	4.9	6.4	13.0	19.6	12.9	19.6

Comparing the RMS estimation errors in the reconstructed forces obtained for the different MIMO systems a trend can be identified. Clearly, the accuracy of any of the two force identification techniques increases with increasing degree of overdetermination. The influence of overdetermination on the estimation accuracy can also be measured in terms of the spectral error in the reconstructed forces, as plotted in Figure 4.27 for the different MIMO models assuming 10 % noise corrupted response data. In addition, the spectral estimation error obtained for the noise free (2x9) MIMO system is plotted (black dashed line) which serves as reference and represents the best possible solution for the given FRF data.

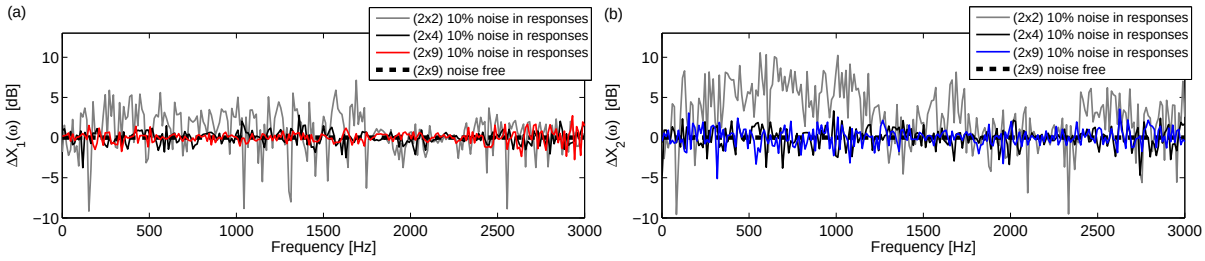

Figure 4.27. Influence of the degree of overdetermination on the estimation accuracy. Spectral estimation error $\Delta X(\omega)$ in the reconstructed force x_1 (a) and x_2 (b) obtained with the generalised TDM for the determined (2x2) and the overdetermined (2x4) and (2x9) MIMO system: ── with 10% noise added to all responses; ▪▪▪▪ without noise.

Clearly, one can see the significant improvement in the reconstructed forces one achieves when employing the double determined (2x4) or the highly overdetermined (2x9) MIMO system for force identification instead of using the determined (2x2) system. Doing so, will reduce the maximal spectral estimation errors in the reconstructed force x_1 from $\Delta X_{1,(2\times2)} \approx |9.2\,\text{dB}|$ to $\Delta X_{1,(2\times4)} \approx |3.7\,\text{dB}|$ and $\Delta X_{1,(2\times9)} \approx |2.7\,\text{dB}|$, respectively, and in the force x_2 from $\Delta X_{2,(2\times2)} \approx |10.6\,\text{dB}|$ to $\Delta X_{2,(2\times4)} \approx |4.7\,\text{dB}|$ and $\Delta X_{2,(2\times9)} \approx |3.8\,\text{dB}|$, respectively. Similar conclusions can be drawn from the simulation results obtained for different noise levels as provided in Appendix A.2. In the following, the influence of overdetermination is further investigated for cases where the system model is assumed to comprise errors.

4.6.4. Sensitivity to errors in the system model

To investigate the performance of the generalised TDM for cases where the system model is inconsistent to some extent, the assumed noise free MIMO models from section 4.6.2 are degraded artificially. For this purpose, all measured impulse response functions (IRFs) are modified by addition of uncorrelated white noise sequences according to Eq. (4.15). As error magnitudes 5% and 10% of the RMS value of the respective noise free IRFs are chosen so that signal-to-noise ratios of approximately $SNR_{5\%} = 26\,\text{dB}$ and $SNR_{10\%} = 20\,\text{dB}$ result.

Simulations for the determined (2x2), the double overdetermined (2x4) and the highly overdetermined (2x9) MIMO system are carried out for the different levels of inconsistencies. Figure 4.28 depicts the simulation results obtained with the generalised TDM for the (2x9) MIMO system with 10 % disturbances added to all IRFs. Note that simulation results for the remaining MIMO models and different noise levels are provided in Appendix A.2.

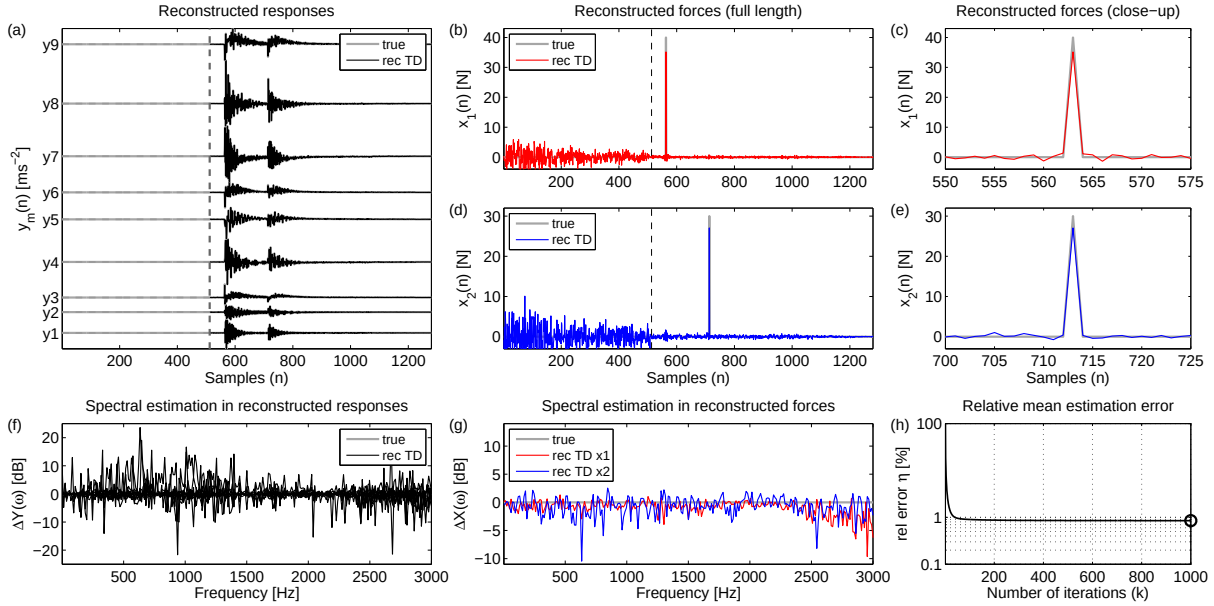

Figure 4.28. Numerical results for (2x9) MIMO system with 10 % errors added to all impulse response functions. Time signatures of structural responses (a) and reconstructed force signatures in full-length (b,d) and as close-up (c,e); spectral estimation error in reconstructed responses (f) and identified forces (g): ▬ true signal; ── reconstructed signal using TDM. Relative mean prediction error (E-RMPE) as performance measure of the adaptive inversion routine (h).

The evolution of the E-RMPE (Figure 4.28 - (h)) indicates that a convergent iterative process is achieved and that the iterative process is carried out sufficiently. As mentioned before, the residual E-RMPE value is influenced by the additional disturbances included in the impulse response functions resulting in a relatively high residual value of the E-RMPE.

The additional disturbances in the system model and the use of the averaged error gradients in the generalised TDM cause considerable errors in the reconstructed responses, as evidenced by the corresponding spectral estimation errors in Figure 4.28 - (f). For some paths the maximal estimation error can exceed values of $\Delta Y_m(\omega) = |20\,\mathrm{dB}|$ at discrete frequencies. The corresponding time domain RMS estimation errors $\varepsilon_{y,\%RMS}$ range from 4.7 % to 12.2 %, as depicted in Table 4.12. However, the errors in the identified forces are orders of magnitudes below the ones in the reconstructed responses, as it can be concluded by comparing the corresponding spectral estimation errors in diagram (f) and (g), respectively. Again, the superior estimation accuracy in the forces is due to the use of the averaged error gradients involved in the generalised TDM to update the forces recursively. Within a wide frequency range the forces can be estimated with an error less than $\Delta X_1(\omega) = |2.0\,\mathrm{dB}|$ for force x_1 and $\Delta X_2(\omega) = |3.3\,\mathrm{dB}|$ for x_2, respectively (see Figure 4.28 - (g)).

The good force identification accuracy can also be seen from the corresponding force time histories depicted in (Figure 4.28 – (b)-(e)). Despite the highly inconsistent system model the transient pulses in both force signatures are recovered with high precision (see diagrams (c) and (e)) and only little errors can be spotted beside these peaks (diagrams (b) and (d)). The corresponding time domain RMS errors in the estimated forces $\varepsilon_{x,\%RMS}$ are 20.5 % and 28.4 % for force x_1 and x_2, respectively (see Table 4.12).

In Figure 4.29, the identified forces calculated with the generalised TDM are contrasted to the ones obtained with the standard FDM. Comparing first the spectral estimation errors in the reconstructed forces (Figure 4.29 - (b) and (d)) it can be found that the FDM is more sensitive to inconsistencies included in the system model than the TDM.

In general, the scatter in the estimated spectra in both identified forces is higher if the FDM is used. This also provokes higher estimation errors in the reconstructed force signatures as depicted in diagrams (a) and (c). The corresponding time domain RMS estimation errors $\varepsilon_{x,\%RMS}$ are 28.3 % and 48.7 % for force x_1 and x_2, respectively. Equivalent conclusions can be drawn for the simulations carried out with different levels of inconsistencies and different degrees of overdetermination.

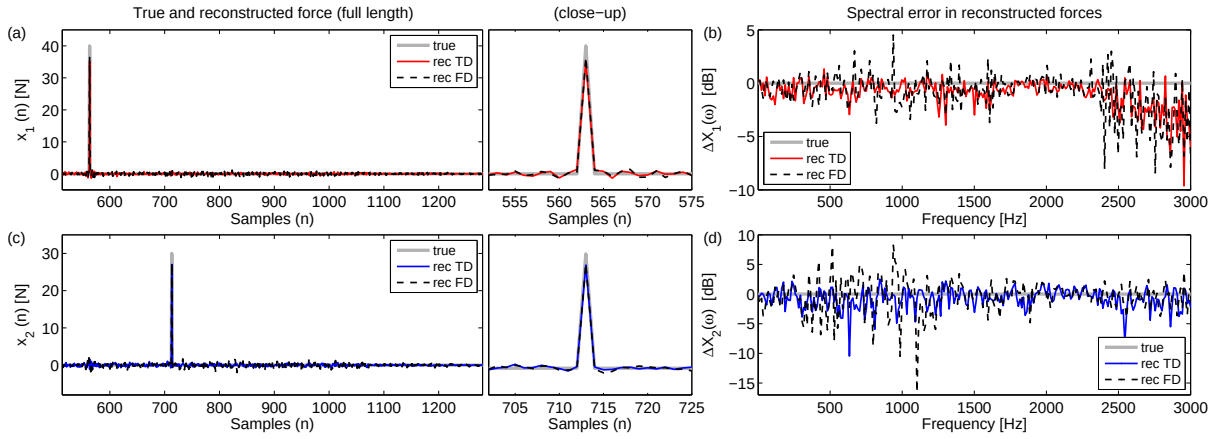

Figure 4.29. Comparison of the generalised time domain inverse method (TDM) with the standard frequency domain inverse method (FDM) for the (2x9) MIMO system with 10 % errors added to all impulse response functions. Time signatures of reconstructed forces (a,c) and spectral estimation error in the identified force (b,d): ▬ true signal; — reconstructed force using the MIMO TDM; – – identified force using the FDM.

A summary of the simulation results obtained for the determined (2x2), the double overdetermined (2x4) and the highly overdetermined (2x9) MIMO system with 10 % disturbances added to all impulse response functions is given in Table 4.12. Note that

simulation results for different levels of inconsistencies are provided for all investigated MIMO models in Appendix A.2.

Table 4.12. Summary of simulation results achieved with the generalised time domain inversion routine and the standard frequency domain inverse method for all MIMO systems with 10 % noise corrupted system model.

Degree of over-determination (used system)		10% noise added to IRFs ($SNR_m \approx 20$ dB)												
		TD inversion routine											FD inverse method	
		Error ε_{RMS} in reconstructed responses [%]									Error ε_{RMS} in reconstructed force [%]		Error ε_{RMS} in reconstructed force [%]	
		$y_1(n)$	$y_2(n)$	$y_3(n)$	$y_4(n)$	$y_5(n)$	$y_6(n)$	$y_7(n)$	$y_8(n)$	$y_9(n)$	$x_{1,TD}(n)$	$x_{2,TD}(n)$	$x_{1,FD}(n)$	$x_{2,FD}(n)$
1	(2x2)	0.0	-	-	0.0	-	-	-	-	-	64.5	124.3	99.4	202.1
2	(2x4)	4.9	7.2	-	2.1	-	-	-	1.3	-	45.1	74.2	47,3	78.4
4.5	(2x9)	8.9	11.0	12.2	6.7	8.6	9.4	4.8	4.7	6.9	20.5	28.4	28.3	48.7

As can be concluded from Table 4.12 the accuracy of both the TDM and the FDM decreases if the degree of overdetermination is decreased. This is consistent with the findings of the last section. Furthermore, for all investigated cases the TDM yields more reliable force reconstruction results than the FDM as evidenced by the time domain RMS estimation errors $\varepsilon_{x,\%RMS}$ provided in Table 4.12. The influence of overdetermination on the estimation accuracy is further illustrated in Figure 4.30 where the spectral estimation errors in the force x_1 and x_2 are plotted as functions of the degree of overdetermination for the 10 % degraded system models achieved with the FDM (Figure 4.30 - (a),(b)) and the generalised TDM (Figure 4.30 - (c),(d)), respectively. In addition, the spectral estimation errors obtained for the noise free (2x9) MIMO system is plotted (black dashed lines) which serves as reference and represents the best achievable solution for the measured FRF data.

From Figure 4.30 it becomes apparent that, when employing the FDM instead of the TDM, one generally has to expect larger errors in the reconstructed forces. By comparing the shapes of the force estimation errors obtained with the FDM and the TDM, in particular for the force x_1 (cf. diagrams (a) and (b)), one can find similar spectral patterns highlighting the frequency ranges at which force reconstruction generally tends to be difficult. For example, the force x_1 can be estimated with best accuracy at frequencies between about 1500 Hz and 2400 Hz while its reconstruction is subject to relative large uncertainty at frequencies below and above this frequency range. It is noted that the same tendencies can be found for the force x_2, in particular for the (2x9) MIMO system, although this is hard to see from the diagrams (c) and (d) since the estimated forces tend to oscillate considerably.

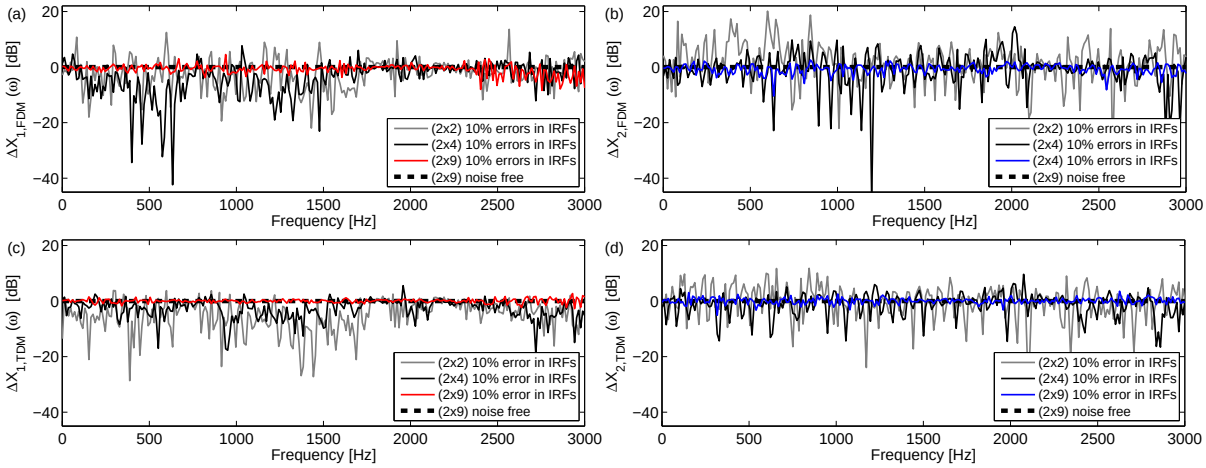

Figure 4.30. Influence of the degree of overdetermination on the estimation accuracy. Spectral estimation error in the reconstructed force x_1 (a) and x_2 (b) obtained with the standard FDM and corresponding errors (c) and (d) obtained with the generalised TDM for the determined (2x2) and the overdetermined (2x4) and (2x9) MIMO system: ── with 10% errors added to all impulse response functions (IRFs); ▪ ▪ ▪ without errors.

Important to note is, however, that an equivalent spectral pattern can be found in the reconstructed responses if the generalised TDM is used for force identification (see e.g. Figure 4.28 – (f)). Moreover, equivalent patterns in the reconstructed responses and forces can also be found for simulations in which the system model is assumed to be free from any disturbances but instead responses are corrupted by noise (see e.g. Figure 4.25 – (f) and (g)). Note that no such pattern appears if both the system model and the structural responses are free from noise (see e.g. Figure 4.23 – (f) and (g)).

However, since in all simulations additional disturbances in either the response data or the system models are designed as random signals (white noise), i.e. they have a flat (constant) power spectral density, the disturbances may indeed provoke the appearance of the spectral error patterns in the reconstructed quantities but they cannot cause their characteristic shape. Instead it is suspected that the underlying system models which in all simulations are based on the same basic FRF measurements are responsible for these characteristic patterns. To clarify this conjecture the employed system models are analysed in more detail. It is well known from the standard FDM that the sensitivity of the least-squares solution to perturbations of the FRF matrix, $\mathbf{H}(\omega)$, and errors in the response measurements can be measured by the frequency dependent condition number of $\mathbf{H}(\omega)$ [29]. The 2-norm condition number is defined by

$$\kappa(\omega) = cond(\mathbf{H}(\omega)) = \left\|\mathbf{H}(\omega)\right\|_2 \left\|\mathbf{H}^{+}(\omega)\right\|_2 = \sigma_1 / \sigma_{rank(\mathbf{H}(\omega))} \tag{4.36}$$

where super-script '+' denotes Moore-Penrose pseudo-inverse and σ_1 and $\sigma_{rank(\mathbf{H}(\omega))}$ are the largest and smallest singular values of the FRF matrix, respectively, of which the latter depends on the rank of the FRF matrix. (For more details see also the discussion given in section 2.4).

Mathematically the condition number is a dimensionless quantity which is used to evaluate the degree of singularity of the FRF matrix. Large condition numbers indicate a nearly singular matrix which is likely to lead to numerical inversion problems. Although the magnitude of the condition number is problem dependent and, for engineering vibration problems, can range from 1 to more than 10000 [7] the general consensus is that force identification based on the standard FDM at frequencies with high condition numbers can go dramatically wrong since small perturbations included in the used data tend to be amplified considerably after inverting the FRF matrix at these frequencies.

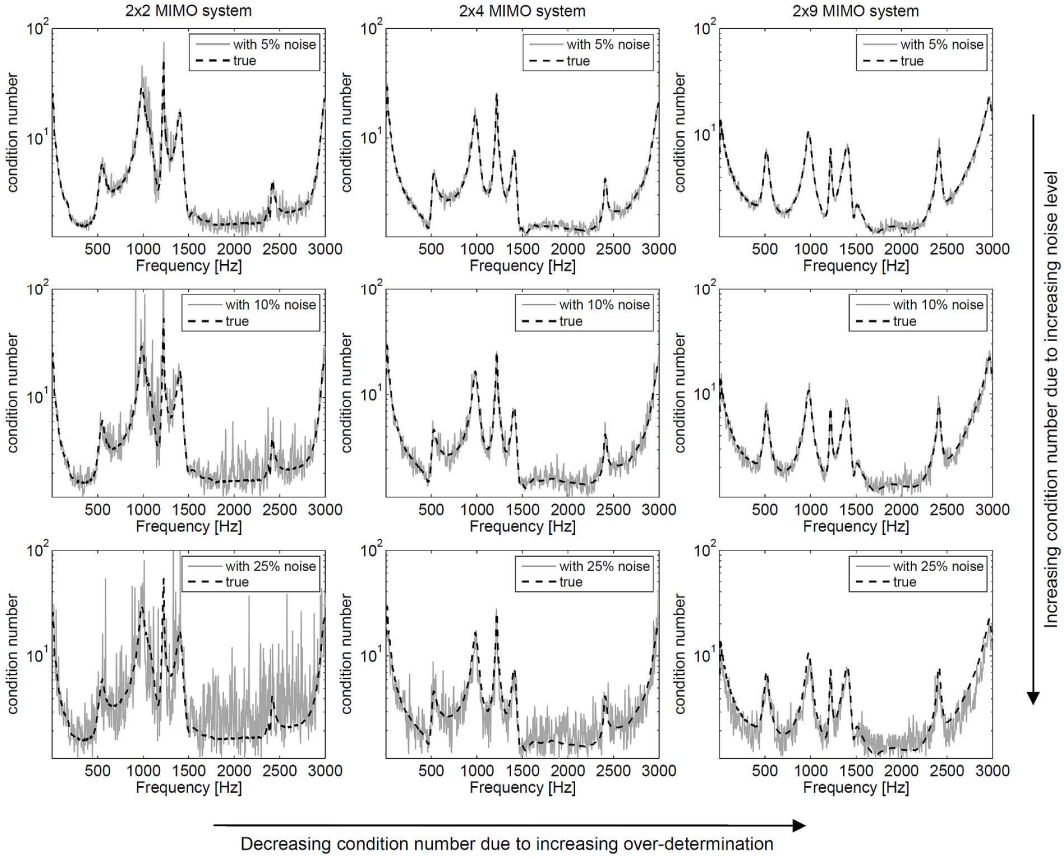

Figure 4.31. Sensitivity of the condition number to different degrees of over-determination (determined (2x2), double (2x4) and large over-determined (2x9) MIMO system) and different levels of disturbances (5%, 10% and 25%) included in the impulse response function measurements: ---- true system, —— noise corrupted system.

Since the FRF matrix for the given application case is obtained by Fourier transformation of per-measured impulse response functions, of which the latter are also employed for force reconstruction based on the generalised TDM, analysis of the corresponding condition numbers seems to be worthwhile. In Figure 4.31, the condition numbers of the determined (2x2) and the overdetermined (2x4) and (2x9) FRF matrices are depicted assuming noise free, as well as, 5 %, 10 % and 25 % errors in the measured impulse response functions.

Clearly, the condition numbers of all noise free FRF matrices (dashed lines) feature similar spectral shapes which are determined by the dynamic characteristics of the steering gear housing. For all investigated MIMO systems it can be seen that the corresponding FRF matrices are best conditioned at frequencies between about 1500 Hz and 2400 Hz while the condition numbers at lower and higher frequencies generally indicate inferior conditioning.

Concerning the sensitivity of the condition numbers to the degree of overdetermination, it can be found that consideration of more responses, i.e. increasing the degree of overdetermination, results in decreasing condition numbers (see Figure 4.31 – from left to right). It is stressed that for all investigated MIMO systems the number of applied forces is always equal to $S = 2$ while the number of considered responses M is modified according to the constraint $M \geq S$ which is required to guarantee solvability of the inverse force identification problem. As a consequence of this the corresponding FRF matrices always have rank 2. Note that the condition numbers would increase if despite considering a larger number of responses also the number of independent excitation mechanisms were increased.

Analysing further the sensitivity of the condition numbers to the level of disturbances added to all impulse response functions, which are ultimately used to build the different FRF matrices, it can be found that increasing noise levels cause the condition numbers to increase (see Figure 4.31 – from top to bottom). The additional random errors tend to have less impact on the condition numbers of systems with relative large overdetermination whereas they can considerably influence the condition numbers of the determined system.

According to these findings, the determined (2x2) MIMO system with 25 % corrupted impulse response functions (IRFs) (Figure 4.31 – bottom-left diagram) is most critical with respect to inverse force identification while the best force estimation accuracy is expected for the large overdetermined (2x9) MIMO system with 5% degraded or rather noise free IRFs (top-right diagram). Simulations conducted for all MIMO systems referred to in Figure 4.31 have unambiguously proved that this conjecture is true. Moreover, comparing the overall

spectral shapes of the condition numbers for the different MIMO systems with the patterns detected in the spectral force estimation errors it can be concluded that force reconstruction in frequency ranges with predominantly high condition numbers generally is prone to large errors while frequency ranges with low condition numbers allow predicting the forces more reliable. Basically, the spectral characteristics of the condition numbers (see Figure 4.31) seem to correlate well with the spectral patterns detected for the estimation errors in the forces identified with either the FDM or the TDM (see Figure 4.28 and Figure 4.30). Furthermore, it can be found that, when using the TDM for force identification, the spectral estimation errors in the reconstructed responses also correlate well with the characteristics of the condition numbers and consequently with the spectral error patterns in the identified forces. This can be observed for simulations in which either the system model is assumed to be inconsistent (see Figure 4.25and Figure 4.28) or in which the response data is assumed to contain noise (see Figure 4.28 and Figure 4.30). With respect to practical force identification problems where spectral force estimation errors cannot be calculated since the true forces are unknown, the spectral errors in the reconstructed responses provided by the TDM may constitute important additional information to detect frequency ranges in which force identification is likely to be erroneous. Note that this information is not available if the standard FDM is used for force identification.

Moreover, in all conducted simulations in which inconsistent system models have been used, the generalised TDM has unambiguously outperformed the FDM in terms of the achieved force identification accuracy. According to the previous analysis, poor conditioning of the FRF matrix and the need to invert this matrix in the standard FDM can now be named as the principal reason for the inferior performance of the FDM if considerable inconsistent system models are present. Since the TDM uses the same fundamental data it is further concluded that the generalised TDM is more robust for inconsistent system models than the FDM.

4.6.5. Conclusions

Employing the principles of overdetermination and linear superposition to account for contributions from several excitations to at least the same number of observable responses a generalised time domain inversion routine (TDM) has been derived. The generalised TDM facilitates robust force identification in multiple input multiple output (MIMO) systems (see Table 4.8). The generalisation is based on the introduction of an individual iterative recursion

for each applied force to be identified. In each recursion an average error gradient is used to update the estimated forces recursively. Furthermore, the averaged error gradients allow for suppression of uncorrelated noise in the response data or inconsistencies in the employed system model by overdetermining the system. In case of overdetermination, the choice of the response positions is generally not as crucial as in standard frequency domain inverse methods (FDM) since response positions with weak contribution from the excitation forces at a certain frequency do not govern the averaged error gradients. The adaptive process will automatically be controlled by the strongest signals. Inconsistencies in the impulse response functions (IRFs) or noise in the response data appear as considerable errors in the reconstructed structural responses but do not influence the force reconstruction process to a high degree.

In numerical simulations the sensitivity of the generalised TDM to noise and inconsistencies included in the structural responses and the system model, respectively, was investigated. The performance of the MIMO TDM was further compared to the standard frequency domain FDM. All time domain estimation errors obtained from simulations for the determined (2x2) and the overdetermined (2x4) and (2x9) MIMO system are summarized in Table 4.13 assuming 5 %, 10 % and 25 % corrupted response data and in Table 4.14 assuming 5 % and 10 % defective system models, respectively. Note that the corresponding diagrams of all simulations are provided in Appendix A.2.

Table 4.13. Summary of simulation results achieved with the generalised time domain inversion routine and the standard frequency domain inverse method for the determined (2x2) and the overdetermined (2x4) and (2x9) MIMO system with 5 %, 10 % and 25 % noise added to all responses.

Degree of over-determination (used system)		5% noise added to responses ($SNR_m \approx 26$ dB)												
		TD inversion routine											FD inverse method	
		Error ε_{RMS} in reconstructed responses [%]									Error ε_{RMS} in reconstructed force [%]		Error ε_{RMS} in reconstructed force [%]	
		$y_1(n)$	$y_2(n)$	$y_3(n)$	$y_4(n)$	$y_5(n)$	$y_6(n)$	$y_7(n)$	$y_8(n)$	$y_9(n)$	$x_{1,TD}(n)$	$x_{2,TD}(n)$	$x_{1,FD}(n)$	$x_{2,FD}(n)$
1	(2x2)	0.2	-	-	0.0	-	-	-	-	-	56.9	135.2	67.3	159.1
2	(2x4)	3.5	4.3	-	1.9	-	-	-	1.2	-	15.9	28.7	16.0	28.5
4.5	(2x9)	3.9	4.1	4.6	3.3	3.9	4.1	2.9	2.5	3.5	6.3	9.7	6.4	9.6
		10% noise added to responses ($SNR_m \approx 20$ dB)												
		TD inversion routine											FD inverse method	
		Error ε_{RMS} in reconstructed responses [%]									Error ε_{RMS} in reconstructed force [%]		Error ε_{RMS} in reconstructed force [%]	
		$y_1(n)$	$y_2(n)$	$y_3(n)$	$y_4(n)$	$y_5(n)$	$y_6(n)$	$y_7(n)$	$y_8(n)$	$y_9(n)$	$x_{1,TD}(n)$	$x_{2,TD}(n)$	$x_{1,FD}(n)$	$x_{2,FD}(n)$
1	(2x2)	0.5	-	-	0.0	-	-	-	-	-	118.4	274.1	144.1	328.5
2	(2x4)	6.9	8.7	-	4.1	-	-	-	2.4	-	30.2	54.8	30.1	54.9
4.5	(2x9)	7.9	8.4	9.1	6.8	7.7	8.0	5.5	4.9	6.4	13.0	19.6	12.9	19.6
		25% noise added to responses ($SNR_m \approx 12$ dB)												
		TD inversion routine											FD inverse method	
		Error ε_{RMS} in reconstructed responses [%]									Error ε_{RMS} in reconstructed force [%]		Error ε_{RMS} in reconstructed force [%]	
		$y_1(n)$	$y_2(n)$	$y_3(n)$	$y_4(n)$	$y_5(n)$	$y_6(n)$	$y_7(n)$	$y_8(n)$	$y_9(n)$	$x_{1,TD}(n)$	$x_{2,TD}(n)$	$x_{1,FD}(n)$	$x_{2,FD}(n)$
1	(2x2)	1.1	-	-	0.1	-	-	-	-	-	310.3	700.2	385.5	864.4
2	(2x4)	17.1	2.2	-	10.6	-	-	-	6.4	-	75.8	129.5	77.0	133.4
4.5	(2x9)	19.1	20.7	23.6	17.0	18.9	19.6	14.3	12.4	15.7	31.8	47.6	31.7	47.5

Table 4.14. Summary of simulation results achieved with the generalised time domain inversion routine and the standard frequency domain inverse method for the determined (2x2) and the overdetermined (2x4) and (2x9) MIMO system with 5 % and 10 % disturbances added to all impulse response functions.

Degree of over-determination (used system)		5% noise added to IRFs ($SNR_m \approx 26$ dB)												
		TD inversion routine											FD inverse method	
		Error ε_{RMS} in reconstructed responses [%]									Error ε_{RMS} in reconstructed force [%]		Error ε_{RMS} in reconstructed force [%]	
		$y_1(n)$	$y_2(n)$	$y_3(n)$	$y_4(n)$	$y_5(n)$	$y_6(n)$	$y_7(n)$	$y_8(n)$	$y_9(n)$	$x_{1,TD}(n)$	$x_{2,TD}(n)$	$x_{1,FD}(n)$	$x_{2,FD}(n)$
1	(2x2)	0.0	-	-	0.0	-	-	-	-	-	46.6	94.9	134.4	195.7
2	(2x4)	3.1	4.5	-	1.5	-	-	-	0.9	-	23.3	41.7	28.0	42.5
4.5	(2x9)	4.7	5.4	6.2	3.8	4.3	5.3	2.7	2.5	3.6	9.7	13.8	15.9	26.2
		10% noise added to IRFs ($SNR_m \approx 20$ dB)												
		TD inversion routine											FD inverse method	
		Error ε_{RMS} in reconstructed responses [%]									Error ε_{RMS} in reconstructed force [%]		Error ε_{RMS} in reconstructed force [%]	
		$y_1(n)$	$y_2(n)$	$y_3(n)$	$y_4(n)$	$y_5(n)$	$y_6(n)$	$y_7(n)$	$y_8(n)$	$y_9(n)$	$x_{1,TD}(n)$	$x_{2,TD}(n)$	$x_{1,FD}(n)$	$x_{2,FD}(n)$
1	(2x2)	0.0	-	-	0.0	-	-	-	-	-	64.5	124.3	99.4	202.1
2	(2x4)	4.9	7.2	-	2.1	-	-	-	1.3	-	45.1	74.2	47,3	78.4
4.5	(2x9)	8.9	11.0	12.2	6.7	8.6	9.4	4.8	4.7	6.9	20.5	28.4	28.3	48.7

For the conducted simulations it has been found that

- exact force identification is possible with the FDM and the generalised TDM if neither the structural responses nor the system model comprises any errors (cf. Table 4.10) and the system is sufficiently overdetermined,
- both methods, the standard FDM and the generalised TDM, perform exactly the same if only the structural responses are corrupted by additional (uncorrelated) noise. The residual errors in the identified forces correlate with the amount of noise added to the response, i.e. the errors increase with increasing noise levels. Due to the use of the averaged error gradients the transient force pulses can be reconstructed with high precision while, at the same time, errors and noise beside these pulses are sufficiently suppressed. The use of the generalised TDM has been found to be advantageous since the additional spectral estimation errors in the reconstructed responses are related to the force estimation errors and thus provide helpful information to identify at which frequencies certain FRFs are sensitive to noise and which frequencies in the estimated forces are likely to be prone to errors. This additional information is not available if the standard FDM is employed for inverse force identification.
- the generalised TDM outperforms the standard FDM in terms of the achieved force identification accuracy if inconsistent system models are used. Since the MIMO recursion involved in the generalised TDM does not require solution of an equation system by inversion of a possibly ill-conditioned FRF matrix the TDM has been found to be more robust to uncorrelated errors in the system description than the FDM although both methods in essence rely on the same data. In the investigated numerical examples it has been found that force spectra estimated with the generalised TDM can be at least an order of magnitude superior to the ones obtained with the FDM at frequencies at which the corresponding FRF matrices are poorly conditioned. The spectral estimation errors in the reconstructed responses provided as additional information by the TDM further help to evaluate frequency ranges in which force identification is subject to large uncertainty. Increasing the degree of overdetermination generally improves the force estimation accuracy and it has been shown that large overdetermination enables satisfying force identification even in the presence of considerable defective system models.

The expanded relative mean prediction error (E-RMPE) has been found to be a good means to monitor the convergence behaviour of the iterative process involved in the generalised TDM although its absolute values cannot be used to define an objective criterion to interrupt the iterative process.

4.7. Summary and concluding remarks

In a series of steps, the conventional Least Mean Square (LMS) algorithm has been modified to derive a generalised time domain inverse method (TDM) which is capable of reconstructing simultaneous multi-channel force signatures for structures with known and fixed force input locations utilising measured structural responses.

The physical system is modelled by means of impulse response functions (IRFs) that can be calculated by employing inverse Fourier transformation to frequency response functions (FRFs) which can be measured experimentally invoking conventional system identification methods, such as (roving hammer) impact testing or shaker testing. In this way it is possible to realise reliable system models even for highly complex technical structures.

The obtained IRFs are then used in the TDM to filter a set of estimated input force signatures so as to predict the corresponding set of structural responses. The instantaneous errors between the estimated and measured responses are then used to update the input force time histories recursively. In a way, all data-processing steps involved in the TDM are carried out in an invariable forward manner which is believed to pose one of the major advantages of the TDM in contrast to other inverse methods, such as standard frequency domain inverse methods (FDM). At no stage the iterative process involved in the generalised TDM needs to rely on inversion of a possibly ill-conditioned FRF matrix nor requires extensive regularisation techniques to improve the solutions. In the standard FDM ‘weak’ paths bring about dominant contributions after inversion, which are highly susceptible to noise. Instead, it is always the measurement point with the strongest signal that dominates the inversion process in the generalised TDM so that the choice of measurement positions is generally not very critical.

It has been shown that the novel time domain inversion routine allows reconstruction of multiple uncorrelated, correlated or partially correlated forces that can feature any kind of sparse or non-sparse time signature including random, periodic, impulsive, irregular or steady state signals. Sharp discontinuities contained in the force time signatures have been found to affect the convergence speed negatively but can be reconstructed precisely if the iterative

process is carried out often enough. Furthermore, under the assumption that the available response data is at least twice the length of the used IRFs, the method facilitates continuous processing of time data of arbitrary length thus allowing all sorts of post-processing for each individual identified force signature which is an attractive prospect for many practical demands like time domain TPA [19],[86], auralisation purposes [6] or condition monitoring [176].

The implementation of an averaged error gradient in the iterative recursion to update each force individually allows for overdetermining the system. In numerical simulations it has been found that for overdetermined systems the generalised TDM is very robust to noise included in the response data or errors inherent in the system model. Under the assumption that these disturbances are uncorrelated and the system is sufficiently overdetermined the averaged error gradients will significantly suppress the negative influences of the perturbations on the force reconstruction process even when the used data comprises considerable errors. In the presence of defective data the averaged error gradients can cause substantial errors in the reconstructed response spectra. However, the spectral shapes of these errors has been found to be suitable indicators to identify frequency bands in which force reconstruction is generally subject to high uncertainty due to insufficient system descriptions. This additional information is not available when conducting inverse force identification with the standard FDM.

By comparison it has been found that the FDM and the TDM perform equally if the used data can be assumed to be noise free or if noise is only included in the response data. Due to the availability of additional information concerning the reliability of the identified forces it has been argued that the use of the generalised TDM is at least of avail. However, as soon as the system model comprises (uncorrelated) errors the novel time domain inversion routine has proved to generally yield more robust and accurate force reconstruction results than the standard FDM. It has been found that force spectra estimated with the generalised TDM can be at least an order of magnitude superior to the ones obtained with the standard FDM at frequencies at which the corresponding FRF matrices are poorly conditioned. The advantages of the TDM over the FDM become more significant with increasing degree of overdetermination and increasing levels of perturbation.

Notwithstanding these benefits, it has also been shown that the generalised TDM lacks a reliable measure to evaluate the accuracy of the force prediction or rather to define an objective criterion to interrupt the iterative force reconstruction process. Observing the

evolution of the expanded relative mean prediction error (E-RMPE) has, however, been found to be a good means to monitor the overall progress of the iterative process. It has further been outlined that defining interruption criteria based on the E-RMPE's gradient or its curvature may be promising possibilities for future work. Note that two alternative criteria will be proposed in later sections that can be applied with respect to test bench measurements required for characterisation of transient sound sources in electrical steering systems.

The stability and speed of adaptive algorithm involved in the generalised TDM is dependent on the choice of the convergence-determining step size parameter μ_s [202], [175], [209]. A large step size parameter makes the adaption fast, while a small value is likely to make the residual error between the true and the reconstructed forces close to the minimum. An implementation of a variable step size parameter, as proposed e.g. in [210] or [211], could offer potential to optimise the prediction accuracy and the speed of the adaptive process at the same time. Alternatively, the step size parameter could also be adjusted according to the evolution of the E-RMPE. For example, for each individual step size parameter a proportionality factor defined in terms of the upper stability bounds (Eq. (4.35)) could be introduced in the corresponding update recursions (Eq. (4.34)) which then could be controlled according to the E-RMPE evolution. At the beginning of the iterative process where the gradient of the E-RMPE is large one may preferably use large values (close to 100 %) for the proportionality factor in order to achieve rough and fast adjustment of the forces. When the E-RMPE converges towards a fixed value, i.e. its gradient tend to zero, the factor is to be minimised in order to allow for slow but more accurate correction of the reconstructed forces and further to reduce the residual E-RMPE.

As it has been discussed, the proposed TDM will only provide reliable force estimates if all excitation positions are known. Unaccounted forces will go into the force prediction as (correlated) disturbances (section 4.5). With respect to applications of the generalised TDM to real force identification problems it has been advised to rather account for additional force input locations than leaving possible excitations unconsidered. Ideally, the generalised TDM yield zero force signals at considered locations if in fact no force is acting at this point.

With respect to applications of the novel time domain force identification routine for independent source characterisation, as discussed in chapter 2, it is speculated that the generalised TDM could provide a significant contribution towards obtaining simultaneous blocked force time signatures of arbitrary length from measurements carried out in-situ. In the

following chapter, the use of the generalised TDM will be demonstrated in the context of independent characterisation of transient sound sources in electrical steering systems. It is believed that both the generalisation of the TDM and its application in independent source characterisation is original.

Chapter 5

Characterisation of structure-borne sound sources in electrical steering systems

5.1. Introduction

During driving on rough roads, rattle noise may emanate from (electric power) rack-and-pinion steering gears as a result of reverse feedback from the road. As elaborated in chapter 3, excitations provided by the road surface (EBR), fed into the steering system via both tie rods, force adjacent components inside the steering gear to temporarily separate from each other followed by abrupt equalising movements of these assemblies which ultimately result in transient (impact) excitation at the internal source regions. The conceptual source-path-receiver model, developed in section 3.4 has been found to disclose the theoretical locations and the associated mechanisms of all possible transient sound sources inside the steering gear. This information forms the basis for subsequent measurement steps required to experimentally quantify the strength of each individual source. In detail, the measurement approach applied in this study is based on a time domain equivalent of the in-situ blocked force method (see section 2.3.4); thus facilitating independent source characterisation on the steering gear whilst connected to an arbitrary receiver structure, e.g. a vehicle body or a test bench. One key factor of the introduced measurement approach is to solve the inherent inverse problem in a reliable manner in time domain which can be achieved by employing the generalised time domain inversion routine derived in section 4.6. Another important factor to achieve reliable characterisation of the transient structure-borne sound sources inside the steering gear is the generation of realistic rattle excitation. As a test bench evaluation method for rattle noise has already been established in industrial practice the existing rattle test bench may be used for this purpose.

In a nutshell, all necessary steps to theoretically conduct sufficient characterisation of the rattle sources located inside electrical steering systems have been achieved. Therefore, this chapter is intended for demonstrating how the different steps are to be combined in order to conduct identification and quantification of the transient structure-borne sound sources within electrical steering systems. It is noted that this chapter rather constitutes a feasibility study of the developed methodology than a profound analysis of rattle phenomena.

Starting with a brief introduction of the established test bench approach, section 5.2 aims to discuss some assets and drawbacks of the state-of-the-art approaches used in industrial practice to evaluate rattle phenomena within electrical steering systems. Section 5.3 highlights the additional measurement stage involved in the proposed time domain characterisation

method compared with the conventional rattle evaluation approach in which the passive structure of the steering system and the test bench is characterised by impulse response functions. Furthermore, some existing as well as a novel data evaluation criterion is presented that may be useful to evaluate the quality of the additional measurements. Based on numerical and experimental examples, the applicability of the derived methodology is then demonstrated in section 5.4 for source characterisation in electrical steering systems being subject to artificial impact excitation of the internal source regions. In order to achieve realistic rattle excitation of the internal transient sources the steering gear has to be operated on the rattle test bench. With respect to independent source characterisation using this test bench approach comes along with some significant limitations. Section 5.5 aims to discuss these limitations and to derive different strategies to overcome these hurdles. Being able to account for the difficulties introduced by the test bench approach it will be demonstrated how the derived time domain characterisation method can be used to quantify transient structure-borne sound sources within electrical steering systems provoked by realistic EBR excitation using the rattle test bench. A summary and some concluding remarks are provided in section 5.6.

5.2. The test bench measurement approach

In order to determine the internal dynamic forces responsible for the origination of rattle noise within electrical steering systems external dynamic excitation applied to the tie rods of the steering gear is required. This can be achieved in two ways: (i) Measurements are carried out on the steering system whilst mounted in a vehicle and realistic operation conditions are achieved by driving on roads with rough surfaces. (ii) Measurements are conducted under laboratory conditions and oscillating loads are achieved by operating the steering system on specially designed test benches that are able to simulate the reverse force feedback to the rack that would act under normal operation conditions when driving on rough roads. Assets and drawbacks can be found for both approaches, as summarised in Table 5.1.

However, in order to minimize uncertainty in the prevailing excitation and measurement conditions, test bench measurements have generally been accepted to be more appropriate for evaluation of steering induced rattle noise than vehicle measurements [3],[212]. In the following, the standard test bench used in industrial practice for evaluation of rattle noise in electric powered steering systems is briefly introduced.

Table 5.1. Assets and drawbacks of (i) vehicle and (ii) test bench measurements to provoke rattling inside (electric power) rack-and-pinion steering gears.

	ADVANTAGES	DISADVANTAGES
(i) VEHICLE MEASUREMENTS	• real excitation conditions • real mounting conditions • axle kinematics fully regarded • high range of excitations possible • subjective rating while measuring is possible	• repeatability of excitation is not given (e.g. operational profile, steering angle, ...) • unsteady boundary conditions (e.g. temperature, ...) • difficult access to steering system • unknown influences on internal mechanisms • limited vehicle availability • restictions for mechanical modifications due to possible impacts on the driving dynamics
(ii) TEST BENCH MEAS.	• steady boundary conditions (e.g. temperature, steering angle, mounting conditions, ...) • good accessibility to points on the steering system • high range for mechanical modification • repeatable excitation and measurement conditions	• unreal mounting and driving conditions • influence of test bench on internal source mechanisms • axle kinematics cannot completely regarded • limited test bench availabilty

5.2.1. The test bench

As a test bench evaluation method for rattle noise has already been established at ZFLS, the standard rattling test bench can also be used for the purpose of this project. The fundamental principle and the basic components of the test bench are illustrated in Figure 5.1.

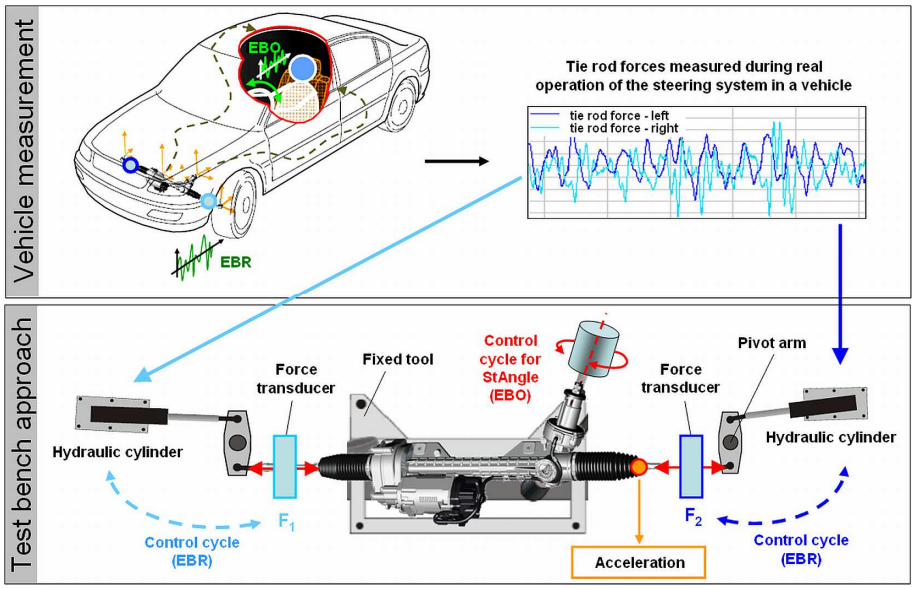

Figure 5.1. Functional principle and basic components of the standard test bench for evaluations of rattle noise originated inside steering gears due to external excitation provided by the roadway surface (EBR).

Since the axle kinematics highly influences the internal source mechanisms, it has been found that the required external excitation, normally provided by the road surface (EBR) whilst driving on poorly conditioned pavement, can be best achieved by simulating dynamic tie rod forces by means of oscillating loads provided by controlled hydraulic cylinders. Generally, the

tie rod forces can either be designed numerically or pre-measured tie rod forces obtained from vehicle measurements can be fed into the hydraulic cylinders. The latter method is preferred in this study since tie rod forces recorded under normal driving and mounting conditions of the steering system in a vehicle are believed to best approximate realistic conditions for the test bench excitation. In this way, influences of the axle kinematics on the tie rod forces are also included in the simulated test bench excitations.

A pivot arm connects each hydraulic cylinder with the respective tie rod of the steering gear so as to contain additional loading of the steering rack introduced by the heavy-weight hydraulic cylinders. It is noted that the pivot arms prohibit dynamic motion of the tie rods in vertical direction so that the present test bench does not allow simulation of landing gear shock strut compression, for instance.

In order to counterbalance possible feedback and associated influences of the test bench on the dynamics of the steering system the provided tie rod excitations are controlled. At each time, force transducers located on both tie rods measure the instantaneous excitation forces applied to the steering gear. An electronic control unit (ECU) calculates the difference between the actual test bench forces with the excitation forces previously measured during the vehicle tests in order to adjust the hydraulic powered forces according to the set values.

Additionally, an actuator can be connected to the steering pinion. The actuator is controlled by the ECU and allows for the adjustment of the steering angle and the steering velocity. In different set-ups the actuator can also be used to achieve excitation provided by the operator so as to investigate transient ‘clunk noise’ as discussed in section 3.3. However, with regard to rattle investigations the actuator attached to the steering pinion is solely required to ensure constant steering angle throughout the entire rattle test cycle and to simulate inertia from the steering wheel.

To evaluate rattle noise caused by the external tie rod excitation conventional accelerometers are placed at certain locations on the housing of the steering gear. The measured vibration responses are then used in subsequent analysis steps to identify transient events included in the acceleration time signals which are likely to result from the internal rattle sources, as briefly discussed in the following.

5.2.2. State-of-the-art analysis

The dynamic excitations applied externally to both tie rods induce rattling inside the steering gear. As a result of the external excitation a number of the internal sources are activated causing impact excitations inside the steering gear which ultimately contribute energy to the overall vibration field observable on the housing of the steering gear. Hence, in industrial practice, the conventional approach to evaluate rattle noise in (electrical power) steering gears is similar to the classical approach to machine condition monitoring where information about the embedded possible active components is extracted from structural responses measured on the machine housing by employing signal processing techniques (see for example [3],[212] or [14]). Using the previously discussed test bench set-up additional information can be employed to extract transient events from the measured structural acceleration responses which are likely to be linked to the internal active rattle sources. For example, the observance of the tie rod forces fed into the steering system to excite the internal rattle sources has been found to be useful as a feature to detect transient events in the structural response data. For this reason the state-of-the-art rattle evaluation approach incorporates vibration accelerations measured at discrete spatial locations on the housing of the steering gear as well as the dynamic forces applied externally to both tie rods measured directly with force transducers implemented in the standard rattle test bench to control the EBR excitation (see Figure 5.1). By means of example, Figure 5.2 illustrates how the additional information is employed to identify transient peaks in one recorded acceleration signal. The operational measurement was obtained on the standard rattle test bench by simulating dynamic forces at both tie rods provoked by reverse road feedback when driving straight ahead on cobblestone pavement with a speed of about 15 km/h.

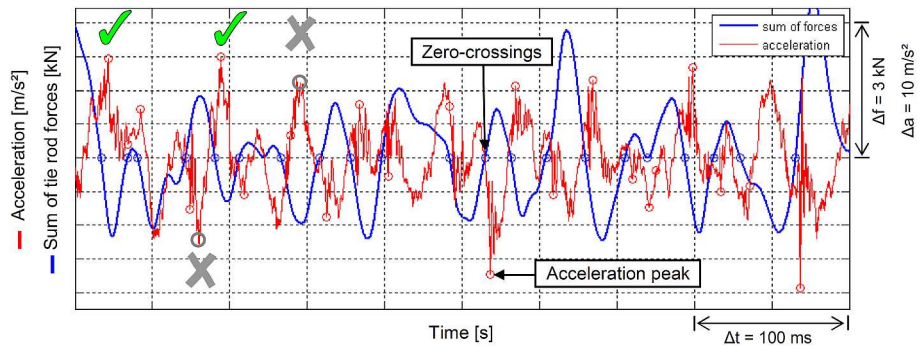

Figure 5.2. Information employed to detect transient events in measured acceleration time histories to evaluate rattle noise in electric power steering systems: — acceleration measured on steering gear housing; — sum of tie rod forces provided by the test bench.

As can be seen, the acceleration time history (red curve) comprises a number of impulsive events. However, without any additional information it is hardly possible to evaluate whether or not a specific transient event is caused by an internal rattle source or not. To detect times at which rattle excitation inside the steering gear is likely to occur the sum of the right and left tie rod force is calculated at each time and plotted over time (blue curve). The physical reasoning for this approach is based on the consideration that possible clearance between adjacent components inside the steering gear becomes maximal at times where the external tie rod forces, that usually cause considerable pre-loading of assemblies inside the steering gear, cancel each other. Hence, the zero-crossings of the sum of the tie rod forces, depicted by blue circles in Figure 5.2, indicate times at which the internal transient source regions are most likely to originate rattle noise. Due to the internal transient excitation one can also expect corresponding transient events in the observed response signal, as indicated by the red circles in Figure 5.2. Note that the transient events in the measured responses may appear shortly after the tie rod forces cancel each other (zero-crossings) which is rooted in internal stiffness and inertia always present in practice. However, based on the knowledge of the zero-crossings in the tie rod net force, different evaluation algorithms have been developed that, aim (i) to detect transient events in the measured responses which are possibly linked to the internal rattle excitation and (ii) to extract the transient peaks in the measured responses and apply some form of signal processing to them so as to achieve objective measures to evaluate the rattle phenomena.

Although this evaluation method has established as a state-of-the-art approach and has sufficiently been employed to quantify the performance of steering systems being subject to rattle excitation its basic principle features some essential limitations.

One major shortcoming is that the approach does not disclose which source actually contributes at a specific time to the observed response position. This distinction is required in order to rank-order different internal source mechanisms so as to allow designers and engineers to effectively address the problem of rattle noise by design. Note that current approaches to locate the most dominant transient sound sources inside the steering gear are based on time delay analysis of transient events recorded in parallel at different response positions. However, the effort to perform such analysis is very high and reasonably results can only be achieved in cases where solely the rough location of a single source is of interest, e.g. to distinguish whether the most dominant rattle source is located in the ball nut assembly

(BNA) or within the pinion-yoke domain (PY) (cf. Figure 3.10).

Another drawback of the conventional rattle evaluation method results from the fact that only events in the measured responses related to the external EBR excitation are considered while even dominant contributions from other transient sources which cannot be linked to the zero-crossings in the sum of the tie rod forces may remain unconsidered. By means of example, two dominant transients that are related to the sum force zero-crossings (indicated by green ticks) are detected as rattle phenomena by the conventional approach in Figure 5.2 while other transients with similar impact on the measured response signal (marked by grey crosses) are not detected and therefore are not included in subsequent rattle evaluation steps. The reasons for the origination of such events cannot be investigated.

Moreover, it is stressed that accelerations measured on the housing of the steering gear are also influenced by the characteristics of the structure to which the steering system is connected. With respect to test bench measurements the entire structure of the test bench may influence the vibration field observed at discrete points on the steering gear while, when conducting equivalent measurements in a vehicle, the vehicle body may essentially influence the vibration field. Thus, hypothetically, operating a steering system under the same conditions when connected to the rattling test bench will produce different vibration signals than the ones provoked whilst operating the steering system in a real vehicle. However, time dependent blocked forces as obtainable with the proposed time domain inversion routine will be the same in both cases. It is speculated that this independence from the downstream structure, i.e. the complete structure away from the internal source regions including additional structures like a test bench or a vehicle body, will reduce the uncertainty in evaluating rattle noise. It is further believed that the proposed time domain in-situ blocked force approach allows for fair comparison between test bench and vehicle measurements which is essential if one aims to find a correlation between the predicted internal source forces and the sound perceived by passengers inside the vehicle. The latter consideration is an important aspect with respect to using the achieved blocked force time signatures for future applications in virtual acoustic prototypes (see section 1.2), (time domain) TPA or to further study the obtained rattling force signatures from a perceptual point of view.

5.2.3. Operation and testing conditions

Operational measurements are to be carried out while the internal transient sources are active, i.e. the steering system is excited by EBR yielding the operational accelerations. It has been

found that the transient fraction of the measured accelerations which is related to the internal sources is affected by the steering angle. In general, large steering angles increase the effects of rattle phenomena in steering systems. Furthermore, it has been found that the tie rod angles with respect to the axis of the steering rack affect the generation of rattling. Other important influencing factors are (i) the temperature or rather the temperature difference between different parts of the steering system that may become considerable if the steering system is mounted in a vehicle close to the exhaust manifold, (ii) production tolerances taking effects on the internal clearances or, most important, (iii) the (external) excitation forces governed by the actual driving conditions (vehicle speed, loading etc.) and the conditions of the roadway surface. Note that these findings are consistent to the industrial practice and the general consensus provided in the specialist literature concerning sound generation in rack-and-pinion steering gears (see for example [14], [3], [212] or [13]).

In consideration of the multitude of factors influencing the generation of rattle noise inside electrical steering systems a ‘standard rattle test profile’ has been defined for all test bench experiments within the scope of this project. The used rattle profile is taken from vehicle measurements when driving straight ahead with a speed of 15 km/h over rough cobblestone pavement yielding excitation frequencies below 40 Hz (see also Figure 5.2). In order to achieve different levels of tie rod excitation the amplitudes of the dynamic forces applied to the steering rack can be adjusted on the test bench to take values between ± 0.5 and ± 5 kN. To ensure stable test conditions throughout the entire rattle test cycle an actuator connected to the pinion of the steering gear is used to control the actual steering angle in such a way that it can be assumed constant. The angles between the tie rods and the steering rack as well as all internal clearances are set up according the vehicle specifications although they can be manipulated on purpose in order to enable or disable the internal rattle sources.

5.2.4. Conclusions

It has been discussed that rattle noise within (electric power) rack-and-pinion steering gears can sufficiently be provoked by means of specially designed test benches that simulate the dynamic excitation feedback from the roadway surface (EBR) using pre-measured tie rod forces from actual vehicle tests. Since test bench rattle evaluation approaches have already been established for industrial purpose a standard rattle test bench will be used to excite the internal transient structure-borne sound sources inside electric power steering systems as required within the scope of this study. Nevertheless, it has been found that the conventional

state-of-the-art approaches to evaluate rattle phenomena for industrial purposes lack in generality with respect to gaining characteristic and independent data for the individual internal sources. It is concluded that vibration signals measured on the housing of the steering gear, as used in the conventional approaches, are comprised of a mixture of the excitation from all internal active sources as well as the influence of the resonances of the overall passive structure. For this reason it is expected that sufficient separation of the internal excitation signals themselves would provide more focussed information about the active sources. Furthermore no additional information about the external tie rod excitation would be required so that all internal sources could be quantified no matter whether or not a specific source mechanism can be related to the additional information provided by the standard rattle test bench. For these reasons, it is believed that independent source characterisation based on a time domain equivalent to the in-situ blocked force method by employing the time domain inversion routine derived in the previous chapter could deliver significant insight into the generation of rattle noise within electric steering systems. It is noted that equivalent conclusions are drawn in [176] where the use of the developed time domain in-situ blocked force approach is discussed with respect to possible condition monitoring applications to which the conventional rattle evaluation approach is very similar.

5.3. Obtaining suitable system models

Compared with conventional rattle evaluation approaches used in industrial practice the proposed time domain in-situ blocked force method requires an additional measurement stage in which the passive structure of the steering system and any other structure to which it is connected is characterised by impulse response functions obtained from in-situ measurements. The following sections explain how these measurements can be conducted in order to achieve suitable system models for sophisticated multi degree of freedom (MDOF) structures. Furthermore, some criteria are presented that may be useful to evaluate the quality and consistency of the system model.

5.3.1. Measurement of (in-situ) frequency response functions

As discussed in section 2.3.1 different forms of frequency response functions (FRFs) such as compliance, mobility or accelerance exist. The use of a specific type of FRF over another one is problem dependent. In the following accelerances are used to build system models of the physical structures under test. Employing accelerances is favoured since (i) established

system identification techniques allow obtaining FRFs directly from vibration responses measured on the structure by means of conventional accelerometers and (ii) operational acceleration responses can directly be employed in the proposed time domain inversion routine so as to conduct time domain source characterisation in subsequent analysis steps. In this way issues with integration of the measured operational acceleration data to achieve time domain data consistent with the corresponding system description, as would be required if mobility or compliance functions were used in the system model, can be avoided. However, all mentioned approaches could also be employed for any other FRF type by simple transformation into accelerance functions (see also section 2.3.1).

In theory, the accelerance is a complex valued function of frequency defined as the ratio of the Fourier transform of the structural acceleration response divided by the Fourier transform of the causative excitation, as discussed in section 2.3.1. However, in practice accelerances (or accordingly any other FRF type) are computed differently. Instead of using the relationship given in Eq. (2.2) one rather uses FRF estimators that are less sensitive to statistical errors in the employed measurements of the input and the output signal. This is beneficial in order to remove random noise and randomly excited non-linearity (distortion) from the FRF estimates [213]. A standard technique to do so is known as tri-spectrum averaging which can be used to calculate FRFs in several different ways. Usually the $H_1(\omega)$ estimator is used if random noise and distortion is assumed to influence the output signal only while the input can be assumed being unaffected by additional noise (and further the noise in the output is uncorrelated with the input). Assuming the output at response DOF *m* is given by the acceleration time signal $a_m(t)$ and the input at DOF *s* is represented by the known excitation force $f_s(t)$, an least squared error estimate of the accelerance $A_{ms}(\omega)$ (FRF) can be calculated by

$$H_1(\omega) = A_{1,ms}(\omega) = \frac{S_{af}(\omega)}{S_{ff}(\omega)} \tag{5.1}$$

where $S_{af}(\omega)$ denotes an estimate of the cross power spectrum between the input and the output and $S_{ff}(\omega)$ is the auto power spectrum estimate of the input signal. Similar to the H_1 estimator, the assumption that noise and distortion is only included in the input signal whilst the output signal is free from noise results in the H_2 estimator which is defined by

$$H_2(\omega) = A_{2,ms}(\omega) = \frac{S_{aa}(\omega)}{S_{af}(\omega)} \tag{5.2}$$

where $S_{aa}(\omega)$ is the auto power spectrum estimate of the output signal.

In a noise free scenario both formulations (Eq. (5.1) and (5.2)) provide the same result. However in a noisy environment they may yield essential different results. It can be shown (see e.g. [214],[215]) that the H_1 estimator is unbiased with respect to the presence of output noise yet it will underestimate the magnitude of the true FRF, i.e. $|H_1(\omega)| < |H(\omega)|$, if additive disturbances are included in the input signal. Instead the H_2 estimator is unbiased with respect to the presence of noise in the input while it tends to overestimate the true FRF, i.e. $|H_2(\omega)| > |H(\omega)|$, if errors are added to the output signal. Generally, the decision which estimator is to be preferred in practice depends on the amount of noise included in the measurements. If one of the signals (input or output) contains markedly less noise than the other one, the function which uses the better auto power spectrum should be used, i.e. $H_1(\omega)$ for low-noise input and $H_2(\omega)$ for low-noise output. At all events, the actual FRF is between $H_1(\omega)$ and $H_2(\omega)$. Although not discussed here, it is noted that other estimators exist that consider both noise in the input and the output (see e.g. [216]).

With respect to estimating accelerance functions within the scope of this study the H_1 estimator is invariably used since all measurements of the structural dynamics will be conducted by means of (roving) hammer impact tests so that the input force can be assumed to be free of considerable measurement noise. Impact testing is further preferred due to the complex physical structure of the steering system in combination with the relative large number of source and response DOFs prohibiting convenient and possibly non-reactive use of shakers to artificially excite the structure in the required DOFs. In all conducted FRF measurements the structures under test will be equipped with accelerometers positioned at all considered response locations in parallel while the steering system is excited with an impact hammer at a single input DOF at a time. In this way single input multiple output (SIMO) impact testing can be performed enabling measurement of multiple FRFs at the same time while using the single fixed input force as a reference. To achieve the previously discussed H_1 estimates of the accelerance functions the structure is impacted 3 times at each excitation location allowing the cross power spectrum and auto power spectrum to be estimated by averaging over the 3 corresponding Fourier spectra for the input force and the acceleration response, respectively. Note that adequate settings for the pre-trigger delay and the sampling window are used. It is assumed that in all impact tests the measured response signals decay

sufficiently to zero before the end of the sampling window, so that no exponential windowing is required to reduce leakage in the spectrum of the measured responses. Also, no special windowing for the input force will be used to remove possible noise from the measured impulse (excitation) signal.

In order to evaluate the quality of the measurement used to calculate an estimate for each accelerance the coherence function is used. The coherence function is a measure of the degree of linearity between two signals (e.g. the input force $f_s(t)$ and the acceleration response $a_m(t)$) versus frequency ω and is related to the respective cross power spectrum and auto power spectrum as

$$\gamma_{af}^2(\omega) = \frac{\left|S_{af}(\omega)\right|^2}{S_{aa}(\omega) \cdot S_{ff}(\omega)} = \frac{H_1(\omega)}{H_2(\omega)}. \tag{5.3}$$

The coherence function can take values between $0 \le \gamma_{af}^2(\omega) \le 1$, i.e. $\gamma_{af}^2(\omega)$ is unity if $f_s(t)$ and $a_m(t)$ are linearly related, $\gamma_{af}^2(\omega)$ is zero if both signals are uncorrelated or $\gamma_{af}^2(\omega)$ is greater than zero but less than one if the signals are partially linearly related. Thus, large coherence values (close to one) signify good measurements in which high dependency between the respective in- and outputs exist. Possible departures from linear relationship between the input $f_s(t)$ and the output $a_m(t)$ can be caused (i) by (uncorrelated) noise included in either of the two signals, (ii) by non-linearity included in the transfer path between the input location (*s*) and the output location (*m*) or (iii) if the output signal $a_m(t)$ does not only result from the considered input force $f_s(t)$ but also depends on other (unconsidered) excitation [215].

It is emphasised that the coherence function provides an important tool with respect to accelerance measurements carried out in the following since the complex physical structure of the steering system can comprise internal clearance in certain transfer paths which may result in non-linearity that can be identified by examining the corresponding coherence function. Thus, if measurements for a specific transfer path show poor coherence over wide frequency ranges they will be rejected and the measurements are to be repeated. If the coherence cannot significantly be improved in subsequent measurement attempts the error-prone transfer path is rejected completely and instead a more suitable transfer path is sought after by iteratively changing the position of the accelerometer until satisfying coherence for the alternative transfer path can be achieved. If so an estimate of the respective accelerance function is calculated according to Eq. (5.1) and the previous descriptions. The obtained accelerance

function is then considered to sufficiently describe the dynamic properties of the structure under test in the respective transfer path. In this way, it is assumed that satisfactory accelerance functions can be measured between all considered input DOFs and the selectable output DOFs.

Further it is noted that within this study the measured accelerance functions are to be used for conducting independent characterisation of the structure-borne sound sources inside electric power steering systems. Thus additional constraints have to be considered when conducting measurements to obtain the structural passive properties, as discussed in section 2.3.4. To recapitulate, all measurements have to be carried out in-situ, i.e. whilst the steering system is connected to a receiver structure; the latter can be represented by a standard rattle test bench or any other structure supporting the steering gear in the following experiments. Furthermore, all locations at which operational acceleration responses are measured, which in the time domain inversion routine are to be propagate back towards the initial excitations, need to be located outside the assumed source regions. In practice, this is achieved by selecting corresponding response positions only on the receiver structure. To identify the theoretical source regions inside the steering gear the conceptual source-paths-receiver model from chapter 3 is employed. Accelerance functions then have to be measured in-situ between all expected sources and the selected response positions according to the aforementioned impact testing approach. However, since the boundaries of the internal source regions are not directly accessible for impact excitation the principle of vibro-acoustic reciprocity [43] is employed which allows excitation and response locations to be reversed without altering the dynamic properties of the structure in between. In this way, the more difficult task of sufficiently exciting the structure can be made at the receiver locations, which can be arbitrarily selected at accessible points, and the simpler task of response measurement is carried out at the internal source interfaces, which can be conducted with embedded accelerometers.

5.3.2. Data evaluation criteria based on reciprocity principle

When dealing with sophisticated multi-point excited structures such as electric power steering systems, for instance, several FRFs describing the passive structural properties in different transfer paths are to be combined in order to build adequate system models of the entire structure. Small errors included in the different FRF measurements in this way can sum up and may result in insufficient system models. In the previous section it has been discussed

how (in-situ) FRFs (e.g. accelerances) can sufficiently be measured. However, despite of all diligence in experimentally determining each single FRF systematic errors are always included in the measurements. In essence, systematic errors can occur as global and local errors.

Global errors affect all measured FRFs in similar degree and may result, for example, from faulty sensor calibration or insufficient suspension of the structure under test [217]. As a consequence of this, system descriptions on the basis of measured FRFs being subject to global systematic errors are biased although the entire set of FRFs is consistent in itself.

Instead, local errors affect the FRF measurement solely in a specific DOF, thus resulting in an inconsistent set of measured FRFs. Local errors may, for example, result from time varying test conditions, inaccurate FRF measurement in a certain DOF (e.g. due to mismatch of the actual excitation direction and the theoretical exact one, insufficient signal-to-noise ratio, non-linear effects due to overexciting the physical structure etc.) or mass effects due to roving instrumentation.

System models built up of inconsistent or physically wrong FRF measurements will inevitably yield erroneous results when used for predicting sound and vibration. A major concern to achieve accurate source characterisation therefore is to identify possible errors and inconsistencies in the experimental FRF data before conducting source characterisation. A number of methods to evaluate the consistency of particular large FRF matrices have already been established. Some widely used approaches are based on invoking the reciprocity principle [43] for structural FRFs. Since interchanging the excitation and the response position theoretically does not change the transfer paths of the system in between these points, one can use the reciprocity postulation to compare two FRF measurements obtainable for each transfer path, i.e. the direct FRF $H_{ms}(\omega)$ when excited at DOF s with response measurement at DOF m and the reciprocal FRF $H_{sm}(\omega)$ when excited at DOF m with response measurement at DOF s. If both FRFs correlate well with each other the underlying measurements can be considered to be of high quality.

In order to make such a comparison convenient for even large FRF matrices Brechlin [217] and Allemang [218] suggest using techniques known as the Frequency Response Assurance Criterion (FRAC) and the Phase Assurance Criterion (PAC), respectively. The FRAC criterion is a measure of correlation between the magnitude responses of any two FRFs to be compared whereas the PAC criterion is a measure of correlation between the according phase responses.

Both procedures allow for comparison over the full or partial frequency range of the FRFs as long as the same discrete frequencies are used in the comparison. By definition, each of the evaluation criteria, i.e. FRAC and PAC, yields a frequency independent single value to measure the correlation between the compared FRFs. It is convenient to plot these single value correlation measures as coloured matrices which are arranged according to the degree of freedoms considered in the system model (see e.g. Figure 5.4). In this way, quick identification of inconsistent FRF data comprised in the system model and convenient evaluation of the overall measurement quality can be achieved. Note that more information about FRAC and PAC as well as the mathematical foundations are provided in Appendix A.3.

However, employing FRAC and PAC procedures to evaluate the consistency and quality of complex FRF matrices is not always sufficient. As major drawbacks one may name the restriction to transfer FRFs only while no evaluation of driving point FRFs is possible as well as the fact that both correlation measures only indicate erroneous FRF pairs while they are not able to reveal which FRF measurement, e.g. direct or reciprocal FRF, actually contains more reliable information or rather if any of the two measurements contain physical meaningful information at all. It is speculated that alternative evaluation criteria providing this clarification could potentially prevent carrying out erroneous or unnecessary measurements which in particular for sophisticated multi-point excited structures may consume additional time and costs. On all accounts it is believed that alternative evaluation criteria providing information about the physical correctness of particularly large FRF matrices while requiring similar measurement effort could at least present valuable completions and may help to reduce uncertainty of established data quality tests. Therefore, two different criteria will be introduced in the following that in combination with each other have been found to be very helpful means when evaluating the quality of particular large FRF matrices.

5.3.3. Data evaluation criteria based on conductance of the mobility matrix

As discussed in section 2.3.1, the dynamic properties of any multi-point excited mechanical structure can be characterised by its complex FRF matrix. Note that accelerance, mobility or receptance functions could be used to build this matrix. For the following discussion it is assumed that the system description is given in terms of mobility matrices. However, it is stressed that any other FRF matrix can be converted into a mobility matrix (see section 2.3.1).

Therefore, all presented approaches are considered to be generally applicable for any type of FRF measurement.

The complex mobility matrix, as introduced in Eq. (2.6), can also be written in terms of its real and imaginary parts as

$$\mathbf{Y}(\omega) = \Re e\{\mathbf{Y}(\omega)\} + j \cdot \Im m\{\mathbf{Y}(\omega)\} = \mathbf{G}(\omega) + j \cdot \mathbf{B}(\omega) \tag{5.4}$$

where the real part $\mathbf{G}(\omega)$ is called the conductance and the imaginary part $\mathbf{B}(\omega)$ susceptance. Assuming a square matrix, ideally the mobility matrix has to be symmetric about the main diagonal because of the principle of reciprocity. As a consequence of this its real part, i.e. the conductance matrix $\mathbf{G}(\omega)$, also needs to be symmetric. Another important property of the real part of the mobility matrix is that it is either positive definite or positive semi-definite. This condition results from the passivity since the total vibrational power transmitted by external forces must always be positive [219]. Furthermore the condition requires that the diagonal elements of the mobility matrix, which are related to the driving-point mobility functions, are constrained to be positive real or zero. On the other hand, transfer mobility functions, i.e. off-diagonal elements of the mobility matrix, are not bound to be positive real.

The mentioned properties of the real part (conductance) of the mobility matrix can be used as a check on measured mobility data. Concerning single point mobilities first, a widely used check for driving-point mobilities is that their real part should always be positive since the flow of energy cannot go from the structure into direction of the exciter. Thus, a negative real part indicates errors in the measurement of the mobility function. In order to evaluate the measurement quality based on a frequency independent single value, Hudelmaier [220] introduces the so-called 'conductance value'. The conductance value incorporates a logical vector $\mathbf{l} = [l(\omega_{\min}), \ldots, l(\omega_{\max})]$ which at each considered frequency grid point ($\omega_{\min} \le \omega_c \le \omega_{\max}$) determines a logical number $l(\omega_c) = \{-1, 0, 1\}$, according to the function

$$l(\omega_c) = \operatorname{sgn}\left(\Re e\{Y_{ii}(\omega_c)\}\right) = \begin{cases} -1 & \text{for } \Re e\{Y_{ii}(\omega_c)\} < 0 \\ 0 & \text{for } \Re e\{Y_{ii}(\omega_c)\} = 0 \\ +1 & \text{for } \Re e\{Y_{ii}(\omega_c)\} > 0 \end{cases} \tag{5.5}$$

where 'sgn(·)' denotes the signum function extracting the sign of the expression in the brackets and $\Re e\{Y_{ii}(\omega_c)\}$ denotes the real part of the examined driving-point mobility at DOF

i. The corresponding conductance value $CV(Y_{ii})$ is then obtained as the normalised sum over all positive numbers of the logical vector $\mathbf{l}$ for the chosen frequency range

$$CV(Y_{ii}) = \frac{\sum_{\omega_c=\omega_{\min}}^{\omega_{\max}} \mathbf{l}(Y_{ii}(\omega_c))\big|_{l>0}}{N_c} \tag{5.6}$$

where N_c is the number of the considered frequency grid points. Due to the normalisation only values of $0 \le CV(Y_{ii}) \le 1$ are possible. Conductance values close to unity indicate physical correct point mobility measurements, i.e. the real part of the point mobility is positive all over the considered frequency range. Instead, conductance values close to zero indicate erroneous measurements which may result from neglecting boundary conditions during measuring the driving point mobility or from instrumentation phase errors [220].

Unfortunately, the conductance value cannot be applied for the evaluation of transfer mobilities because both positive and negative real parts are permissible. However, one can examine the eigenvalues for the real part of the mobility matrix instead to detect possible measurement errors in some of the matrix entries including the transfer mobilities. The positive definite property of the real part of the mobility matrix holds for any structure and any number of points. Thus, to locate measurement errors in an arbitrary ($n \times n$) mobility matrix the eigenvalues of all 2x2 sub-matrices formed by each pair of points have to be calculated and analysed. By definition, the eigenvalues of a positive definite matrix need to be positive also so that a negative eigenvalue for any of the calculated sub-matrices indicate measurement errors in the respective transfer mobility. Although this strategy to locate erroneous transfer mobility measurements has been mentioned earlier by Moorhouse and Gibbs in [221] no procedure has been developed that allows convenient application for large mobility matrices. One reason for this possibly results from the difficulty to clearly illustrate the analysis results for large mobility matrices since evaluation of two eigenvalues per sub-matrix and frequency grid point is necessary. However, a solution to this problem has been achieved within this research project and is presented in the following.

In essence, three basic steps are to be carried out in order to perform this analysis for arbitrary (square) mobility matrices. These steps are illustrated Figure 5.3 and are discussed in more detail in the following.

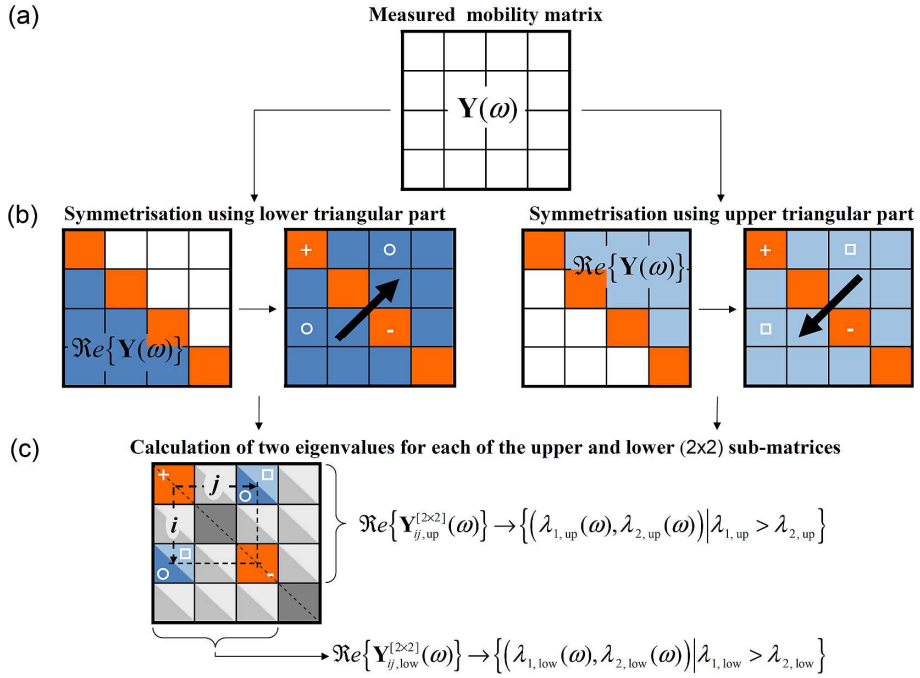

Figure 5.3. Methodology involved in the calculation of eigenvalues for the proposes Eigenvalue Measure (EM): (a) Measured square mobility matrix; (b) symmetrisation using lower and upper triangular real part of the matrix and (c) partitioning of upper and lower symmetric matrices into (2x2) sub-matrices which are used to calculate two eigenvalues per sub-matrix.

In an initial step (a) any measured (square) FRF matrix has to be converted into a mobility matrix. Since all passive structural dynamics within this study are measured in terms of accelerances the corresponding accelerance matrix, at each frequency, is to be multiplied by the complex scalar $(1/j\omega)$. The result is the $(n\times n)$ mobility matrix $\mathbf{Y}(\omega)$ as illustrated in Figure 5.3 – (a). However, in the following only the real part of the mobility matrix $\Re e\{\mathbf{Y}(\omega)\}$ is used for further analysis. Note that $\Re e\{\mathbf{Y}(\omega)\}$ can also be termed the 'conductance matrix'.

In order to achieve the non-negative definite property of the real part of the mobility matrix a symmetrisation step (b) is required. This can be done in different ways, as illustrated in Figure 5.3 – (b). If all elements of the square mobility matrix are measured symmetry of its real part can be achieved by either (i) mirroring the lower triangular part of the conductance matrix on the main diagonal or (ii) mirroring the upper triangular part of the conductance matrix on the main diagonal. If not all entries of the mobility matrix are known, a general restriction to achieve symmetrisation is that all driving point mobilities $Y_{ii}(\omega)$ and at least one transfer mobility per transfer path, i.e. $Y_{ij}(\omega)$ or its reciprocal element $Y_{ji}(\omega)$, need to be known. One

possible downside coming along with this restriction is that measurements of driving point mobilities may not always be practical, especially for in-plane DOFs away from an edge. On the other side, FRAC or PAC analysis generally require measurement of all transfer mobilities so that excitation in the same potentially difficult DOFs is necessary. However, under the assumptions that all elements of the mobility matrix are measured the previously symmetrisation step will yield one symmetric $(n\times n)$ conductance matrix built of the lower part of $\Re e\{\mathbf{Y}(\omega)\}$ (in Figure 5.3 highlighted in dark blue) and one $(n\times n)$ symmetric conductance matrix built of the upper part of $\Re e\{\mathbf{Y}(\omega)\}$ (in Figure 5.3 highlighted in light blue). Both the upper and lower symmetric conductance matrix share the same driving point mobilities along their main diagonals, i.e. $\Re e\{Y_{ii,low}(\omega)\} = \Re e\{Y_{ii,up}(\omega)\}$ for $i = [1, 2, \ldots, n]$, as highlighted in orange in Figure 5.3.

In the following step (c) the lower and upper symmetric $(n\times n)$ conductance matrices are processed independently of each other. First, they are partitioned into sets of (2×2) sub-matrices, as illustrated in Figure 5.3 – (c), before the eigenvalues for each of the sub-matrices are calculated. By way of example this procedure is illustrated for a lower and an upper (2×2) conductance sub-matrix depicted by $\Re e\{Y_{ij,low}^{[2\times 2]}(\omega)\}$ and $\Re e\{Y_{ij,up}^{[2\times 2]}(\omega)\}$, respectively. Note that at each frequency two eigenvalues, $\lambda_1(\omega)$ and $\lambda_2(\omega)$ where $\lambda_1(\omega) > \lambda_2(\omega)$, have to be calculated for each of the sub-matrices. In order to achieve a single frequency independent evaluation criterion for each of the eigenvalues, i.e. $\lambda_n(\omega)$ for $n = [1, 2]$, a logical vector $\mathbf{l}_n = \left[l_n(\omega_{\min}), \ldots, \mathrm{l}_n(\omega_{\max})\right]$ is introduced that, at each considered frequency grid point ($\omega_{\min} \le \omega_c \le \omega_{\max}$), determines the sign of the respective eigenvalue $\lambda_n(\omega_c)$ according to

$$l_n(\omega_c) = \operatorname{sgn}\left(\lambda_n(\omega_c)\right) = \begin{cases} -1 & \text{for } \lambda_n(\omega_c) < 0 \\ 0 & \text{for } \lambda_n(\omega_c) = 0 \\ +1 & \text{for } \lambda_n(\omega_c) > 0 \end{cases} \tag{5.7}$$

where the sub-script '*n*' distinguishes between the maximum ($n = 1$) and the minimum ($n = 2$) eigenvalue. Based on these vectors a frequency independent single number, in the following termed 'Eigenvalue Measure' $EM(\lambda_n)$, can be calculated which is defined as the normalised sum over all negative numbers of the logical vector $\mathbf{l}_n$ for the chosen frequency range

$$EM(\lambda_n) = \frac{\sum_{\omega_c=\omega_{\min}}^{\omega_{\max}} \mathbf{l}_N(\lambda_n(\omega_c))\big|_{l_n<0}}{N_c} \tag{5.8}$$

where N_c is the number of the considered frequency grid points. Due to the normalisation only values of $0 \le EM(\lambda_n) \le 1$ are possible. It is stressed that the EM, by definition (see Eq. (5.8)), counts the (normalised) number of appearances of the negative eigenvalues for which reason it constitutes a measure of the non-physical information included in the examined mobility matrix. Hence, EM values close to zero indicate physical correct measurements while values close to unity signify violation of the postulated positive definite properties of the real part of the mobility matrix. This violation inevitably results from measurement errors to which the minimum eigenvalues $\lambda_2(\omega)$ are particular sensitive. Therefore, sufficient evaluation of transfer mobility measurements in practice can usually be performed by solely calculating the Eigenvalue Measure for the minimum eigenvalues, i.e. $EM(\lambda_2)$.

The frequency independent EM value can be visualised in coloured matrices which are arranged according to the original $(n \times n)$ mobility matrix; thus allowing easy identification of transfer mobility measurements containing unphysical information. To distinguish between EM values calculated from sub-matrices which were obtained from symmetrisation using the lower or the upper triangular real part of the mobility matrix, respectively, the corresponding EM value is plotted below or above the main diagonal of the colour matrix, respectively. By way of example, to evaluate the measurement quality for the transfer mobility function $Y_{31}(\omega)$, denoted by the '○' symbol in Figure 5.3, one (i) needs to use the lower triangular real part of the mobility matrix to obtain the corresponding (lower) (2×2) conductance sub-matrix $\Re e\{\mathbf{Y}^{[2\times2]}_{31,\,\mathrm{low}}(\omega)\}$ where

$$\mathbf{Y}^{[2\times2]}_{31,\,\mathrm{low}}(\omega) = \begin{vmatrix} Y_{11,\,\mathrm{low}}(\omega) & Y_{13,\,\mathrm{low}}(\omega) \\ Y_{31,\,\mathrm{low}}(\omega) & Y_{33,\,\mathrm{low}}(\omega) \end{vmatrix} \tag{5.9}$$

and $Y_{31}(\omega) = Y_{13}(\omega)$ due to the symmetrisation before (ii) calculating the eigenvalues at each frequency for the conductance sub-matrix so as to (iii) determine (at least) the EM value for the minimum eigenvalues according to Eq. ((5.7) and(5.8)). If the respective EM value is to be visualised in the $(n \times n)$ colour matrix its value has to be plotted according to a defined colour map in the 3rd row and the 1st column. Correspondingly, an EM value could also be calculated for the reciprocal transfer function $Y_{13}(\omega)$ assuming upper symmetry for the real part of the mobility matrix and performing the same steps as before. The corresponding elements are denoted by the '□' symbol in Figure 5.3. A comparison of both EM values

should show which of the two transfer function measurements contain more physical meaningful information.

However, the calculation of the EM involves the driving point mobilities which may also contain measurement errors. As discussed earlier in this section, the conductance value $CV(Y_{ii})$ can be used to verify whether or not the point mobilities contain physical correct information. By definition, the conductance value counts the (normalised) number of the frequency grid points at which the real part of the point mobility is positive yielding a CV close to unity if the data is physically correct. Instead an EM close to unity indicates errors in the measurements. In order to achieve consistency between the different criteria the conductance value as defined in the Eqs. (5.5) and (5.6) can be slightly modified in such a way that a CV close to unity indicates erroneous measurements while a CV close to zero indicates physical correct point mobilities. This enables one to use the same colour map for both the CV and the EM so that both criteria can be visualised in the same ($n \times n$) colour matrix. The combination of both criteria, the Conductance Value for the point mobilities and the Eigenvalue Measure for the transfer mobilities, represents a useful means to evaluate the measurement quality for any square mobility matrix. For convenience, the combination of both criteria and their visualisation in form of a colour matrix will be termed 'Conductance Assurance Criteria (CAC)' in the following.

By way of example, the Conductance Assurance Criteria (CAC) are compared to the Frequency Response Assurance Criterion (FRAC) and the Phase Assurance Criterion (PAC) (see also Appendix A.2). As data accelerance measurements conducted in-situ for a steering system whilst mounted on the standard rattle test bench are used. Note that this set-up will be used to characterise the internal rattle sources in section 5.6 where also detailed information about the physical set-up and the considered DOFs is provided (see also Figure 5.7). However, in order to evaluate the ability of the different criteria to locate possible errors in the measured data some elements of the accelerance matrix are modified. The respective elements are denoted by numbers in round brackets in Figure 5.4. In detail, measurement errors are considered that in practice may result from (1) confusion with the sign convention (e.g. an accelerometer measuring vibration with opposite sign or an excitation applied in the opposite direction) which is simulated by inverting the phase for a whole column of the accelerance matrix, and from noise included in either (2) the driving-point FRFs or (3) the transfer FRFs which is simulated by replacing the measured accelerances with synthesised random noise

sequences. The analysis results for the modified accelerance measurements using the different criteria (FRAC, PAC, and CAC) are illustrated in Figure 5.4.

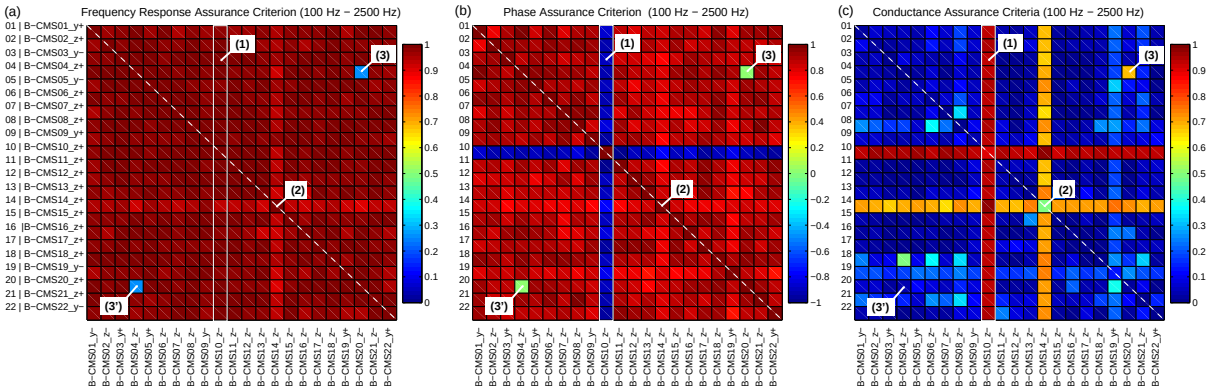

Figure 5.4. Evaluation of accelerance measurements conducted in-situ for a steering system whilst mounted on the standard rattle test bench using (a) the Frequency Response Assurance Criterion, (b) the Phase Assurance Criterion and (c) the Conductance Assurance Criteria. Some elements of the accelerance matrix are modified to simulate (1) phase errors for a whole column as well as (2) random errors in driving-point and (3) the transfer accelerance measurements, respectively.

Despite the simulated errors all criteria, i.e. the FRAC (Figure 5.4 - (a)), the PAC (b) and the CAC (c), indicate generally consistent and physically correct accelerance measurements. Note that in the FRAC and PAC plot warm colours (red, yellow) indicate good agreement and cold colours (green, blue) poor agreement between the compared FRFs while the CAC use the cold colours to indicate physically correct data and the warm colours to indicate errors in the measurements.

Due to employing the principle of reciprocity the FRAC and PAC can only indicate errors for a pair of transfer function measurements but they cannot determine which of the two measurements contain physical more reliable information. This becomes apparent from the small FRAC and PAC values for the matrix elements depicted in Figure 5.4 by (3) and (3'), respectively, where (3) refers to the accelerance function containing the artificial noise sequence and (3') represents its 'reciprocal' element containing a measured accelerance function. Note that the corresponding magnitude and phase responses are plotted in terms of mobilities in Figure 5.5 - (a,c) for the FRF (3') and in Figure 5.5 - (b,d) for FRF (3). However, compared to FRAC or PAC the CAC yield an individual evaluation value for each of the measured FRFs (Figure 5.4 - (c)) so that the physically correct FRF (3') can be detected by a small CAC value (approx.: 4 %; see Figure 5.5 – (g)) and the unphysical FRF (3) is unambiguously indicated by a high CAC value (approx. 72 %; see Figure 5.5– (g)). For better understanding the underlying FRFs as well as the associated eigenvalue spectra and sign

vectors of the real part of the corresponding mobility sub-matrices required to calculate the CAC-Eigenvalue Measure according to Eq. (5.8) are illustrated in Figure 5.5 for the uncorrupted FRF measurement (3') (see (a,c,e,g)) and the simulated noise signal (3) (b,d,f,h). Note that in the diagrams (e) to (h) both the maximum and the minimum eigenvalues of the real part of the according lower (e,g) and upper (f,h) (2×2) mobility sub-matrices are illustrated although the CAC plot in Figure 5.4 only considers the minimum eigenvalues which are more sensitive to errors in the measurements.

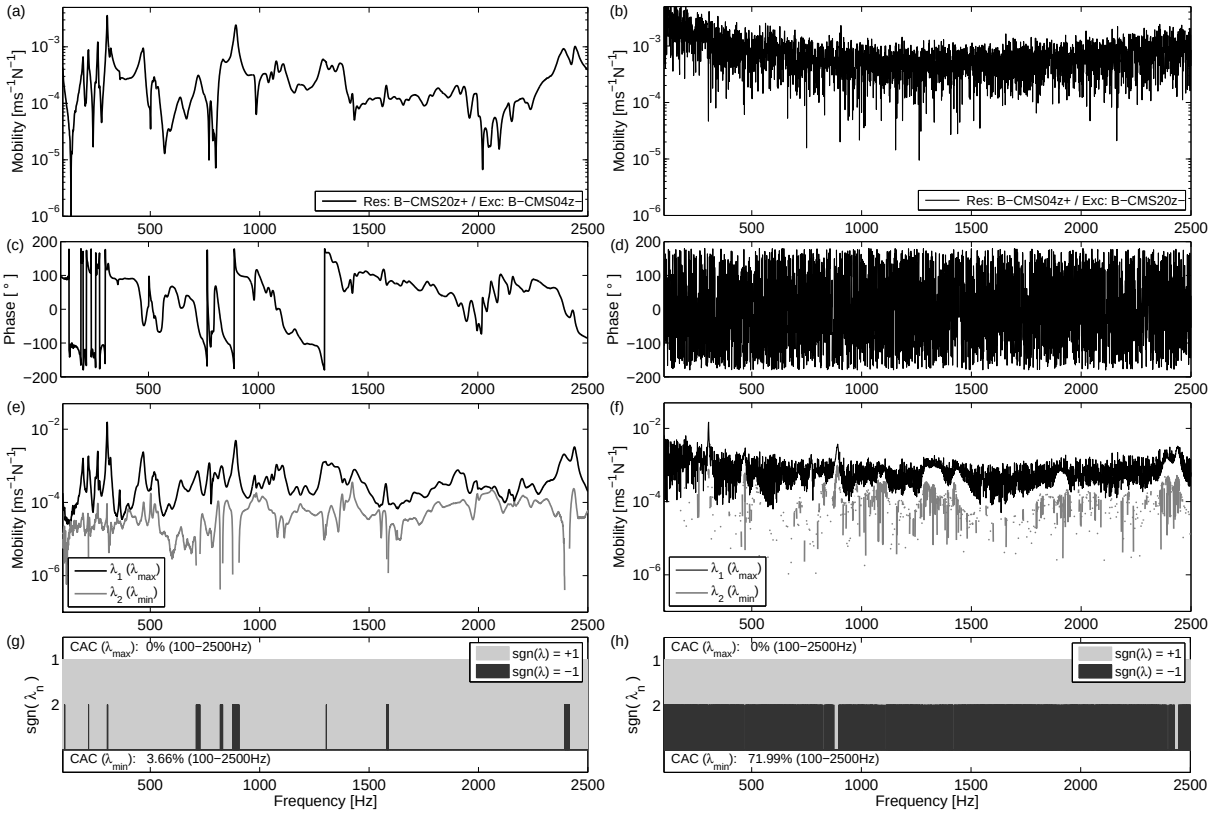

Figure 5.5. Employed data in the CAC analysis: Magnitude and phase response of the obtained mobility functions for the measured (a,c) and the simulated (b,d) FRF and corresponding eigenvalues and sign vectors of the real part of the lower (e,g) and the upper (f,h) (2x2) mobility sub-matrices.

As can be seen from Figure 5.4 - (c), the CAC is also able to detect erroneous FRF measurements due to unphysical phase information (indicated by the white rectangle labelled by (1)). Since in this example the phase is inverted for a whole column of the FRF matrix the conductance of the driving-point mobility is also negative so that all sub-matrices involving this measurement will have negative eigenvalues of the real part of the respective mobility sub-matrices yielding CAC values close to unity for a whole column and row. By comparison the PAC analysis (Figure 5.4 – (b)) also detects the phase errors included in the measurements while this is not possible with the FRAC that only considers the magnitude responses.

According to the given explanations, errors included only in the driving-point mobility, as denoted by (2) in Figure 5.4, also influence the CAC values for a whole column and row. However, it is noted that individual CAC values are calculated for all transfer FRFs so that one is still able to compare the relative measurement quality between FRFs involving the defective driving-point FRF. Further it is noted that the random noise sequence used to simulate the errors in the point mobility can be identified by a conductance value of about 0.5 meaning that the real part of the mobility takes equally positive and negative values due to the random signal. By definition, measurement errors included only in the driving point FRFs cannot be identified employing FRAC or PAC analysis since these methods rely on the reciprocity principle.

In summary, as illustrated in the presented example, the ability to unambiguously detect errors in transfer function measurements as well as in driving-point FRF measurements, particular for large FRF matrices, is a big advantage of the CAC compared to the conventional FRAC or PAC analysis. Although the basic idea of the presented data evaluation approach is not new the procedure to calculate the CAC values as well as their representation in easy-to-read colour matrices is believed to be original.

5.3.4. Impulse response functions from transformation

The time domain inversion routine requires a system model defined in time domain. In essence, impulse response functions (IRFs), $h_{ms}(i)$, between each assumed source region $s=[1,2,\ldots,S]$ and all considered response positions $m=[1,2,\ldots,M]$ are required to describe the passive properties of the true system so as to achieve a system model that can be employed by the iterative force reconstruction routine. As discussed in section 5.3.1, conventional system identification techniques can be used to measure the corresponding FRFs, $H_{ms}(\omega)$, in-situ on the StSys whilst connected to an arbitrary receiver structure. In order to obtain suitable IRFs from the pre-measured FRFs two steps are needed.

First the frequency dependent transfer functions have to be transformed into time domain. This is achieved by employing inverse discrete Fourier transformation to the measured FRFs

$$h_{ms}(i)=\frac{1}{N_{IRF}}\sum_{l=0}^{I-1}H_{ms}(l)\,e^{j(2\pi/N_{IRF})i\cdot l} \tag{5.10}$$

where i indicates discrete-time-dependency of the IRF, N_{IRF} is the finite length of the impulse response function after transformation, l is the integer frequency variable

and $j = \sqrt{-1}$. It is emphasised that care is to be taken during the whole procedure of obtaining the finite impulse responses (FIRs), i.e. proper selection of sampling parameters and time windows already when measuring the FRFs in order to avoid leakage problems in time domain.

The computational effort required to carry out the adaptive algorithm involved in the time domain inversion routine significantly depends on (i) the number S of forces to be identified, (ii) the number M of considered response positions, (iii) the utilised length I of the pre-measured impulse responses and (iv) the length N of the operational responses. Note that (iii) and (iv) are related by the constraint $N \geq 2 \cdot I$. Considering further that for each accounted-for force position a set of $1 \times M$ impulse responses functions has to be implemented in the system model optimising (iii) clearly poses the best potential to achieve reasonable computation times. Therefore, it is advisable to truncate the N_{IRF} - length impulse response functions calculated by Eq. (5.10) to a shorter length *I* before implementing them in the system model of the iterative routine.

However, truncation of the obtained impulse response functions requires care in order to achieve a good compromise between neglecting information of the system description in order to minimise the computation times and considering sufficient information of the system impulse responses so as to gain accurate system models required for accurate force prediction. The general consensus is that the final length *I* of IRFs after truncation should be chosen so that they have sufficiently decayed within the time window [174].

Since background noise is almost uniformly distributed throughout the impulse response the minimum level of a measured impulse response is limited by the noise floor. On the other hand, the energy related to structural vibration roughly decays in an exponential manner so that this energy is concentrated at the beginning of the impulse response. Therefore, vibrational energy is usually considerably bigger than the noise energy at the beginning of the impulse response while noise dominates the measurement toward its end.

By means of example, an impulse response function and the corresponding energy distribution is depicted in Figure 5.6. The impulse response ($h_{23,2}(i)$) is obtained from measurements conducted in-situ on the steering system whilst connected to a front axle carrier (cf. Figure 5.7). Note that this example will be discussed in more detail in section 5.4.1.

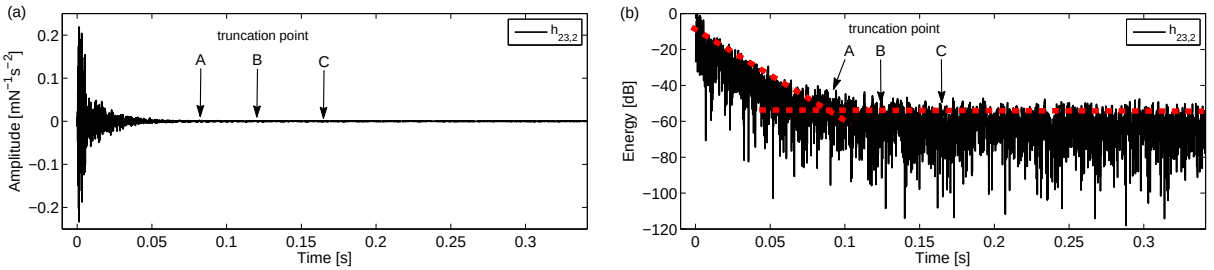

Figure 5.6. Sample impulse response measured on the steering system whilst coupled to a receiver structure with corresponding truncation points (a) and squared impulse response (b) with dashed lines indicating decay slope and noise floor for evaluation of the truncation time.

According to the previously discussion, the optimal truncation point of the impulse response, in theory, is located at the knee (A) where the main decay slope of the squared impulse response intersects the noise floor (indicated by dashed lines). Truncation at (A) enables separating the useful information of the impulse response, which describes the structural dynamics of the structure under test, from the part that only contains noise. However, it is stressed that exact estimation of the knee for structural impulse responses is not always possible since the assumption of exponentially decaying vibration amplitudes only holds as a first approximation. Nevertheless, for all investigated examples the mentioned approach yield sufficient determination of the truncation point. To achieve conservative system models one shall choose the point of truncation at later times where the noise level unambiguously dominates the measurement, as indicated in Figure 5.6 by the point (B), for example. This may negatively effect the computation time required for the iterative force identification process but the inversion routine is able to suppress possible negative influences of the additional noise if overdetermined systems are used and noise in different paths is uncorrelated (see chapter 4).

If force identification for systems with multiple response locations is to be conducted further care is required when truncating the set of pre-measured impulse response functions. By definition the adaptive algorithm in the derived time domain inversion routine relies on a system model built of multiple IRFs which have to be of the same length *I*. For the mentioned reasons the truncation length *I* should be chosen with respect to the slowest decaying IRF. In case of the sample impulse response function depicted in Figure 5.6, which will be implemented in overdetermined system models (cf. section 5.4), following these steps results in shifting the final truncation point (C) even to later times since the slowest IRF involved in the system model has been shown to require about 170 ms to decay sufficiently.

In a nutshell, to obtain suitable impulse response functions that can sufficiently be implemented in a time domain system model to inversely identify forces using the derived adaptive algorithm requires (i) employing inverse Fourier transformation to all measured FRFs yielding corresponding (full-length) FIRs which then (ii) have to be truncated in length. Theoretically, the optimal truncation point (A) is located at the intersection of main decay slope and noise floor. In practice, a conservative truncation point (B) may be defined at later times to account for the insufficient exponential decay of structural impulse responses. If overdetermined system models an overall truncation point (C) has to be defined that need to be chosen according to the slowest decaying impulse response. This procedure will invariably be used in all following examples.

5.3.5. Conclusions

A methodology to obtain suitable system models to perform independent source characterisation with the developed time domain equivalent of in-situ blocked force method has been introduced. It has been discussed that employing accelerance functions instead of the more popular mobility functions in the time domain inverse routine is favoured. In this way difficulties with integrating measured operational acceleration responses can be avoided. With respect to measuring accelerance functions in-situ on the steering system whilst coupled to a test bench or another receiver, impact testing methods have been found to be most suitable since measurement is easy and further allows exciting the structure in DOFs difficult to reach with bigger instrumentation such as shakers, for example. It has been emphasised that measurements should be performed with care in order to achieve good quality data. Observance of the ordinary coherence function while performing the measurements as well as the use of the H1 estimator to suppress noise in the measured accelerance data has been suggested. However, since system models for multi-degree of freedom structures always are made up of several FRFs the according data matrices have to be evaluated with regard to measurement errors, their general consistent appearance or otherwise unphysical information included in the data. Two conventional data evaluation criteria has been discussed that perform analysis based on the reciprocity constraint. The FRAC criterion is a measure of correlation between the magnitude responses of any two FRFs to be compared whereas the PAC criterion is a measure of correlation between the according phase responses. As a major drawback of both methods it has been found that they can only identify a pair of defective FRFs but they lack in clarity which of the two FRFs contain physical less meaningful

information. Two different criteria have been introduced which can provide this information for any element of a square mobility matrix. Both criteria are based on the positive definite property of the real part of the mobility matrix; the latter is sometimes denoted as conductance. The ‘Conductance Value’ (CV) has been found to be a simple check on measured driving-point mobilities while the developed ‘Eigenvalue Measure’ (EM) can be used to evaluate the quality of measured transfer functions. Both criteria, the CV and the EM, are grouped under the term ‘Conductance Assurance Criteria’ (CAC) yielding normalised frequency independent single values between zero and one that facilitates convenient illustration in coloured matrices arranged according to the actual matrices. In this way easy and fast evaluation of all transfer and point FRF measurements is possible. It has been found that CAC can provide more detailed and clear information than FRAC or PAC analysis while requiring only insignificant bigger measurement effort. Furthermore, the CAC has been found able to disclose whether or not FRF measurements contain physical meaningful information for cases in which only one transfer mobility and the according two point mobilities can be measured.

Further it has been discussed how the obtained frequency domain system models have to be processed in order to achieve suitable models for the time domain inverse method. Of major importance in this respect is adequate transformation from the frequency domain into time domain using inverse Fourier transformation and to sufficiently truncate the resulting impulse response functions (IRFs) in order to improve the performance of the time domain inversion routine. In summary, the presented practical approaches to obtain suitable time domain representations for even sophisticated technical structures complete the time domain source characterisation methodology. In the following this methodology will be tested to conduct in-situ source characterisation on electric power steering systems whilst connected to certain passive test rigs.

5.4. Characterisation using artificial excitations

In this section the applicability of the time domain inversion routine is discussed in the context of source characterisation in electrical steering systems using a time domain equivalent to the in-situ blocked force method (see section 2.3.4). The complexity of the force identification problem will be increased subsequently considering cases in which an electrical steering system is assumed to comprise single and multiple parallel acting source mechanisms, respectively. For verification reasons only artificial excitations are used in the

following examples allowing exact knowledge of the applied source forces which will be employed to validate the force reconstruction results provided by the time domain inversion routine. Numerical and experimental vibration tests will be conducted on the sophisticated test structure in order to investigate the influence of noise on the source characterisation accuracy.

5.4.1. Experimental set-up

The applicability of the derived force identification method for complex technical structures is investigated in the following. In particular, an electrical steering system (StSys) mounted on a front axle carrier is considered as test structure. The assembly is depicted in Figure 5.7. Note that due to the physical assembly of the steering system two different coordinate systems are used. The global coordinate system (x, y, z) is depicted in the lower left corner of Figure 5.7 while the local coordinate system (x2, y2, z2) for the pinion-yoke area is depicted in the upper right corner. Further it is noted that the perpendicular axes of the pinion-yoke system are rotated to the global ones so that, for example, measuring the response in z2-directon corresponds to partial measurements in all 3 directions (x, y, z) of the global system.

For the experiment it is assumed that the StSys comprises three unknown internal point-like structure-borne sound sources (S_u) for $u=[1,2,3]$ and two external structure-borne sound sources (S_u) for $u=[4,5]$, each exciting the assembly in one degree of freedom (DOF).

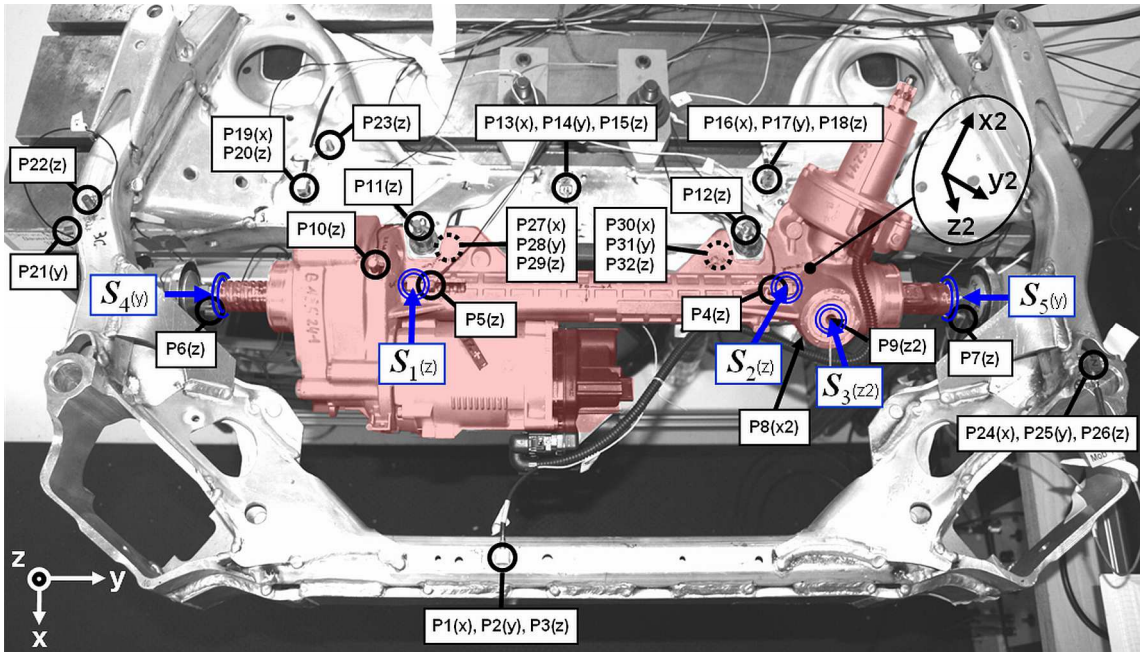

Figure 5.7. Steering system connected to front axle carrier with sources (S_u) and response positions (P_m).

The internal source (S_1(z)), close to the ball screw drive unit, as well as the internal source (S_2(z)), close to the pinion are located directly on the steering rack inside the gear housing. The internal source (S_3(z2)) is located on the lateral area (side) of the yoke. All internal sources are only accessible through cut-outs in the housing. At the source positions (S_4(y)) and (S_5(y)) external excitations can be applied to both ends of the tie rods. Their meaning with respect to rattle excitation in electrical steering systems will be discussed in more detail in section 5.5. The vibration responses are measured in terms of accelerations at multiple DOFs spatially distributed over the coupled structure as indicated by the points (P_m) for $m = [1, 2, \ldots, 32]$.

In order to identify dynamic forces applied to the StSys, the structural dynamic properties between the assumed source locations (S_u) and all response DOFs (P_m) as well as the corresponding operational responses need to be known. Note that all measurements are conducted according to the definitions of the in-situ blocked force method, as discussed in section 2.3.4.

The structural dynamic properties of the coupled system are identified using impact testing methods. The obtained frequency response functions (FRFs), $H_{m,s}(\omega) = A_m(\omega) / F_s(\omega)$, are represented by accelerance functions, that is the complex ratio of the acceleration spectrum $A_m(\omega)$, measured at response DOF m, over the force spectrum $F_s(\omega)$, measured at the excitation points s. To evaluate the measured accelerance data the FRAC, PAC and the novel CAC method were used. Since a time domain system model is required an impulse response function (IRF) is calculated from each of the pre-measured FRFs by inverse Fourier transformation. In a subsequent step the set of obtained IRFs is then truncated in length, as discussed in section 5.3. Following these steps and using a sample frequency of $f_s = 12\,\text{kHz}$ the length of the truncated set of measured impulse response functions was chosen to be $I = 2048$ samples, corresponding to a duration of about 170 ms. This set of IRFs is considered to describe the complete system under test, being aware of possible inconsistencies caused by unavoidable errors and noise in the measurements.

5.4.2. Steering system with single internal source: Numerical examples

In a first study the obtained structural dynamic data (IRFs) is used to build a numerical model of the StSys. It is assumed that only the source (S_2(z)) is acting inside the StSys while all other sources are assumed to be inactive. As internal excitation a numerical impulsive (blocked) force is used that is designed to be representative for transient excitations provoking rattling

inside electrical StSys as a result of reverse feedback from the road (EBR – see section 3.3). To simulate the input force a purpose-made computation routine is used to generate arbitrary numbers of impulses with random modulus and sign stochastically distributed across the signal length $N = 5 \cdot I$ (see Figure 5.8 – (a),(c)). The required operational acceleration responses are then calculated by convolving the synthesised force time history with the truncated IRFs according to the modelling approach discussed in section 4.3. To account for noise, which in practice will always spoil the measurements, the calculated response data can artificially be corrupted by normally distributed, zero mean noise with unit standard deviation, proportional to the root mean square (RMS) of the respective acceleration signal (see Eq. (4.15)). In this way, the noise sequences as well as the true structural responses and applied 'rattling excitations' are exactly known at any time so that they can serve as reliable references to evaluate the accuracy of the adaptive force reconstruction procedure.

A first simulation is carried out aiming to reconstruct the impulsive force signature by means of a single 'operational' response. In order to investigate scatter in the reconstructed force caused by the spatial location of the response measurement on the assembly, the force identification process is carried out individually for each of the 32 measurement positions (see also Figure 5.7). However, the discussion in the following will only refer to a small number of selected remote points though all following findings and conclusions are valid for all investigated points. The positions considered in the following are chosen according to the following observations (see also Figure 5.7): Point 1 (P1) is placed on the 'cantilever' of the sub-frame resulting in a distinct resonant behaviour for frequencies below 400 Hz and a relatively high dynamic range of its FRF; the source contributes well to (P10) since they are strongly coupled via the rigid housing of the StSys; structural responses at (P14) suffer from almost blocked conditions and furthermore represent in-plane quantities for which reason the measured FRF is likely to be erroneous; (P23) has found to be representative for the majority of points on the sub-frame.

For force identification the SISO time domain inversion routine from Table 4.1 is used. The iterative process is interrupted according to the error criterion η = 0.001 % (Eq. (4.14)). Simulation results are shown in time and frequency domain in Figure 5.8. Note that estimates for times smaller than t_d = 170 ms, corresponding to the decay time $t_d = I / fs$ of the IRFs, denoted by the vertical dashed line, are not reliable due to the reasons mentioned in section 4.2.2. Hence, this range is not considered in the frequency domain estimation errors, which

are defined according to Eq. (4.19) for the reconstructed responses and Eq. (4.18) for the identified force, respectively.

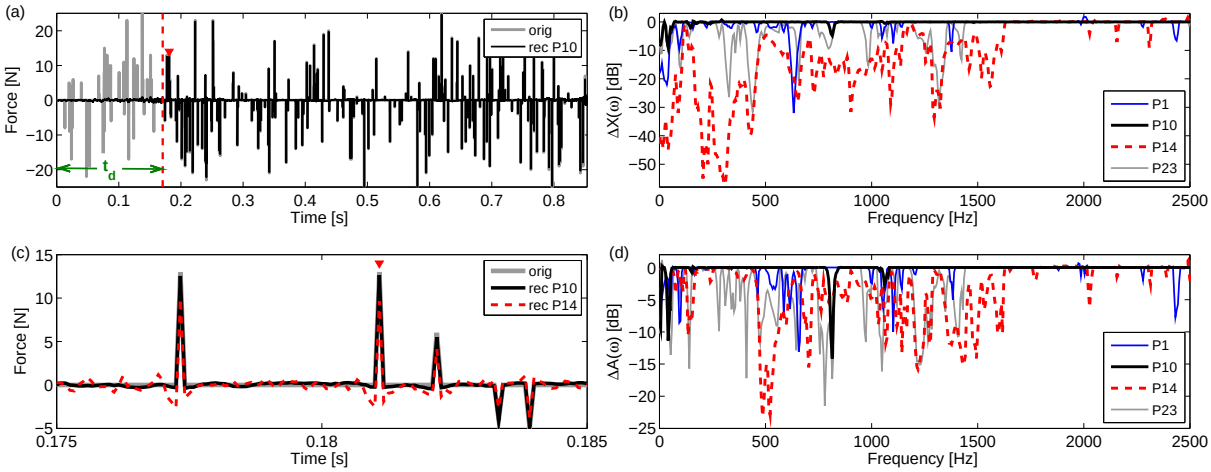

Figure 5.8. Simulation results for 4 different noise free SISO systems: Measured and reconstructed forces in full length (a) and close up (c), estimation error of reconstructed force spectrum (b) and approximated acceleration spectrum (d) for different points on the assembly.

Although numerical models without any unconsidered noise are used, the time history of the applied dynamic force (orig) can not be reconstructed completely, as illustrated in (a) and (c) for the best (P10) and the worst (P14) response position on the assembly. Visually small variations in time domain may lead to profound errors in the estimated force spectra as demonstrated in (b). Using structural responses measured at (P14) will lead to underestimating the actual force up to about 57 dB (at 310 Hz). The large deviations in the reconstructed force can be traced back to errors in the measured impulse response function resulting from the almost blocked conditions at (P14). The measurements of the corresponding FRF showed very poor coherence for frequencies below 450 Hz. Only for frequencies above 1.6 kHz satisfying coherence was achieved which becomes evident in the small estimation errors for both, the reconstructed force and the approximated acceleration, when using (P14).

In contrast, response position (P10), to which the source contributes strongly, achieves constant estimation accuracy of about $\Delta X_{10}(\omega) \approx |0.2\,\mathrm{dB}|$ across almost the whole frequency range. Merely for frequencies below 40 Hz as well as in narrow bands around 150 Hz, 814 Hz and 1060 Hz the error in the reconstructed force increases (see also Figure 5.9 - (a)). At these frequencies large errors can also be spotted in the reconstructed acceleration spectrum for (P10). The ordinary coherence function for the measurements of the corresponding FRF showed dips at these frequencies so that the increase in the estimation error is believed to

result from inconsistent FRF data. Similar conclusions can be drawn for all remaining points on the structure. However, comparing estimation results for different response positions reveals that the spatial variation across the structure is quite considerable, even when the response measurements do not include any noise.

In reality, noise in the measured structural responses will be present and thus further affects the accuracy of the force identification process. In order to evaluate the effects of noise on the estimation accuracy if only a single response is used to reconstruct the unknown input force, the previous simulation is expanded. This time 5 % and 10 % RMS noise is added to each acceleration signal. Simulation results for response position (P10) are illustrated in Figure 5.9.

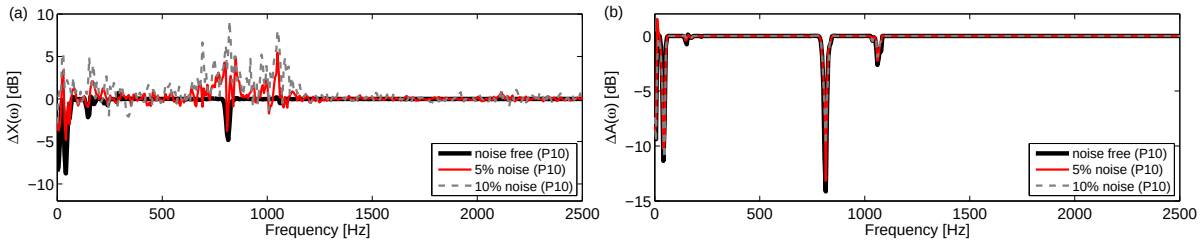

Figure 5.9. Simulation results for SISO system considering point (P10): Estimation error of reconstructed force spectrum (a) and approximated acceleration spectrum (b) for noise free, 5 % and 10 % noise corrupted acceleration response.

As expected, additional noise in the operational response is gained and decreases the accuracy of the force reconstruction process (see Figure 5.9 - (a)). This emerges especially around frequencies at which the reconstructed acceleration spectrum in (b) also shows high deviations from the original responses. It has been discussed in section 4.4.1 that for ideal SISO systems the reconstructed response should always be identical to the desired one. However, at the error-prone frequencies inconsistencies in the measured FRF have been detected. It is important to see that errors in the reconstructed acceleration spectrum at frequencies related to the inconsistent system description do not depend on the amount of the added random noise. No matter if the response is assumed to be noise free or corrupted by additional 5% or 10% noise, the acceleration signal can always be reconstructed with consistent accuracy. Note that this finding is only valid for SISO systems. However, this finding is important since it states, that errors in the reconstructed acceleration spectrum relate to inconsistencies in the measured FRFs no matter whether the operational response is corrupted by noise or not. On this account, plots of the error in the reconstructed acceleration spectrum have turned out to be very useful with regard to identifying frequencies at which a FRF may be defective or sensitive to noise and at which frequencies the uncertainty in the

estimated force spectrum increases. In [174] similar conclusions have been drawn for measurements on a single degree of freedom excited beam.

In order to reduce the prior discussed discrepancies in the reconstructed forces obtained by using SISO models only additional simulations based on overdetermined (OD) system models are carried out. The same 'rattle-like' force signature as used before for the SISO models is to be recovered by the newly created SIMO system. All 32 available response positions are considered in the model. Different simulations are carried out considering noise free responses and operational responses to which noise of 5 % and 10 % of their respective RMS value is added. Figure 5.10 illustrates the results when reconstructing the force according to the expanded SIMO time domain inversion routine from Table 4.3.

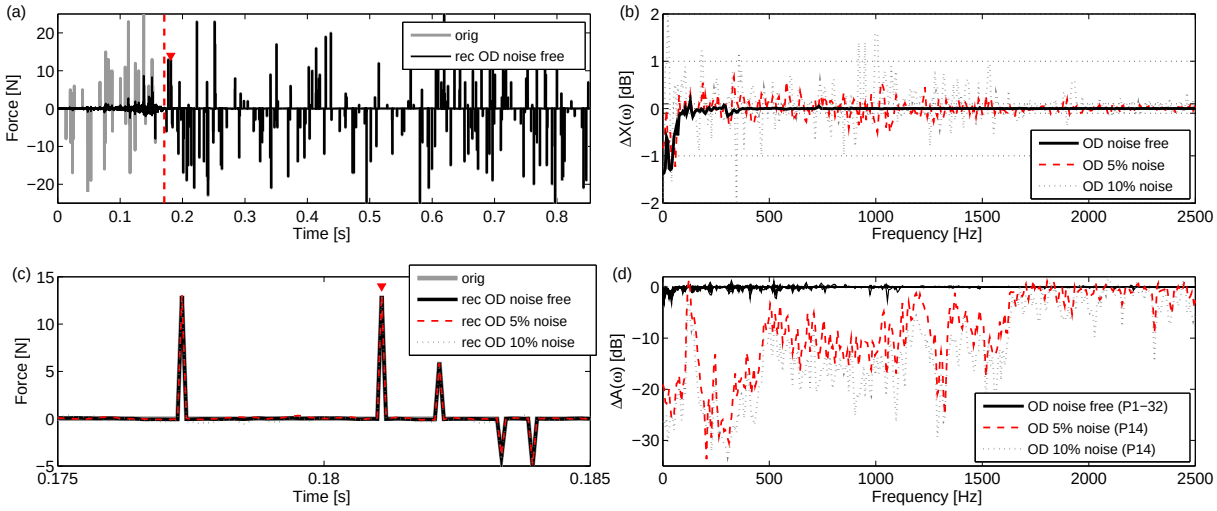

Figure 5.10. Simulation results for over-determined (1x32) SIMO system: Measured and reconstructed forces in full length (a) and close up (c), estimation error of reconstructed force spectrum (b) and approximated acceleration spectrum (d) for noise free, 5 % and 10 % noise corrupted acceleration responses.

Since the averaged error gradient is used in the expanded adaptive process (see section 4.5.1), the simulation results show large errors in the reconstructed acceleration spectra. These errors increase if noise is added to the acceleration responses and can take very high values for certain response positions, e.g. values up to 32 dB at measurement position (P14) if 10 % white noise is added. However, by means of the averaged error gradient the error in the reconstructed force is only slightly affected by the additional noise. For the noise free system the negative influence of inconsistencies in the FRFs is almost eliminated, yielding insignificant errors smaller than |0.1 dB|, as indicated by the horizontal dashed lines in Figure 5.10 - (b). The time history of the assumed unknown input force in (c) in this case is reconstructed precisely. Due to the over-determination, the force estimation accuracy is even

better than for the best point (P10) obtained by the SISO model in Figure 5.8 and Figure 5.9, respectively. Even for a considerable amount of noise (10 %), the force spectrum can be identified with an uncertainty smaller than |1 dB| throughout the whole frequency range, apart from frequencies below 100 Hz. It is likely that only a few modes contribute to the measured responses at these low frequencies for which reason over-determination may not be effective.

The influence of overdetermination on the force identification accuracy in the presence of 10 % noise corrupted response data is further illustrated in Figure 5.11 where the solution obtained with the expanded SIMO time domain inversion routine (cf. Figure 5.11 – OD 10% noise) is contrasted with the force identification results achieved with the basic SISO routine considering only the best response position (P10) (cf. Figure 5.8–10% noise (P10)).

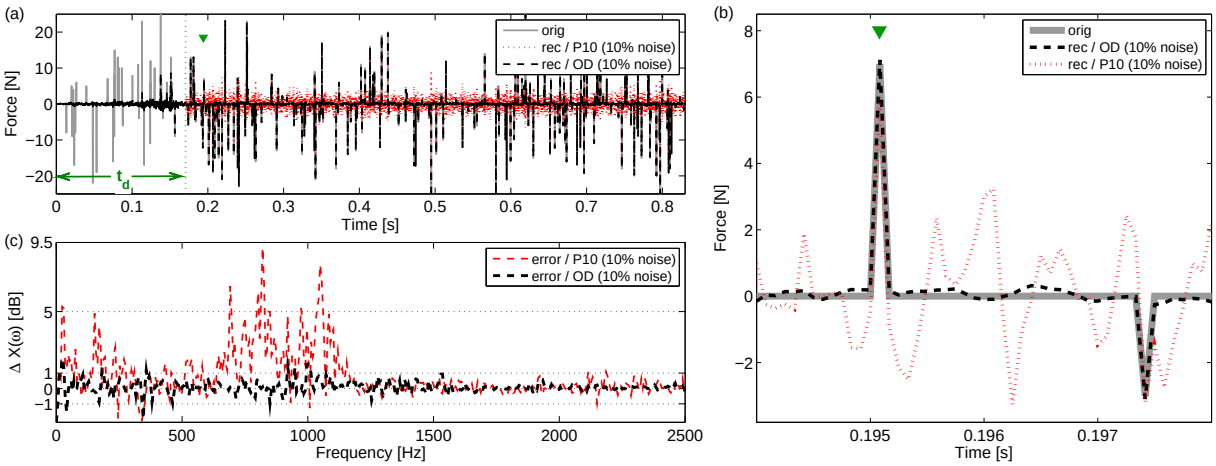

Figure 5.11. Effect of overdetermination (OD) on the force estimation accuracy for 10% noise corrupted response data. Original and reconstructed force signature in full length (a), close-up (b) and spectral estimation error (c): —— true force; – – – reconstructed from overdetermined system; ▪▪▪▪▪ reconstructed from single response position (P10).

Clearly, attempts to recover the impulsive force from a single noisy response fail, even for the best measurement point 'P10' to which the source contributes well. The recovered transient force signature (Figure 5.11 – (a),(b)), in this case, is buried in noise and large spectral estimation errors up to $\Delta X_{P10}(\omega) \approx |10\,\mathrm{dB}|$ prevail (Figure 5.11 – (c)). Instead, the averaged error gradient significantly suppresses negative influences of the uncorrelated errors included in the system model and the structural responses, even if a considerable amount of noise is added (10 % added noise). These findings are consistent with the ones mentioned in [174],[206] and [207].

5.4.3. Steering system with single internal source: Experimental example

In order to evaluate the suitability of the time domain force identification method for real-life source characterisation purposes operational responses from experimental tests on the steering system are used in the following. The experimental vibration test data was obtained by exciting the assembly at the assumed source DOF ($S_2(z)$) (see Figure 5.7) using an instrumented hammer. In this way a long duration (20 seconds) impulsive force signal was applied to the structure. The actual dynamic excitation forces and the resulting operational accelerations at all response positions were measured at the same time according to the requirements of the in-situ blocked force method. The structural dynamic properties in terms of measured IRFs are identical to the ones used for the prior simulations and thus include errors which are considered to be representative for typical measurement scenarios. The time history of the applied input force is identified using the expanded time domain recursion for over-determined SIMO systems (cf. Table 4.3). The experimental results are shown in Figure 5.12. Note, the FRF measurements showed generally poor coherence at frequencies below 100 Hz and above 2.5 kHz, thus accurate force identification has not been possible at these frequencies. In order to allow comparing the measured and recovered force signatures all time series data has been band-pass filtered according to the valid frequency range. It is also stressed that the actual excitation force was measured so that the benchmark force ('meas') may also contain errors.

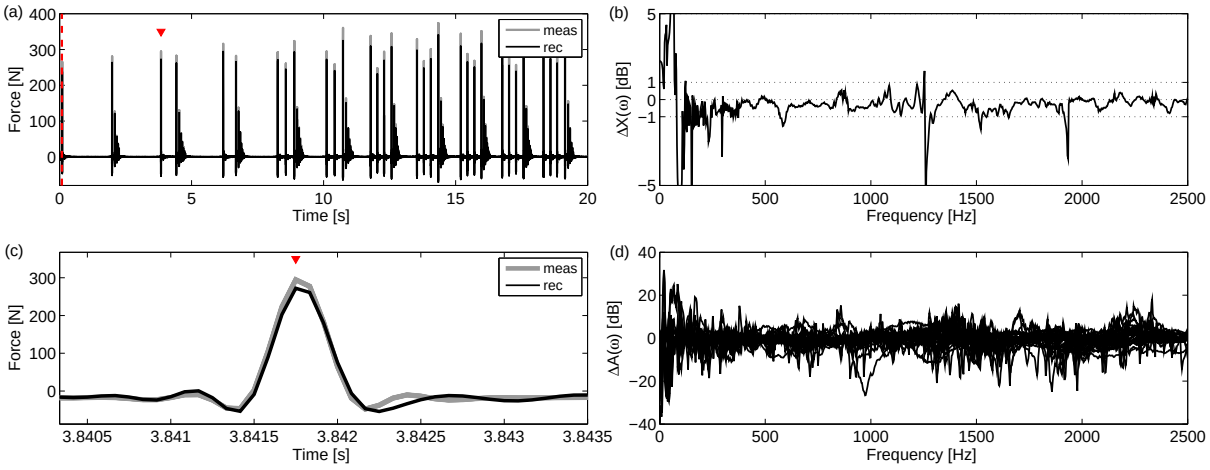

Figure 5.12. Experimental results for large (1x32) over-determined system: Measured (——) and reconstructed (——) force time history in full length (a) and close up (c), estimation error of reconstructed force spectrum (b) and approximated acceleration spectra (d) for all 32 response positions.

As can be seen from Figure 5.12 - (a), it is possible to reconstruct the applied dynamic force for the full length of the measurement (except the first I values) with satisfying accuracy.

Figure 5.12 - (c) evidences the good estimation result in time domain by zooming in on an arbitrary impulse of the force sequence. The error in the reconstructed force spectrum (b) is less than |1 dB| for a wide frequency range. Only narrow bands around the frequencies 150 Hz (-8 dB), 230 Hz (-2 dB), 295 Hz (-3 dB), 1260 Hz (-6 dB) and 1930 Hz (-3 dB) do not allow for estimating forces accurately. Again, the prediction accuracy at frequencies below 100 Hz is poor for the aforementioned reasons. On the contrary, the scatter in the error of the reconstructed acceleration spectra (d) is very high which indicates inconsistencies in the measured FRFs and the presence of noise in the response measurments. However, noise in the measured responses and considerable errors included in the used FRFs, as discussed before, are significantly suppressed in the reconstructed force by the averaged error gradient approach. Furthermore, it is stressed that more or less random measurement positions were considered when placing the sensors on the test structure. It has turned out that points with even very weak contribution from the source, such as (P14), do not govern the force reconstruction process negatively so that generally robust and accurate force identification is possible.

To sum up, a long duration impulsive force signature was recovered satisfactorily under realistic measurement conditions using measurements carried out on the StSys whilst connected to the front axle carrier according to the in-situ blocked force requirements. Therefore, it can be concluded that using the time domain inversion routine in the described manner constitutes a time domain equivalent of the in-situ blocked force method that theoretically facilitates independent source characterisation on the fully assembled test structure.

5.4.4. Steering system with multiple internal sources: Numerical example

Under normal operation conditions multiple source mechanisms act in parallel inside electrical steering systems. As elaborated in chapter 3, these mechanisms can either result from forces originated due the function of the steering system, e.g. electric-magnetic forces, or from transient excitations. In this section an example is presented so as to demonstrate one of the main potential benefits of the achieved time domain in-situ blocked force approach, i.e. the potential to separate out excitations from different components while the blocked forces obtained have the property of independence from the structure outside the source region.

Again the sophisticated experimental set-up from section 5.4.1 is considered as test structure in which the electrical steering system is mounted on the front axel carrier. This time it is assumed that the StSys comprises four ideally point-like structure-borne sound sources, each exciting the assembly in one DOF, denoted in Figure 5.7 by (S_1(z)), (S_2(z)), (S_3(z2)) and (S_4(y)). Note that despite (S_4(y)) all sources are located inside the StSys and are only accessible for measurements through cut-outs in the housing.

A numerical model of the steering system is used considering $M = 9$ structural responses measured at the points (P_m) for $m = [11, 12, 18, 20, 21, 22, 26, 29, 32]$ (cf. Figure 5.7). It is stressed that these response points are spatially distributed over the front axle carrier but not on the steering gear itself. This strategy is preferred since it will also be employed for test bench measurements later on so as to achieve response measurements that only require installation of sensors on the test bench structure while unequipped steering systems may easily be swapped without the need of time-consuming re-installation of the measurement equipment. Further it is noted that the resulting (4x9) MIMO model of the assembly is based on the same (in-situ) FRF measurements and the associated truncated IRFs as in the previous examples.

In a first example a virtual vibration test is conducted based on the (4x9) MIMO model. Operational responses are calculated by convolving numerical blocked force signatures with the obtained IRFs. Inconsistencies in the measured IRFs thus become part of the system whilst the generated responses are free from errors. For each source a different blocked force signature is simulated as input: $x_1(n)$ – a logarithmic chirp accounting for non-stationary operation of the source (S_1(z)) (e.g. run-up of the electric motor); $x_2(n)$ – a signal composed of two sinusoids and superposed with $x_1(n)$ (correlation coefficient $\rho_{x2,x1} \approx 0.2$) for source (S_2(z)) (e.g. meshing of pinion and rack) ; $x_3(n)$ – a random signal partially correlated with $x_1(n)$ ($\rho_{x3,x1} \approx 0.25$) for source ($S_3$(z2)); and $x_4(n)$ – an uncorrelated impulsive signal for source (S_4(y)) (e.g. road feedback). Uncorrelated white noise with amplitudes of 5% of the respective RMS value can be added to each response so as to evaluate the robustness of the inversion process for a noisy measurement scenario. The generalised time domain inversion routine from Table 4.8 is used to reconstruct the blocked force signatures from the calculated responses which are then compared with the exact input signals. Results are illustrated in Figure 5.13.

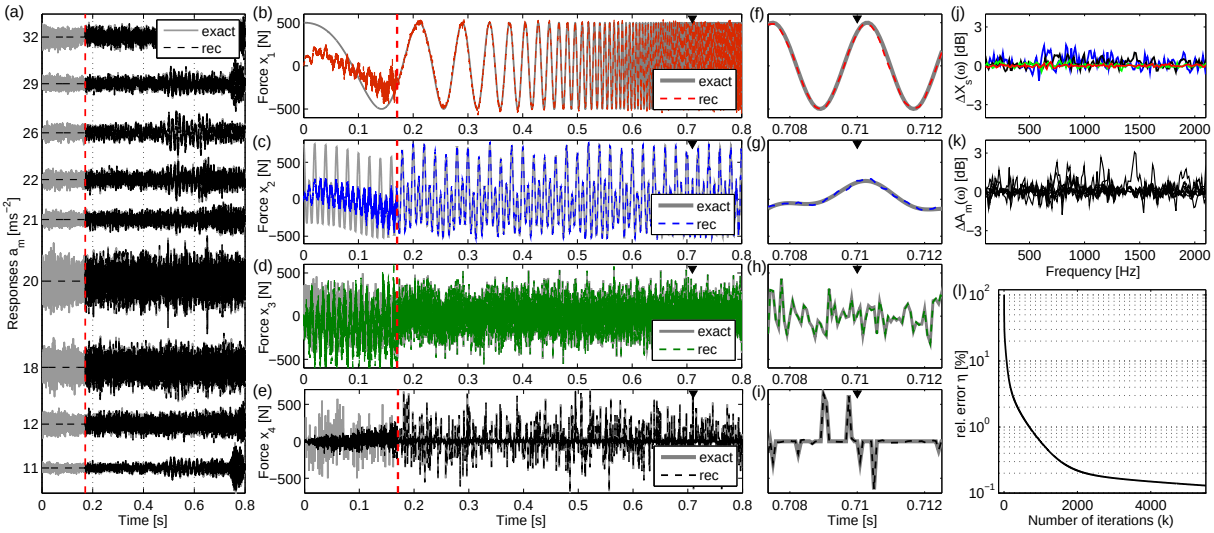

Figure 5.13. Numerical result for (4x9) over-determined MIMO system. Time signatures of structural responses (a) and in-situ blocked forces in full length (b)-(e) and as close-up (f)-(i): ——— exact; – – –recovered from noisy responses. Spectral estimation error in identified forces (j) and reconstructed responses (k). Relative mean estimation error as performance measure of the adaptive inversion routine (l).

Considering noise free responses first, the generalised MIMO deconvolution routine allows reconstructing all blocked forces precisely although the set of measured IRFs has been found to comprise severe inconsistencies. However, due to the averaged error gradient negative effects caused by random errors in the system description are sufficiently suppressed. Note that blocked forces recovered from noise free responses are not depicted in Figure 5.13 since they are indistinguishable from the exact curves. If uncorrelated noise is added to all responses the solution is affected only slightly. All blocked force signatures can be identified accurately as shown in Figure 5.13 - (b–i). Only the first 170 ms of the time series data cannot be recovered from the available data as discussed in the previous examples. The spectral estimation errors of the reconstructed input forces are plotted in Figure 5.13 - (j). Accordingly, the blocked forces of the source (S_1(z)) and (S_3(z2)) can be identified with an error $\Delta X_{S1,S3}(\omega) \leq |0.5\,\mathrm{dB}|$ in the entire frequency range whereas source characterisation for (S_2(z)) and (S_4(y)) is possible with an uncertainty $\Delta X_{S4}(\omega) \leq |1\,\mathrm{dB}|$ and $\Delta X_{S2}(\omega) \leq |1.5\,\mathrm{dB}|$, respectively. The spectral estimation errors in the recovered responses $\Delta A_m(\omega)$ can reach higher values, up to |3 dB|, which is due to the averaged error gradient that is always dominated by the strongest force paths. To monitor the performance of the adaptive algorithm the expanded relative mean prediction error (see Eq. (4.30)) between the exact and the estimated response time signals (Figure 5.13-(a)), which is formulated for the reliable time range (> 170 ms), is plotted in Figure 5.13 - (l). In summary, a convergent and robust solution has been achieved.

5.4.5. Steering system with multiple internal sources: Experimental example

The generalised MIMO time domain inversion routine is verified experimentally in the following. Operational data was obtained by exciting the steering system whilst connected to the front axle carrier at the assumed internal source regions (S_1(z)), (S_2(z)) and (S_3(z2)) (see Figure 5.7) using three instrumented hammers. In this way long duration (20 seconds) impulsive force signatures were applied to the structure. The actual excitations and the operational accelerations at all 9 response DOFs were measured in parallel. The IRFs from the previous examples are used to model the system so that errors, representative for typical measurement scenarios, are included. The time histories of the three applied forces are identified using the generalised algorithm from Table 4.8. Results are shown in Fig 4. Note, the FRF measurements showed poor coherence at frequencies below 100 Hz and above 2.1 kHz, thus accurate force identification has not been possible at these frequencies. To allow comparing measured and estimated force signatures, all time series data has been band-pass filtered according to the valid frequency range. It is also stressed that the actual excitations were measured so that errors in the benchmark values ('meas') cannot be excluded.

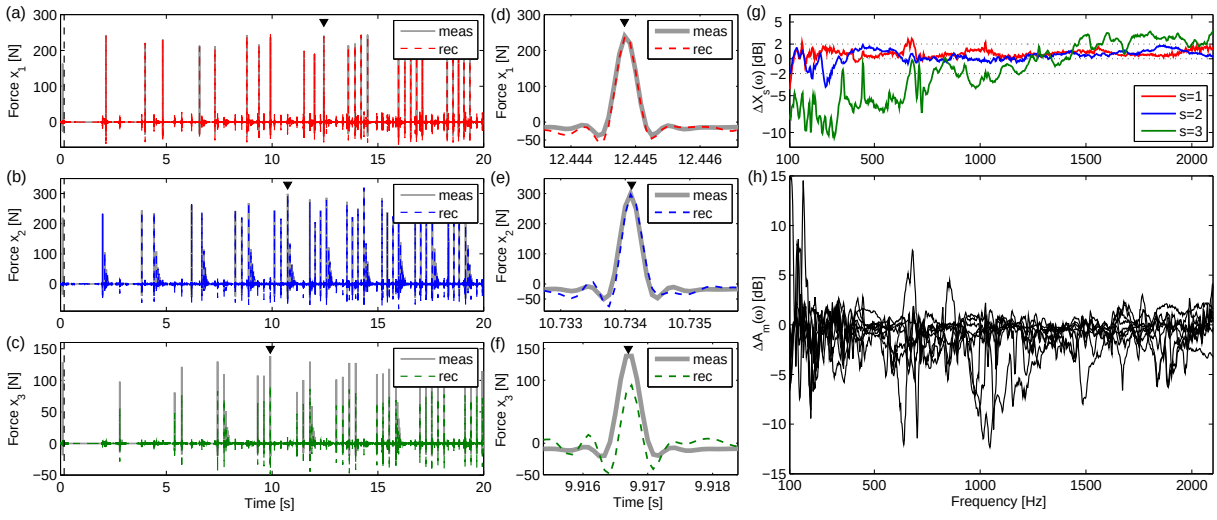

Figure 5.14. Experimental result for (3x9) over-determined MIMO system. Dynamic force signatures in full length (a,b,c) and close-up (d,e,f): measured ——— ; recovered from structural responses — — —. Spectral estimation error of identified forces (g) and reconstructed responses (h).

As can be seen form Figure 5.14 - (a),(b),(c) the time series of all applied forces can be separated from the measured operational responses for the full length of the signals; except for the first 170 ms. The temporal positions of all impulsive peaks can clearly be detected for all considered sources (S_1(z)), (S_2(z)) and (S_3(z2)). Discrepancies in the reconstructed magnitudes are evidenced in the diagrams (e),(f),(g) by zooming in on one arbitrary impulse

for each of the reconstructed force sequences. Their appearance in the full-length signals is indicated by black triangles. The best force reconstruction accuracy can be achieved for source (S_1(z)), i.e. the force signature $x_1(n)$ (see Figure 5.14 - (a),(d)), followed by source (S_2(z)) (see $x_2(n)$ in Figure 5.14 - (b),(e)). The corresponding spectral force estimation errors, $\Delta X_s(\omega)$ for $s=[1,2]$, are below |2 dB| throughout wide frequency ranges, as indicated by the two horizontal dashed lines in Figure 5.14 - (g). Instead, large errors in the reconstructed force for source region (S_3(z2)) clearly emerge in the frequency domain where estimation errors $\Delta X_3(\omega)$ between $-12\,\text{dB}$ and $3.5\,\text{dB}$ can be found. The considerable underestimation of the force can also be seen in the magnitude of the reconstructed time series $x_3(n)$ (Figure 5.14 - (c),(f)).

The uncertainty in the reconstructed acceleration spectra $\Delta A_m(\omega)$ is also high (Figure 5.14-(h)). Especially below 200 Hz, around 650 Hz, 1.1 kHz and above 1.7 kHz the response errors can exceed |5 dB|. As discussed in the previous examples, large errors in the reconstructed response spectra indicate frequencies at which the considered FRFs may contain errors or rather the inversion process is sensitive to noise. This, in turn, can help to identify frequencies at which force reconstruction may be subject to increased uncertainty.

The poor estimation accuracy for source (S_3(z2)) is likely to result from measurement problems. Due to the installation position of the steering system and the sub-frame on the test rig, impact excitation turned out to be difficult due to reduced accessibility. Furthermore, the source region was assumed to be located at the curved surface area of the yoke and a stinger was needed for the excitation as the source was not directly accessible for impact hammer excitation through the small cut-out in the housing. Due to the relative long stinger (approximately 7 cm) it is likely that the direction of excitation did not fall in line with the considered degree of freedom. The mentioned difficulties appeared when measuring the actual applied force $x_{3,meas}(n)$ and the structural dynamic properties (FRFs) between source location (S_3(z2)) and all response positions (P_m). Reciprocity tests (FRAC, PAC) and the porposed CAC test attested problems in the FRF measurements.

Although all impulsive peaks can be identified in the three recovered force time signatures (Figure 5.14 - (a),(b),(c)), smaller ‘secondary’ peaks can be found at times where no force is applied to a respective source region. Those secondary peaks correlate with primary peaks of other sources and result from cross-coupling between different paths. It is likely that the point or the direction of excitation did not exactly correspond with the respective DOF considered

in the FRF measurements. Excitation through the small cut-outs in the housing was generally difficult. Nevertheless, in all identified force signatures the secondary peaks can clearly be distinguished from the primary peaks so that, at each time, it is possible to unambiguously identify whether a specific internal source is active or not. Regarding the aims of the research (chapter 1), this information is one of the main objectives of the research project, since it allows for detection of the instantaneous active internal sources based on measured operational responses.

One of the major drawbacks of the state-of-the-art 'rattling' measurement procedures (cf. section 5.2) is that knowledge about whether internal 'rattling' sources are active or not is derived on identifying transient events in the measured operational responses. This can lead to wrong interpretations although, in some circumstances, additional information such as zero-crossings in the measured sum of the tie rod forces may help to reduce uncertainty when detecting transient events in the measured responses caused by internal mechanism. However, even if the transient events in the responses can reliably be related to the internal excitations it is not possible to determine which source actually causes a problem at a specific time. To exemplify this issue, operational responses measured in 3 DOFs on the 'cantilever' of the sub-frame (see Figure 5.7 - (P_1),(P_2),(P_3)) are used. The responses are plotted as solid black lines in Figure 5.15. Owing to the sufficient separation of the originating force signatures achieved by employing the time domain inversion routine the transient peaks in the structural responses can unambiguously be linked to the respective internal sources, as indicated by the coloured triangles and dashed lines (red - (S_1(z)), blue - (S_2(z)), green - (S_3(z2))).

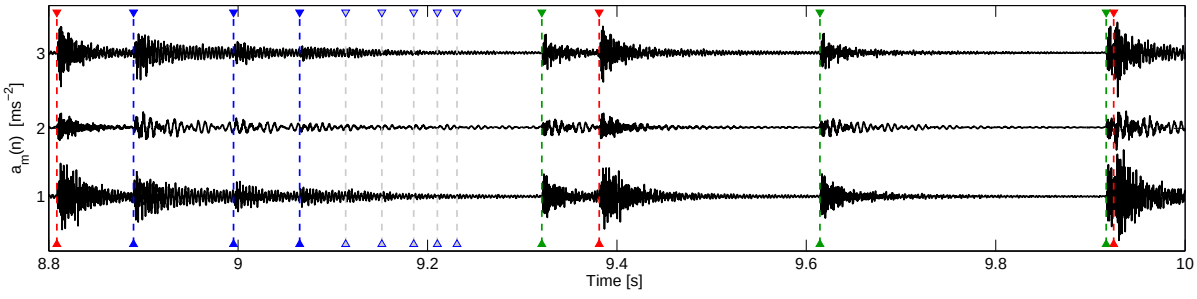

Figure 5.15. Relating transient events in the measured operational responses to the internal sources: Transient event caused by — — — source (S_1(z)); — — — source (S_2(z)) and — — — source (S_3(z2)).

Figure 5.15 illustrates that simply monitoring the operational responses do not necessarily allow identifying the times at which internal sources are active. For example, the five vertical grey lines around 9.2 seconds indicate impulsive peaks identifiable from the reconstructed

time signature of source ($S_{2(z)}$) (cf. Figure 5.14 – (b)). Without this information, one would probably simply diagnose decays in the measured responses leading to the misinterpretation that no internal source is active at these times. Furthermore, misinterpretation may arise if two sources contribute to the responses at the same time or temporal very close to each other, as indicated by the red and green line around 9.93 seconds for source ($S_{1(z)}$) and ($S_{3(z2)}$), respectively. Events like this could easily be misconstrued as one single event.

Summing up, the proposed MIMO force identification routine has been successfully used for separating three long-duration impulsive force signatures from noisy response measurements. Satisfying results were obtained for two of the recovered forces (sources ($S_{1(z)}$) and ($S_{3(z2)}$)) while considerable errors in the third force have been found to result from issues with exciting the corresponding internal source region ($S_{3(z2)}$) sufficiently. Although errors in the reconstructed magnitudes are present, the exact times at which impulses are applied to the different source regions can clearly be identified. It has been demonstrated that this information can be used to link transient events in the measured responses to the actual active internal sources in order to avoid misinterpretation of the observed operational responses and to unambiguously identify and evaluate which source contributes in which degree at a certain time. Furthermore, it has been discussed that all measurements were carried out according to the in-situ blocked force method so that it can be concluded that the derived time domain inversion routine yields fairly accurate identification results under normal experimental conditions and in theory is capable of separating blocked force signatures from physically separated sources inside the steering system.

5.4.6. Characterisation of the internal sources using test bench excitation

In this section the derived methodology is demonstrated with respect to identifying and quantifying structure-borne sound sources inside pinion-rack steering gears based on realistic test bench excitation. However, it is stressed that the presented example constitutes a feasibility study only. Several important steps required to perform reliable source characterisation could not be achieved during the measurements.

In order to excite the transient sound source inside the steering gear the steering system need to be operated on a standard rattle test bench. To mount the steering system on the test bench a front axle carrier is used. The assembly is depicted in Figure 5.16. Note that due to the physical assembly of the steering system two different coordinate systems are used. The

global coordinate system (x, y, z) is depicted in the lower part of Figure 5.16 while the local coordinate system (x2, y2, z2) for the pinion-yoke area is depicted in the upper right corner. Further it is noted that the perpendicular axes of the pinion-yoke system are rotated to the global ones so that, for example, measuring the response in z2-directon corresponds to partial measurements in all 3 directions (x, y, z) of the global system.

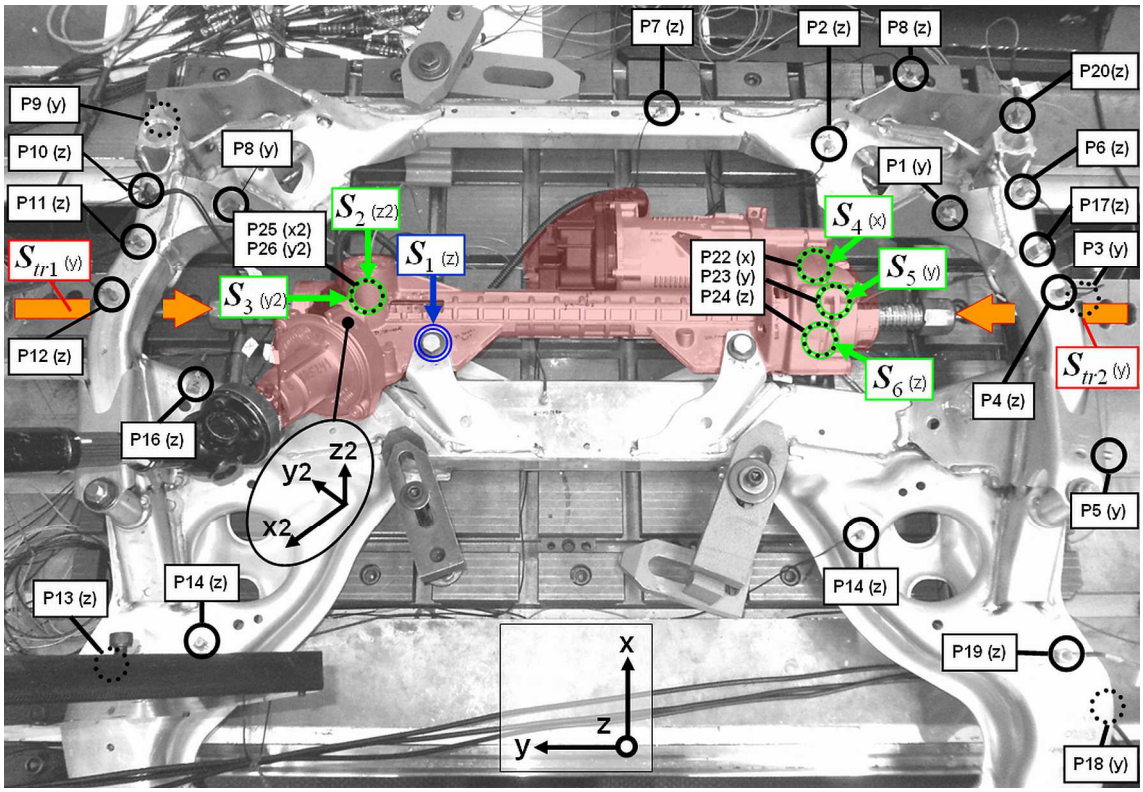

Figure 5.16. Steering system mounted on the standard rattle test bench with known source (S_1), assumed internal sources (S_2 - S_6), external tie rod excitation (S_{tr1}) - (S_{tr1}) and response positions (P_m).

For the experiment it is assumed that the StSys comprises one external known source (S_1) on the surface of the steering system, 5 internal point-like structure-borne sound sources (S_u) for $u = [2,3,\ldots,6]$ which has been chosen in accordance with the findings from the source-path-receiver model (see section 3.4) and two external structure-borne sound sources ($S_{tr,r}$) for $r = [1,2]$ representing the required tie rod excitations. It is assumed that each of the named sources excite the assembly in one degree of freedom (DOF) only. This, of course, is an idealisation and cannot be achieved in practice. It is noted that the internal source locations were chosen as close to the theoretical correct locations identified from the source-path-receiver model. However, due to issues with accessing the internal source regions, required for example to conduct in-situ FRF measurements to characterise the transfer paths between each source and all response sensors the possibility to define source regions on the physical

structure was very difficult. In detail, the internal sources ($S_{2(z2)}$) and ($S_{3(y2)}$) are located on the yoke accounting for rattle excitation in two degree of freedoms which can be caused either due to the contact of pinion and rack or due to relative movement between the yoke and the pinion or the yoke and the housing , respectively (c.f. Figure 3.11). On the opposite of the steering system three internal sources ($S_{4(x)}$), ($S_{5(y)}$) and ($S_{6(z)}$) are defined that account for rattle excitation onside the ball nut unit (c.f. Figure 3.11). Since none of the internal sources is accessible for impact excitation to measure in-situ FRFs accelerometers were installed at the assumed source locations. Invoking the principle of reciprocity corresponding accelerance functions can be measured by exciting the structure at the response positions. The purpose of considering the additional external force ($S_{1(z)}$) located on one of the fastening points is, to apply a known force using an impact hammer and to use these known force as a reference. This means, the additional force will also be reconstructed by the iterative process and can be compared with the actual one in order to judge the accuracy of the approach.

Concerning the external tie rod forces ($S_{tr,r(y)}$) for $r = [1,2]$ measuring useful transfer function to any of the internal sources using impact hammer testing have been found impractical. Reasons for this result mainly from the accessibility of the tie rod ends in combination with clearance present if the system is unloaded. However, first attempts to characterise these transfer functions by operating the hydraulic cylinders of the test bench as shakers with defined excitation signals and using the force transducers on both tie rod ends as well as accelerometers installed at the assumed source and response points on the assembly as the corresponding in- and output signals, the conventional LMS algorithm has been found to yield suitable IRFs for the frequency range governed by the external tie rod excitations. These IRFs could be considered in the time domain inverse routine to compensate for contributions from the tie rod excitations on the operational responses as discussed in the next section. Unfortunately, no FRFs could be measured for the presented example so that the external tie rod excitations contribute to all measured responses.

The vibration responses are measured in terms of accelerations at multiple DOFs spatially distributed over the coupled structure. However, it is stressed that responses used for source characterisation are only taken from sensors located on the front axle carrier, i.e. the receiver structure downstream the assumed sources. The receiver accelerometers are located at the points (P_r) for $r = [1,2,\ldots,22]$. According the methodology discussed in section 5.3 the structural dynamic properties of the coupled system were identified according to the in-situ

blocked force requirements. Following these steps and using a sample frequency of $f_s = 12\,\text{kHz}$ the length of the truncated set of measured impulse response functions was chosen to be $I = 2048$ samples, corresponding to a duration of about 170 ms.

To obtain operational responses under realistic driving conditions the test bench approach as described in section 5.2 was employed. The defined 'standard rattle test profile' simulating driving on cobble stone pavement was used to provoke rattle inside the steering gear. The resulting structural responses on the receiver points were measured. The generalised time domain inversion routine from Table 4.8 was then used to reconstruct blocked force time signatures from the measured receiver responses for the potential internal rattle sources and the additional external force; the latter is then used to compare the predicted force with the measured one so as to judge the general performance of the procedure. Results are illustrated in Figure 5.17.

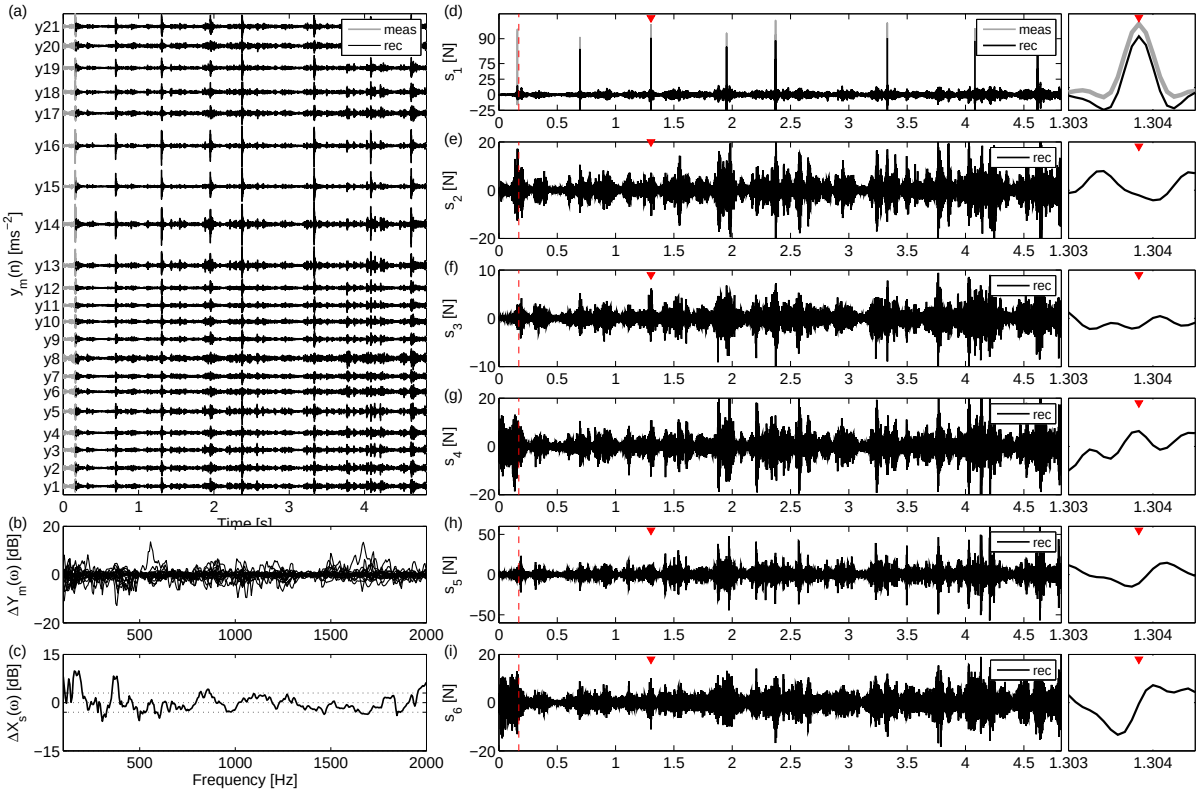

Figure 5.17. Experimental result using test bench rattle excitation: Time signatures of structural responses (a) and in-situ blocked forces in full length and as close-up for the known external force (d) and the 5 internal sources (e)-(i): ——— exact; ——— recovered from noisy responses. Spectral estimation error in the identified known forces (c) and the reconstructed responses (b). The red triangle indicate one external force impulse as magnified in the right diagrams.

As can be seen, the time domain inverse routine is able to separate out an individual blocked force time signature for each of the considered sources. Considering first the force signature obtained for the external source ($S_1(z)$) (Figure 5.17 –(a)) by comparing with the measured force (grey line) it can be found that the impulsive signature of the original force can be retained. All impulses can be identified at the correct times. Although, errors in the magnitude of the force peaks prevail the shape of the transient peak can be reconstructed with satisfying accuracy. Beside the force peaks the identified force contains significant perturbations. In analysis of the applied tie rod forces (not shown here) it has been found that these perturbations appear at times where the external tie rod excitations are generally contributing much to the overall vibration field on the assembly. Since no FRFs could be measured for the tie rods these contributions remain unconsidered in the force reconstruction so that they appear as correlated noise possibly in all of the predicted force signatures. However, the spectral estimation error in the reconstructed force ($S_1(z)$) is less than |3 dB| throughout most part of the considered frequency range. Higher deviations at low frequency again could be traced back to the external rattle excitation. It was found the external tie rod forces were orders of magnitudes higher than the applied impulsive force for frequencies below about 350 Hz. However, the FRF measurements have also shown to be of poor quality at several different frequency ranges. These errors show up in the reconstructed response spectra that can reach values of up to |15 dB|.

Concerning the potential internal rattle sources ($S_2(z2)$)- ($S_6(z)$) it can be found that all of the predicted blocked force signatures indicate transient behaviour. Interestingly, none of them seem to correlate with the additional external force ($S_1(z)$) which can be seen as an indicator for sufficient separation of the different signals. Furthermore, the reconstructed blocked force signatures provide rough information of the strength of the internal rattle sources. Until today, even such rough estimation of the source strength could not be provided. The discussed example at least demonstrates that comparable small internal (blocked) forces may emanate audible rattle noise as experienced while conducting the operation measurements. However, in order to identify which source contributes at a certain time transient events included in the blocked force time series should be identified.

Identification of these events can be realised in different ways. A simple criterion to identify the most dominant sources at a certain time can for example be achieved by detecting dominant peaks in the energy signals of the reconstructed blocked force signatures. This

procedure is illustrated in Figure 5.18 where a squared blocked force signature is calculated and normalised to one. This allows defining a threshold which can be used to detect the times at which a certain source signal exceeds this threshold. In the illustrated example the threshold was set to a value of half of the maximum signal energy.

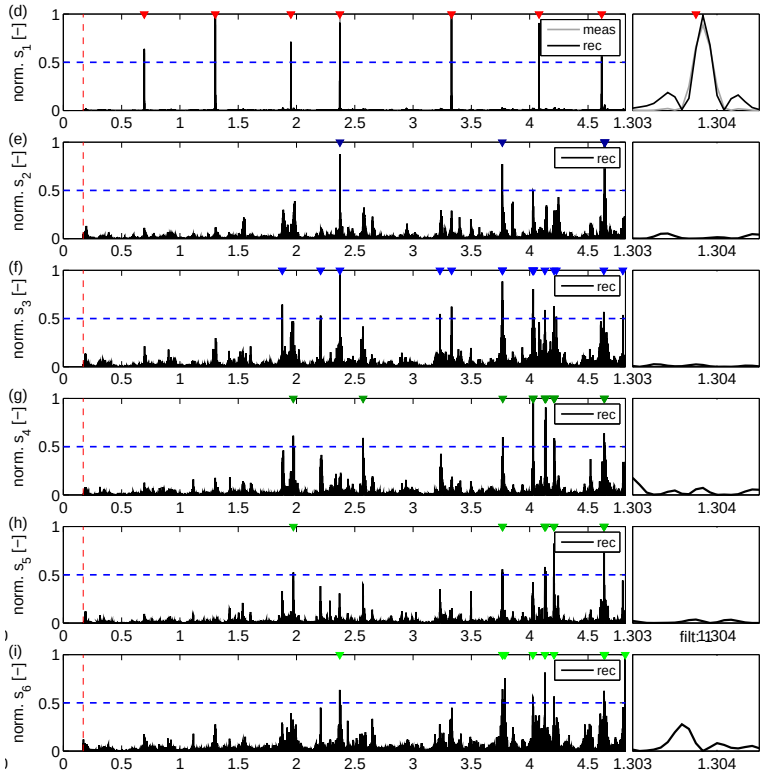

Figure 5.18. Normalised blocked force energy signals of the external (d) and the 5 internal sources (e)-(i). Times at which a signal exceeds the defined threshold are denoted by coloured triangles.

As can be seen from Figure 5.18, transient events can be found in all of the identified source signatures. They appear more often to later times since the magnitudes of the tie rod forces in the used profile are designed to increase with time. Based on the coloured indicators it would now be possible to further analyse how the specific sources contribute the responses for example, as elaborated in section 5.4.5.

Another possibility to examine whether the reconstructed blocked force signatures contain characteristic transient information is to evaluate if the identified peaks can physically be provoked by rattle excitation at all. In order to clarify this question a strategy usually employed in the state-of-the-art rattle evaluation method is used. As discussed in section 5.2.2 the zero-crossings in the sum of the applied tie rod forces indicate the times at which rattle excitation inside the steering gear is most likely to be provoked due to increasing internal clearance. Figure 5.19 shows the relationship between the zero –crossings of the sum of the

tie rod forces and the energy signal of one of the identified blocked force source signatures. Note that red dots denotes values in the squared blocked force signal at which both tie rod forces cancel each other.

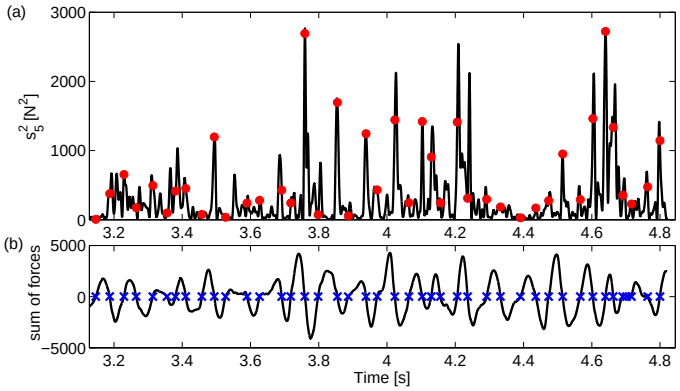

Figure 5.19. Relation between zero-crossings of the sum of the tie rod forces and the reconstructed blocked force signatures.

Clearly the identified transient events correlate well with the additional information provided by the test bench approach. With respect to future applications of the time domain source characterisation technique it may be worthwhile investigating how this additional information could be used to validate the predicted blocked force signatures.

To conclude, the developed time domain in-situ blocked force method was applied for the first time to reconstruct time domain blocked forces for multiple transient sources excited by external rattle excitation. Despite problems with measuring the FRFs between the tie rods to the assumed internal sources or points on the passive receiver satisfying force reconstruction was achieved for an experimentally applied reference force. Blocked force time signatures were achieved for all assumed internal sources retaining distinct transient features of the sources. At this stage no further research could be devoted to validate the reconstructed time signatures. However, this first attempt to conduct in-situ source characterisation based on an alternative rattle test bench approach have already yield some new interesting details about the characteristics of the internal sources. Furthermore, two criteria were presented that can be used to identify the most dominant transient events in the achieved source signals. Most important is however that all measurements and calculations were achieved with the developed methodology so that it has been tested under realistic conditions. Furthermore, an approach to better characterise the transfer paths from the tie rods to all other points on the assembly was mentioned that is speculated to offer big potential for future test bench

measurements. However, the external excitation required to provoke rattle inside steering systems will always cause problems if nor handled with care. In the following section this will be elaborated in more detail.

5.4.7. Conclusions

The feasibility of the time domain inversion routine has been demonstrated in the context of source characterisation in electrical steering systems using a time domain equivalent to the in-situ blocked force method. By way of example an electrical steering system mounted on a front axle carrier was considered as test structure. All measurements were conducted according to the requirements of the in-situ blocked force method.

Based on numerical and experimental examples it can be concluded that the proposed time domain in-situ blocked force approach provides a significant contribution towards better understanding the basic problem of transient structure-borne sound originated within electrical steering systems.

On the negative side, the time domain method requires additional FRF measurements compared with the state-of-the-art test bench measurement in which solely transient events in the operational responses are observed. Furthermore, it is necessary to solve an (possibly ill-posed) inverse problem. However, the introduced time domain inversion routine has proved to yield robust and accurate solutions to the inverse problem without the need of employing any form of regularisation even in the presence of considerable noise and errors included in the used measurements.

On the positive side, it is emphasised that the identified blocked force signatures could provide significant advantages over the conventional measurement approach. First, there is the potential to separate blocked force signatures from physically separated sources inside the steering system. It has been discussed that separation yields reliable and highly significant information about the activity of the internal sources. This information is believed to be very helpful in terms of locating the dominant transient sound sources inside the steering system and to achieve rank ordering of the underlying source and transmission mechanisms. It is also emphasised that the independence property of the resulting blocked forces is useful in terms of establishing evaluation criteria and limits for each of the possible internal sources whilst avoiding uncertainties associated with different steering systems. Second, since sensors are only required on the receiver-side, i.e. the front axle carrier in the presented examples or later

on the structure of the test bench, the proposed method does not require installation of sensors each time when the steering system is swapped making it very appealing with respect to end-of-line testing, for example.

In the presented experimental examples single and multiple long-duration (20 seconds) impulsive force signatures have been satisfactorily recovered from noisy response measurements conducted in-situ on a sophisticated technical structure. Errors in the identified forces have been traced back to errors in the employed FRF measurements or problems with exciting the source regions in the considered degree of freedom. Despite possible errors in the magnitudes of the reconstructed force time histories all transient peaks in the signals can unambiguously detected allowing for identifying which source contributes at which time to the observed structural responses. This information cannot be gained with the standard measurement approach. Based on the plausible experimental results it is believed that the time domain in-situ blocked force approach can also successfully be employed for characterisation of the internal structure-borne sound sources responsible for rattling in electrical steering systems. To do so, measurements on a specially designed rattling test bench are required involving additional difficulties when characterising the internal sources, as elaborated next.

5.5. Correction strategies for test bench measurements

In order to cause rattling in a steering system (StSys) it need to be coupled with either a test bench or mounted in a vehicle. This is inevitable since external dynamic forces, such as excitation provided by the road surface (EBR), have to be applied to both tie rod ends of the StSys so as to excite the internal structure-borne sound sources (see also chapter 3.4). Identifying the corresponding internal (rattling) forces is only possible by invoking inverse methods due to (i) the lack of accessibility and space for mounting transducers for measuring the forces in all required degree of freedoms directly, (ii) the risk of changing the interfacial conditions within the sensitive source regions, which may directly influence the actual forces, by the implemented instrumentation and (iii) possible impacts on the functionality of the StSys. It has been discussed that the novel generalised time domain inversion routine derived in the previous chapter will be used to recover the sought internal source forces from measured structural responses. However, invoking inverse methods for identifying the internal source forces from measurements carried out in-situ on rattling test benches is not directly possible. As discussed in the following, special care is to be taken due to the required external excitations.

5.5.1. Limitations of test bench approach

Since the StSys is coupled to either a test bench or a vehicle body all excitations acting on the overall assembly may contribute to each of the measured structural responses. As excitations, one needs to consider the sought internal source mechanisms and the external tie rod forces as well as additional forces caused by unknown disturbances within the structure. Assuming the structural dynamic properties of the assembly are given in terms of (measured) impulse response functions with finite length *I*, the operational (desired) responses at any point *m* on the assembly can be expressed as

$$d_{op,m}(n) = \underbrace{\sum_{s=1}^{S}\sum_{i=0}^{I-1} h_{ms}(i)\,x_{int,s}(n-i)}_{\text{contribution from internal sources}} + \underbrace{\sum_{r=1}^{R}\sum_{i=0}^{I-1} h_{mr}(i)\,x_{ex,r}(n-i)}_{\text{contribution from external tie rod forces}} + \underbrace{\sum_{d=1}^{D}\sum_{i=0}^{I-1} h_{md}(i)\,\varepsilon_d(n-i)}_{\text{contribution from unknown disturbances}} \quad (5.11)$$

where $x_{int,s}(n)$, $x_{ex,r}(n)$ and $\varepsilon_d(n)$ are the time signals of the $s=[1,2,\ldots,S]$ internal source forces to be identified, the $r=[1,2,\ldots,R]$ external tie rod forces (EBR) in order to provoke rattling inside the StSys and the $d=[1,2,\ldots,D]$ additional unknown disturbances, respectively. The corresponding impulse responses between the respective forces and each response point are denoted by $h_{ms}(i)$, $h_{mr}(i)$ and $h_{md}(i)$, respectively. Accordingly, the contributions from all forces to each point on the structure are given by a convolution sum between the actual excitation and the respective impulse response. The total desired response that can be measured on the assembly at each time *n* is the superposition of all the individual contributions. Note, uncorrelated noise such as inconsistencies or noise included in the measurements are omitted in Eq. (5.11) since the averaged error gradient involved in the expanded and generalised time domain inversion routine is able to deal with this problem, as discussed in section 4.5 and section 4.6 for SIMO and MIMO applications, respectively.

The rightmost term in (5.11) represents the fraction of the structural responses caused by unaccounted-for disturbances. In this context, disturbances represent additional force or moment excitations acting at unknown positions on the assembly for which reason they cannot be considered in the inverse model. Since those unconsidered excitations may contribute to several or all measurement positions their influence on the structural responses can be understood as ‘correlated’ noise. In consequence of this forces inferred from such garbled response measurements will always be erroneous. If the steering system is mounted in the car such disturbances are unavoidable since a multitude of operational forces generated by

or applied to the overall structure of the vehicle contribute to the observed measurement positions. It is likely that the sought internal source forces may be smaller by several magnitudes compared to the spurious unconsidered excitations and thus do not contribute much to the overall structural responses. However, in the presence of unknown disturbances acting at positions not taken into account by the inverse routine, the time signatures of the sought internal sources cannot be recovered from the measured responses.

To avoid problems arising from correlated noise in the response measurements, solely test bench measurements will be carried out. Due to the special design of the rattling test bench, i.e. test bench is mounted on isolators to provide vibration decoupling from the environment and actuators like hydraulic cylinders are decoupled from the test bed, the influence of unconsidered disturbances on the measured operational responses can be assumed to be insignificant. Thus, equation (5.11) can be reduced to the first two terms

$$d_{op,m}(n) = \sum_{s=1}^{S}\sum_{i=0}^{I-1} h_{ms}(i)\, x_{int,s}(n-i) + \sum_{r=1}^{R}\sum_{i=0}^{I-1} h_{mr}(i)\, x_{ex,r}(n-i). \tag{5.12}$$

This still means that the structural responses are affected by the external excitations applied to both tie rods in order to provoke rattling by EBR. Simply inferring the internal source forces $x_s(n)$ from responses measured on the test bench therefore would still yield erroneous estimation results. The reason for this is that the tie rod forces $x_r(n)$ affect the structural vibrations and hence need to be considered by the inverse model. Otherwise, they will have the same impact on the force identification process as ‘correlated noise’ (see also discussion in section 4.6.1).

In order to demonstrate how external forces applied to the tie rods can influence the estimation accuracy if they are not considered in the inverse model a numerical model of the StSys is created. The model is based on data obtained from the experiments discussed in section 5.4. The model considers 3 internal sources and 9 structural response positions. The 3 internal sources (see Figure 5.7 $S_1(z)$, $S_2(z)$ and $S_3(y)$) are assumed to generate dynamic forces in the form of a pure sinusoid $x_{int,1}(n)$, accounting for functional excitation that may be caused e.g. by the belt drive (cf. section 3.3.1), and two impulsive signals $x_{int,2}(n)$ and $x_{int,3}(n)$, representing rattling of the yoke in two degree of freedoms. As additional external excitations two random white noise signals $x_{ex,1}(n)$ and $x_{ex,2}(n)$ applied to both ends of the tie rods (see Figure 5.7 $S_4(z)$ and $S_5(y)$) are simulated. Their contributions to the calculated ‘operational’

responses are considered by convolving the random white noise signals with the respective impulse responses h_{mr}. A 'naive' simulation based on these garbled responses is carried out according to the proposed MIMO force identification algorithm given in Table 4.8. By using the term 'naive' it is emphasized that the identification routine is employed to identify only the 3 internal sources $x_{int,s}(n)$ but not taking the additional tie rod forces $x_{ex,r}(n)$ into account, which in practise would be necessary to excite the rattling sources. Simulation results for the (3x9) MIMO model are shown for the reconstructed forces and responses in time domain in Figure 5.20 and for the reconstructed responses in frequency domain in Figure 5.21.

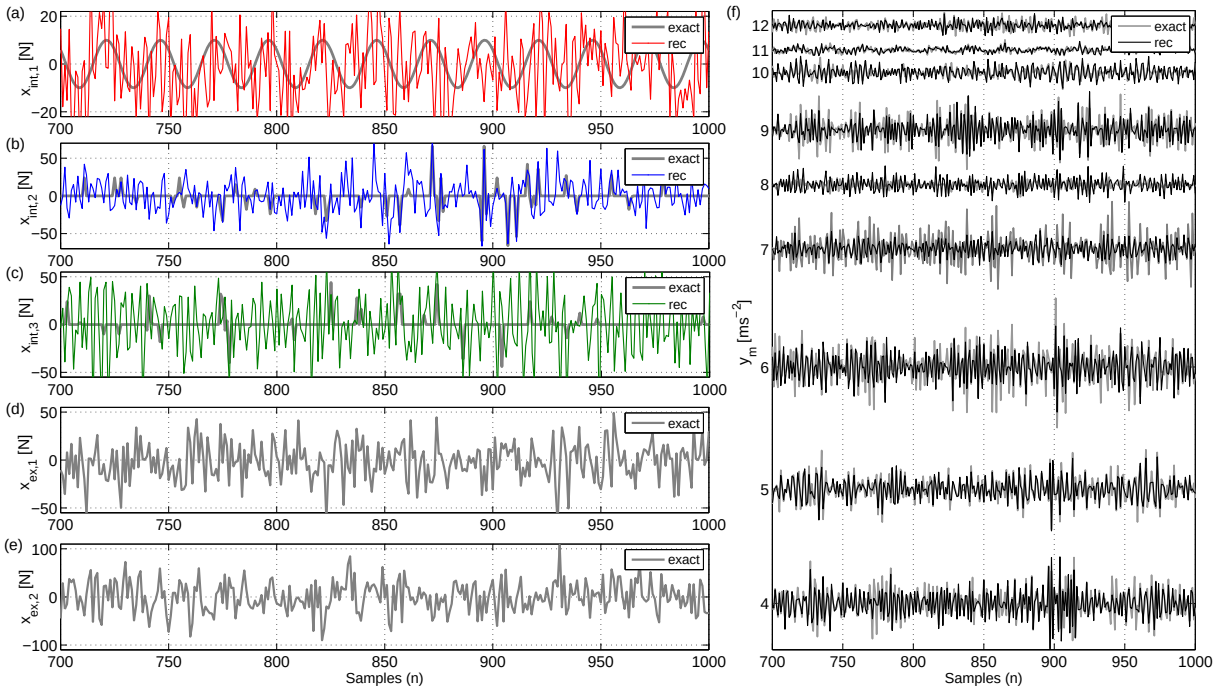

Figure 5.20. Simulation results for (3x9) MIMO system when tie rod forces are not considered in the inverse model. Exact and reconstructed internal source forces (a)-(c), additional unconsidered tie rod force (d) and (e), measured and reconstructed structural responses (f): ——— exact signal; —— reconstructed signal.

The additional tie rod forces, depicted in Figure 5.20 - (d),(e), contribute to all (exact) structural responses. In consequence, the averaged error gradient involved in the generalised MIMO recursion (Eq. (4.34)) adjusts the reconstructed response signals to the provided ones. However, since the originating tie rod forces are not taken into account in the inverse model, their contributions are missing in the reconstructed operational responses, as evidenced by the deviations between the measured and the reconstructed response time signals in Figure 5.20 - (f). It is important to note, that the responses cannot be recovered completely in this case. This finding is essential since it implies that large errors in the reconstructed responses may indicate the presence of additional forces not considered in the adaptive identification process.

A similar finding has been discussed with respect to inconsistencies in the impulse response functions (section 4.6.4). It has been shown that the error in the reconstructed acceleration spectrum increases significantly at frequencies where the corresponding FRF is defective [206],[207],[208]. However, the influence of unconsidered forces on the reconstructed response spectra will be reflected as substantial errors across wide frequency ranges for several or all measurement positions. The error in the frequency domain thereby is dependent on the spectra of the unconsidered excitation filtered by the respective transfer functions. Since white noise signals are used to simulate the additional tie rod forces, large errors throughout the whole frequency range can be found, as illustrated in Figure 5.21.

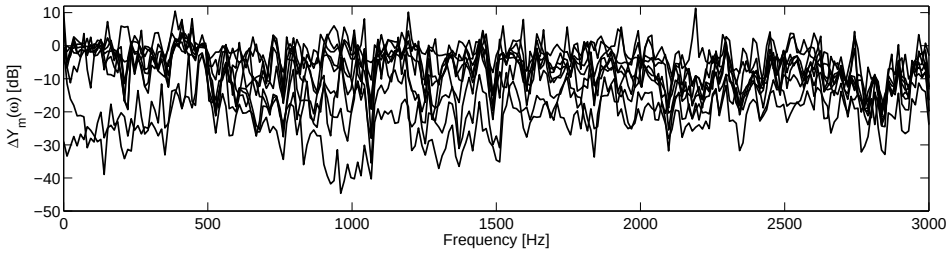

Figure 5.21. Spectral estimation error in the reconstructed accelerations for all 9 response positions when tie rod forces are not considered in the inverse model.

The large deviations in the estimated responses go along with rigorous errors in the reconstructed forces. As can be seen from Figure 5.20 - (a), (b) and (c), none of the sought internal force signals can be recovered. The unconsidered external tie rod forces lead to large distortion in all estimated force signatures so that the original signals cannot be identified.

However, carrying out experimental tests on the StSys whilst coupled to a rattling test bench allows for monitoring the additional tie rod forces. Force transducers measure the dynamic forces applied to the tie rods so that they are exactly known at any time (cf. section 5.2). This additional information can be used in order to counterbalance influences resulting from the required external excitations. Knowledge of the additional tie rod excitations facilitates for inferring the sought internal source forces from operational responses measured on the test bench set-up. Using the proposed adaptive force identification algorithm this is possible by following two different strategies, as discussed in the following.

5.5.2. Strategy I: Correction of the measured operational responses

Assuming that the external tie rod forces as well as the corresponding impulse response functions between all excitation and response positions are known, the measured operational

responses can be decomposed into contributions from the external tie rod forces and residual contributions caused by the internal sources. The time domain formulation given in Eq. (5.12) enables, at each time *n*, the latter contributions to be separated from the measured operational response signatures

$$d_{rattle,m}(n) = \sum_{s=1}^{S}\sum_{i=0}^{I-1} h_{ms}(i)\, x_{int,s}(n-i) = d_{op,m}(n) - \sum_{r=1}^{R}\sum_{i=0}^{I-1} h_{mr}(i)\, x_{ex,r}(n-i) \qquad (5.13)$$

where $d_{rattle,m}(n)$ is the fraction of the measured responses which is solely caused by the sought internal forces. The separated rattling responses represent ‘clean’ versions of the measured responses, that is, all contributions from the external tie rod forces are removed. In this way, the original measured structural responses can be corrected. Applying the time domain force identification technique to the corrected response signals allows for reconstructing the time signatures of the unknown internal source forces $x_{int,s}(n)$. In order to implement the correction approach in the generalised time domain inversion routine the iterative MIMO recursion need to be modified. This can be done by considering equation (5.13) when calculating the multiple error signals as given in Eq. (4.32). Accordingly, the corrected errors can be obtained as

$$e_m(n_k) = d_{op,m}(n_k) - \sum_{r=1}^{R}\sum_{i=0}^{I-1} h_{mr}(i)\, x_{ex,r}(n_k - i) - \sum_{s=1}^{S}\sum_{i=0}^{I-1} h_{ms}(i)\, x_{int,s}(n_k - i). \qquad (5.14)$$

Using the corrected recursion, i.e. Eq. (4.31), Eq. (5.14) and Eq. (4.34) together with the stability constraint Eq. (4.35), a new simulation is carried out with the previous (3x9) MIMO model in order to test the effectiveness of this correction strategy. The simulation results are summarised in Figure 5.22.

Clearly, all sought internal source signatures can fully be recovered from the corrected structural responses (Figure 5.22 - (a),(b) and (c)). The corresponding maximal frequency domain prediction errors are less than |0.1 dB| for all reconstructed forces although not illustrated here. The contributions from the external tie rod forces can be spotted as the difference between the original measured and the corrected recovered response signals, depicted in Figure 5.22 - (f). Note, the reconstructed responses would match exactly with the corrected responses from Eq. (5.13). However, here the difference between the corrected and the ‘measurements’ that in practice would be obtained from test bench measurements are contrasted.

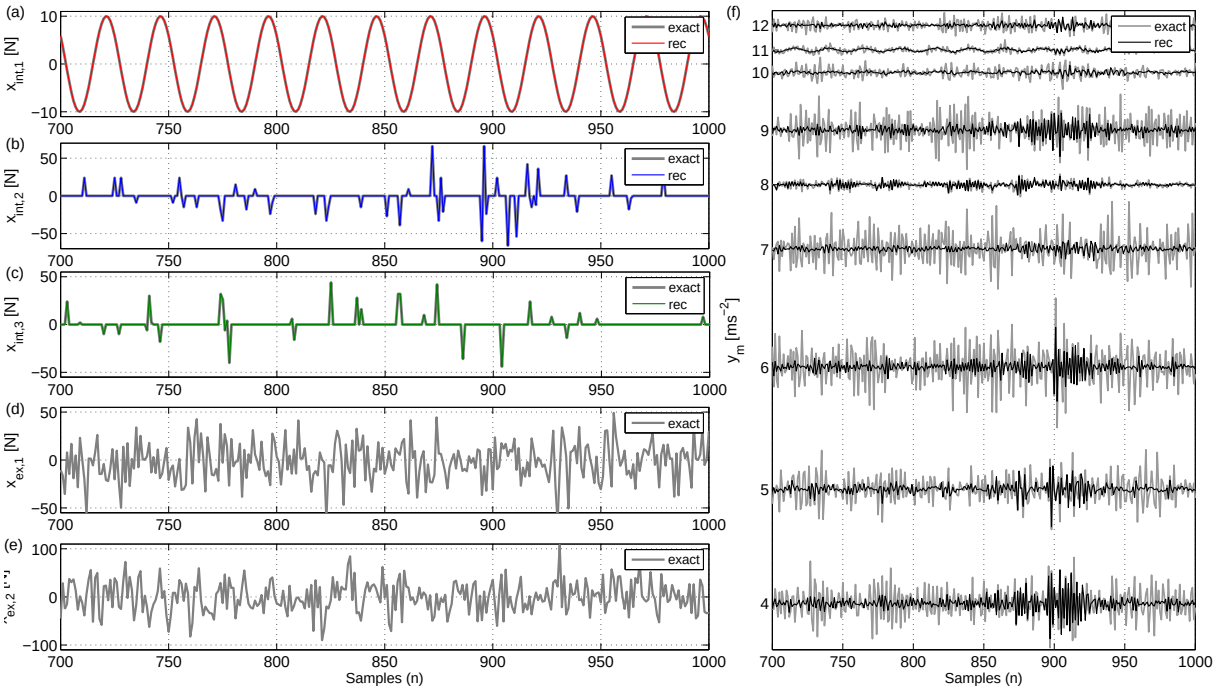

Figure 5.22. Simulation results for (3x9) MIMO system when measured responses are corrected (strategy 1). Exact and reconstructed internal source forces (a)-(c), applied tie rod force (d) and (e), measured and reconstructed structural responses (f): ▬▬ exact signal; ── reconstructed signal.

The advantage of this correction strategy is that the involved inverse model only considers the unknown internal sources but no additional assumed known forces. Since the adaptive time domain routine used for solving the inverse problem is based on an iterative algorithm, its computational effort significantly depend on (i) the number of forces to be identified, (ii) the number of considered response positions and (iii) the length of the involved impulse responses as well as the length of the operational response data. Note that a solution to decrease the computational effort due to (iii) has been discussed in section 5.3.4 while issues resulting from (i) are in the focus, here. This means that the proposed correction strategy should be applied whenever a large number of unknown forces is to be inferred from a large number of response positions, especially for structures with slowly decaying impulse responses or if long-duration operating data need to be processed. For all other applications where additional known forces are applied to structures, the strategy discussed below is preferable.

5.5.3. Strategy II: Reconstruction of an expanded set of input forces

Another strategy to infer the sought internal source forces from structural responses measured whilst StSys and test bench are coupled is to consider all forces acting on the overall assembly

by means of an enhanced MIMO model. Hence, the generalised time domain inversion routine has to solve for both, the unknown internal sources as well as the external tie rod excitations. The required adaptive algorithm can be derived by considering the additional force terms in the multiple error equations (4.32) and by including an individual update equation for the additional tie rod forces. Thus, an 'enhanced' MIMO algorithm can be achieved by

$$e_m(n_k) = d_{op,m}(n_k) - \sum_{s=1}^{S}\sum_{i=0}^{I-1} h_{ms}(i)\, x_{int,s}(n_k - i) - \sum_{r=1}^{R}\sum_{i=0}^{I-1} h_{mr}(i)\, x_{ex,r}(n_k - i) \tag{5.15}$$

$$\mathbf{x}_{int,s}(n_{k+1}) = \mathbf{x}_{int,s}(n_k) + 2\mu_s \left\langle e_m(n_k)\mathbf{h}_{ms}(n_k) \right\rangle \quad \text{for} \quad s = [1,2,\ldots,S] \tag{5.16}$$

$$\mathbf{x}_{ex,s}(n_{k+1}) = \mathbf{x}_{ex,s}(n_k) + 2\mu_r \left\langle e_m(n_k)\mathbf{h}_{mr}(n_k) \right\rangle \quad \text{for} \quad r = [1,2,\ldots,R]. \tag{5.17}$$

Note that the basic constraints of the time domain inversion routine, i.e. (i) consideration of only a part of the input and the desired response signals both of which are assumed to be of length N and (ii) cyclic operation of the iterative process by repeating the FIR and the desired signal periodically with period length *N*, remain valid although, for convenience, they are not depicted here. Further it is noted that the stability bound according to which the step size parameter μ_r involved in the update of the external tie rod forces has to be chosen can be obtained according to Eq. (4.35).

Although the computational effort for solving the expanded problem is larger compared to invoking the aforementioned correction strategy, this approach offers other advantages. Since the tie rod forces provided by the test bench are exactly known at any time, comparing the measured external forces with their reconstructed counterparts can be used for evaluating the estimation accuracy of the iterative process. The instantaneous estimation error in the reconstructed tie rod forces can be calculated at each iteration loop and its progression can serve as a more reliable performance measure for the iterative process than the previous introduced relative mean prediction error (see also discussion in section 4.7). In fact, the progression of the error in the reconstructed tie rod forces equates to the so-called 'misalignment vector' which is used in many adaptive filtering applications to measure the distance (difference) between the true filter coefficients and the estimated ones [209],[222]. Accordingly, a normalised misalignment vector for each tie rod force can be formulated as

$$\nu_r = 20\log_{10}\left(\frac{\sqrt{\sum_{n_k=I+1}^{N}\left(x_{ex,r}(n_k)-x_{meas,r}(n_k)\right)^2}}{\sqrt{\sum_{n_k=I+1}^{N}\left(x_{meas,r}(n_k)\right)^2}}\right) \quad \text{for} \quad r=[1,2,\ldots,R], \qquad (5.18)$$

where $x_{ex,r}(n_k)$ are the reconstructed external tie rod forces and $x_{meas,r}(n_k)$ are the measured tie rod forces provided by the test bench. Note, the misalignment measure is only defined within the valid estimation range, i.e. for all times $n_k \geq I+1$. In order to demonstrated the enhanced inverse approach, a simulation based on the equations (5.15), (5.16) and (5.17) is carried out. Due to considering both tie rod forces the time domain routine was applied to the enhanced (5x9) MIMO model. The simulation results are depicted in Figure 5.23

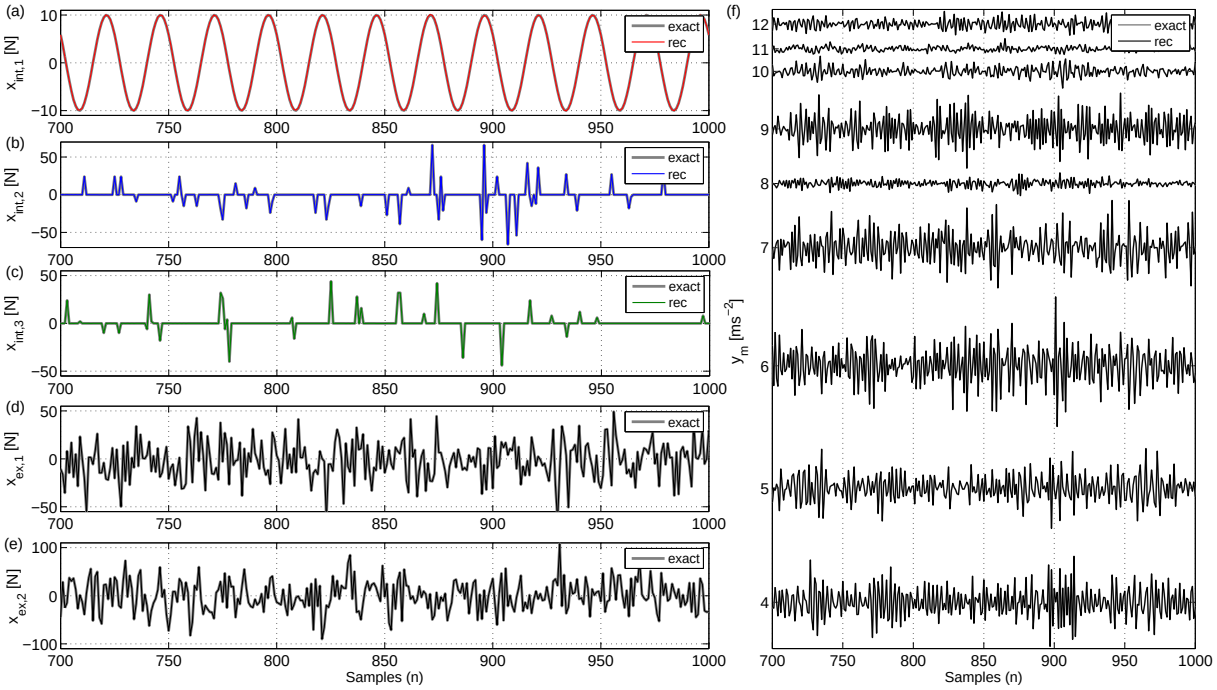

Figure 5.23. Simulation results for (5x9) MIMO system when all applied forces are considered in the inverse model (strategy 2). Exact and reconstructed internal source forces (a)-(c), applied tie rod force (d) and (e), measured and reconstructed structural responses (f): ——— exact signal; —— reconstructed signal.

As expected, the time histories of the sought internal forces, Figure 5.23 - (a),(b) and (c), as well as the two additional tie rod forces, Figure 5.23 - (d) and (e) are recovered precisely. Again, the corresponding maximal errors in all recovered force spectra are less than |0.1 dB| across almost the whole frequency range. Since the measured response signals this time were not corrected, the reconstructed structural responses also match perfectly with the original measurements, as depicted Figure 5.23 - (f). The respective spectral errors for the estimated responses are of the same order of magnitude as the spectral force reconstruction errors.

The introduced normalized misalignment (5.18) is computed for both tie rod forces. The misalignment vectors together with the spectral estimation errors for both tie rod forces are illustrated in Figure 5.24.

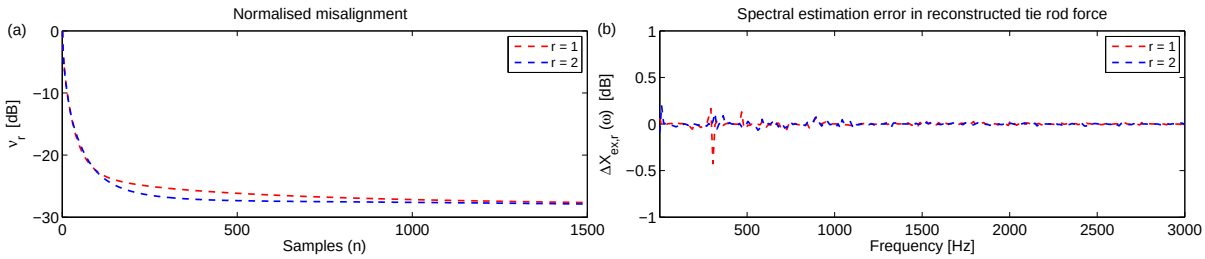

Figure 5.24. Normalised misalignment (a) and spectral estimation errors (b) for both external tie rod forces.

From Figure 5.24 - (a) it can be seen that the normalised misalignment of the reconstructed forces is a good means to monitor the convergence of the iterative process. The estimation discrepancies for both tie rod forces decrease monotonically with increasing numbers of iterations and tend to a lower limit. In practice, however, this limit will not be reached since unavoidable noise in the measured structural responses or inconsistencies in the involved impulse response functions will always affect the force reconstruction process. Nevertheless, it is possible to use the normalised misalignment as interruption criterion for the adaptive process based on its asymptotic behaviour. For example, if the misalignment does not significantly decrease within a certain number of iterations, e.g. 200 iterations, the adaptive process is close to the best achievable solution based on the given data.

The influence of defective impulse responses can also be identified in the spectral estimation error for the reconstructed tie rod forces, as depicted in Figure 5.24 - (b). Based on the spectral error, band pass filters could be designed which implemented in the adaptive force reconstruction process could be used to improve the prediction accuracy in certain frequency ranges. Similar procedures are known from applications of the conventional LMS algorithm used for filter design tasks. Moreover, as against the spectral estimation errors in the reconstructed responses the spectral force estimation errors reflect a measure of the estimation accuracy based on the desired quantity. Hence, using the spectral force estimation errors to monitor the progress of the time domain inversion routine is believed to be more straightforward than evaluating the accuracy of the reconstructed responses. Considering this, one could also define an interruption criterion for the iterative process based on the spectral force estimation errors, e.g. by defining error bands for certain frequency ranges.

To sum up, the normalised misalignment monitoring the convergence of the iterative process together with the spectral tie rod estimation errors have been found to provide significant additional information. Both criteria should be considered when internal sources are to be identified from real-life test bench measurements. For this reason strategy 2, that is the reconstruction of an enhanced set of input forces, should be applied in future works.

5.5.4. Conclusions

Provoking rattling inside of steering systems (StSys) requires external dynamic forces to be applied to both tie rods of the StSys. Furthermore, unconsidered forces may act on the assembly under test as the StSys is either coupled to the vehicle body or a test bench. All internal and external forces contribute to the operational responses which are measured at different spatial positions on the assembly. Since the internal source forces are to be inferred indirectly from these measured responses, the contributions from all applied forces need to be considered. In this section a time domain formulation for the total operational responses has been discussed. Contribution terms for the internal source forces, the required external tie rod excitations and additional disturbances have been introduced. The influence of additional disturbances, reflected as ‘correlated noise’ in the measured responses, on the force identification process has been discussed. It has been concluded that test bench measurements need to be carried out in order to minimise the risk for garbled response data. Based on the introduced time domain formulation for the operational responses, two strategies for inferring the internal source forces from test bench measurements have been derived. Strategy 1 allows for correcting the measured structural response data by separating the internal source contribution term from the tie rod excitation term. The generalised MIMO force identification algorithm has been modified in order to account for these corrected response signals. Strategy 2 relies on considering all internal and external forces in the MIMO identification algorithm at once. Consequently, the computational effort for the force reconstruction procedure is higher than for strategy 1 but, in return, two useful criteria for monitoring the inverse force reconstruction process have been introduced. The normalised misalignment defined for the known tie rod excitations can be used to analyse the convergence behaviour of the iterative reconstruction process whereas the spectral estimation error of the reconstructed tie rod forces have been found to serve as indicator for frequencies at which forces cannot be recovered exactly. It has been emphasised that both criteria are good means for identifying the internal rattling forces from noisy test bench measurements.

5.6. Summary and concluding remarks

In this chapter the methodology to characterise transient structure-borne sound sources inside electrical steering systems based on a novel time domain inversion routine has been complemented and tested sufficient. Different approaches have been discussed to facilitate independent source characterisation for the steering system based on test bench measurements.

It has been discussed that rattle noise within (electric power) rack-and-pinion steering gears can sufficiently be provoked by means of specially designed test benches that simulate the dynamic excitation feedback from the roadway surface (EBR) using pre-measured tie rod forces from actual vehicle tests. It has been found that standard rattle test benches used in industrial practice serve well to excite the transient structure-borne sound sources inside electric power steering systems as required within the scope of this study. However, it has been found that the conventional state-of-the-art approaches to evaluate rattle phenomena for industrial purposes lack in generality with respect to gaining characteristic and independent data for the individual internal sources. Instead it has been concluded that sufficient separation of the internal excitation signals themselves would provide more focussed information about the active sources. It is believed that independent source characterisation based on a time domain equivalent to the in-situ blocked force method achievable by employing the novel time domain inversion routine could deliver significant insight into the generation of rattle noise within electric steering systems.

The in-situ blocked force method generally requires characterisation of the dynamic properties of the involved passive structures. With regard to perform source characterisation based employing rattle test bench excitation this involves in-situ FRF measurements on the steering system whilst mounted on the test bench. Different approaches to obtain suitable system models even for complex technical applications have been elaborated. Focus have been put on practical measurement approaches as well as on methods that can help to identify errors in the obtained system models. In detail, two different criteria has been discussed that facilitate evaluation of the measurement quality for any element of a square mobility matrix. Both criteria are based on the positive definite property of the real part of the mobility matrix; the latter is sometimes denoted as conductance. The ‘Conductance Value’ (CV) has been introduced as a simple check on measured driving-point mobilities and is based on the passivity condition requiring their real parts always to be positive. For transfer mobilities the

so-called ‘Eigenvalue Measure’ (EM) has been defined which utilises a partitioning approach to obtain eigenvalues for the real part of the corresponding mobility sub-matrices. Due to the positive definite property these eigenvalues need to be positive otherwise they indicate erroneous measurements. Both criteria, the CV and the EM, are grouped under the term ‘Conductance Assurance Criteria’ (CAC) yielding normalised frequency independent single values between zero and one that facilitates convenient illustration in coloured matrices arranged according to the actual matrices. In this way easy and fast evaluation of all transfer and point FRF measurements is possible. Compared to conventional data evaluation criteria based on the reciprocity principle such as the Frequency Response Assurance Criterion (FRAC) or the Phase Assurance Criterion (PAC), the CAC has been found to provide more detailed information about the physical correctness of the used data while requiring only insignificant bigger measurement effort. Furthermore, the CAC is still able to disclose whether or not FRF measurements contain physical meaningful information for cases in which only one transfer mobility and the according two point mobilities are measurable. Although the basic idea of the presented data evaluation approach is not new the procedure to calculate the CAC values as well as their representation in easy-to-read colour matrices is believed to be original.

Furthermore it was elaborated how the obtained frequency domain system models have to be processed in order to achieve suitable models for the time domain inverse method. Of major importance in this respect is adequate transformation from the frequency domain into time domain using inverse Fourier transformation and to sufficiently truncate the resulting impulse response functions (IRFs) in order to improve the performance of the time domain inversion routine.

In a number of experiments this developed methodology has been satisfactory tested for steering systems comprising a single or multiple internal sources achieved by numerical simulations or realistic experiments. All measurements were conducted according to the requirements of the in-situ blocked force method. Considering artificial excitation first, single and multiple long-duration (20 seconds) impulsive force signatures were satisfactorily recovered from noisy response measurements conducted in-situ under normal testing conditions. Errors in the identified forces have been traced back to errors in the employed FRF measurements or problems with exciting the source regions in the considered degree of freedom. Despite possible errors in the magnitudes of the reconstructed force time histories all

transient peaks in the signals were unambiguously detected allowing for identifying which source contributes at which time to the observed structural responses.

Based on test bench measurements a first attempt to characterise the time domain blocked force signatures of multiple transient sound sources excited by realistic rattle excitation was conducted. Despite problems with measuring the FRFs between the tie rods to the assumed internal sources or points on the passive receiver satisfying force reconstruction was achieved for an experimentally applied reference force. Blocked force time signatures were achieved for all assumed internal sources retaining distinct transient features of the sources. At this stage no further research could be devoted to validate the reconstructed time signatures. However, this first attempt to conduct in-situ source characterisation based on an alternative rattle test bench approach has already yielded some new interesting details about the characteristics of the internal sources.

Furthermore, some basic limitations of test bench measurement approach have been discussed. One major drawback of the test bench measurement approach has been found to result from the need to apply external (EBR) excitation to both tie rods of the steering system which have found to contribute to the structural responses utilised in the time domain inversion routine. Two strategies have been derived that in theory can compensate for contributions to the operational responses induced by the EBR excitation. One of these strategies further allows defining two useful criteria to monitor and interrupt the iterative process involved in the time domain inverse method. The normalised misalignment has been defined for the known tie rod force and which can potentially serve as reliable indicator of the convergence behaviour of the iterative process. Further, the spectral estimation error in the reconstructed tie rod forces have been found to serve as useful indicators of frequencies at which forces cannot be recovered exactly.

To conclude, a number of different approaches have been introduced in this chapter that all have found to contribute well to achieve a general methodology to characterise transient structure-borne sound sources inside electrical steering systems based on a novel time domain in-situ blocked force routine. Although, further research, in particular with regard to realistic test bench measurements to excite the internal source regions is required it is speculated that the developed time domain source characterisation routine is a significant contribution towards better understanding the general problem of transient structure-borne sound within electrical steering systems.

Chapter 6

Concluding remarks and future work

During certain driving situations, e.g. driving on poorly conditioned pavement or rapid (standstill) steering, transient forces at random times can be originated at multiple different source regions inside (electric power) rack-and-pinion steering systems resulting in unintended acoustical phenomena with likewise transient sound patterns. Depending on the underlying excitation and driving conditions such stochastic phenomena can emerge as rattle, klonk or groan noise which are summarised under the generic term ‘transient sound’. Whenever transient sound emanates from the steering system it is possible that passengers inside the cabin perceive the disturbance and associate its appearance with a defect, even though no mechanical faults are present or the functionality of the steering system is affected. This so-called `perception of a fault´ (PF) is purely dependent on the subjective judgement of the passenger, thus posing high risk for complaints. In order to minimise PF by design, engineers and designers need to have exact knowledge of the internal source locations and the mechanisms that originate transient sound inside the steering gear. It was found that this information cannot be delivered by conventional state-of-the-art approaches used in industrial practice to analyse transient sound phenomena in electrical steering systems. To achieve this information, however, this research project was launched in collaboration with a German steering system manufacturer with the overall aim to develop a methodology and a practical approach facilitating identification and quantification of transient structure-borne sound sources within electrical steering systems. Ideally such a method should be able to separate out intrinsic information about the activity for each of the multiple internal sources from vibration measurements conducted while the steering system is operated either in a car or under similar conditions on a test bench.

To achieve these aims, first the physical problem behind steering induced (transient) structure-borne sound was elaborated. Based on psychological distinguishing criteria a general classification system of steering induced sound was achieved comprising two main groups, i.e. functional steering sound and interfering steering noise. The latter class comprises all types of steering induced transient sound. As fundamental generation mechanisms of transient sound dynamic forces were found that are induced by stick-slip or impact excitation as a result of relative movements between contacting assemblies inside the steering gear. With respect to impact excited transient sound rattling was ranked as the most relevant noise phenomenon. Rattle noise emanates from (electric power) rack-and-pinion steering gears as a result of reverse feedback from the road, the so-called ‘excitation provided by the roadway

surface' (EBR). It was found that the range of operation conditions for EBR cannot exactly be specified due to the diversity of influencing factors including the indeterminacy of the road surface and the time variance of the axle kinematics amongst others.

A conceptual source-path-receiver (SPR) model for rack-and-pinion steering gears was developed that discloses the theoretical locations and the associated generation mechanisms of all potential internal transient sound sources. Furthermore, the SPR model allows for theoretical studies of the vibro-acoustic processes inside the steering system. To achieve this model a methodology based on a systematic sub-structuring approach was suggested in which components located inside the steering gear are grouped according to their relative movement. In this way different component layers with static, rotational or translational motion were identified. Intersections of adjacent layers with different movements were defined as the contact zones at which transient sound sources inside the physical assembly can be expected. On the basis of the available literature and the industrial expertise some of the identified source locations have been ascertained although different approaches are in common practice to identify these sources. In general it was found that no systematic approach comparable to the derived source-path-receiver model or a comparable comprehensive mapping of potential structure-borne sound sources inside (electrical) steering systems has been published to date. For this reason it is speculated that the achieved source-path-receiver model constitutes a significant contribution towards ascertaining the causes of steering induced structure-borne sound within (electric power) rack-and-pinion steering gears. Regarding the general validity of the derived SPR model it is noted that the model should only be used for EPS type steering systems since these are based on the same functional principle. Future work may therefore concentrate on employing the derived sub-structuring methodology to derive equivalent SPR models for steering systems with different functional principles in order to reveal the internal active components and the associated sound generation mechanisms. Furthermore, it is believed that expansion of those models by considering not only sources of transient sound but also sources of functional steering sound could potentially provide further guidance for engineers and designers to address a variety of different NVH problems by theoretical studies of the underlying structure-borne sound generation, transmission and propagation processes inside the steering system. However, the main contribution of the presented source-path-receiver model to the development of a source characterisation approach for transient structure-borne sound sources was the disclosure of all theoretical source locations inside the

steering gear. This information formed the basis to develop a measurement procedure to experimentally characterise the internal structure-borne sound source independently of whether the steering system is installed on a test bench or inside a vehicle.

To address the problem of independent source characterisation an extensive literature research on experimental methods was conducted. In a comprehensive review the most promising measurement approaches were discussed. In general, theses techniques require the measurement of passive properties, normally characterised by frequency response functions (FRFs) such as mobility or accelerance functions, as well as active properties; of which the latter are generally more difficult to measure. One line of research focuses on source characterisation in terms of power using prediction approaches, such as the source descriptor [63], the characteristic power, the mirror power or the maximum power [38]. A second line of research employs measurement approaches that characterise the source activity in terms of the free velocity [39],[84],[45],[54] or the blocked force [85], which were found to be more suitable for the given characterisation purpose. It was discussed that measuring free velocity and blocked forces incorporates several practical limitations. For example, measurement of the free velocity requires operation of the vibration source whilst it is separated from any rigid support structure which prohibits characterisation of sources running under load or rather to account for internal excitation mechanisms that vary with the external loading. On the other hand, the blocked force approach theoretically allows operating vibration sources under load but limitations result from the need for large and rigid test rigs to approximate true blocked terminations over sufficient frequency ranges and from difficulties with directly measuring all interfacial blocked forces between the source and the receiver for sophisticated multi-point-connected systems without influencing the interfacial conditions.

Research into alternative characterisation methods revealed that partially conducted in-situ measurements of operational forces at the source receiver interface using inverse force synthesis [34] ensure realistic operation and mounting conditions and prevent placing instrumentation within the sensitive contact zone. However, it was argued that the obtained forces are not an independent property of the source but they also depend on the structural dynamic properties of the connected receiver so that source characterisation is only possible for a specific installation. Finally, the in-situ blocked force method [9] was found capable to conduct independent source characterisation without the need, at any stage, to separate the source from the receiver, thus facilitating both practicability and operation of the source under

realistic conditions. The in-situ blocked force method employs inverse methods in frequency domain, in which measured structural responses are propagated back to the assumed known source regions by inverting matrices containing pre-measured FRFs. This, however, was found to be disadvantageous. In this respect it was argued that the associated inversion problem is an ill-posed one to which solutions based on matrix inversion in frequency domain are generally known to be sensitive to measurement noise and to suffer from numerical ill-conditioning at frequencies associated with the natural frequencies of the structures. Usually, the robustness of such solutions has to be improved artificially by applying some form of regularisation. Furthermore, it was argued that addressing source characterisation in frequency domain could lead to obscuring some essential features of the originating source mechanisms, such as transient or impulsive signatures, and that source characterisation under non-stationary operation conditions may be difficult. To overcome these hurdles, the idea of achieving independent source characterisation in time domain was proposed.

To achieve such a time domain approach a comprehensive literature research was conducted and a comprehensive review on time domain force identification was achieved considering direct deconvolution techniques, modal filtering techniques, state-space methods such as inverse filtering and Kalman filtering, as well as sensitivity methods. It was found that some of these methods have fundamental limitations while others lack in generality with respect to the underlying assumptions, the way they describe the physical system or the need for additional information to parameterise the algorithms, so that they are not practicable for sophisticated structure-borne sound problems. The most promising approach was found to be a method incorporating an adaptive algorithm in time domain that has only been studied for relatively simple structures with single-degree of freedom excitation. Due to the expected significant potential advantages, it was decided to generalise the adaptive force identification technique for multi-degree of freedom excited structures and to develop a time domain equivalent of the in-situ blocked force method facilitating simultaneous calculation of multi-channel blocked force signatures from measurement made in-situ. Both the generalisation of the time domain inversion routine and its application in independent source characterisation is believed to be original.

By gradually modifying the Least Mean Square (LMS) algorithm, which is widely used in adaptive filter design due to its robustness and simplicity, the generalisation of the time domain inversion routine (TDM) was achieved. This novel time domain inversion routine is

capable of separating simultaneous multi-channel force signatures from a set of operational responses measured on structures with known and fixed force input locations. It was discussed that the TDM incorporates a model of the physical system built up of impulse response functions (IRFs) which can be obtained by employing inverse Fourier transformation to pre-measured frequency response functions (FRFs). Since the latter can easily be measured experimentally invoking conventional system identification methods, such as (roving hammer) impact testing reliable system models can be realised even for highly sophisticated technical structures, such as electric power steering systems. The iterative process involved in the TDM was elaborated. In brief, the iterative process, at each time step, utilises the obtained IRFs to filter a set of estimated input force signatures so as to predict a corresponding set of structural responses. The instantaneous errors between the estimated and measured responses are then used to update the input force time histories recursively. It was shown that all data-processing steps involved in the TDM are carried out in an invariable forward manner which is believed to pose one of the major advantages of the method in contrast to other inverse methods, such as standard frequency domain inverse methods (FDM). At no stage the iterative process involved in the generalised TDM needs to rely on inversion of a possibly ill-conditioned FRF matrix nor requires extensive regularisation techniques to improve the solutions. It was discussed that in the standard FDM ‘weak’ paths bring about dominant contributions after inversion, which are highly susceptible to noise. Instead, it was shown that always the measurement point with the strongest signal dominates the inversion process in the generalised TDM. This was also found to be the reason why the TDM is generally insensitive to the choice of measurement positions as against the conventional FDM.

In numerical experiments it was proved that the novel time domain inversion routine allows reconstruction of multiple uncorrelated, correlated or partially correlated forces that can feature any kind of sparse or non-sparse time signature including random, periodic, impulsive, irregular or steady state signals. Furthermore, it was discussed that under the assumption that the available response data is at least twice the length of the employed IRFs, the TDM facilitates continuous processing of time data of arbitrary length thus allowing all sorts of post-processing for each individual identified force signature which speculated to pose an attractive prospect for many industrial demands like time domain TPA, auralisation purposes or condition monitoring applications.

Due to the implementation of an averaged error gradient in the iterative recursion to update each force individually the TDM can be applied to perform inverse force identification in

overdetermined system. Based on numerical simulations it was affirmed that for overdetermined systems the generalised TDM is very robust to noise included in the response data or errors inherent in the system model. Under the assumption that these disturbances are uncorrelated and the system is sufficiently overdetermined the averaged error gradients were found capable to significantly suppress the negative influences of the perturbations on the force reconstruction process even when the used data comprises considerable errors. It was further discussed that in the presence of defective data the averaged error gradients can cause substantial errors in the reconstructed response spectra. However, the spectral shapes of these errors were found to be suitable indicators to identify frequency bands in which force reconstruction is generally subject to high uncertainty due to insufficient system descriptions. This additional information is not available when conducting inverse force identification with the standard FDM.

By comparison it was found that the FDM and the TDM perform equally if the used data can be assumed to be noise free or if noise is only included in the response data. Due to the availability of additional information concerning the reliability of the identified forces it was argued that the use of the generalised TDM for these cases is at least of avail. However, in the presence of (uncorrelated) errors comprised in system model comprises the novel time domain inversion routine proved to generally yield more robust and accurate force reconstruction results than the standard FDM. It was found that force spectra estimated with the generalised TDM can be at least an order of magnitude superior to the ones obtained with the standard FDM at frequencies at which the corresponding FRF matrices are poorly conditioned. Further is was found that the advantages of the TDM over the FDM become more significant with increasing degree of overdetermination and increasing levels of perturbation.

As a major drawback of the TDM it was found that the method lacks in a reliable measure to evaluate the accuracy of the force prediction or rather to define an objective criterion to interrupt the iterative force reconstruction process. Future work is required to obtain such a criterion. Some potential ways to achieve this were elaborated. Amongst them, the observance of the evolution of the introduced expanded relative mean prediction error (E-RMPE) was found to be a good means to monitor the overall progress of the iterative process. It was outlined that the gradient or the curvature of the E-RMPE could be used to develop reliable interruption criteria in future studies.

It was discussed that the stability and speed of adaptive algorithm involved in the generalised TDM is dependent on the choice of the convergence-determining step size parameter μ_s. A large step size parameter makes the adaption fast, while a small value is likely to make the residual error between the true and the reconstructed forces close to the minimum. In this respect it was argued that an implementation of a variable step size parameter, as proposed e.g. in [210] or [211] with respect to adaptive filter design, could offer big potential to optimise the prediction accuracy and the speed of the adaptive process at the same time. An alternative approach to the variable step size parameter was also outlined in which the step size parameter could be adjusted according to the evolution of the E-RMPE. The practicability and implementation of adjustable or variable step size parameters in the time domain inversion routine should be investigated in future research projects.

In order to use the novel time domain inversion routine for independent characterisation of the structure-borne sound sources in electrical steering systems a test bench measurement approach to obtain operational response data as well as the structural dynamic of the passive structure is required. It was found that rattle noise within (electric power) rack-and-pinion steering gears can sufficiently be provoked by means of specially designed test benches that simulate the dynamic excitation feedback from the roadway surface (EBR) using pre-measured tie rod forces from actual vehicle tests. Thus, operational data can be sufficiently provided by performing standard test bench measurements.

Considering the passive properties, an in-situ measurement approach was discussed allowing measurement of frequency response functions (FRFs) whilst the steering system is connected to the rattle test bench. To obtain suitable system models two different criteria were presented that facilitate evaluation of the measurement quality for driving-point and transfer FRFs. Both criteria are based on the positive definite property of the real part of the square mobility matrix; the latter is sometimes denoted as conductance. The ‘Conductance Value’ (CV) was introduced as a simple check on measured driving-point mobilities and is based on the passivity condition requiring their real parts always to be positive. For transfer mobilities the so-called ‘Eigenvalue Measure’ (EM) was defined which utilises a partitioning approach to obtain eigenvalues for the real part of the corresponding mobility sub-matrices. Due to the positive definite property these eigenvalues need to be positive otherwise they indicate erroneous measurements. Both criteria, the CV and the EM, were grouped under the term ‘Conductance Assurance Criteria’ (CAC) yielding normalised frequency independent single

values between zero and one that facilitates convenient illustration in coloured matrices arranged according to the actual matrices. In this way easy and fast evaluation of all transfer and point FRF measurements is possible. Compared to conventional data evaluation criteria based on the reciprocity principle such as the Frequency Response Assurance Criterion (FRAC) or the Phase Assurance Criterion (PAC), the CAC was found to provide more detailed information about the physical correctness of the used data while requiring only insignificant bigger measurement effort. Furthermore, the CAC can still be used to disclose whether or not FRF measurements contain physical meaningful information for cases in which only one transfer mobility and the corresponding two point mobilities are measurable. Although the basic idea of the presented data evaluation approach is not new the procedure to calculate the CAC values as well as their representation in easy-to-read colour matrices is believed to be original and to be a useful contribution.

Further it was discussed how the checked FRF data has to be processed in order to obtain impulse response functions of suitable length that can be utilised by the time domain inverse method.

One major drawback of the test bench measurement approach was found to result from the need to apply external (EBR) excitation to both tie rods of the steering system. It was discussed that this additional excitation contributes to the structural responses utilised in the TDM to predict blocked force signatures for the sources inside the steering gear. Based on an introduced time domain formulation for the operational responses, two strategies were derived that compensate for contributions to the operational responses induced by the EBR excitation. Strategy 1 allows for correcting the measured structural response data by separating the internal source contribution term from the tie rod excitation term. The adaptive algorithm used in the generalised TDM was modified in order to account for these corrected response signals. Strategy 2 relies on considering all internal and external forces in the TDM at once at the expense of the computational effort. However, two useful criteria for monitoring the inverse force reconstruction process were introduced based on strategy 2. The normalised misalignment was defined for the known tie rod excitations and was found to be a reliable indicator of the convergence behaviour of the iterative process. Further, the spectral estimation errors in the reconstructed tie rod forces were found to serve as useful indicators of frequencies at which forces cannot be recovered exactly. It was emphasised that both criteria are good means to define more reliable interruption criteria for the iterative process involved in the TDM than the expanded relative mean prediction error (E-RMPE).

To test the methodology discussed so far different experiments were carried out considering artificial and test bench excitation applied to the steering system whilst connected to a test bench. All measurements were conducted according to the requirements of the in-situ blocked force method. Considering artificial excitation first, single and multiple long-duration (20 seconds) impulsive force signatures were satisfactorily recovered from noisy response measurements conducted in-situ under normal testing conditions. Errors in the identified forces were traced back to errors in the employed FRF measurements or problems with exciting the source regions in the considered degree of freedom. Despite possible errors in the magnitudes of the reconstructed force time histories all transient peaks in the signals were unambiguously detected, allowing for identifying which source, at which time, contributed to the observed structural responses. This information cannot be gained with the conventional state-of-the-art approach. Further, the experiments showed that sufficient source characterisation is possible by placing sensors only on the receiver-side, i.e. the test bench, so that the proposed method does not require installation of sensors on the housing of the steering system each time when the steering system is swapped as against the conventional approach. It was discussed that the time domain in-situ approach therefore is very appealing with respect to end-of-line testing. However, additional research is required to investigate if such an end-of-line test could be realised at all.

Considering source characterisation based on test bench excitations the developed time domain in-situ blocked force method was applied for the first time to reconstruct time domain blocked forces for multiple transient sources excited by external rattle excitation. Despite problems with measuring the FRFs between the tie rods to the assumed internal sources or points on the passive receiver satisfying force reconstruction was achieved for an experimentally applied reference force. Blocked force time signatures were achieved for all assumed internal sources retaining distinct transient features of the sources. At this stage no further research could be devoted to validate the reconstructed time signatures. However, this first attempt to conduct in-situ source characterisation based on an alternative rattle test bench approach has already yielded some new interesting details about the characteristics of the internal sources. Furthermore, two criteria were presented that can be used in future applications to identify the most dominant transient events in the achieved source signals. Furthermore, an approach to better characterise the transfer paths between the tie rods and all other points on the assembly was discussed. However, future research is required in order to further test the methodology in the context of test bench excited transient sound.

The concept of Virtual Acoustic Prototyping (VAP) was mentioned as a powerful tool that in combination with the derived source characterisation method could potentially enable noise control engineers to rank order the different internal transient sound sources according to their partial contributions to the perceived interior vehicle sound. In this way, engineers would be able to identify and optimise dominant internal sources or to evaluate whether primary design modifications on the active sources or secondary actions on the conducting passive structure are required to minimise PF. Therefore, future research should be devoted to developing a detailed VAP of a steering system considering multiple internal sources. In this respect, the achieved time domain source characterisation method could be use to provide blocked force time signatures for the individual sources of arbitrary length making auralisation and post-processing convenient.

References

[1] K. Genuit, *Sound-Engineering im Automobilbereich - Methoden zur Messung und Auswertung von Geräuschen und Schwingungen*, Springer Verlag, 2012.

[2] P. Pfeffer and M. Harrer, *Lenkungshandbuch - Lenksysteme, Lenkgefühl, Fahrdynamik von Kraftfahrzeugen*, Vieweg+Teubner Verl., 2011.

[3] T. Verkoyen, *Aktive Sekundärmaßnahmen zur Vermeidung von fahrzustandsabhängigen Geräuschen in hydraulischen Lenksystemen*, Shaker Verlag, 2009.

[4] A.T. Moorhouse, "Virtual Acoustic Prototype as a tool for low-noise design", *Proceedings of the Institute of Acoustics*, vol. 24, 2002.

[5] A. Moorhouse and L. Gavric, "Source characterisation of active internal components for Virtual Acoustic Prototypes", *Processings of Euronoise 2003*, Naples, Italy, 2003, paper ID: 289.

[6] A. Moorhouse, "Virtual Acoustic Prototypes: Listening to machines that don't exist", *Acoustics Australia*, vol. 33(3), 2005, pp. 97-105.

[7] M. Bauer, *Virtual Acoustic Prototyping: Characterisation of a steering system and prediction of structure-borne sound*, PhD Thesis, University of Salford, 2011.

[8] M. Hesselmeier, *Virtual Acoustic Prototyping*, Diplomarbeit, Hochschule für angewandte Wissenschaften Coburg, 2012.

[9] A.T. Moorhouse, A.S. Elliott and T.A. Evans, "In situ measurement of the blocked force of structure-borne sound sources", *Journal of Sound and Vibration*, vol. 325(4), 2009, pp. 679-685.

[10] M. Bauer, A.T. Moorhouse and T. Alber, "Virtual Acoustic Prototyping for electrical steering systems", *Proceedings of DAGA 2011*, Berlin, Germany, 2011, pp. 787-788.

[11] H.-H. Braess and U. Seifert, *Handbuch Kraftfahrzeugtechnik*, Friedr. Vieweg & Sohn Verlag, 2007.

[12] P. Zeller, *Handbuch Fahrzeugakustik: Grundlagen, Auslegung, Berechnung, Versuch*, Vieweg+Teubner Verl., 2009.

[13] P. Pfeffer and M. Harrer, *Lenkungshandbuch - Lenksysteme, Lenkgefühl, Fahrdynamik von Kraftfahrzeugen*, Vieweg+Teubner Verl., 2011.

[14] Y. Kozaki, G. Hirose, S. Sekiya and Y. Miyaura, "Electric Power Steering (EPS)", *NSK Technical Journal - Motion&Control*, vol. 6, 1999, pp. 9-15.

[15] Q.-H. Vo, *Soundengineering: kundenbezogene Akustikentwicklung in der Fahrzeugtechnik*, Expert-Verlag, 1994.

[16] L. Cremer, M. Heckl and E.E. Ungar, *Structure-Borne Sound*, Springer-Verlag, 1987.

[17] A. Elliott, *Characterisation of structure borne sound sources in-situ*, PhD Thesis, University of Salford, 2009.

[18] A. Elliott and A.T. Moorhouse, "Characterisation of structure borne sound sources from measurement in-situ", *Proceedings of Acoustics 2008*, Paris, France, 2008.

[19] P.V.D. Ponseele, H.V.D. Auweraer and K. Janssens, "Source-Transfer-Receiver approaches: a review of methods", *Proceedings of International Conference on Noise and Vibration Engineering (ISMA)*, Leuven, Belgium, 2012, pp. 3617-3630.

[20] A.N. Thite and D.J. Thompson, "The quantification of structure-borne transmission paths by inverse methods. Part 1: Improved singular value rejection methods", *Journal of Sound and Vibration*, vol. 264(2), 2003, pp. 411-431.

[21] A.N. Thite and D.J. Thompson, "The quantification of structure-borne transmission paths by inverse methods. Part 2: Use of regularization techniques", *Journal of Sound and Vibration*, vol. 264(2), 2003, pp. 433-451.

[22] P. Hynnä, *Vibrational power methods in control of sound and vibration*, Research report, VTT Technical Research Centre of Finland, 2002.

[23] M.H.A. Janssens and J.W. Verheij, "A pseudo-forces methodology to be used in characterization of structure-borne sound sources", *Applied Acoustics*, vol. 61(3), 2000, pp. 285-308.

[24] B.A.T. Petersson and B.M. Gibbs, "Towards a structure-borne sound source characterization", *Applied Acoustics*, vol. 61(3), 2000, pp. 325-343.

[25] B.M. Gibbs, N. Qi and A.T. Moorhouse, "A practical characterisation for vibro-acoustic sources in buildings", *Acta Acustica united with Acustica*, vol. 93(1), 2007, pp. 84-93.

[26] P. Gardonio and M.J. Brennan, "Mobility and impedance methods in structural dynamics", *Advanced Applications in Acoustics, Noise & Vibration*, vol. 9, 2004, pp. 389-447.

[27] M. Ohlrich, "Predicting transmission of structure-borne sound power from machines by including terminal cross-coupling", *Journal of Sound and Vibration*, vol. 330(21), 2011, pp. 5058-5076.

[28] H.W. Engl, M. Hanke and M. Neubauer, *Regularization of Inverse Problems*, Kluwer Academic Publisher, 2000.

[29] P.C. Hansen, *Rank Deficient and Discrete Ill Posed Problems: Numerical Aspects of Linear Inversion*, Society for Industrial and Applied Mathemetics, 1998.

[30] K. Worden and G.R. Tromlinson, *Nonlinearity in structural dynamics - Detection, Identification and Modelling*, Institute of Physics Publishing (UK), 2001.

[31] M. Street, "Identification of non-linear systems using multi-scale ridges and skeletons of the wavelet transform", *Journal of Sound and Vibration*, vol. 214(4), 1998, pp. 639-658.

[32] D.E. Adams and R.J. Allemang, "Survey of nonlinear detection and identification techniques for experimental vibrations", *Proceedings of the International Seminar on Modal Analysis (ISMA)*, Leuven, Belgium, 1998, pp. 269-282.

[33] K. Worden and A.F. Vakakis, "Past, present and future of nonlinear system identification in structural dynamics," *Mechanical Systems and Signal Processing*, vol. 20(3), 2006, pp. 505-592.

[34] B.J. Dobson and E. Rider, "A review of the indirect calculation of excitation forces from measured structural response data", *Proceedings of the Institution of Mechanical Engineers Part C: Journal of Mechanical Engineering Science*, vol.204(2), 1990, pp. 69–75.

[35] H. Inoue, J.J. Harrigan and S. Reid, "Review of inverse analysis for indirect measurement of impact forces", *Applied Mechanics Reviews*, vol. 54(6), 2001, pp. 503-524.

[36] R.J. Hundhausen, D.E. Adams, M. Derriso, P. Kukuchek and R. Alloway, "Transient loads identification for a standoff metallic thermal protection system panel," *Proceedings of 23rd International Modal Analysis Conference (IMAC XXIII)*, Orlando,Florida, 2005.

[37] K.F. Steinberg, *With all senses*, WJR-Verlag, 2007.

[38] A.T. Moorhouse, "On the characteristic power of structure-borne sound sources", *Journal of Sound and Vibration*, vol. 248(3), 2001, pp. 441-459.

[39] T. Ten Wolde and T.G.R. Gadefelt, "Development of standard measurement methods for structure-borne sound emission", *Noise Control Engineering Journal*, vol. 28, 1987, pp. 5-14.

[40] H. Bodén, "Characterisation of fluid-borne and structure- borne sound sources," *Proceedings of the 9th International Congress on Sound and Vibration*, Florida, USA, 2002.

[41] M. Ohlrich, "Structure-borne sound sources and their power transfer," *Proceedings of Inter-Noise 2001*, The Hague, Netherlands: 2001.

[42] J.W. Verheij, “Inverse and reciprocity methods for machinery noise source characterization and sound path quantification, Part 1: Sources”, *International Journal of Acoustics and Vibration*, vol. 2(3), 1997, pp. 11-20.

[43] J.W. Verheij, “Inverse and Reciprocity Methods for machinery noise source characterization and sound path quantification, Part 2: Transmission paths”, *International Journal of Acoustics and Vibration*, vol. 2(3), 1997, pp. 103-112.

[44] R.A. Fulford and B.M. Gibbs, “Structure-borne sound power and source characterisation in multi-point-connected systems, Part 1: Case studies for assumed force distributions”, *Journal of Sound and Vibration*, vol. 204(4), 1997, pp. 659-677.

[45] R.A. Fulford and B.M. Gibbs, “Structure-borne sound power and source characterisation in multi-point-connected systems, Part 2: About mobility functions and free velocities”, *Journal of Sound and Vibration*, vol. 220(2), 1999, pp. 203-224.

[46] R.A. Fulford and B.M. Gibbs, “Structure-borne sound power and source characterisation in multi-point-connected systems, Part 3: Force ratio estimates”, *Journal of Sound and Vibration*, vol. 225(2), 1999, pp. 239-282.

[47] B.M. Gibbs and A.T. Moorhouse, “Case studies of machine bases as structure-borne sound sources in buildings,” *International Journal of Acoustics and Vibration*, vol. 4(3), 1999, pp. 125-133.

[48] T. Evans, *Estimation of uncertainty in the structure- borne sound power transmission from a source to a receiver*, PhD Thesis, University of Salford, 2010.

[49] G. Pavić and A.S. Elliott, “Structure-borne sound characterization of coupled structures - Part I: Simple demonstrator model”, *Journal of Vibration and Acoustics*, vol. 132(4), 2010.

[50] G. Pavić and A.S. Elliott, “Structure-borne sound characterization of coupled structures - Part II: Feasibility study”, *Journal of Vibration and Acoustics*, vol. 132(4), 2010.

[51] A.T. Moorhouse, T.A. Evans and A.S. Elliott, “Some relationships for coupled structures and their application to measurement of structural dynamic properties in situ”, *Mechanical Systems and Signal Processing*, vol. 25(5), 2011, pp. 1574-1584.

[52] H.A. Bonhoff, “Drei Linien der Entwicklung von Methoden zur Charakterisierung von Körperschallquellen”, *Proceedings of DAGA 2011*, Düsseldorf, Germany, 2011, pp. 783-784.

[53] H.A. Bonhoff and B.A.T. Petersson, “Towards a structure borne sound source characterisation for design and optimisation,” *Proceedings of Recent Advances in Structural Dynamics (RASD)*, Southampton, UK: 2010.

[54] International Standards Organisation ISO 9611, “Acoustics—characterisation of sources of structure-borne sound with respect to sound radiation from connected

structures—measurement of velocity at the contact points of machinery when resiliently mounted", 1996.

[55] A.T. Moorhouse, R.D. Cookson and G. Seiffert, "Measurement of operating forces of an electric motor", *Proceedings of the National Conference on Noise Control Engineering (Noise-Con 04),* Baltimore, Maryland, 2004, pp. 64-75.

[56] M.M. Späh and B.M. Gibbs, "Reception plate method for characterisation of structure-borne sound sources in buildings: Assumptions and application", *Applied Acoustics*, vol. 70(2), 2009, pp. 361-368.

[57] M.M. Späh and B.M. Gibbs, "Reception plate method for characterisation of structure-borne sound sources in buildings: Installed power and sound pressure from laboratory data", *Applied Acoustics*, vol. 70(11), 2009, pp. 1431-1439.

[58] J. Lu, B. Louvigne, J.C. Pascal and J. Tourret, "The perforated reception plate; a practical method for the characterization of structure-borne noise emitted by small equipment", *Proceedings of Inter-Noise'90*, Goteborg, Sweden, 1990, pp. 217-220.

[59] M.M. Späh, B.M. Gibbs, and H.-M. Fischer, "Measurement of structure- borne sound power of mechanical installations in buildings", *Proceedings of the 11th International Congress on Sound and Vibration*, St.Petersburg, Russia: 2004, pp. 3377–3384.

[60] European Standard EN 15657-1, "Acoustic properties of building elements and of buildings -Laboratory measurement of airborne and structure borne sound from building equipment - Part 1: Simplified cases where the equipment mobilities are much higher than the receiver mobilities", 2009.

[61] European Standard EN 12354-5, "Building acoustics – Estimation of acoustic performance of buildings from the performance of elements – Part 5: Sound levels due to the service equipment", 2009.

[62] H.A. Bonhoff and B.A.T. Petersson, "Towards a structure-borne sound source characterization for low-noise design", *Applied Acoustics*, 2010.

[63] J.M. Mondot and B. Petersson, "Characterization of structure-borne sound sources: The source describtor and the coupling function", *Journal of Sound and Vibration*, vol. 114(3), 1987, pp. 507-518.

[64] B. Petersson and J. Plunt, "On effective mobilities in the prediction of structure-borne sound transmission between a source structure and a receiving structure, part I: Theoretical background and basic experimental studies", *Journal of Sound and Vibration*, vol. 82(4), 1982, pp. 517-529.

[65] B. Petersson and J. Plunt, "On effective mobilities in the prediction of structure-borne sound transmission between a source structure and a receiving structure, part II: Procedures for the estimation of mobilities", *Journal of Sound and Vibration*, vol. 82(4), 1982, pp. 531-540.

[66] B.A.T. Petersson and B.M. Gibbs, "Use of the source descriptor concept in studies of multi- point and multi-directional vibrational sources", *Journal of Sound and Vibration*, vol. 168(1), 1993, pp. 157-167.

[67] A.T. Moorhouse and B.M. Gibbs, "Measurement of the characteristic power of structure- borne sound sources", *Proceedings of International Congress on Sound and Vibration*, Lyngby, Denmark: 1999, pp. 2161–2168.

[68] S. Laugehsen and M. Ohlrich, "The vibrational source strength descriptor using power input from equivalent forces: a simulation study", *Acta Acustica*, vol. 2(6), 1994, pp. 449-459.

[69] M.H.A. Janssens, J.W. Verheij and D.J. Thompson, "The use of an equivalent force method for the experimental quantification of structural sound transmission", *Journal of Sound and Vibration*, vol. 226(2), 1999, pp. 305-328.

[70] M.H.A. Janssens, J.W. Verheij and T. Loyau, "Experimental example of the pseudo-forces method used in characterisation of a structure-borne sound source", *Applied Acoustics*, vol. 63(1), 2002, pp. 9-34.

[71] H.-Y. Lai, "Alternative test methods for measuring structure-borne sound power", *Proceedings of Inter-Noise and Noise-Con*, Honolulu, Hawai: 2006, vol.2006(5), pp. 2515-2524.

[72] R.J. Pinnington and D.C. Pearce, "Multipole expansion of the vibration transmission between a source and a receiver", *Journal of Sound and Vibration*, vol. 142(3), 1990, pp. 461-479.

[73] R.J. Pinnington, R.A. Fulford and M. Terry, "The use of polar mobilities for predicting the coupled response of machine mounting systems", *Proceedings of Inter-Noise'96*, Liverpool, UK, 1996, pp. 1587-1592.

[74] L. Ji, B.R. Mace and R.J. Pinnington, "A power mode approach to estimating vibrational power transmitted by multiple sources", *Journal of Sound and Vibration*, vol. 265(2), 2003, pp. 387-399.

[75] A.T. Moorhouse and B.M. Gibbs, "Simplified characterisation of multiple point excited structures using mobility eigenvalues and eigenvectors", *Acta Acustica united with Acustica*, vol. 84(5), 1998, pp. 843-853.

[76] J. Su, A.T. Moorhouse and B.M. Gibbs, "Towards a practical characterisation for structure-borne sound sources based on mobility techniques", *Journal of Sound and Vibration*, vol. 185(4), 1995, pp. 737-741.

[77] H.A. Bonhoff and B.A.T. Petersson, "The influence of cross-order terms in interface mobilities for structure-borne sound source characterization: Plate-like structures," *Journal of Sound and Vibration*, vol. 311(1), 2008, pp. 473-484.

[78] H.A. Bonhoff and B.A.T. Petersson, “The influence of cross-order terms in interface mobilities for structure-borne sound source characterization: Frame-like structures,” *Journal of Sound and Vibration*, vol. 319(1), 2009, pp. 305-319.

[79] H.A. Bonhoff, “Interface Mobilities for low-noise design of structure-borne sound sources”, *Proceedings of Forum Acusticum*, Aalborg, Denmark: 2011, pp. 2351-2356.

[80] H.A. Bonhoff and B.A.T. Petersson, “The influence of cross-order terms in interface mobilities for structure-borne sound source characterization”, *Journal of Sound and Vibration*, vol. 329(16), 2010, pp. 3280-3303.

[81] P. Hynnä, *Mechanical mobility technique*, Research report, VTT Technical Research Centre of Finland, 2002.

[82] S.A. Sands, P. Camilleri, R.A. Breuer, G.K. Cambrell, R.J. Alfredson, E.M. Skuza, P.J. Berger and M.H. Wilkinson, “A novel method for the measurement of mechanical mobility,” *Journal of Sound and Vibration*, vol. 320(3), 2009, pp. 559-575.

[83] L.H. Ivarsson and M.A. Sanderson, “MIMO technique for simultaneous measurement of translational and rotational mobilities”, *Applied Acoustics*, vol. 61(3), 2000, pp. 345-370.

[84] L. Cremer, M. Heckl and B.A.T. Petersson, *Structure-borne sound: structural vibrations and sound radiation at audio frequencies*, Springer Verlag, 2005.

[85] P. Gardonio and M.J. Brennan, “Mobility and impedance methods in structural dynamics”, *Advanced Applications in Acoustics, Noise and Vibration*, vol. 2004(9), pp. 389-447.

[86] A. Schuhmacher and D. Tcherniak, “Engine contribution analysis using a noise and vibration simulator”, *Sound and Vibration*, vol. 43(1), 2009, pp.16.

[87] D. Tcherniak and A. Schuhmacher, “Application of decomposition-based technique in NVH source contribution analysis”, *Proceedings of ISMA*, Leuven, Belgium: 2008, pp. 3139-3152.

[88] A. Elliott, A.T. Moorhouse and G. Pavic, “Characterisation of a structure-borne sound source using independent and in-situ measurement”, *Proceedings of 19th International Congress on Acoustics (ICA’07)*, Madrid, Spain: 2007.

[89] A. Moorhouse, T. Evans and A. Elliott, “Structure-borne sound from building-mounted wind turbines”, *Proceedings of Forum Acusticum*, Aalborg, Denmark: 2011, pp. 2405-2410.

[90] A. Moorhouse, A. Elliott and T. Evans, “Indirect measurement of structural frequency response function (FRF) matrices and free velocity”, *Proceedings of Forum Acusticum*, Aalborg, Denmark: 2011, pp. 2297-2302.

[91] Y.I. Bobrovnitskii, "A theorem on the representation of the field of forced vibrations of a composite elastic system," *Acoustical Physics*, vol. 47(5), 2001, pp. 586-589.

[92] H.-Y. Lai, "Alternative test methods for measuring structure-borne sound power", *Proceedings of Inter-Noise and Noise-Con*, Honolulu, Hawai: 2006, vol.2006(5), pp. 2515-2524.

[93] A.S. Elliott and A.T. Moorhouse, "Characterisation of vibration sources in-situ", *Proceedings of Novem 2009*, Oxford, UK: 2009, pp. 132.

[94] A.T. Moorhouse and A.S. Elliott, "Application of an in situ measurement method for characterisation of structure-borne sound generated by building-mounted wind turbines", *Proceedings of Inter-Noise and Noise-Con*, vol. 2010(8), 2010, pp. 2780-2789.

[95] A. Moorhouse, A. Elliott, G. Eastwick, T. Evans, A. Ryan, V. Bescond and D. Waddington, *Noise and vibration from building-mounted micro wind turbines (NANR244), Part 2: Results of measurement and analysis*, Defra, London: 2011.

[96] A.S. Elliott and A.T. Moorhouse, "In-situ characterisation of structure borne noise from a building mounted wind turbine", *Proceedings of ISMA 2010*, Leuven, Belgium: 2010, pp. 2055-2068.

[97] M. Thivant and A. Carbonelli, "Derivation of the force interaction within strongly coupled systems - application to diesel engine oil pumps", *Proceedings of ISMA 2010*, Leuven, Belgium: 2010, pp. 2103-2116.

[98] A.S. Elliott, A.T. Moorhouse, T. Huntley and S. Tate, "In-situ source path contribution analysis of structure borne road noise", *Journal of Sound and Vibration*, vol. 332(4), 2013, pp.6276-6295.

[99] A.S. Elliott and A.T. Moorhouse, "A quarter vehicle transfer path analysis by in-situ measurement", *Proceedings of Novem 2012*, Sorrento, Italy: 2012.

[100] Z. Fu, C. Wei and Y. Yang, "Force identification by using SVM and CPSO technique", *Advances in Swarm Intelligence*, Springer Verlag, 2010, pp. 140-148.

[101] F.E. Gunawan, H. Homma and Y. Kanto, "Two-step B-splines regularization method for solving an ill-posed problem of impact-force reconstruction", *Journal of Sound and Vibration*, vol. 297(1), 2006, pp. 200-214.

[102] Q. Zhang, Ł. Jankowski and Z. Duan, "Identification of coexistent load and damage," *Structural and Multidisciplinary Optimization*, vol. 41(2), 2010, pp. 243-253.

[103] L.J.L. Nordström and F. Larsson, "A strategy for input estimation with sensitivity analysis," *International Journal for Numerical Methods in Engineering*, vol. 69(11), 2007, pp. 2219-2246.

[104] T. Alber, G. Speidel, M. Sturm and M. Hudelmaier, “Methods for the characterization of structure-borne sound sources using the example of electrical steering systems”, *Proceedings of Stuttgarter Symposium 2013*, Stuttgart, Germany: 2013.

[105] M. Sturm, T. Alber and T. Akyol, “Determination of dynamic contact forces for MDOF-structures”, *Proceedings of DAGA 2010*, Berlin, Germany: 2010.

[106] A. Gunduz, A. Inoue and R. Singh, “Estimation of interfacial forces in time domain for linear systems”, *Journal of Sound and Vibration*, vol. 329(13), 2010, pp. 2616-2634.

[107] D.C. Kammer, “Input force reconstruction using a time domain technique”, *Transactions-American Society of Mechanical Engineers Journal of Vibration and Acoustics*, vol. 120, 1998, pp. 868-874.

[108] M.S. Allen and T.G. Carne, “Delayed, multi-step inverse structural filter for robust force identification”, *Mechanical Systems and Signal Processing*, vol. 22(5), 2008, pp. 1036-1054.

[109] L. Ljung, *System Identification - Theory for the user*, Prentice-Hall and System Science Series, New Jersey, 1999.

[110] C. Chen and F.-G. Yuan, “Impact source identification in finite isotropic plates using a time-reversal method: Theoretical study”, *Smart Materisals and Structures*, vol. 19(10), 2010, p.105028.

[111] T. Uhl, “The inverse identification problem and its technical application”, *Archive of Applied Mechanics*, vol.77(5), 2007, pp. 325-337.

[112] C.-H. Huang, “An inverse non-linear force vibration problem of estimating the external forces in a damped system with time dependent system parameters”, *Journal of Sound and Acoustics*, vol. 242(5), 2001, pp. 749-765.

[113] E. Jacquelin, A. Bennani and P. Hamelin, “Force reconstruction: Analysis and regularization of a deconvolution problem”, *Journal of Sound and Vibration*, vol. 265(1), 2003, pp. 81-107.

[114] L.J.L. Nordström and P.T. Nordberg, “A time delay method to solve non-collocated input estimation problems”, *Mechanical Systems and Signal Processing*, vol. 18(6), 2004, pp. 1469-1483.

[115] P.C. Hansen, “The L-curve and its use in the numerical treatment of inverse problems”, *IMM*, Department of Mathematical Modelling, Technical University of Denmark, 1999.

[116] C.-H. Huang, “A generalized inverse force vibration problem for simultaneously estimating the time-dependent external forces”, *Applied Mathematical Modelling*, vol. 29(11), 2005, pp. 1022-1039.

[117] L. Jankowski, “Off-line identification of dynamic loads”, *Structural and Multidisciplinary Optimization*, vol. 37(6), 2008, pp. 609-623.

[118] S.S. Simonian, “Inverse problems in structural dynamics - I. Theory”, *International Journal for Numerical Methods in Engineering*, vol. 17(3), 1981, pp. 357–365.

[119] S.S. Simonian, “Inverse problems in structural dynamics - II. Applications”, *International Journal for Numerical Methods in Engineering*, vol. 17(3), 1981, pp. 367–386.

[120] L.J.L. Nordström, “A dynamic programming algorithm for input estimation on linear time-variant systems”, *Computer Methods in Applied Mechanics and Engineering*, vol. 195(44), 2006, pp. 6407-6427.

[121] T.P. Nordberg and I. Gustafsson, “Dynamic regularization of input estimation problems by explicit block inversion”, *Computer Methods in Applied Mechanics and Engineering*, vol. 195(44), 2006, pp. 5877-5890.

[122] B. Hillary and D. Ewins, “The use of strain gauges in force determination and frequency response function measurements”, *Proceedings of IMAC*, vol. 2, 1984.

[123] K.K. Stevens, “Force identification problems-an overview”, *Proceedings of the 1987 SEM Spring Conference on Experimental Mechanics*, Houston, Texas: 1987, pp. 838-844.

[124] J.M. Starkey and G.L. Merrill, “On the ill-conditioned nature of indirect force measurement techniques”, *Journal of Modal Analysis*, vol. 4(3), 1989, pp. 103-108.

[125] J.F. Doyle, “Force identification from dynamic responses of a bimaterial beam”, *Experimental Mechanics*, vol. 33(1), 1993, pp. 64-69.

[126] C.-K. Ma, P.-C. Tuan, D.-C. Lin and C.-S. Liu, “A study of an inverse method for the estimation of impulsive loads”, *International Journal of Systems Science*, vol. 29(6), 1998, pp. 663-672.

[127] Y.M. Mao, X.L. Guo and Y. Zhao, “A state space force identification method based on Markov parameters precise computation and regularization technique”, *Journal of Sound and Vibration*, vol. 329(15), 2010, pp. 3008-3019.

[128] K. Chandrashekhara, A.C. Okafor and Y.P. Jiang, “Estimation of contact force on composite plates using impact-induced strain and neural networks”, *Composites Part B: Engineering*, vol. 29(4), 1998, pp. 363-370.

[129] P. Lecumberri, M. Gómez and A. Carlosena, “Multichannel blind deconvolution of transient impulsive signals”, *Proceedings of Instrumentation and Measurement Technology Conference (IMTC 2006)*, Sorrento, Italy: 2006. Proceedings of IEEE, 2006, pp. 1145-1150.

[130] T.H.T. Chan, L. Yu and S.S. Law, "Moving force identification studies, I: Theory", *Journal of Sound and Vibration*, vol. 247(1), 2001, pp. 59-76.

[131] T.H.T. Chan, L. Yu and S.S. Law, "Moving force identification studies, II : Comparative studies", *Journal of Sound and Vibration*, vol. 247(1), 2001, pp. 77-95.

[132] A.D. Stelzner, D.C. Kammer and P. Milenkovic, "A time domain method for estimating forces applied to an unrestrained structure", *Journal of Vibration and Acoustics*, vol. 123(4), 2001, pp. 524-532.

[133] H. Inoue, K. Kishimoto, T. Shibuya and K. Harada, "Regularization of numerical inversion of the Laplace transform for the inverse analysis of impact force", *JSME international journal. Series A, Solid mechanics and material engineering*, vol. 41(4), 1998, pp. 473-480.

[134] Y. Liu and W.S. Shepard, "Dynamic force identification based on enhanced least squares and total least-squares schemes in the frequency domain", *Journal of Sound and Vibration*, vol. 282(1), 2005, pp. 37-60.

[135] H.G. Choi, A.N. Thite and D.J. Thompson, "Comparison of methods for parameter selection in Tikhonov regularization with application to inverse force determination", *Journal of Sound and Vibration*, vol. 304(3), 2007, pp. 894-917.

[136] Q. Leclère, C. Pezerat, B. Laulagnet and L. Polac, "Indirect measurement of main bearing loads in an operating diesel engine," *Journal of Sound and Vibration*, vol. 286(1), 2005, pp. 341-361.

[137] D. Vandenbroeck and W. Hendricx, "Interior noise road optimization in a multiple input environment", *Institution of Mechanical Engineers Conference Publications*, Medical Engineering Publications LTD, vol. 3, 1994.

[138] G. Desanghere and R. Snoyes, "Indirect identification of excitation forces by modal coordinate transformation," *Proceedings of IMAC*, vol. 3, 1985.

[139] Y.-R. Kim and K.-J. Kim, "Indirect input identification by modal filter technique", *Mechanical Systems and Signal Processing*, vol. 13(6), 1999, pp. 893-910.

[140] K. Mendrok and P. Kurowski, "Operational modal filter and its applications", *Archive of Applied Mechanics*, vol. 83, 2013, pp. 509-519.

[141] J.F. Doyle, "A wavelet deconvolution method for impact force identification", *Experimental Mechanics*, vol. 37(4), 1997, pp. 403-408.

[142] Y. Gao and R.B. Randall, "Reconstruction of diesel engine cylinder pressure using a time domain smoothing", *Mechanical Systems and Signal Processing*, vol. 13(5), 1999, pp. 709-722.

[143] H. Lee and Y.-S. Park, "Error analysis of indirect force determination and a regularisation method to reduce force determination error", *Mechanical Systems and Signal Processing*, vol. 9(6), 1995, pp. 615-633.

[144] M.S. Allen and T.G. Carne, "Comparison of Inverse Structural Filter (ISF) and Sum of Weighted Accelerations Technique (SWAT) time domain force identification methods", *Proceedings of 47th AIAA/ASME/ASCE/AHS/ASC, structures, structural dynamics and materials Conference*, Newport, Rhode Island: 2006.

[145] R.L. Mayes, "Measurement of lateral launch loads on re-entry vehicles using SWAT", (No. SAND-93-1419C; CONF-940146-1), Sandia National Labs., Albuquerque, NM (USA),1993.

[146] V.I. Bateman, T.G. Carne and D.M. McCall, "Force reconstruction for impact tests of a energy-absorbing nose", (No. SAND-90-1575C; CONF-9010172-5), Sandia National Labs., Albuquerque, NM (USA), 1990.

[147] T.G. Carne, R.L. Mayes and V.I. Bateman, "Force reconstruction using the Sum of Weighted Accelerations Technique - Max-Flat Procedure", *Proceedings of the 12th International Modal Analysis Conference (IMAC)*, Honululu, Hawai, 1994.

[148] D.L. Gregory, T.G. Priddy and D.O. Smallwood, "Experimental determination of the dynamic forces acting on non-rigid bodies", *Proceedings of Aerospace Technology Conference and Exposition*, Long Beach, California, SAE Technical Paper Series, 1986, SAE Paper 861791.

[149] D.O. Smallwood and D.L. Gregory, "Experimental determination of the mass matrix using a constrained least squares solution", *AIAA/ASME SDMC Conference*, Monterey, CA (USA), 1887.

[150] T.G. Priddy, D.L. Gregory and R.G. Coleman, "Strategic placement of accelerometers to measure forces by the Sum of Weighted Accelerations", *Proceedings of he 6th International Modal Analysis Conference (IMAC)*, Kissimmee, Florida (USA), 1988.

[151] M.L. Wang, T.J. Kreitinger and H.L. Luo, "Force identification from structural responses", *Proceedings of SEM Spring Conference on Experimental Mechanics*, Houston, Texas, 1987, pp. 851-855.

[152] M.L. Wang and T.J. Kreitinger, "Force identification from nonlinear structure response", *Proceedings of the 6th International Modal Analysis Conference (IMAC)*, Kissimmee, Florida (USA), 1988, pp. 1655-1661.

[153] T.J. Kreitinger, *Force Identification from Structural Responses*, No. WL-TR-89-81, Weapons Lab (AFSC), Kirtland Air Force Base, NM 87117-6008: 1990.

[154] V.I. Bateman, R.L. Mayes and T.G. Carne, "A comparison of force reconstruction methods for a lumped mass beam", *Proceedings of the 63th Shock and Vibration Symposium*, Las Cruces, New Mexico, 1992.

[155] G.H. James, T.G. Carne, K. Elliott and B. Wilson, "Estimation of the Space Shuttle rolling forcing", *Proceedings of 23rd International Modal Analysis Conference (IMAC)*, Orlando, Florida, 2005.

[156] V.I. Bateman, T.G. Carne, D.L. Gregory, S.W. Attaway and H.R. Yoshimura, "Force reconstruction for impact tests", *Journal of Vibration, Acoustics, Stress, and Reliability in Design*, vol. 113(2), 1991, pp. 192-200.

[157] G. Genaro and D.A. Rade, "Input force identification in the time domain", *Proceedings of the 16th International Modal Analysis Conference (IMAC)*, Santa Barbara, California, 1998, pp. 124-129.

[158] A.D. Steltzner and D.C. Kammer, "Input force estimation using an inverse structural filter", *Proceedings of the 17th International Modal Analysis Conference (IMAC)*, Kissimmee, Florida (USA), 1999, pp. 954-960.

[159] D.C. Kammer and A.D. Steltzner, "Structural identification of Mir using inverse system dynamics and Mir / shuttle docking data", *Transactions-American Society of Mechanical Engineers Journal of Vibration and Acoustics*, vol. 123(2), 2001, pp. 230-237.

[160] C.-K. Ma, P.-C. Tuan, J.-M. Chang and D.-C. Lin, "Adaptive weighting inverse method for the estimation of input loads", *International Journal of Systems Science*, vol. 34(3), 2003, pp. 181-194.

[161] C.-K. Ma, J.-M. Chang and D.-C. Lin, "Input foces estimation of beam structures by an inverse method", *Journal of Sound and Vibration*, vol. 259(2), 2003, pp. 387-407.

[162] P.-C. Tuan, C.-C. Ji, L.-W. Fong and C.-H. Huang, "An input estimation approach to on-line two-dimensional inverse heat conduction problems", *Numerical Heat Transfer*, vol. 29(3), 1996, pp. 345-363.

[163] N. Madjarov and L. Mihaylova, "Kalman filter sensitivity with respect to parametric noises uncertainty", *Kypernetika*, vol. 32(3), 1996, pp. 307-322.

[164] C.-K. Ma and D.-C. Lin, "Input forces estimation of a cantilever beam", *Inverse Problems in Engineering*, vol. 8(6), 2000, p. 511–528.

[165] J.-J. Liu, C.-K. Ma, I.-C. Kung and D.-C. Lin, "Input force estimation of a cantilever plate by using a system identication technique", *Computer Methods in Applied Mechanics and Engineering*, vol. 190(11), 2000, pp. 1309-1322.

[166] J. Juang and R.S. Pappa, "An eigensystem realization algorithm for modal identification and model reduction", *Journal of Guidance Control and Dynamics*, vol. 8(5), 1985, pp. 620-627.

[167] J.-S. Hwang, A. Kareem and W.-J. Kim, "Estimation of modal loads using structural response", *Journal of Sound and Vibration*, vol. 326(3), 2009, pp. 522-539.

[168] L.R. Ray, "Nonlinear tire force estimation and road friction identification: Simulation and experiments", *Automatica*, vol. 33(10), 1997, pp. 1819-1833.

[169] C.-K. Ma and C.-C. Ho, "An inverse method for the estimation of input forces acting on non-linear structural systems", *Journal of Sound and Vibration*, vol. 275(3), 2004, pp. 953-971.

[170] D.-C. Lin, "Input estimation for nonlinear systems", *Inverse Problems in Science and Engineering*, vol. 18(5), 2010, pp. 673-689.

[171] S.W. Doebling, F. Alvin and L.D. Peterson, "Limitations of state-space system identification algorithms for structures with high modal density", *Proceedings of SPIE the International Society for Oprical Engineering*, 1994, pp. 633-640.

[172] J.-N. J, L.G. Horta and R.W. Longman, "Identification of observer/Kalman filter Markov parameters: Theory and experiments", *Journal of Guidance Control and Dynamics*, vol. 16(2), 1993, pp. 320-329.

[173] Z.R. Lu and S.S. Law, "Force identification based on sensitivity in time domain", *Journal of Engineering Mechanics*, vol. 132(10), 2006, p. 1050.

[174] W. Kropp and K. Larsson, "Force estimation in the time domain by applying an LMS algorithm", *Proceedings of Conference on Noise and Vibration: Emerging Methods (Novem)*, Saint-Raphaël, France, 2005.

[175] M.G. Bellanger, *Adaptive Digital Filters*, CRC Press, 2001.

[176] A. Moorhouse, "Vibro-acoustic measurement methods in condition monitoring", *Proceedings of the 9th International Conference on Condition Monitoring and Machinery Failure Prevention Technologies 2012 (CM 2012 AND MFPT 2012)*, London, UK, 2012, pp. 74-84.

[177] P. Zeller, *Handbuch Fahrzeugakustik - Grundlagen, Auslegung, Berechnung, Versuch*, Vieweg+Teubner Verlag, 2012.

[178] F.A.N. Chang-Sheng and G.U.O. Yan-Ling, "Design of the auto electric power steering system controller", *Procedia Engineering*, vol. 29, 2012, pp. 3200-3206.

[179] J.H. Kim and J.B. Song, "Control logic for an electric power steering system using assist motor", *Mechatronics*, vol. 12(3), 2002, pp. 447-459.

[180] ZF Lenksysteme, *ZF Servolectric - Electric Power Steering System for Passengers Cars and Light Commercial Vehicles*, 2009.

[181] M.K. Hassan, N.A.M. Azubir, H.M.I. Nizam, S.F. Toha and B.S.K.K. Ibrahim, "Design of electric power assisted steering system (EPAS) using GA-PID method", *Procidia Engineering*, vol. 41, 2012, pp. 614 - 621.

[182] Haus der Technik, “Elektrisch verursachte Vibrationen an Motoren, Seminar-unterlagen: Schwingungsdiagnose an Elektromotoren, Pumpen, Gebläsen und Getrieben,” *Haus der Technik e.V.*, Rostock, Germany, 2002.

[183] M. Sturm, *Bestimmung dynamischer Kontaktkräfte zwischen Komponenten elektrischer Lenksysteme am Beispiel der Koppelstelle Servomotor-Lenkgetriebe*, MSc Thesis, Hochschule Karlsruhe - Technik und Wirtschaft, 2009.

[184] M. Heckl and H. Müller, *Taschenbuch der Technischen Akustik*, Springer Verlag, 1994.

[185] T. Nagel, *Zahnriemengetriebe Eigenschaften, Normung, Berechnung, Gestaltung*, Hanser Verlag, 2008.

[186] B. Merz, *Akustische Untersuchungen am Riemen*, Research report, ZF Lenksysteme GmbH, Schwäbisch Gmünd, Germany, 2009.

[187] R. Perneder, *Handbuch Zahnriementechnik: Grundlagen, Berechnung, Anwendungen*, Springer-Verlag, 2009.

[188] K. Popp and P. Stelter, “Stick-slip vibrations and chaos”, *Philosophical Transactions of the Royal Society of London. Series A: Physical and Engineering Sciences*, vol. 332(1624), 1990, pp. 89-105.

[189] P.E. Rossouw, L.S. Kamelchuk and R.P. Kusy, “A fundamental review of variables associated with low velocity frictional dynamics”, *Seminars in Orthodontics*, vol. 9(4), WB Saunders, 2003, pp. 223-235.

[190] J. Das and A.K. Mallik, “Control of friction driven oscillation by time-delayed state feedback”, *Journal of Sound and Vibration*, vol. 297(3), 2006, pp. 578-594.

[191] S. Hoffmann, *Klappern und Knarzen bei EPS Lenksystemen*, Research report, ZF Lenksysteme GmbH, Schwäbisch Gmünd, Germany, 2009.

[192] S. Hoffmann, *Exzenter-Knarzen / EPSapa*, Research report, ZF Lenksysteme GmbH, Schwäbisch Gmünd, Germany, 2009.

[193] S. Hoffmann, *Flansch-Knarzen / EPSdp*, Research report, ZF Lenksysteme GmbH, Schwäbisch Gmünd, Germany, 2010.

[194] R.P. Harnemik and K.D. Hsueh, “Impulse noise: Some definitions, physical acoustics and other considerations”, *The Journal of the Acoustical Society of America*, vol. 90, 1991, pp. 189-196.

[195] P. Woelfl, *Untersuchung der Korrelation zwischen Prüfstands- und Fahrzeug-messungen für transiente Geräusche von Lenksystemen*, Diplomarbeit, Technische Universität Ilmenau, 2010.

[196] S. Hoffmann, *Klapper- und Klopfphänomene, Übersicht*, Research report, ZF Lenksysteme GmbH, Schwäbisch Gmünd, Germany, 2009.

[197] B. Rommel, *Berechnungsbericht: ETC06207 (Umlenkklopfen)*, , Research report, ZF Lenksysteme GmbH, Schwäbisch Gmünd, Germany, 2006.

[198] B. Rommel, *Berechnungsbericht : EZB080944 (Klappern - Geradeausfahrt)*, Research report, ZF Lenksysteme GmbH, Schwäbisch Gmünd, Germany, 2008.

[199] G. Speidel, *EPSapa PL2 - Klappern / Versuchsbericht KGT-Klappern*, Research report, ZF Lenksysteme GmbH, Schwäbisch Gmünd, Germany, 2009.

[200] B. Rommel, *EPSapa PL2 - Klappern / KGT-Klappern auf Schlechtweg bei Geradeausfahrt*, Research report, ZF Lenksysteme GmbH, Schwäbisch Gmünd, Germany, 2008.

[201] B. Widrow and M.E. Hoff, "Adaptive switching circuits," *IRE WESCON Convention Record, Part 4*, Los Angeles, California (USA), 1960, pp. 96-104.

[202] S. Haykin, *Adaptive Filter Theory*, Prentice-Hall and System Science Series, New Jersey, 1996.

[203] B. Farhang-Boroujeny, *Adaptive Filters: theory and applications*, John Wiley & Sons, 1999.

[204] B. Widrow and S.D. Stearns, *Adaptive Signal Processing*, Prentice-Hall and Signal Processing Series, New Jersey, 1985.

[205] C.F.N. Cowan and P.M. Grant, *Adaptive Filters*, Prentice-Hall, New Jersey, 1985.

[206] M. Sturm, A. Moorhouse, T. Alber and F.F. Li, "Force reconstruction using an adaptive algorithm in time domain", *Proceedings of International Conference on Noise and Vibration Engineering (ISMA)*, Leuven, Belgium, 2012, pp. 3617-3630.

[207] M. Sturm, A. Moorhouse, W. Kropp and T. Alber, "Robust force identification for complex technical structures with single degree of freedom excitation using an adaptive algorithm in time domain", *Proceedings of AIA-DAGA2013*, Merano, Italy, 2013, pp. 1730-1733.

[208] M. Sturm, A. Moorhouse, W. Kropp and T. Alber, "Robust calculation of simultaneous multi-channel blocked force signatures from measurements made in-situ using an adaptive algorithm in time domain", *Proceedings of International Congress on Sound and Virbration (ICSV20)*, Bangkok, Thailand, 2013.

[209] Y. Huang, J. Benesty and J. Chen, *Acoustic MIMO Signal Processing*, Springer Verlag, 2006.

[210] R.H. Kwong and E.W. Johnston, "A variable step size LMS algorithm", *IEEE Transactions on Signal Processing*, vol. 40(7), 1992, pp. 1633-1642.

[211] T. Aboulnasr and K. Mayyas, "A robust variable step-size LMS-type algorithm: Analysis and Simulations," *IEEE Transactions on Signal Processing*, vol. 45, 1997, pp. 631-639.

[212] M. Taenaka, "Establishment of evaluation method for rattle noise of steering gear for column type electric power steering (C-EPS) system", *JTEK Engineering Journal*, 2011, pp. 55-58.

[213] B.J. Schwarz and M.H. Richardson, "Experimental modal analysis", *Proceedings of CSI Reliablility week*, Orlando, Florida (USA), vol. 36(3), 1999, pp. 30-32.

[214] J.S. Bendat and A.G. Piersol, *Engineering applications of correlation and spectral analysis*, John Wiley & Sons, 1993.

[215] J.K. Hammond and K. Shin, *Fundamentals of signal processing for sound and vibration engineers*, Chichester, England, John Wiley & Sons, 2008.

[216] B. Cauberghe, *Applied frequency-domain system identification in the filed of experimental and operational modal analysis*, PhD Thesis, Vrije Universiteit Brussel, 2004.

[217] E. Brechlin, *Methoden und Grenzen der Substrukturkopplung auf der Basis experimenteller Daten*, Osnabrück, Germany, Der Andere Verlag, 2001.

[218] R.J. Allemang, "The Modal Assurance Criterion –Twenty years of use and abuse", *Sound and Vibration*, vol. 37(8), 2003, pp. 14-23.

[219] F. Fahy and P. Gardonio, *Sound and structural vibration: radiation, transmission and response*, Academic Press, Oxford, 2007.

[220] M. Hudelmaier, *Characterisation of an electrical power steering system as structure borne sound source in frequency and time domain using inverse methods*, MSc Thesis, University of Salford, 2012.

[221] A.T. Moorhouse and B.M. Gibbs, "Simplified characterisation of multiple point excited structures using mobility matrix eigenvalues and eigenvectors", *Acta Acustica united with Acustica*, vol. 84(5), 1998, pp. 843 - 853.

[222] Y.A. Huang, J. Benesty and J. Chen, "Optimal step size of the adaptive multichannel LMS algorithm for blind SIMO identification", *IEEE Signal Processing Letters*, vol. 12(3), 2005, pp. 173-176.

A Appendices

A.1 Overview of time domain inverse force identification methods

A priori information of applied input load		Input / output relationship		Analysis procedure		Inverse method	References
location	number	temporal	spatial	processing	system modelling		
						TD state-space method / inverse filtering:	
known, fixed	multiple	linear time-invariant (LTI)	collocated (COL)	online	numerical (FEM)	Causal inverse structural filter (ISF) - section 2.4.4	Kammer, D. C. (1998).
			non-collocated (N-COL)		numerical (FEM) & experimentally (realisation)	Non-causal inverse structural filter (ISF) - section 2.4.4	Steltzner, A. D., & Kammer, D. C. (1999), Steltzner et al. (2001)
					numerical (FEM) & experimentally (realisation)	Non-causal delayed, multi-step inverse structural filter (DMISF) - section 2.4.4	Allen, M. S., & Carne, T. G. (2006). Allen, M. S., & Carne, T. G. (2008).
			COL & N-COL mixed		numerical	Non-causal time delay method - section 2.4.4	Nordström, L. J. L., & Nordberg, P. T. (2004).
					numerical	Block inversion algorithm, Dynamik Tikhonov regularisation - section 2.4.4	Nordberg, T. P., & Gustafsson, I. (2006).
						TD state-space method / Kalman filtering	
known, fixed	multiple	linear time-invariant (LTI)	collocated (COL)	online	numerical (FEM)	Simple Kalman filter in conjunction with a recursive least squares estimator (KF-RLSE) - section 2.4.5	Ma, C.-K., Tuan, P.-C., Lin, D.-C., & Liu, C.-S. (1998) Ma, C.-K., Chang, J.-M., & Lin, D.-C. (2003).
	single		non-collocated (N-COL)		numerical (FEM) & experimentally (realisation)	Simple Kalman filter in conjunction with a recursive least squares estimator (KF-RLSE) - section 2.4.5	Ma, C.-K., & Lin, D.-C. (2000). Liu, J.-J., Ma, C.-K., Kung, I.-C., & Lin, D.-C. (2000).
	multiple		collocated (COL)		numerical (FEM)	Simple Kalman filter in conjunction with adaptive weighting recursive least-square scheme (KF-AIWE) - section 2.4.5.	Ma, C.-K., Tuan, P.-C., Chang, J.-M., & Lin, D.-C. (2003).
	multiple		non-collocated (N-COL)		experimentally (realisation)	Modified KF-RLSE to obtain anlytical procedure which allows for identification of external modal loads (modal space force identification approach)- section 2.4.5	Hwang, J.-S., Kareem, A., & Kim, W.-J. (2009).
known, fixed	multiple	nonlinear time-varying	non-collocated (N-COL)	online	numerical (FEM)	extended Kalman filter (EKF)-in conjunction with a tire model is used to obtain nonlinear tyre forces for adavnced vehicle control - section 2.4.5	Ray, L. R. (1997).
				online	numerical (FEM)	extended Kalman filter in conjunction with a recursive least-square estimator (EKF-RLSE) -section 2.4.5	Ma, C.-K., & Ho, C.-C. (2004). Lin, D.-C. (2010).

A priori information of applied input load		Input / output relationship		Analysis procedure		Inverse method	References
location	number	temporal	spatial	processing	system modelling		
						TD modal filtering :	
known, fixed	single (equivalent)	linear time-invariant (LTI)	COL & N-COL mixed	online	numerical (FEM) & experimentally (system identification)	Tradtional Sum of Weighted Acceleration Technique (SWAT) to estimate the equivalent force acting at the centre-of-gravity of a freely vibrating structure and complementary methods to define optimal number and locations of sensors - section 2.4.3	Gregory, D. L., Priddy, T. G., & Smallwood, D. O. (1986). Smallwood, D. O., & Gregory, D. L. (1887). Priddy, T. G., Gregory, D. L., & Coleman, R. G. (1988). Mayes, R. L. (1994).
							Kreitinger, T. J. (1990) (Review until 1990) Bateman, V. I., Carne, T. G., Gregory, D. L., Attaway, S. W., & Yoshimura, H. R. (1991). James, G. H., Carne, T. G., Elliott, K., & Wilson, B. (2005).
		nonlinear time-varying				Extension of the tradtional (SWAT) to non-linear vibration probelms - section 2.4.3	Wang, M. L., & Kreitinger, T. J. (1988).
		linear time-invariant (LTI)			experimentally (system identification)	SWAT CAL uses initial calibration test to calculate the required weighting factors -section 2.4.3	Bateman, V. I., Mayes, R. L., & Carne, T. G. (1992).
					experimentally (system identification)	SWAT TEEM uses time eleminated elastic modes to calculate the required weighting factors -section 2.4.3	Mayes, R. L. (1994).
						SWAT Max-Flat uses measured FRFs to calculate the required weighting factors -section 1.4.3	Carne, T. G., Mayes, R. L., & Bateman, V. I. (1994).
	multiple				numerical (FEM) & experimentally (system identification)	Extension of SWAT to multiple input forces and arbitary boundary conditions; the method is known as 'partial modal matrix apporach' (PMMA) - section 2.4.3	Genaro, G., & Rade, D. A. (1998).

A priori information of applied input load		Input / output relationship		Analysis procedure		Inverse method	References
location	number	temporal	spatial	processing	system modelling		
known, fixed	multiple	linear time-invariant (LTI)	COL & N-COL mixed	offline	analytical & numerical	**TD sensitivity methods :** The sensitivity of dynamic response with respect to parameters of the input force (amplitude and freqeuncy) are calculated and used to update the estimated parameters iteratively. Only a single response is required - section 2.4.6	Lu, Z. R., & Law, S. S. (2006).
known, fixed	single	linear time-invariant (LTI)	COL & N-COL mixed	offline	experimental (system identification)	**TD methods based on adaptive algorithms** Adaptive inversion routine based on LMS algorithm. Consideration of over-detemined system with single input so as to suppress uncorrelated noise - section 2.4.7 and section 4.2 - 4.5	Kropp, W., & Larsson, K. (2005).
					analysical, numerical, experimental (system identification)	Feasibility study of adaptive inversion routine for applications to complex technical structures. Elaborated derivation of the theory and complementary notes - chapter 4 and chapter 5	Sturm, M., Moorhouse, A., Alber, T., & Li, F. F. (2012). Sturm, M., Moorhouse, A., Kropp, W., & Alber, T. (2013a).
	multiple				analytical, numerical, experimental (system identification)	Generalisation of adaptive inversion routine for structures with multiple inputs and multiple outputs. Feasibility study for applications to complex technical structures with respect to independent source characetrisation - chapter 4 and chapter	Sturm, M., Moorhouse, A., Kropp, W., & Alber, T. (2013b).
known, fixed	single	linear time-invariant (LTI)	COL / N-COL	offline	numerical	**TD direct deconvolution & regularisation methods** Different approaches are reviewed in section 1.4.2	A list of literatre is provided in section 1.4.2

A.2 Additional results: Inverse force identification in time domain

A.2.1 Force reconstruction for single input single output systems

Sensitivity to noise in the structural response

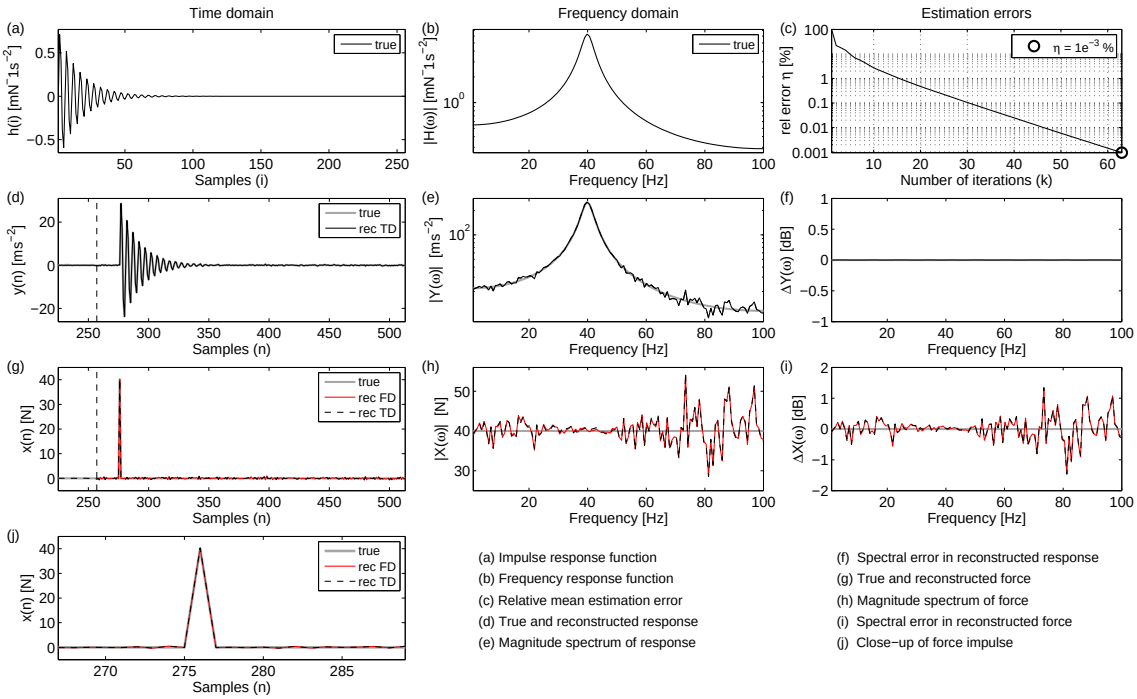

Figure A.1. Numerical result for SISO system with 5% noise added to the acceleration response. Representation of signals in time domain (a, d, g, j), representation of signals in frequency domain (b, e, h,) and different estimation errors (c, f, i): ▬ true signal; ── reconstructed response using TDM; ─ ─ reconstructed force using TDM; ── identified force using FDM.

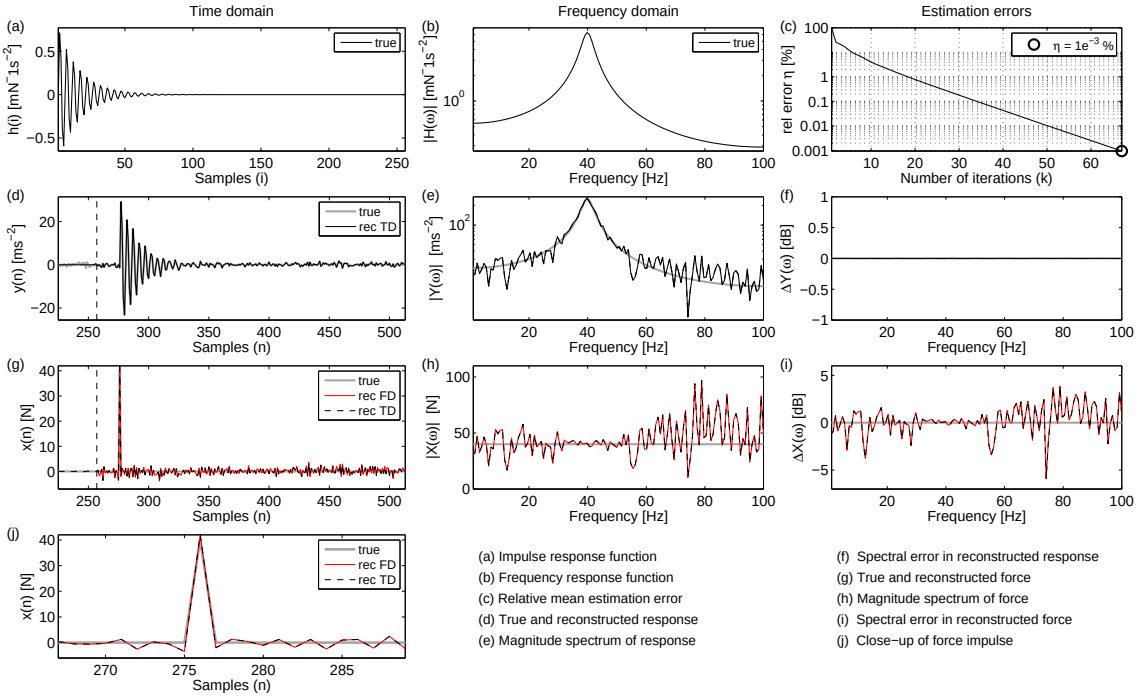

Figure A.2. Numerical result for SISO system with 25% noise added to the acceleration response. Representation of signals in time domain (a, d, g, j), representation of signals in frequency domain (b, e, h,) and different estimation errors (c, f, i): ▬ true signal; ── reconstructed response using TDM; ─ ─ reconstructed force using TDM; ── identified force using FDM.

Sensitivity to noise in the structural response

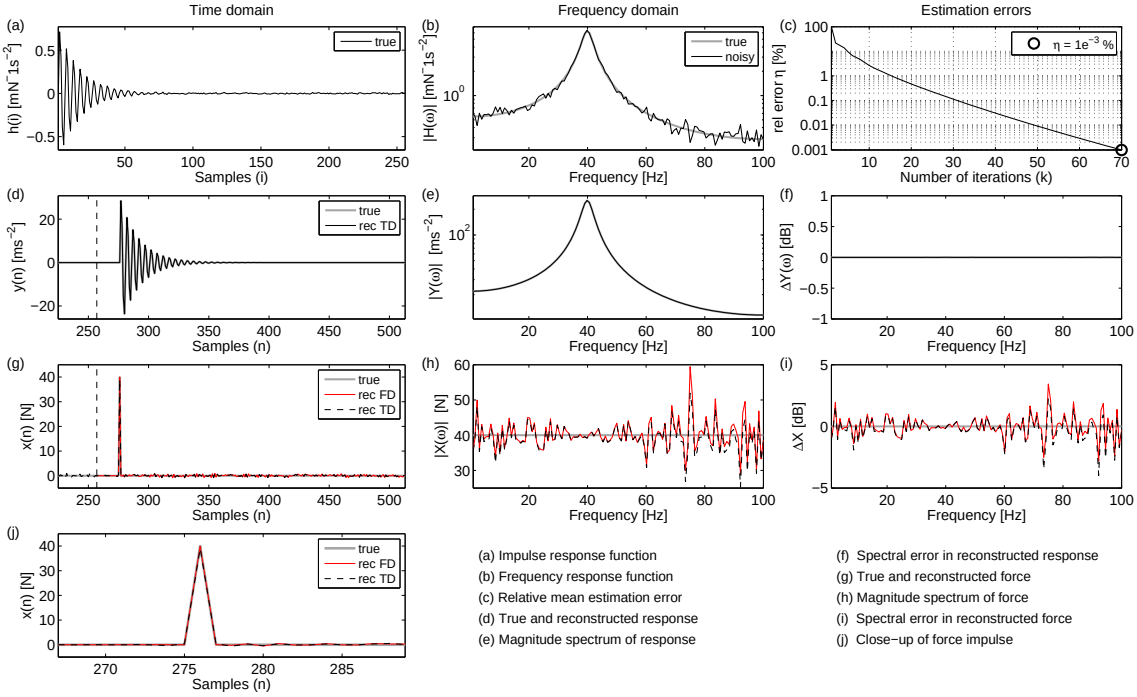

Figure A.3. Numerical result for SISO system with 5% noise added to the impulse response function. Representation of signals in time domain (a, d, g, j), representation of signals in frequency domain (b, e, h,) and different estimation errors (c, f, i): ▬ true signal; ── reconstructed response using TDM; ─ ─ reconstructed force using TDM; ── identified force using FDM.

A.2.2 Force reconstruction for single input multiple output systems

Sensitivity to noise in the structural responses

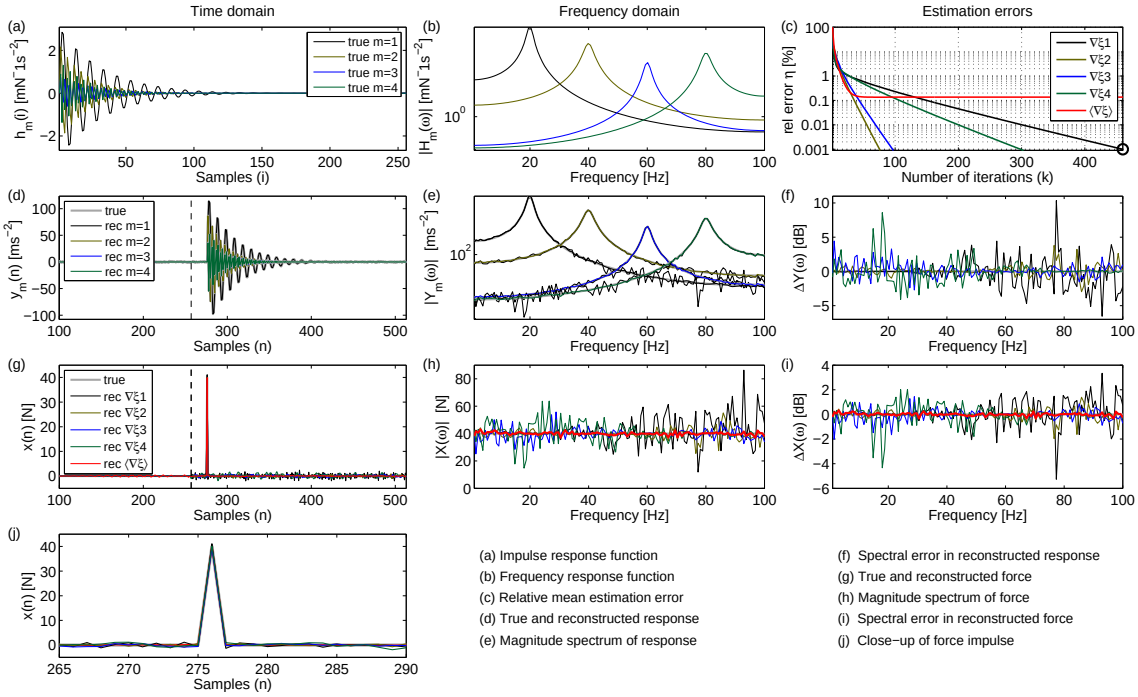

Figure A.4. Numerical result for SIMO system with 5% noise added to the acceleration responses. Representation of signals in time domain (a, d, g, j), representation of signals in frequency domain (b, e, h,) and different estimation errors (c, f, i): Quantities indicated by $\nabla\xi m$ are obtained by the SISO recursion from Table 4.1 whereas $\langle\nabla\xi\rangle$ indicates that the SIMO recursion from Table 4.3 is used.

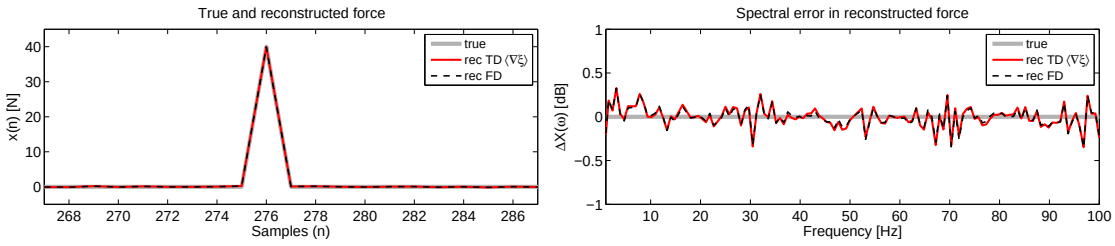

Figure A.5. Comparison of the time domain inverse method (TDM) with the standard frequency domain inverse method (FDM) for SIMO system with 5% noise added to the responses. Reconstructed force time history (left) and spectral estimation error in the identified force (right): ——— true signal; ——— reconstructed force using the SIMO TDM; — — identified force using the FDM.

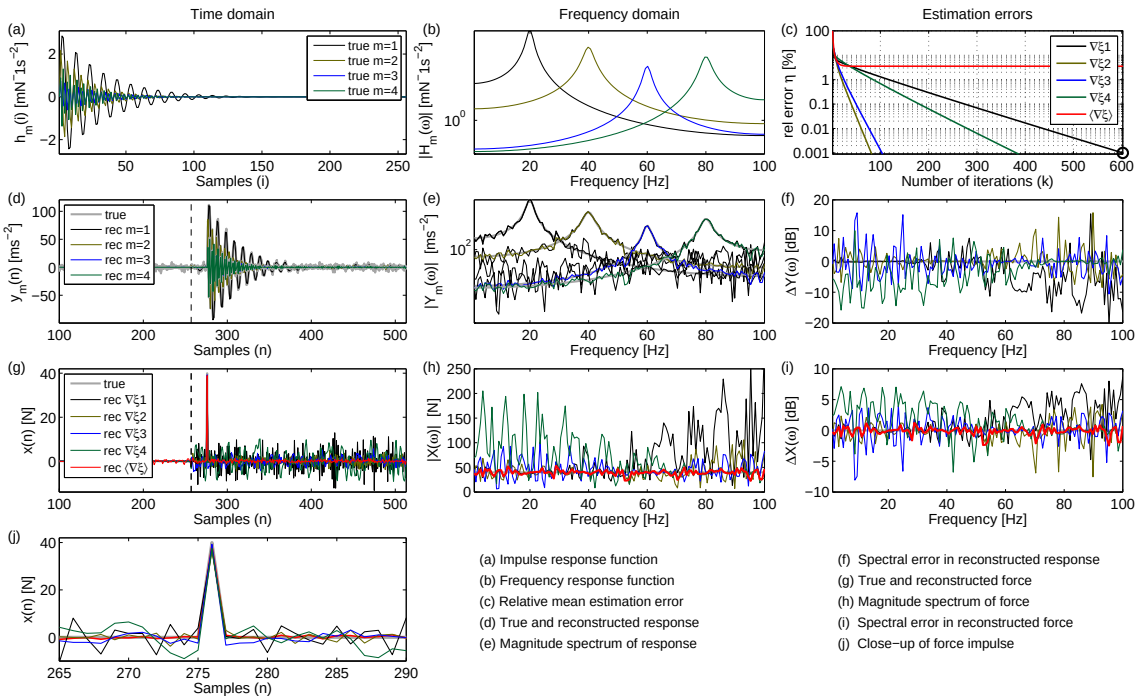

Figure A.6. Numerical result for SIMO system with 25% noise added to the acceleration responses. Representation of signals in time domain (a, d, g, j), representation of signals in frequency domain (b, e, h,) and different estimation errors (c, f, i): Quantities indicated by $\nabla\xi m$ are obtained by the SISO recursion from Table 4.1 whereas $\langle\nabla\xi\rangle$ indicates that the SIMO recursion from Table 4.3 is used.

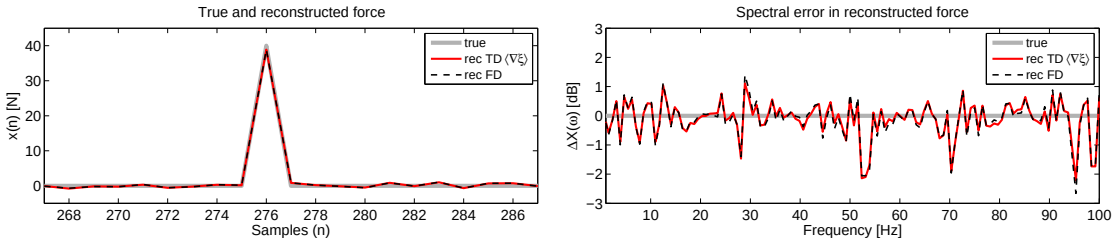

Figure A.7. Comparison of the time domain inverse method (TDM) with the standard frequency domain inverse method (FDM) for SIMO system with 25% noise added to the responses. Reconstructed force time history (left) and spectral estimation error in the identified force (right): ▬▬ true signal; ▬ reconstructed force using the SIMO TDM; ─ ─ identified force using the FDM.

Sensitivity to errors in the system model

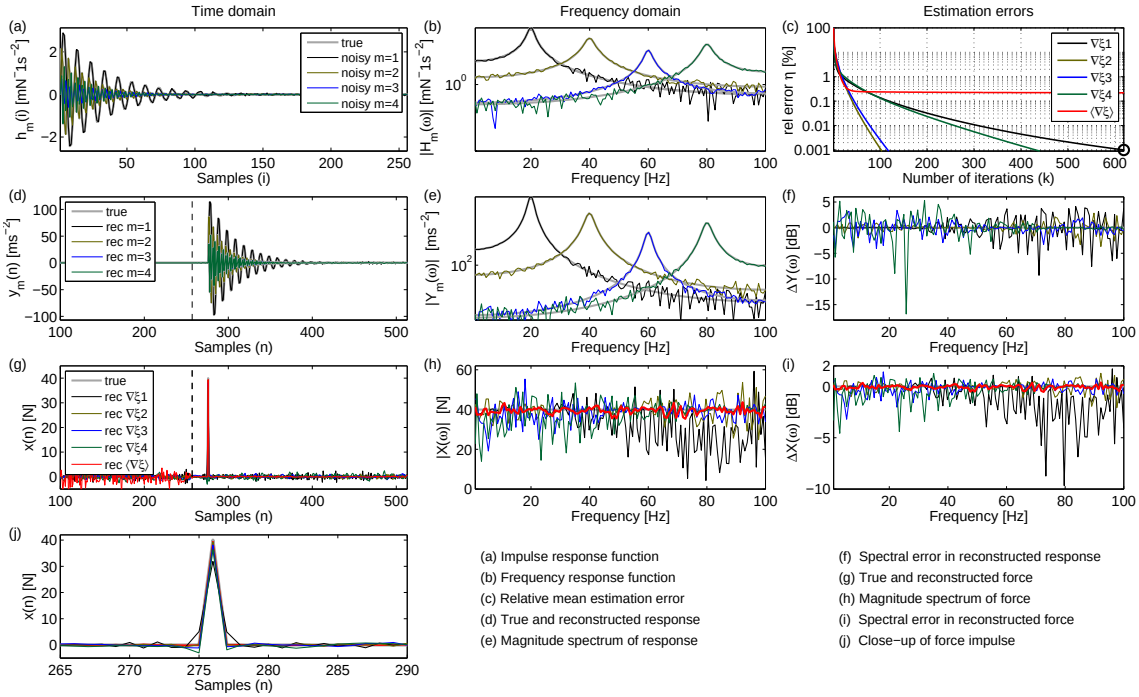

FigureA.8. Numerical result for SIMO system with 5% noise added impulse response functions. Representation of signals in time domain (a, d, g, j), representation of signals in frequency domain (b, e, h,) and different estimation errors (c, f, i): Quantities indicated by $\nabla\xi m$ are obtained by the SISO recursion from Table 4.1 whereas $\langle\nabla\xi\rangle$ indicates that the SIMO recursion from Table 4.3 is used.

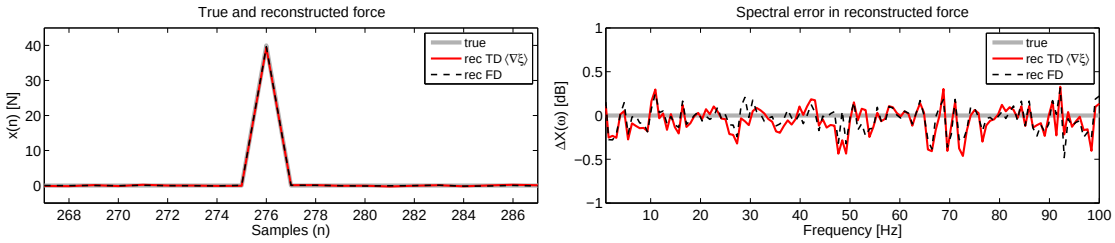

Figure A.9. Comparison of the time domain inverse method (TDM) with the standard frequency domain inverse method (FDM) for SIMO system with 5% noise added to system model. Reconstructed force time history (left) and spectral estimation error in the identified force (right): ▬ true signal; — reconstructed force using the SIMO TDM; ╌ identified force using the FDM.

A.2.3 Force reconstruction for multiple input multiple output systems

Application to noise free system

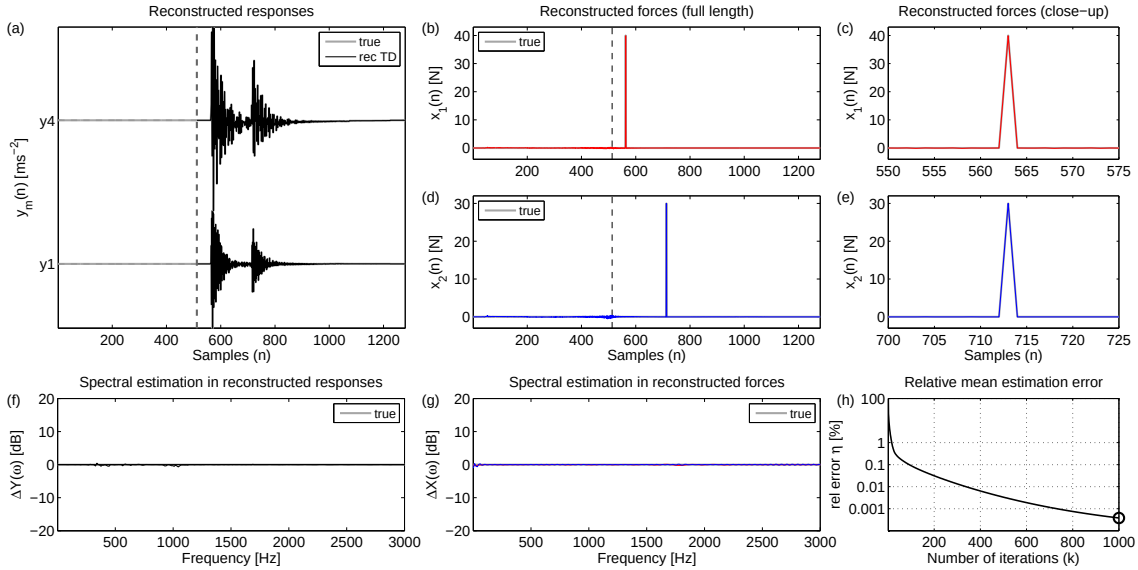

Figure A.10. Numerical results for noise free (2x2) MIMO system. Time signatures of structural responses (a) and reconstructed force signatures in full-length (b,d) and as close-up (c,e); spectral estimation error in reconstructed responses (f) and identified forces (g): ▬ true signal; ── reconstructed signal using TDM. Relative mean prediction error (E-RMPE) as performance measure of the adaptive inversion routine (h).

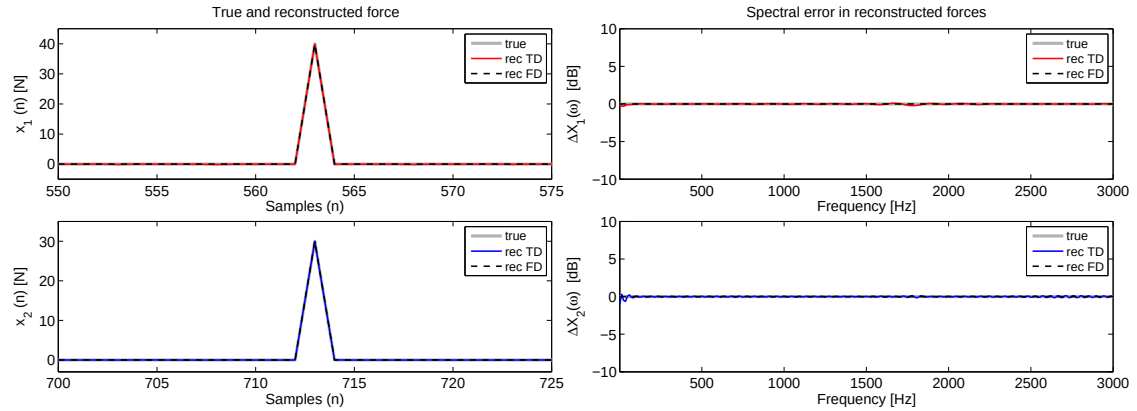

Figure A.11. Comparison of the generalised time domain inverse method (TDM) with the standard frequency domain inverse method (FDM) for the noise free (2x2) MIMO system. Time signatures of reconstructed forces (a,c) and spectral estimation error in the identified force (b,d): ▬ true signal; ── reconstructed force using the MIMO TDM; ─ ─ identified force using the FDM.

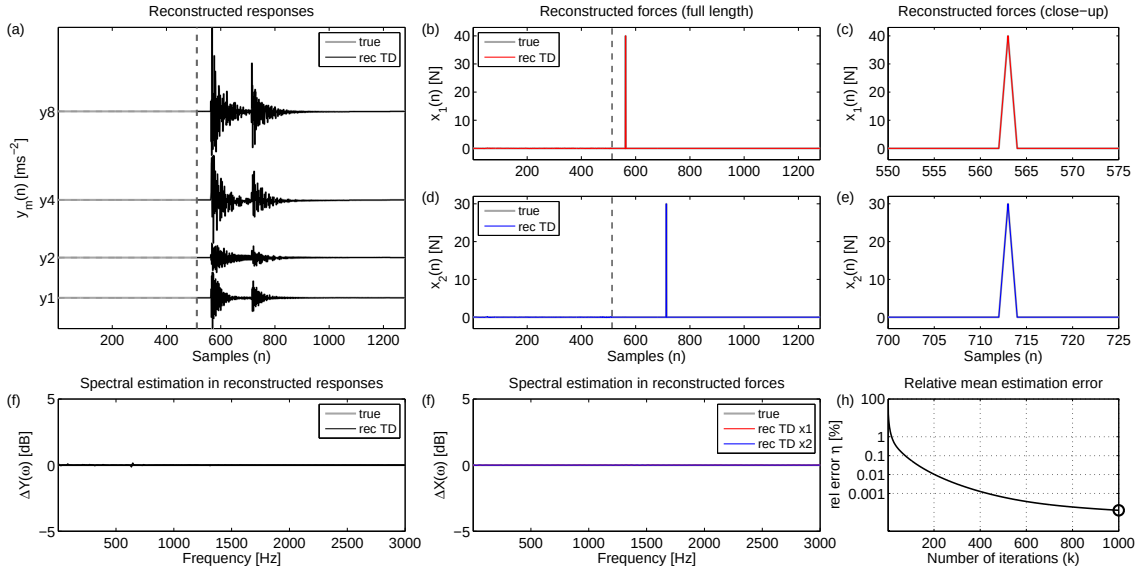

Figure A.12. Numerical results for noise free (2x4) MIMO system. Time signatures of structural responses (a) and reconstructed force signatures in full-length (b,d) and as close-up (c,e); spectral estimation error in reconstructed responses (f) and identified forces (g): ▬ true signal; ── reconstructed signal using TDM. Relative mean prediction error (E-RMPE) as performance measure of the adaptive inversion routine (h).

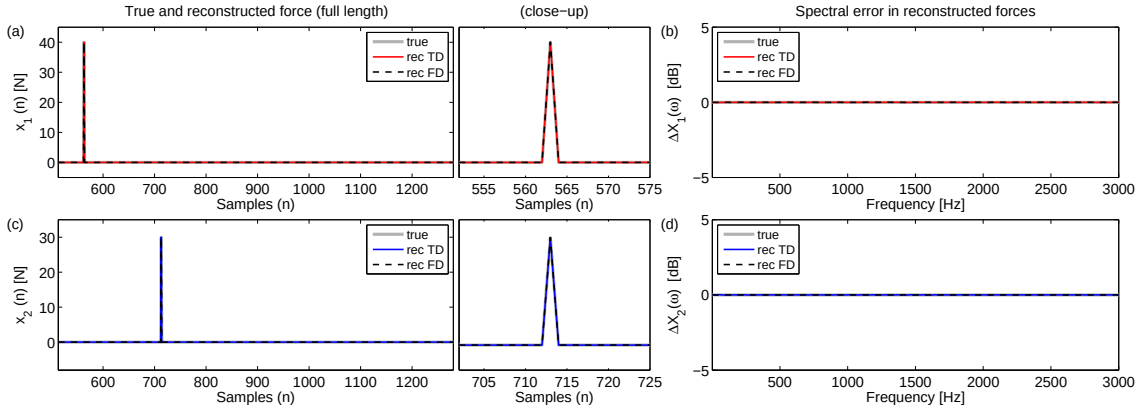

Figure A.13. Comparison of the generalised time domain inverse method (TDM) with the standard frequency domain inverse method (FDM) for the noise free (2x4) MIMO system. Time signatures of reconstructed forces (a,c) and spectral estimation error in the identified force (b,d): ▬ true signal; ── reconstructed force using the MIMO TDM; ─ ─ identified force using the FDM.

Sensitivity to noise in the structural responses

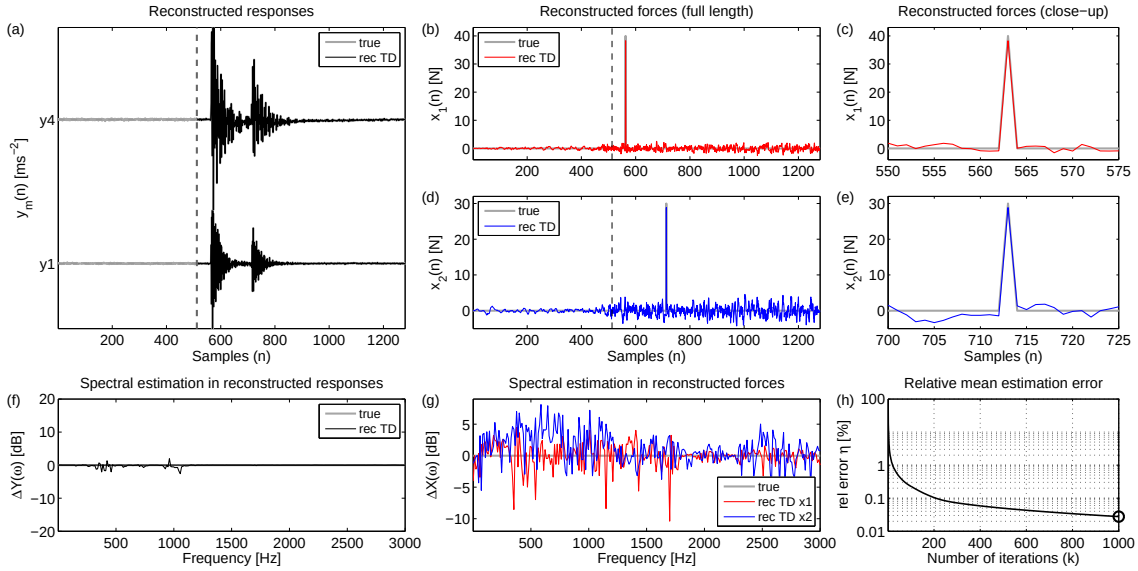

Figure A.14. Numerical results for (2x2) MIMO system with 5 % noise added to all acceleration responses. Time signatures of structural responses (a) and reconstructed force signatures in full-length (b,d) and as close-up (c,e); spectral estimation error in reconstructed responses (f) and identified forces (g): ▬ true signal; ▬ reconstructed signal using TDM. Relative mean prediction error (E-RMPE) as performance measure of the adaptive inversion routine (h).

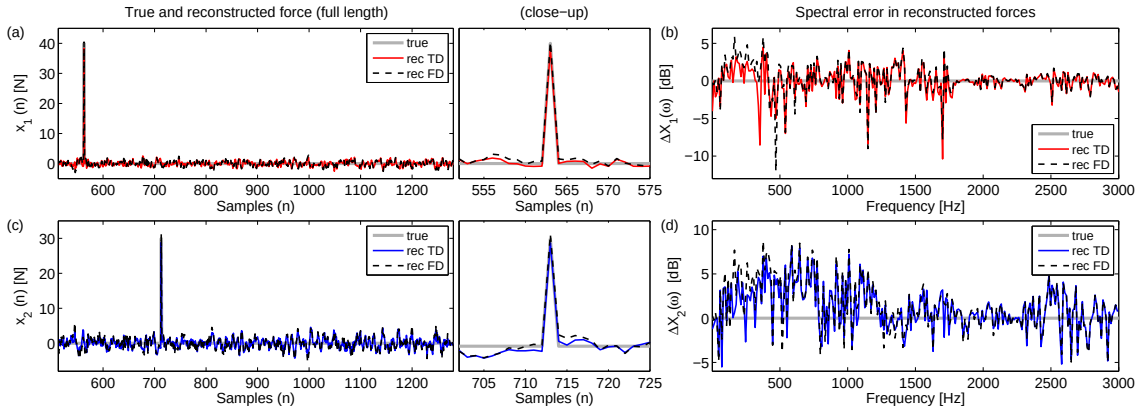

Figure A.15. Comparison of the generalised time domain inverse method (TDM) with the standard frequency domain inverse method (FDM) for the (2x2) MIMO system with 5 % noise added to all responses. Time signatures of reconstructed forces (a,c) and spectral estimation error in the identified force (b,d): ▬ true signal; ▬ reconstructed force using the MIMO TDM; ▬ ▬ identified force using the FDM.

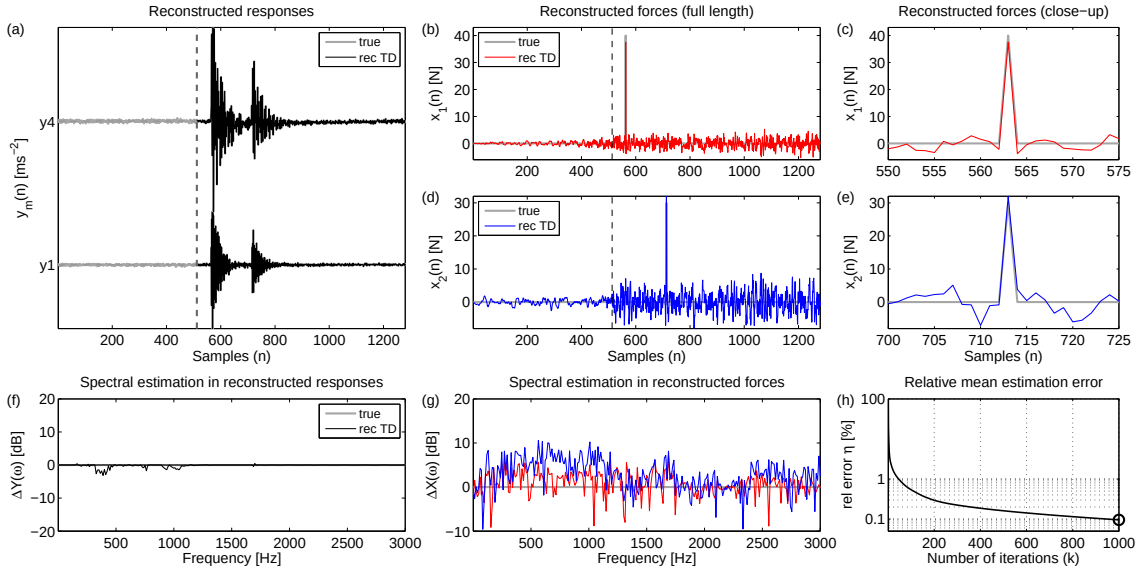

Figure A.16. Numerical results for (2x2) MIMO system with 10 % noise added to all acceleration responses. Time signatures of structural responses (a) and reconstructed force signatures in full-length (b,d) and as close-up (c,e); spectral estimation error in reconstructed responses (f) and identified forces (g): ▬ true signal; ▬ reconstructed signal using TDM. Relative mean prediction error (E-RMPE) as performance measure of the adaptive inversion routine (h).

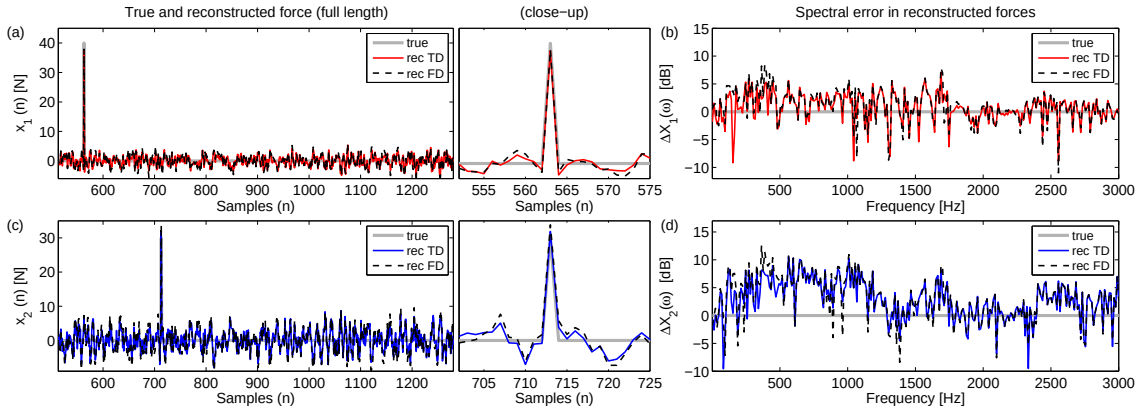

Figure A.17. Comparison of the generalised time domain inverse method (TDM) with the standard frequency domain inverse method (FDM) for the (2x2) MIMO system with 10 % noise added to all responses. Time signatures of reconstructed forces (a,c) and spectral estimation error in the identified force (b,d): ▬ true signal; ▬ reconstructed force using the MIMO TDM; ▬ ▬ identified force using the FDM.

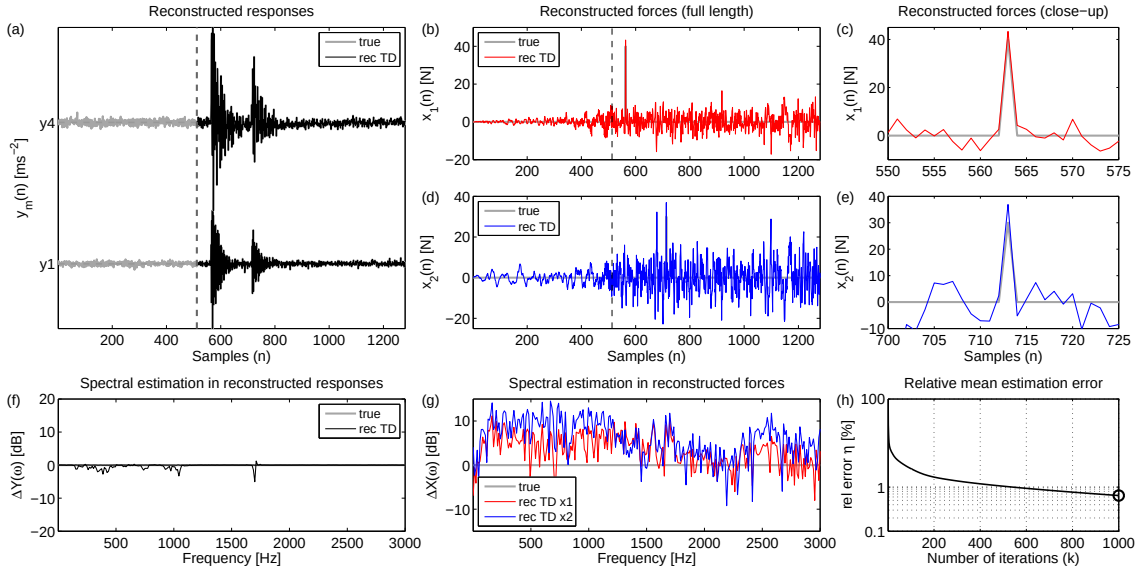

Figure A.18. Numerical results for (2x2) MIMO system with 25 % noise added to all acceleration responses. Time signatures of structural responses (a) and reconstructed force signatures in full-length (b,d) and as close-up (c,e); spectral estimation error in reconstructed responses (f) and identified forces (g): ▬ true signal; ▬ reconstructed signal using TDM. Relative mean prediction error (E-RMPE) as performance measure of the adaptive inversion routine (h).

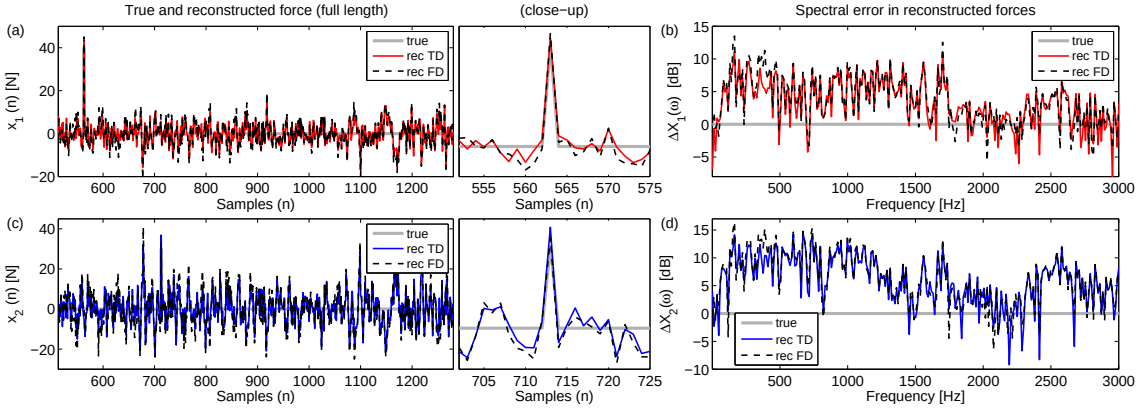

Figure A.19. Comparison of the generalised time domain inverse method (TDM) with the standard frequency domain inverse method (FDM) for the (2x2) MIMO system with 25 % noise added to all responses. Time signatures of reconstructed forces (a,c) and spectral estimation error in the identified force (b,d): ▬ true signal; ▬ reconstructed force using the MIMO TDM; ▬ ▬ identified force using the FDM.

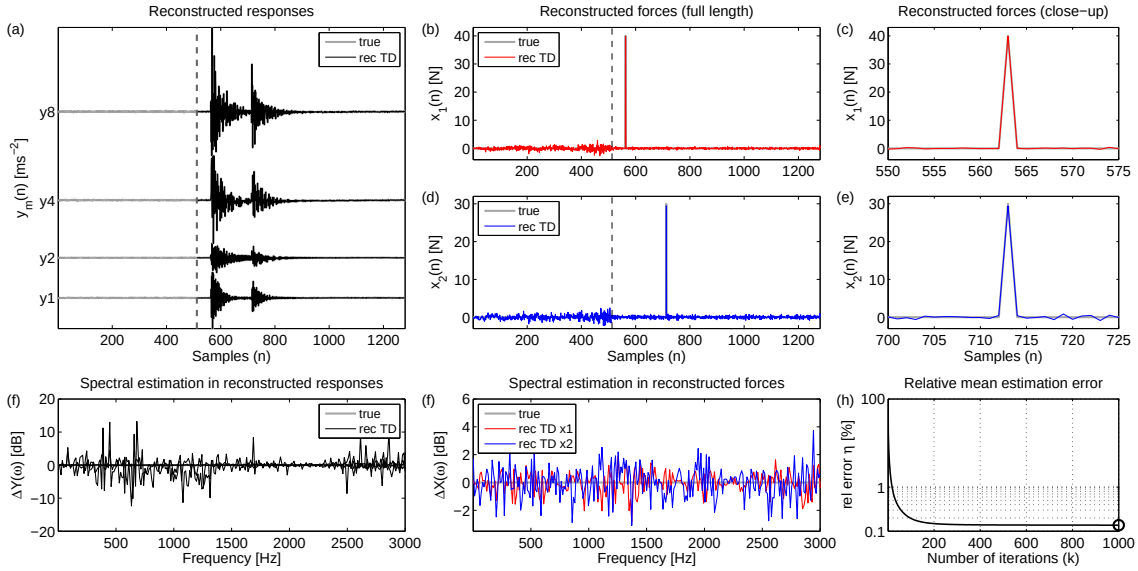

Figure A.20. Numerical results for (2x4) MIMO system with 5 % noise added to all acceleration responses. Time signatures of structural responses (a) and reconstructed force signatures in full-length (b,d) and as close-up (c,e); spectral estimation error in reconstructed responses (f) and identified forces (g): ▬ true signal; ▬ reconstructed signal using TDM. Relative mean prediction error (E-RMPE) as performance measure of the adaptive inversion routine (h).

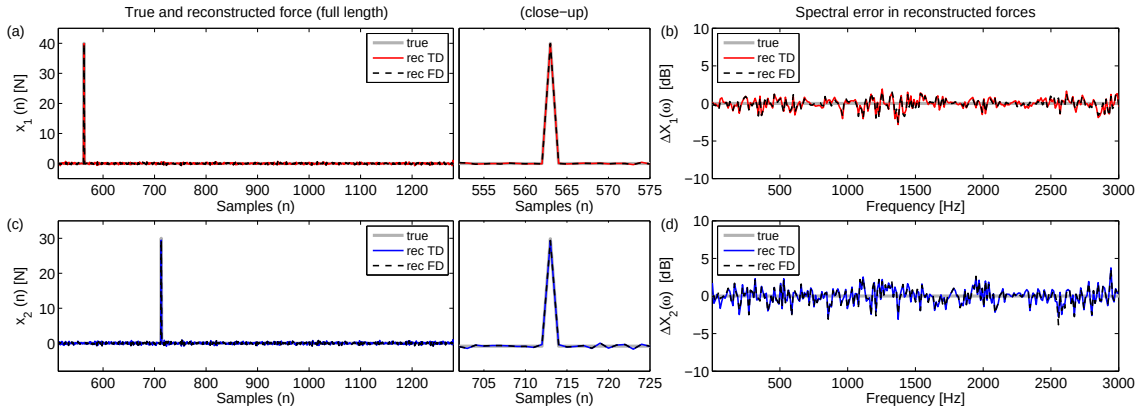

Figure A.21. Comparison of the generalised time domain inverse method (TDM) with the standard frequency domain inverse method (FDM) for the (2x4) MIMO system with 5 % noise added to all responses. Time signatures of reconstructed forces (a,c) and spectral estimation error in the identified force (b,d): ▬ true signal; ▬ reconstructed force using the MIMO TDM; ▬ ▬ identified force using the FDM.

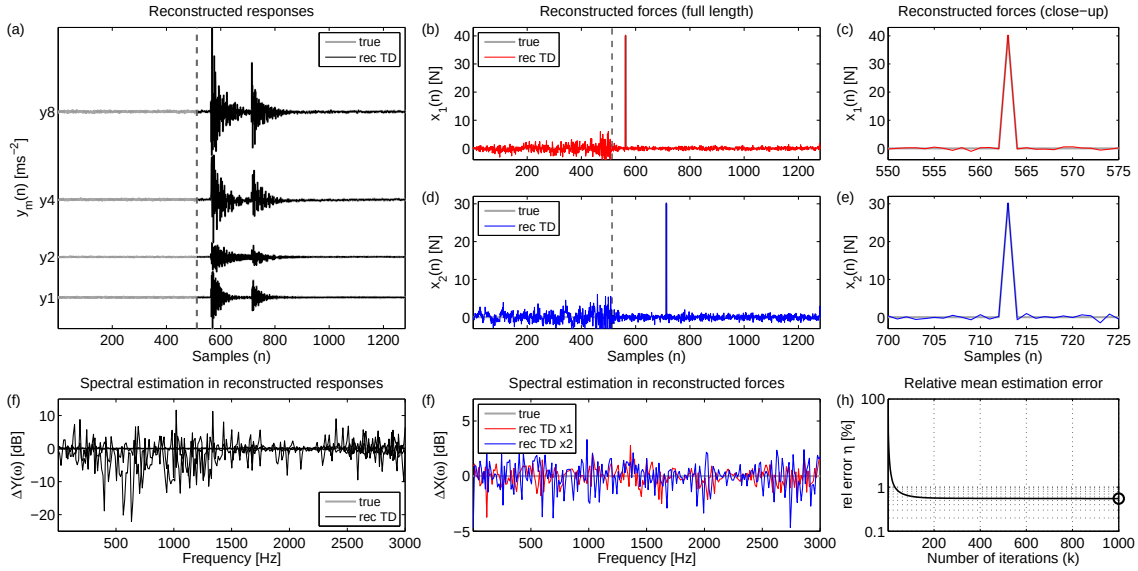

Figure A.22. Numerical results for (2x4) MIMO system with 10 % noise added to all acceleration responses. Time signatures of structural responses (a) and reconstructed force signatures in full-length (b,d) and as close-up (c,e); spectral estimation error in reconstructed responses (f) and identified forces (g): ▬ true signal; ▬ reconstructed signal using TDM. Relative mean prediction error (E-RMPE) as performance measure of the adaptive inversion routine (h).

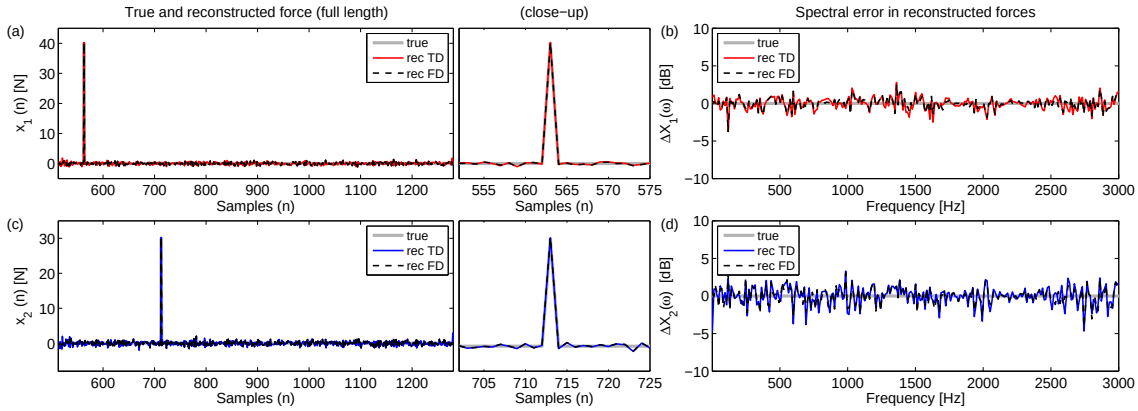

Figure A.23. Comparison of the generalised time domain inverse method (TDM) with the standard frequency domain inverse method (FDM) for the (2x4) MIMO system with 10 % noise added to all responses. Time signatures of reconstructed forces (a,c) and spectral estimation error in the identified force (b,d): ▬ true signal; ▬ reconstructed force using the MIMO TDM; ▬ ▬ identified force using the FDM.

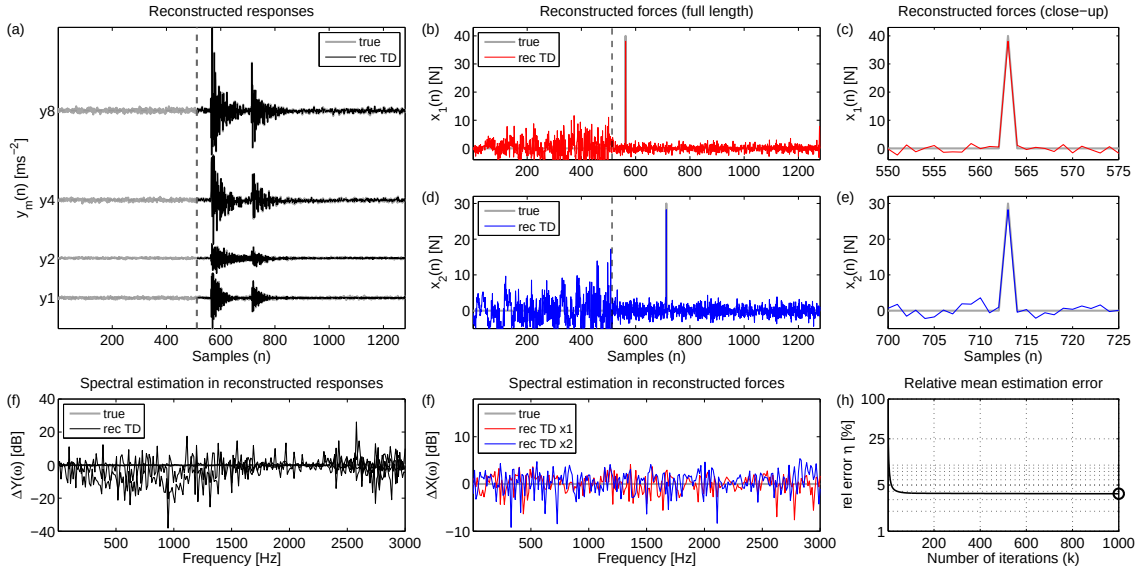

Figure A24. Numerical results for (2x4) MIMO system with 25 % noise added to all acceleration responses. Time signatures of structural responses (a) and reconstructed force signatures in full-length (b,d) and as close-up (c,e); spectral estimation error in reconstructed responses (f) and identified forces (g): ▬ true signal; ▬ reconstructed signal using TDM. Relative mean prediction error (E-RMPE) as performance measure of the adaptive inversion routine (h).

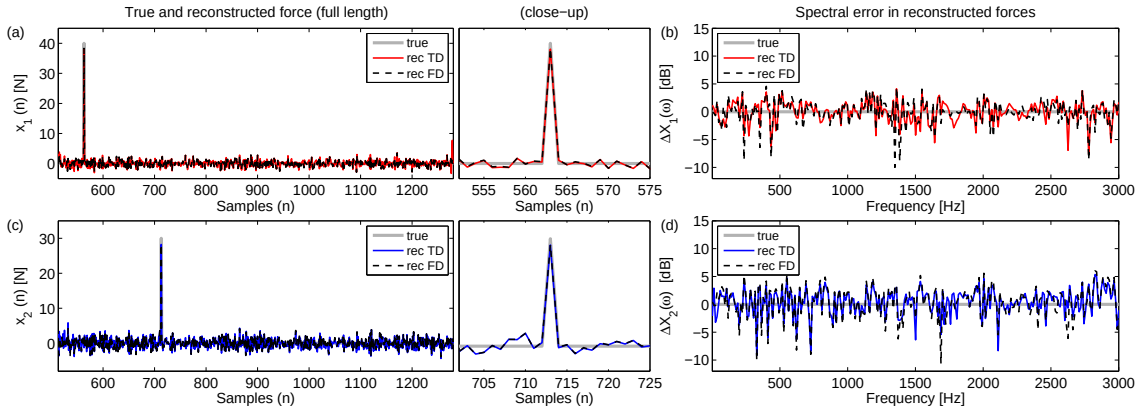

Figure A.25. Comparison of the generalised time domain inverse method (TDM) with the standard frequency domain inverse method (FDM) for the (2x4) MIMO system with 25 % noise added to all responses. Time signatures of reconstructed forces (a,c) and spectral estimation error in the identified force (b,d): ▬ true signal; ▬ reconstructed force using the MIMO TDM; ▬ ▬ identified force using the FDM.

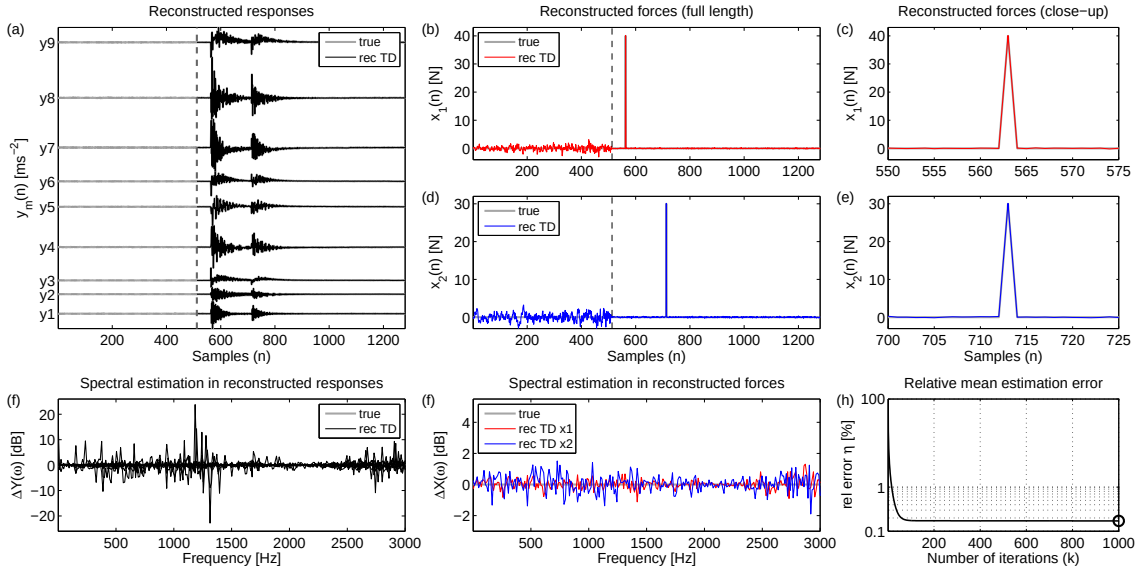

Figure A.26. Numerical results for (2x9) MIMO system with 5 % noise added to all acceleration responses. Time signatures of structural responses (a) and reconstructed force signatures in full-length (b,d) and as close-up (c,e); spectral estimation error in reconstructed responses (f) and identified forces (g): ▬ true signal; ▬ reconstructed signal using TDM. Relative mean prediction error (E-RMPE) as performance measure of the adaptive inversion routine (h).

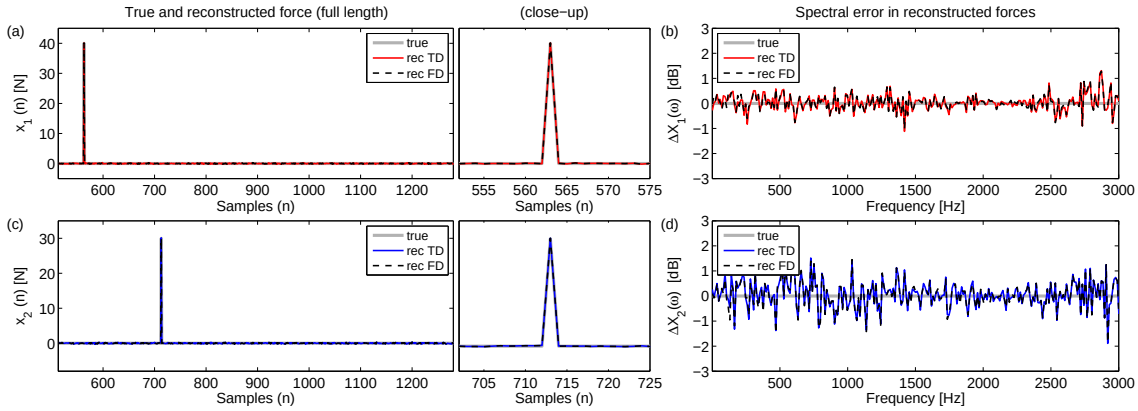

Figure A.27. Comparison of the generalised time domain inverse method (TDM) with the standard frequency domain inverse method (FDM) for the (2x9) MIMO system with 5 % noise added to all responses. Time signatures of reconstructed forces (a,c) and spectral estimation error in the identified force (b,d): ▬ true signal; ▬ reconstructed force using the MIMO TDM; ▬ ▬ identified force using the FDM.

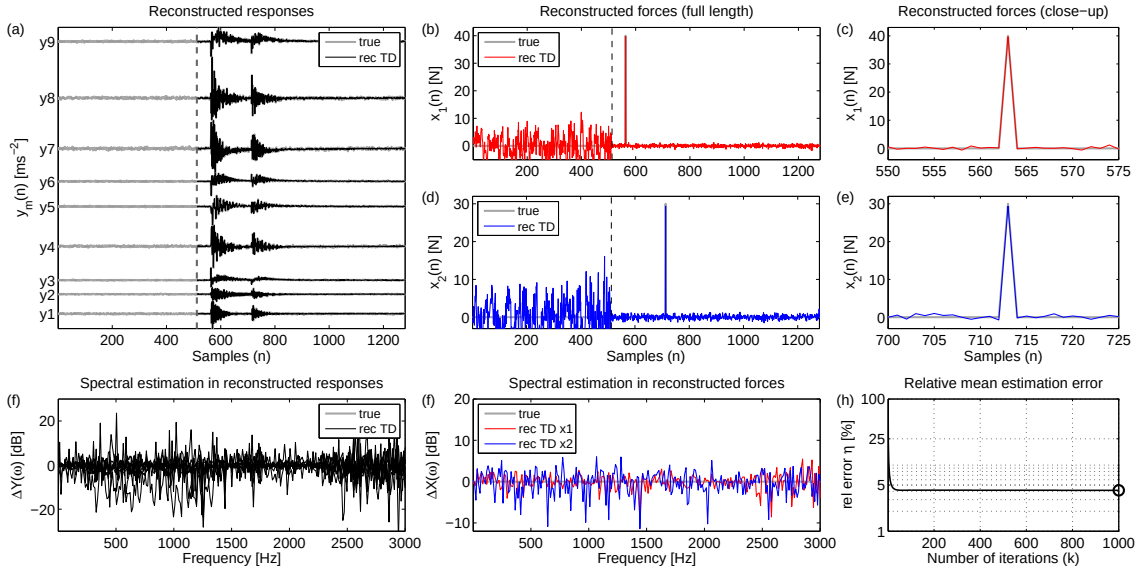

Figure A.28. Numerical results for (2x9) MIMO system with 25 % noise added to all acceleration responses. Time signatures of structural responses (a) and reconstructed force signatures in full-length (b,d) and as close-up (c,e); spectral estimation error in reconstructed responses (f) and identified forces (g): ▬ true signal; ▬ reconstructed signal using TDM. Relative mean prediction error (E-RMPE) as performance measure of the adaptive inversion routine (h).

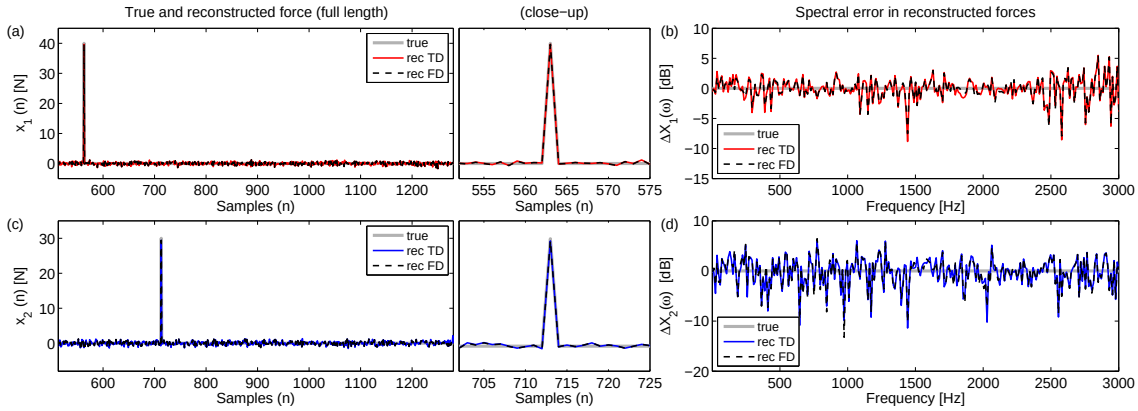

Figure A.29. Comparison of the generalised time domain inverse method (TDM) with the standard frequency domain inverse method (FDM) for the (2x9) MIMO system with 25 % noise added to all responses. Time signatures of reconstructed forces (a,c) and spectral estimation error in the identified force (b,d): ▬ true signal; ▬ reconstructed force using the MIMO TDM; ▬ ▬ identified force using the FDM.

Sensitivity to errors in the system model

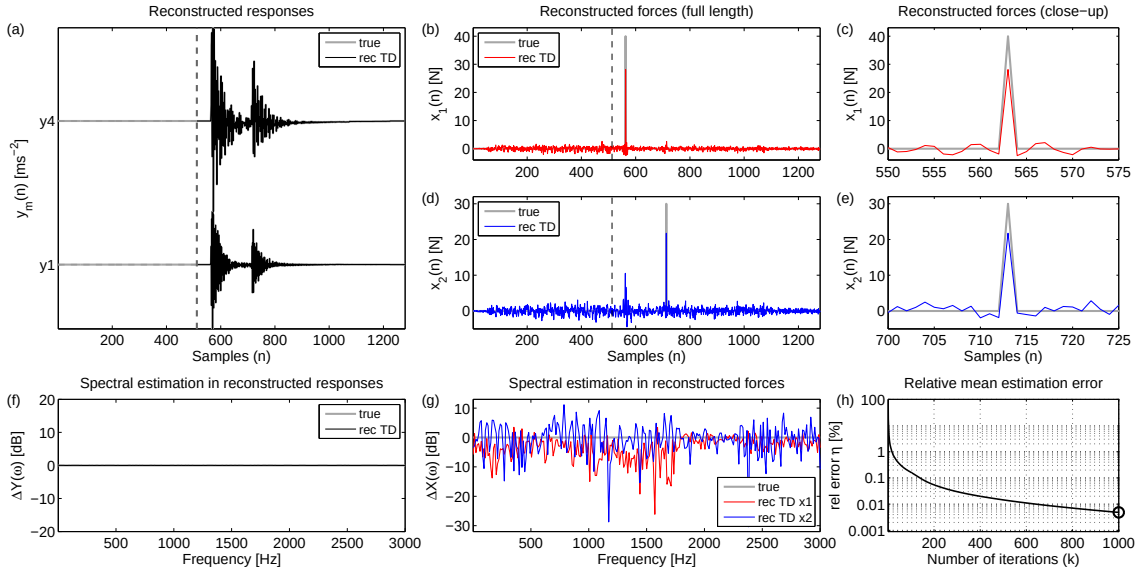

Figure A.30. Numerical results for (2x2) MIMO system with 5 % errors added to all impulse response functions. Time signatures of structural responses (a) and reconstructed force signatures in full-length (b,d) and as close-up (c,e); spectral estimation error in reconstructed responses (f) and identified forces (g): ▬ true signal; ── reconstructed signal using TDM. Relative mean prediction error (E-RMPE) as performance measure of the adaptive inversion routine (h).

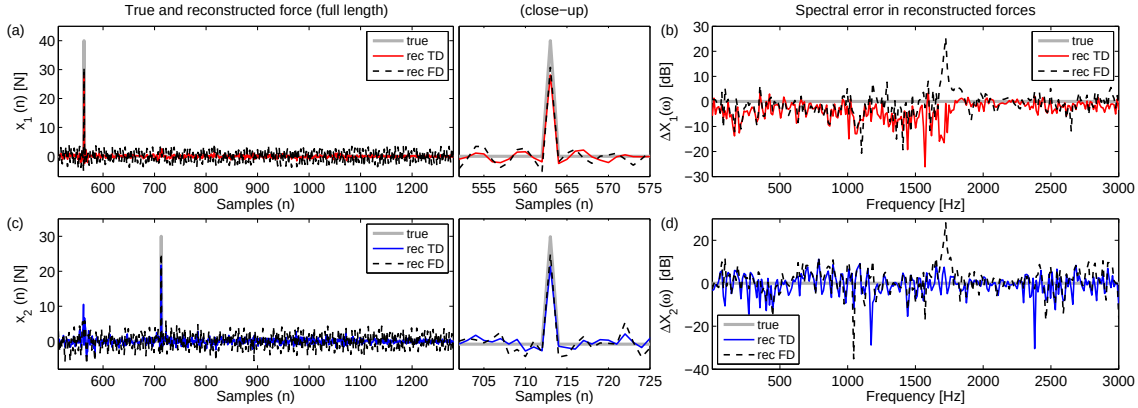

Figure A.31. Comparison of the generalised time domain inverse method (TDM) with the standard frequency domain inverse method (FDM) for the (2x2) MIMO system with 5 % errors added to all impulse response functions. Time signatures of reconstructed forces (a,c) and spectral estimation error in the identified force (b,d): ▬ true signal; ── reconstructed force using the MIMO TDM; ─ ─ identified force using the FDM.

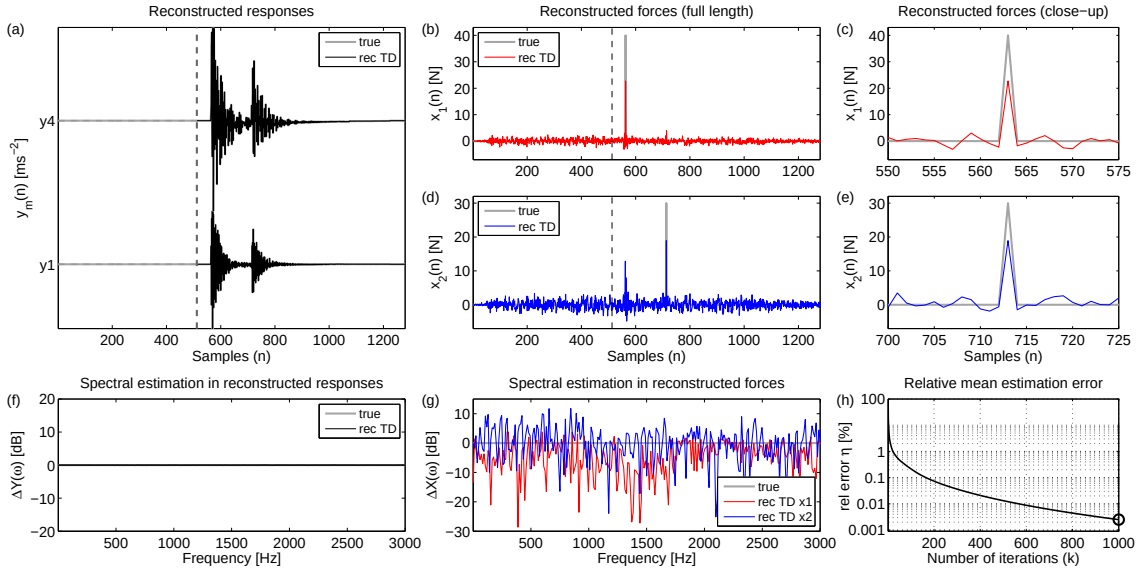

Figure A.32. Numerical results for (2x2) MIMO system with 10 % errors added to all impulse response functions. Time signatures of structural responses (a) and reconstructed force signatures in full-length (b,d) and as close-up (c,e); spectral estimation error in reconstructed responses (f) and identified forces (g): ▬ true signal; ▬ reconstructed signal using TDM. Relative mean prediction error (E-RMPE) as performance measure of the adaptive inversion routine (h).

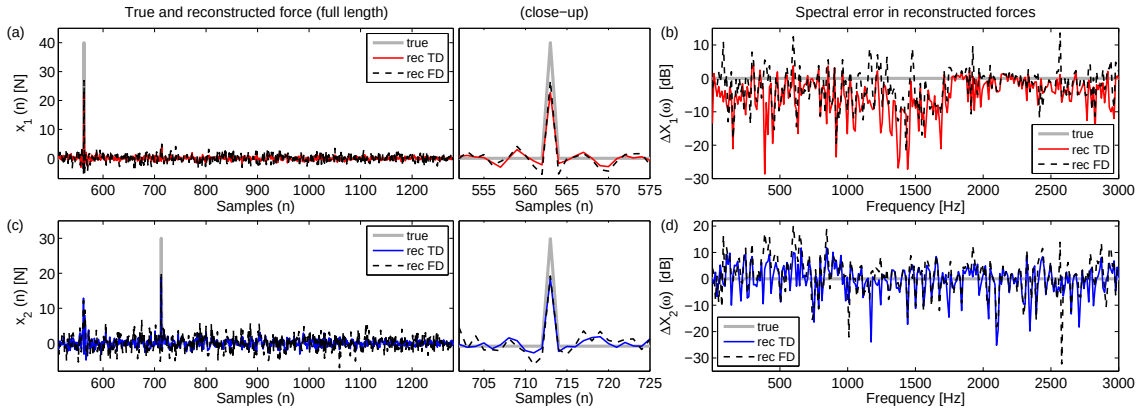

Figure A.33. Comparison of the generalised time domain inverse method (TDM) with the standard frequency domain inverse method (FDM) for the (2x2) MIMO system with 10 % errors added to all impulse response functions. Time signatures of reconstructed forces (a,c) and spectral estimation error in the identified force (b,d): ▬ true signal; ▬ reconstructed force using the MIMO TDM; ▬ ▬ identified force using the FDM.

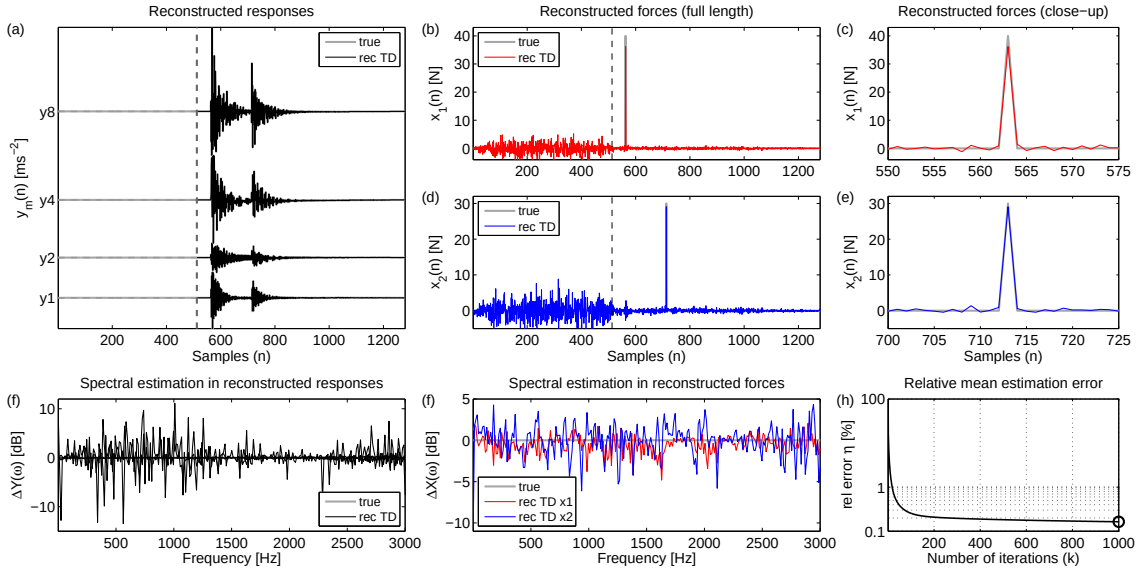

Figure A.34. Numerical results for (2x4) MIMO system with 5 % errors added to all impulse response functions. Time signatures of structural responses (a) and reconstructed force signatures in full-length (b,d) and as close-up (c,e); spectral estimation error in reconstructed responses (f) and identified forces (g): ▬ true signal; ▬ reconstructed signal using TDM. Relative mean prediction error (E-RMPE) as performance measure of the adaptive inversion routine (h).

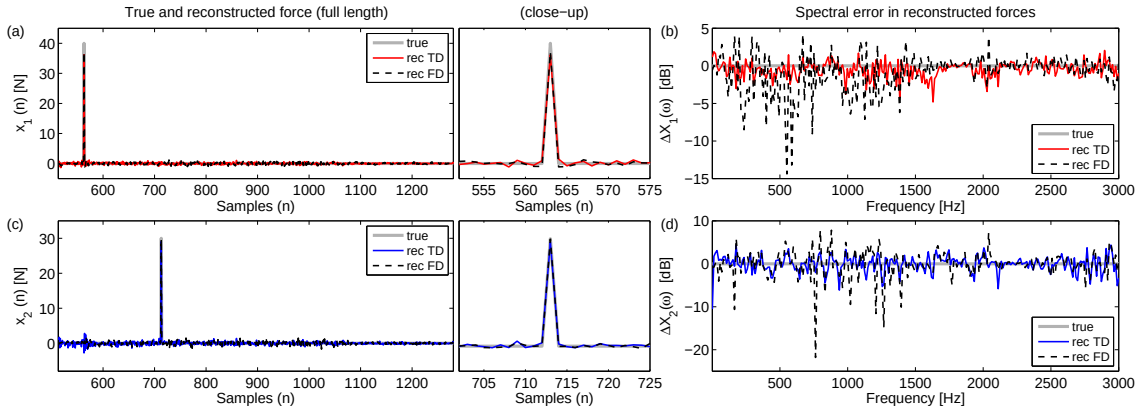

Figure A.35. Comparison of the generalised time domain inverse method (TDM) with the standard frequency domain inverse method (FDM) for the (2x4) MIMO system with 5 % errors added to all impulse response functions. Time signatures of reconstructed forces (a,c) and spectral estimation error in the identified force (b,d): ▬ true signal; ▬ reconstructed force using the MIMO TDM; ▬ ▬ identified force using the FDM.

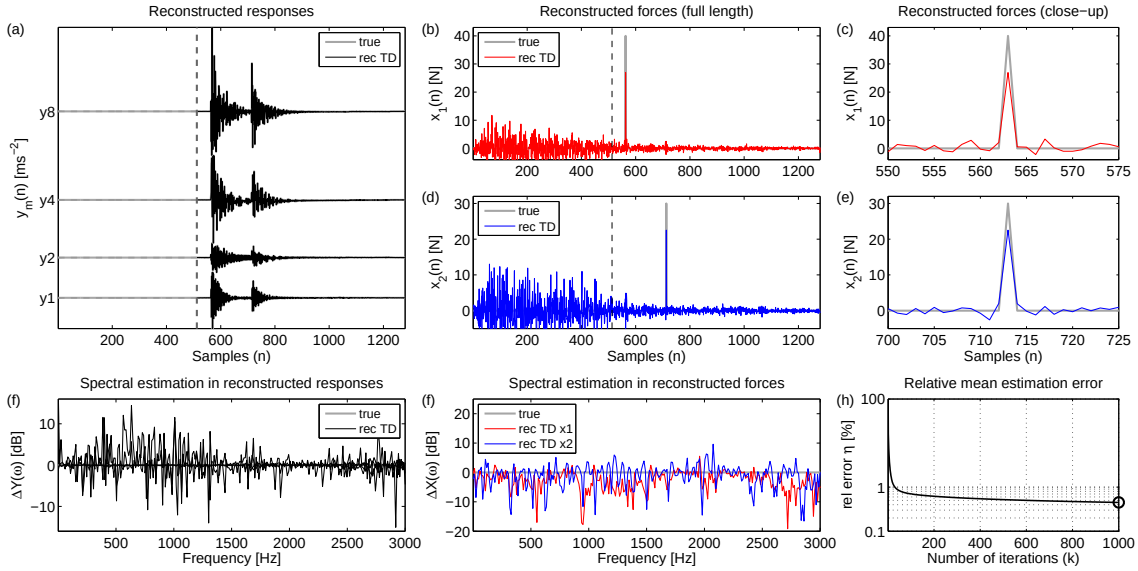

Figure A.36. Numerical results for (2x4) MIMO system with 10 % errors added to all impulse response functions. Time signatures of structural responses (a) and reconstructed force signatures in full-length (b,d) and as close-up (c,e); spectral estimation error in reconstructed responses (f) and identified forces (g): ▬ true signal; ▬ reconstructed signal using TDM. Relative mean prediction error (E-RMPE) as performance measure of the adaptive inversion routine (h).

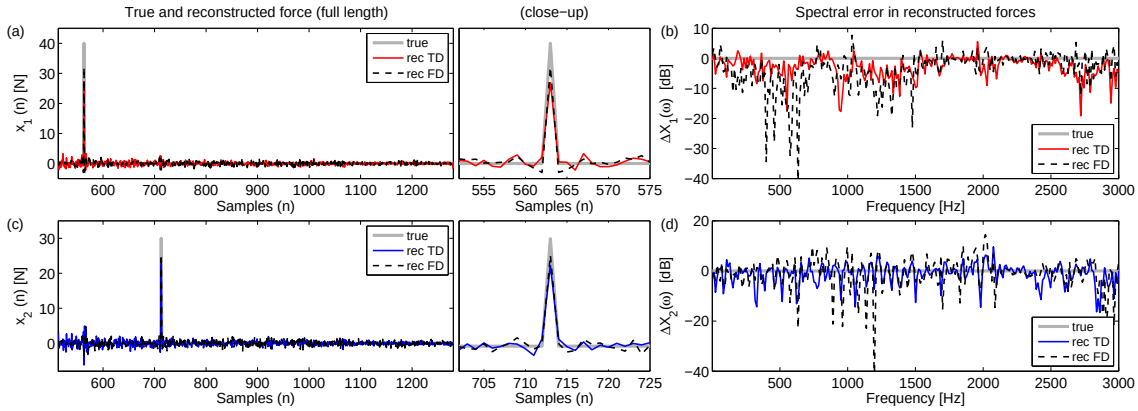

Figure A.37. Comparison of the generalised time domain inverse method (TDM) with the standard frequency domain inverse method (FDM) for the (2x4) MIMO system with 10 % errors added to all impulse response functions. Time signatures of reconstructed forces (a,c) and spectral estimation error in the identified force (b,d): ▬ true signal; ▬ reconstructed force using the MIMO TDM; ▬ ▬ identified force using the FDM.

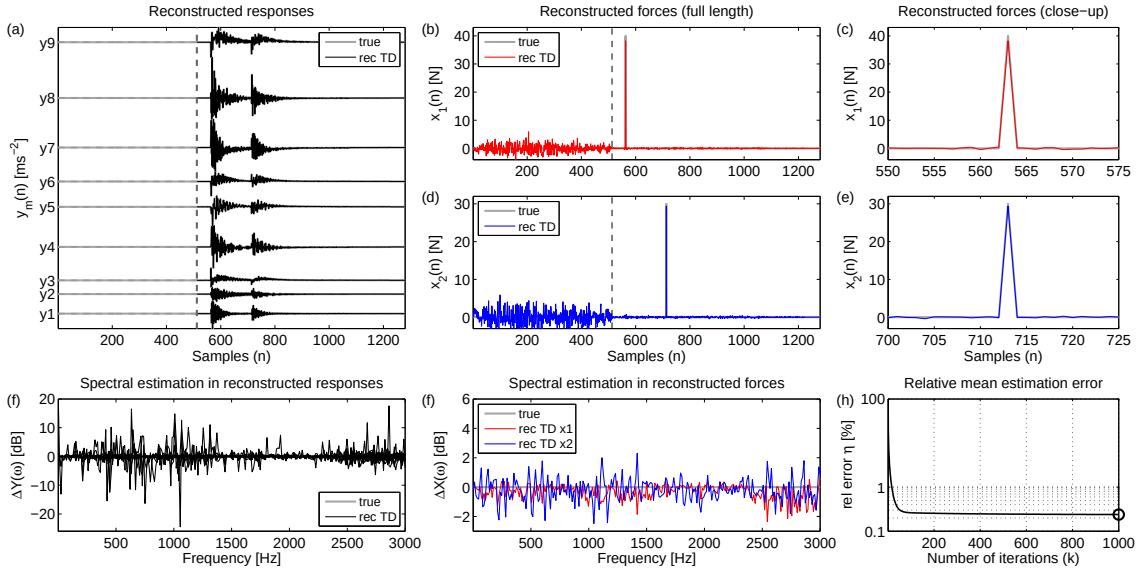

Figure A.38. Numerical results for (2x9) MIMO system with 5 % errors added to all impulse response functions. Time signatures of structural responses (a) and reconstructed force signatures in full-length (b,d) and as close-up (c,e); spectral estimation error in reconstructed responses (f) and identified forces (g): ▬ true signal; ▬ reconstructed signal using TDM. Relative mean prediction error (E-RMPE) as performance measure of the adaptive inversion routine (h).

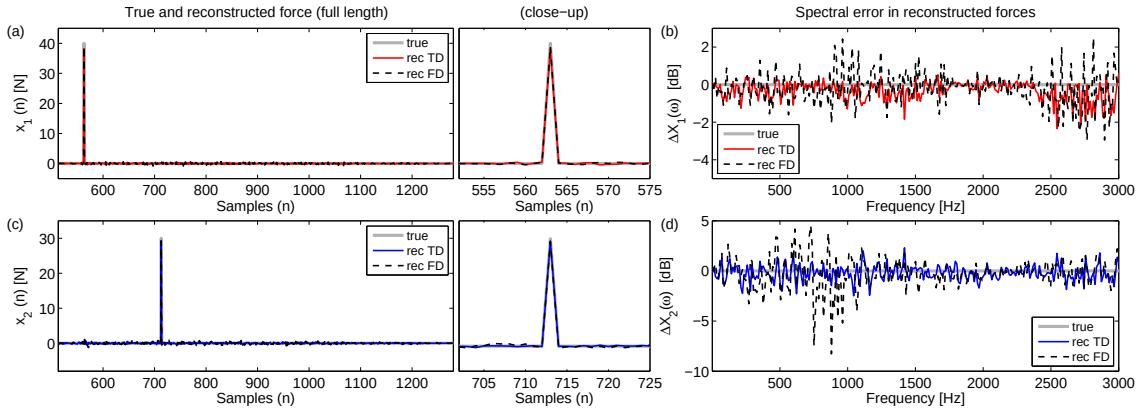

Figure A.39. Comparison of the generalised time domain inverse method (TDM) with the standard frequency domain inverse method (FDM) for the (2x9) MIMO system with 5 % errors added to all impulse response functions. Time signatures of reconstructed forces (a,c) and spectral estimation error in the identified force (b,d): ▬ true signal; ▬ reconstructed force using the MIMO TDM; ▬ ▬ identified force using the FDM.

A.3 FRAC and PAC analysis

The Frequency Response Assurance Criterion (FRAC) represents a frequency independent single-value measure of the correlation between the magnitudes of any two frequency response functions (FRFs) $H_1(\omega)$ and , respectively, the FRAC value is defined by

$$FRAC(H_1, H_2) = \frac{\left|\mathbf{h}_1^H \mathbf{h}_2\right|^2}{\left(\mathbf{h}_1^H \mathbf{h}_1\right)\left(\mathbf{h}_2^H \mathbf{h}_2\right)} \tag{A.1}$$

where $\mathbf{h}_1 = H_1(\omega_c)$ and $\mathbf{h}_2 = H_2(\omega_c)$ are vectors comprising the complex magnitudes of the corresponding FRFs at the considered frequency grid points ω_c in the frequency range of interest, i.e. $\omega_{\min} \le \omega_c \le \omega_{\min}$, and the super-script '*H*' denotes conjugate (Hermitian) transpose of the respective vector. Due to the normalisation only values of $0 \le FRAC(H_1, H_2) \le 1$ are possible. Values close to unity indicate strong correlation between the magnitudes of both FRFs for which reason the underlying measurements can be considered to be of high quality. However, one major drawback of this criterion is the tremendous sensitivity of the FRAC value to magnitude mismatches in the vicinity of even slightly shifted resonances (and anti-resonances) in the measured FRFs inevitably resulting in very small correlation values that indicate low measurement quality although this is not necessarily the case.

In order to better account for possible shifts in the resonance and anti-resonance frequencies it is advisable to employ a different quality evaluation criterion incorporating the phase information of the measured FRFs. In this respect the Phase Assurance Criterion (PAC) has been found to be a helpful means [217]. The PAC uses the effect of changing signs in the phase response of the measured FRFs at resonances and anti-resonances. Determination of the PAC value is based on calculating a sign vector $\mathbf{p}_i = \left[p_i(\omega_{\min}), \ldots, p_i(\omega_{\max})\right]$ for both considered FRFs, i.e. $H_i(\omega)$ for $i = [1, 2]$, and the phase sign $p_i(\omega_c)$ at each considered frequency grid point ($\omega_{\min} \le \omega_c \le \omega_{\max}$) is obtained by

$$p_i(\omega_c) = \operatorname{sgn}\left(\gamma_i(\omega_c) - \gamma_{i,ref}\right) \tag{A.2}$$

where 'sgn(·)' denotes the signum function extracting the sign of the real number expression in the brackets, $\gamma_i(\omega_c)$ is the phase angle in rad of the respective FRF at frequency ω_c and

$$\gamma_{i,ref} = \begin{cases} +\pi/2 & \text{for compliances} \\ 0 & \text{for mobilities} \\ -\pi/2 & \text{for accelerances} \end{cases} \tag{A.3}$$

is the corresponding reference phase angle that needs to be chosen with respect to the prevailing FRF type in order to ensure phase angles between $-\pi/2$ and $+\pi/2$. According to these definitions the PAC value can be calculated as the product of the corresponding phase sign vectors by

$$PAC(H_1, H_2) = \frac{\mathbf{p}_1^T \mathbf{p}_2}{N_c}. \tag{A.4}$$

Note that the inner product of both sign vectors constitutes a summation over all considered frequency grid points so that the PAC value is again a frequency independent single-value. Due to the normalisation to the number of grid points, N_c, PAC values between $-1 \le PAC(H_{ms}, H_{sm}) \le 1$ are possible. Values close to unity indicate good correlation between the phase responses of the compared FRFs while values close to zero indicate no correlation. Negative PAC values close to -1 denote opposite phase relationships between the FRFs which in practice can result from confusion in the sign convention in the measured data [7].

Employing FRAC or PAC techniques to evaluate the consistency of system models is in particular useful if large FRF matrices are involved. The single valued correlation measures can be visualised in coloured matrices which are arranged according to the FRF matrices employed in the system model allowing quick evaluation of the degree of correlation. Theoretically, any two according FRFs could be compared, e.g. FRFs obtained from analytical models or numerical simulations could be employed to evaluate FRF measurements conducted on a real structure. This however is only possible for very simple structures such as beam-like structures, for instance. In practice, FRAC and PAC procedures are often employed by invoking the principle of reciprocity [43] to evaluate the degree of reciprocity between FRF measurements. It is noted that this is only possible if both corresponding FRFs are available, i.e. the direct FRF $H_1(\omega) = H_{ms}(\omega)$ excited at DOF s with response measurement at DOF m as well as the reciprocal FRF $H_2(\omega) = H_{sm}(\omega)$ excited at DOF m with response measurement at DOF s. Thus, only square FRF matrices can be evaluated requiring extensive measurement effort for sophisticated MDOF structures, such as electric power steering systems.